Synthesis and Characterization of Bio-Based Polymers from Oleanolic Acid

Dissertation

Zur Erlangung des akademischen Grades

Doktor der Naturwissenschaften

(Dr. rer. nat.)

Eingereicht an der Fakultät für Mathematik und Naturwissenschaften

der Bergischen Universität Wuppertal

von

Till Laurin Jessewitsch

geb. in Haan, Deutschland

Wuppertal 2025

Die vorliegende Arbeit wurde in der Zeit von Juli 2021 bis Oktober 2024 unter der Leitung von Prof. Dr. Guillaume Delaittre an der Bergischen Universität Wuppertal angefertigt.

Teile dieser Arbeit wurden veröffentlicht:

Jessewitsch, T.; Saou, N.; Steinlein, L.; Bensberg, K.; Kirsch, S. F.; Delaittre, G. Oleanolic Acid-Derived High-Glass-Transition-Temperature Methacrylic Polymers. *ACS Sustainable Chem. Eng.* **2024**, *12* (52), 18499–18507.

Table of contents

1. Introduction and Motivation

The current PhD project was part of the cooperation initiative "Chemistry *of* and *with* Food Loss from Apples" from the Department of Chemistry and Biology at the University of Wuppertal. In the context of sustainable chemistry, apple pomace has been identified as an underexplored and local resource for valuable compounds. It occurs in large quantities – approximately 250 kt/year in Germany – as a byproduct of the apple juice and cider production.[1] Besides lignocellulosic materials and pectin, it is notably rich in bioactive compounds, particularly polyphenols such as flavonoids and phenolic acids, as well as distinct triterpenoids, particularly ursolic acid (UA), oleanolic acid (OA), and betulinic acid (BA).[2] Among them, UA is present at a higher content (0.80 wt%) compared to OA (0.16 wt%).[3] However, OA represents the compound of interest in this study due to its greater availability, stemming from its additional abundance in olive leaves (up to 3.1 wt%) as a byproduct of large-scale olive cultivation.[4] Due to its renewable origin and functional structure, OA is a promising candidate for use in sustainable polymer materials.

In the first research chapter, OA was modified to obtain different stable methacrylate monomers with the bulky triterpenoid forming the side chain (Scheme 1.1). Once their general polymerizability was confirmed, kinetic studies served to demonstrate the controlled behavior of the RAFT process with the novel monomers. Ideally, the polymerization led to a narrow molecular weight distribution while preserving the RAFT end group functionality, enabling the potential to form block copolymers.

In the subsequent chapters, OA was reduced to erythrodiol (**ErDO**), introducing two hydroxyl functionalities that enable its use in diol-based polyaddition and polycondensation reactions and incorporate the triterpenoid structure in the main chain. Bio-based polyurethanes (PUs) are considered promising candidates for future materials.[5] Therefore, the second research chapter focused on the synthesis of linear PUs from **ErDO** and aliphatic or aromatic diisocyanates, investigating both metal-based and organocatalysts. To modify the thermal properties of the PUs, ternary polymers were formed using the potentially bio-based 1,6-hexanediol (HDO).

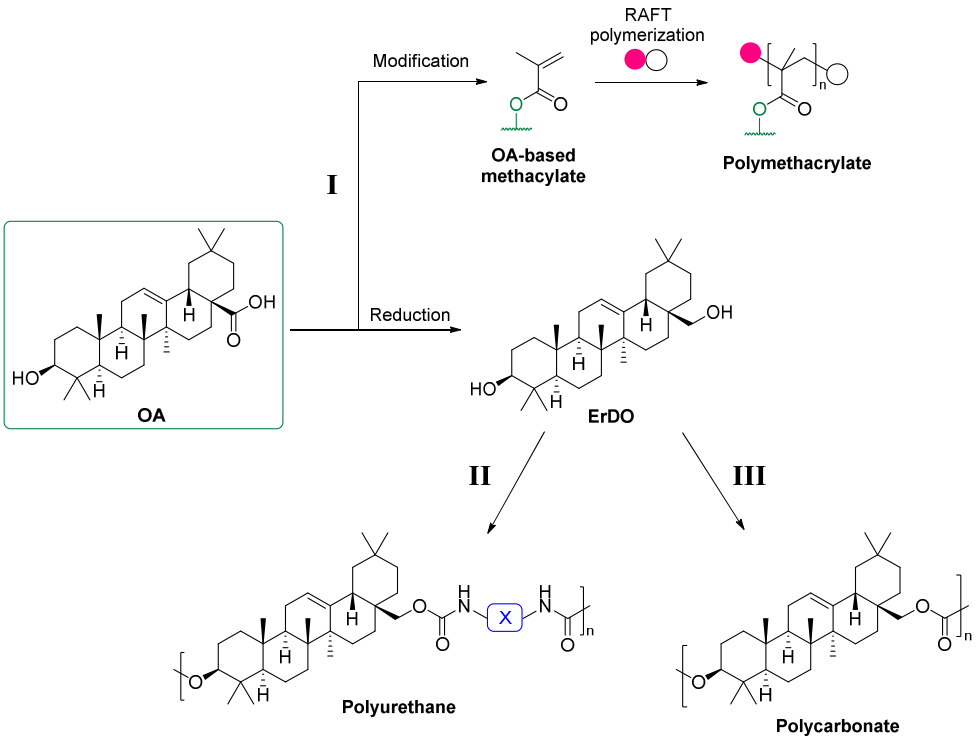

Scheme 1.1. Overview of the synthetic strategy (I: formation of methacrylate monomers and RAFT polymerization, II: polyurethanes by polyaddition with diisocyanates, III: polycarbonates by polycondensation).

In the third part of this study, **ErDO** served as a monomer for polycondensation with carbonylating agents, such as dimethyl carbonate (DMC) or diphenyl carbonate (DPC), in order to obtain sustainable polycarbonates that may serve as alternatives to poly(bisphenol A carbonate). Furthermore, the thermal properties were altered by using HDO as a comonomer.

2. Background

2.1. Bio-Based Polymers

Due to climate change, the use of fossil resources and the environmental impact of plastic waste, moving to a bio-based circular economy has become increasingly important.[6] In contrast to synthetic polymers, biopolymers such as DNA, RNA, proteins, cellulose, and starch are produced by living organisms.[7] Bio-based materials have the advantage of being sustainable or even biodegradable and can be obtained directly from algae, bacteria, plants, fungi, and crustaceans by further partial modification of these polymers or by polymerization of bio-based monomers.[8] Polymers produced by nature can be classified into polysaccharides, proteins, polyesters, and polyphenols, each offering unique properties (Figure 2.1).

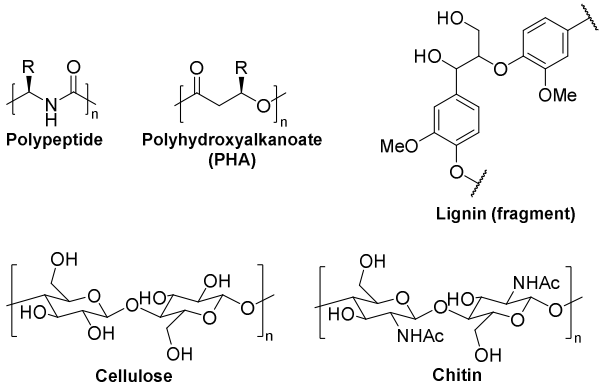

Figure 2.1. Natural biomass polymers.

Polyhydroxyalkanoates (PHAs) are bio-polyesters produced by bacterial fermentation from sugar, vegetable oils, and fatty acids offering a variety of homopolymers, random copolymers, and block copolymers depending on the bacterial species and conditions.[9] PHAs are used in packaging,[10] biomedical applications,[11] and 3D printing.[12] The natural polymer chitin consists of *N*-acetyl-D-glucosamine units and is the second most abundant polysaccharide after cellulose, existing in the shells of crustaceans and insects as well as the cell walls of fungi and algae.[13] Chitosan, obtained by partial deacetylation (>50%) of chitin, is a bioactive compound with versatile applications, including medical uses, cosmetics, and agriculture.[14]

The main first-generation feedstocks to produce bio-based chemicals by fermentation are sucrose- or starch-containing plants such as sugarcane, sugar beet, corn, and wheat.[15] Sucrose is directly fermentable, whereas starch, a mixture of the linear polymer amylose

and the branched amylopectin, requires enzymatic hydrolysis to yield glucose.[9] From the fermentation of the intermediate glucose, several valuable products can be obtained like ethanol as biofuel or precursor for ethylene, lactic acid as the precursor to polylactic acid (PLA), succinic acid for polyesters or further hydrogenation to γ-butyrolactone and 1,4-butanediol (Scheme 2.1).[15] Glucose is industrially used for the catalytic hydrogenation to sorbitol, whereby subsequent complete dehydration forms isosorbide, a highly useful building block for bioplastics.[16] Isomerization of glucose to fructose and subsequent acid-catalyzed dehydration yields 5-(hydroxymethyl)furfural (5-HMF), which is considered the most versatile intermediate for further furan derivatives and can potentially be hydrogenated to 1,6-hexanediol.[10,17]

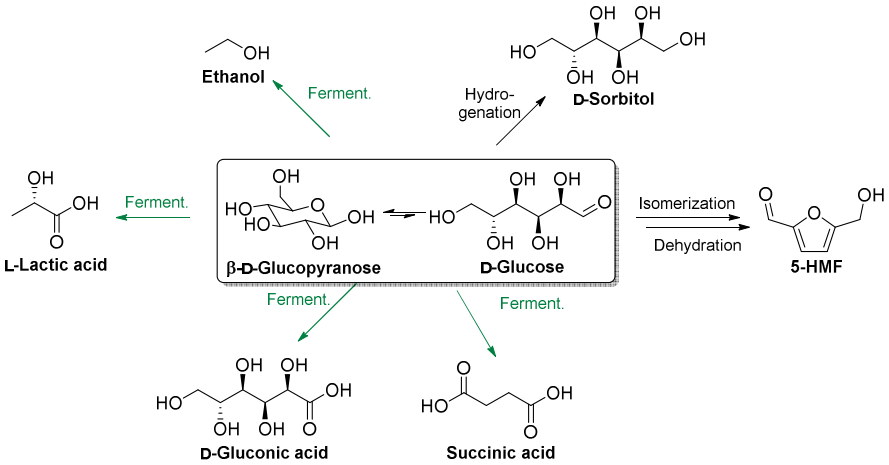

Scheme 2.1. Valuable chemicals from glucose via fermentation or hydrogenation.

Since the use of first-generation feedstocks remains controversial, as they can serve as food sources for humans and animals or compete for agricultural land, the use of the second-generation non-edible lignocellulosic feedstock is gaining importance.[15] Lignocellulosic biomass is the most widespread and renewable resource on earth, consisting of about 35–50% cellulose, 20–35% hemicellulose, and 10–25% lignin, widely present in wood, agricultural waste, and plants.[10] Hemicellulose is composed of several branched heteropolymers with different pentose and hexose units, whereby lignin is an irregular three-dimensional polymer of phenylpropanoid units, functioning as cellular glue or contributing to fiber strength.[18]

Lignocellulose offers the potential for a broader range of platform chemicals, but due to its complex and highly resistant structure it requires pretreatment to increase the porosity, remove lignin or hemicellulose, and reduce the crystallinity of cellulose.[19] Alkaline pretreatment swells and partially dissolves lignin due to the deprotonation of hydroxyl

groups and cleavage of ester bonds between lignin and hemicellulose.[20] In contrast, dilute acid pretreatment hydrolyzes hemicellulose into fermentable C6 (glucose, mannose, galactose) and C5 (xylose, arabinose) sugars.[21] Hydrolysis of cellulose, either through acid or enzymatic treatment, provides glucose as a key precursor for bioconversion. Additionally, extracted lignin can serve as a valuable feedstock for aromatic platform chemicals.[22]

2.2. Plant Metabolites

In general, plants produce two types of metabolites (Figure 2.2). The primary ones are involved in cellular survival, growth, development, and propagation, such as amino acids, sugars, fatty acids, nucleotides, and isoprene-based pyrophosphates.[23–25] Secondary metabolites are mainly biosynthesized from these precursors and are critical for ecological interactions such as defense and resistance against fungi, viruses, bacteria, insects, or even competitors, by suppressing surrounding plant growth.[26–28] Secondary metabolites are commonly classified into the three broad classes consisting of terpenoids, phenolic compounds (phenolic acids, flavonoids, stilbenes, coumarins, lignans, and tannins), and nitrogen-containing compounds (alkaloids, glucosinolates, cyanogenic glycosides, and nonprotein amino acids).[24,29]

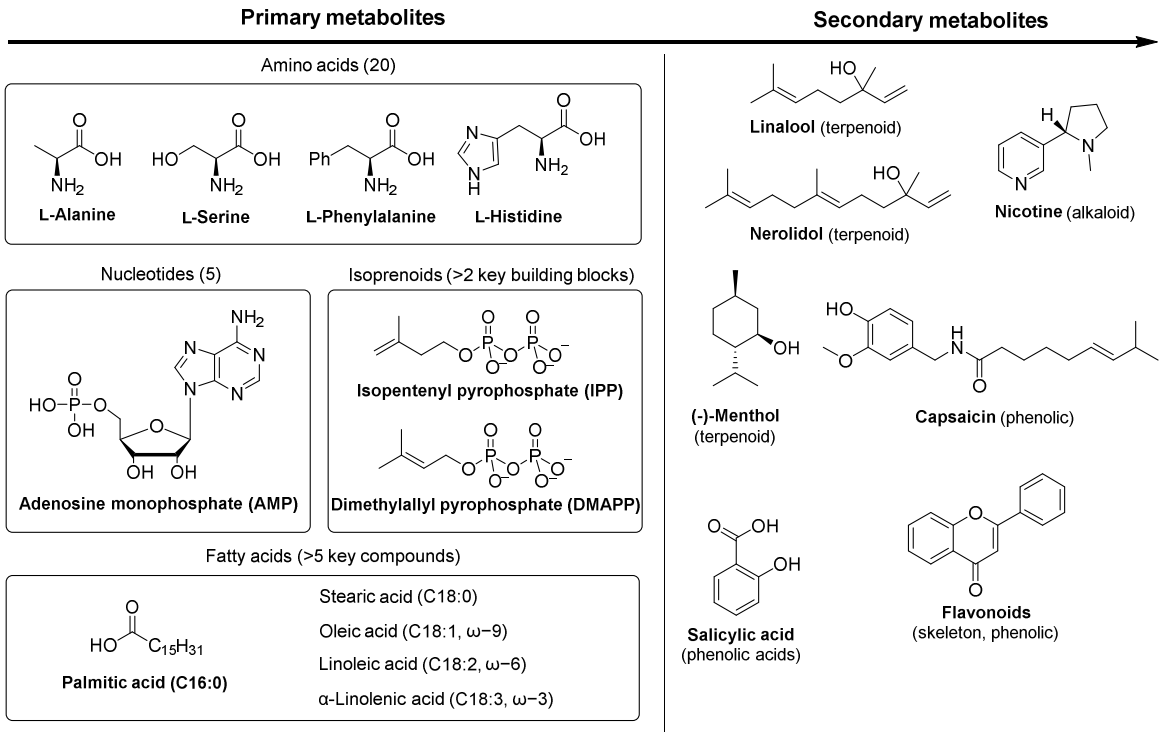

Figure 2.2. Examples of secondary plant metabolites derived from primary metabolites (not all classes of primary metabolites and their compounds are shown).[25]

2.3. Terpenes and Triterpenoids

Terpenes represent the largest, most diverse group of secondary metabolites.[24] Flowering plants exhibit an unusually high amount of terpenoids (terpenes containing oxygen, often used as a synonym), reflecting their adaptive strategies.[30] Terpenes and terpenoids are derived from isoprene, which together comprise around 80 000 different compounds.[31] Terpenes are classified according to the number of isoprene units (1, C_5H_8): monoterpenes (2, $C_{10}H_{16}$), sesquiterpenes (3, $C_{15}H_{24}$), diterpenes (4, $C_{20}H_{32}$), sesterterpenes (5, $C_{25}H_{40}$), triterpenes (6, $C_{30}H_{48}$), and so on.[24]

Squalene (**5**) is a lipophilic molecule, belonging to the class of triterpenes, and is an essential intermediate in the biosynthesis of sterols and cyclic triterpenoids.[32] As can be seen from Scheme 2.2, starting from isopentenyl pyrophosphate (IPP, **2**) and dimethylallyl pyrophosphate (DMAPP, **1**), enzymatic catalysis promotes the elimination of the pyrophosphate group (OPP^-) from substrate **1** to a carbocation, proceeding like a S_N1 mechanism by the nucleophilic attack of **2** followed by deprotonation and C=C double bond formation to geranyl pyrophosphate (GPP, **3**).[33,34] This head-to-tail condensation can continue to farnesyl pyrophosphate (FPP, **4**), whereby subsequently two FPP molecules are condensed head-to-head by the enzyme squalene synthase via a cyclopropyl intermediate forming squalene (**5**). **5** can be found in cell membranes, contributing to their stabilization and regulating diffusion.[35,36]

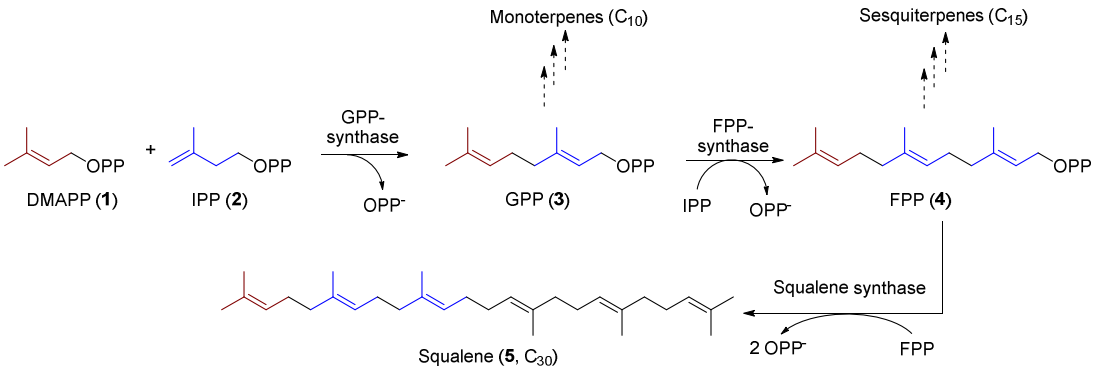

Scheme 2.2. Triterpene squalene biosynthesis (intermediate presqualene pyrophosphate not shown for clarity).

2,3-oxidosqualene (**6**) can be formed from squalene (**5**) by the enzyme squalene epoxidase (Scheme 2.3). The following cyclization can lead to a wide range of different triterpene structures, whereby almost 200 distinct triterpene core structures are known in plants.[37] **6** is pre-folded by the binding site of the cyclase enzyme, whereby the strained three-membered epoxide ring functions as an electrophile.[38] The acidic residue of the enzyme

leads to protonation of the epoxide, triggering ring closure by the nearby double bond and starting a cascade of further C-C ring-forming reactions, as well as rearrangements producing either sterols or cyclic triterpenoids.[38] **6** can be seen as a branch-point between the primary sterol (as essential membrane components) and the secondary triterpenoid metabolism, whereby the initial substrate folding in a chair-boat-chair or for the latter in a chair-chair-chair conformation determines the cyclization pathway.[32,38] By a variety of oxidosqualene cyclases, tricyclic, tetracyclic, or pentacyclic triterpenoids can be formed.[39] From the pentacyclic species, structurally relative to the lupan, oleanan, and ursan fully saturated carbon skeletons, lupeol (**8**), β-amyrin (**10**), and α-amyrin (**12**) are the most widely distributed in plants, occurring in the wax layer of leaves and on fruits.[39–42]

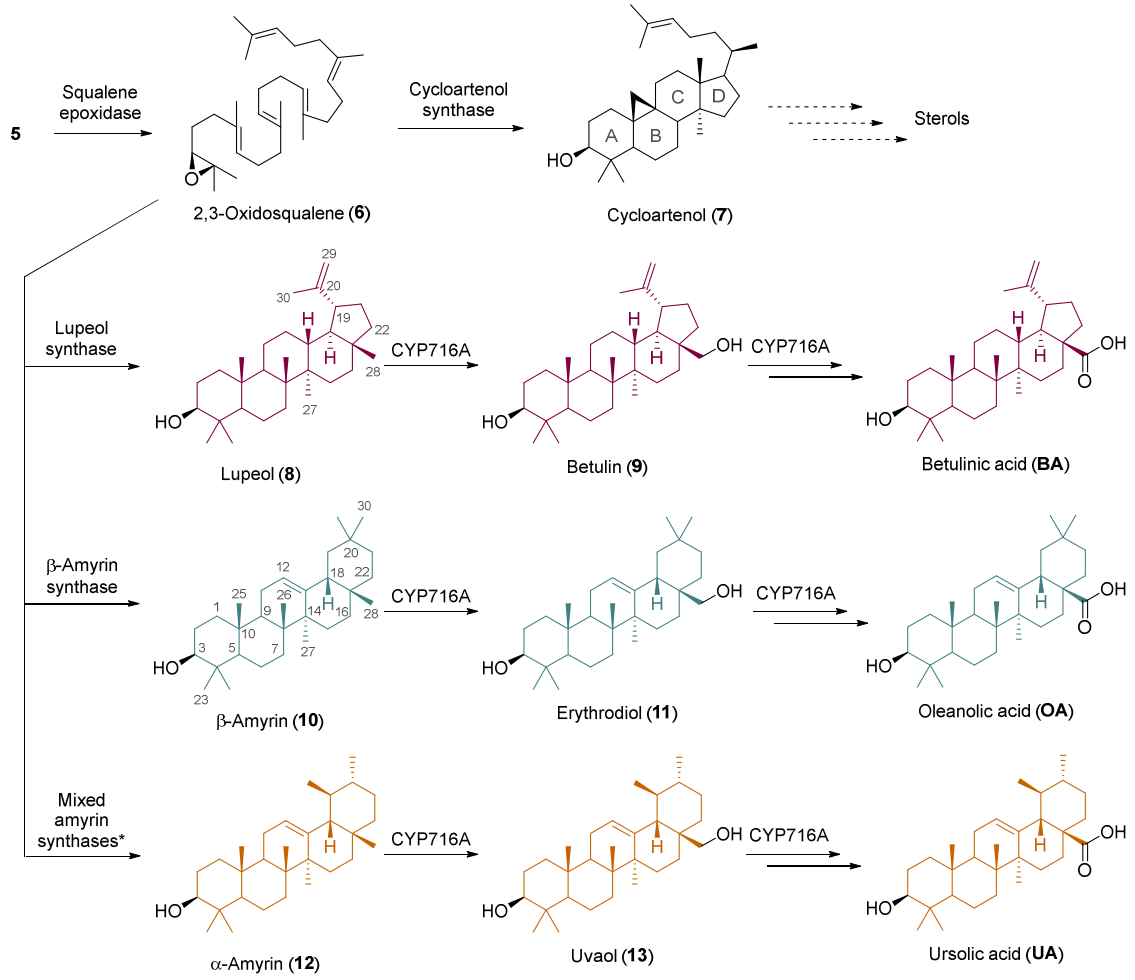

Scheme 2.3. A simplified scheme of the biosynthetic branch point forming either sterols or triterpenoids, highlighting the secondary pentacyclic metabolites BA, OA, and UA (*α-amyrin is mainly produced by multifunctional enzymes, not forming solely α-amyrin).

10 can be formed by β-amyrin synthase over several cationic species with a final deprotonation, creating a double bond between C-12 and C-13. Subsequently, oxidation of the methyl group at C-28 by a CYP716A subfamily enzyme of cytochrome P450

monooxygenases leads to erythrodiol (**11**), the labile oleanolic aldehyde, and lastly oleanolic acid (OA).[43] A product-specific α-amyrin synthase does not exist, in contrast to β-amyrin and lupeol synthases.[44,45] Nevertheless, a mixed-amyrin synthase with α-amyrin (**12**) representing more than 80% of the enzyme product has been identified in apples.[39] The enzymes of the CYP716A subfamily can catalyze C-28 oxidation reactions on various triterpenoid backbones. Therefore, **12** can be oxidized to uvaol (**13**) and UA, as well as lupeol (**8**) to betulin (**9**) and BA. Further C-2α hydroxylation of UA to corosolic acid, as well as OA to maslinic acid, is possible with CYP716C enzymes that are more substrate-specific in this case.[46]

Mechanistically, the cyclization pathway from the pre-folded oxidosqualene **6** in a chair-chair-chair conformation of rings A, B, and C leads to the tetracyclic dammarenyl cation (**14**, Scheme 2.4), which can perform an expansion of the D-ring by rearrangement to the baccharenyl cation (**15**).[47] **15** can form the lupenyl cation (**16**) with the five-membered E-ring, which can potentially deprotonate to yield lupeol (**8**) with the double bond as part of the isopropenyl group. **16** is further a precursor in the formation of amyrins, in which a rearrangement leads to the ring expansion of the E-ring, providing the germanicyl cation (**17**).[48]

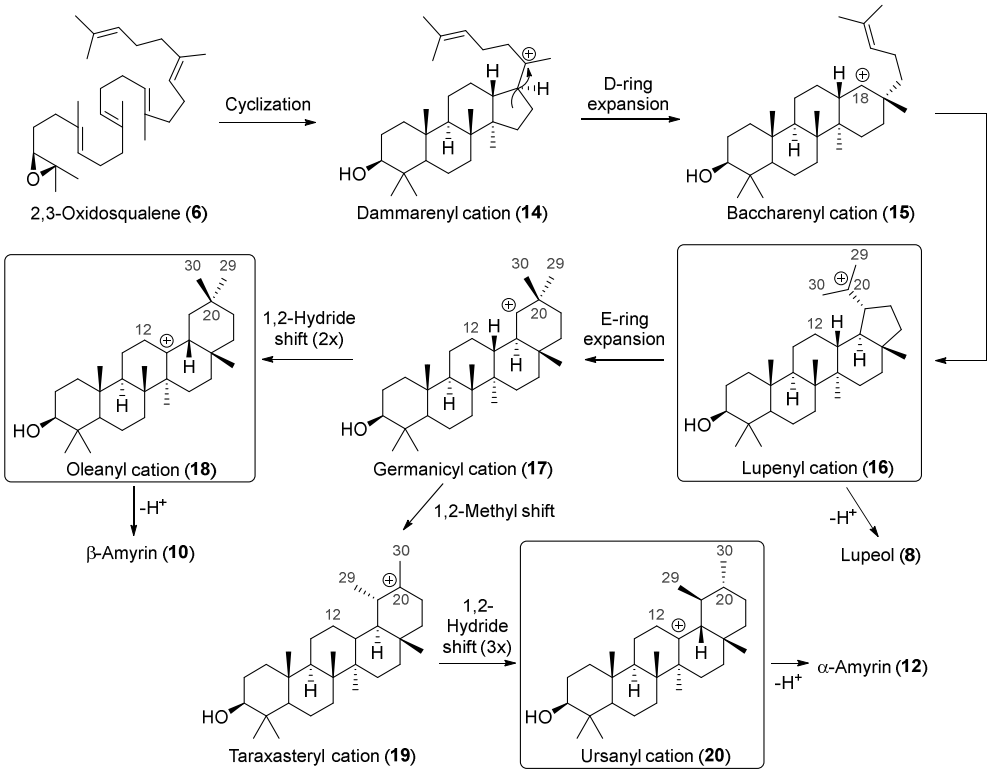

Scheme 2.4. Cationic intermediates in biosynthesis – via cyclization and Wagner-Meerwein rearrangements – followed by deprotonation, forming lupeol, β- and α-amyrin.[38]

17 might undergo 1,2-hydride shifts, yielding the tertiary oleanyl cation (**18**). Alternatively, a 1,2-methyl transfer generates the taraxasteryl cation (**19**), and subsequent 1,2-hydride shifts yield the tertiary ursanyl cation (**20**). Deprotonation of **18** and **20** at H-12 results in the corresponding amyrin structure (**10** or **12**).[47,48]

As lupeol and α/β-amyrin, BA, UA, and OA share structural high similarity and occur mostly in the cuticular wax, a hydrophobic layer covering the surface of the plant on the stem, leaf, flower, and fruit.[49] The cuticular wax includes an intracuticular layer embedded in the cutin matrix (based on a fatty acid-based polyester) and an epicuticular layer on the outer surface.[49] The wax consists of a complex mixture of straight-chain C_{20} to C_{60} aliphatic compounds (fatty acids, alcohols, esters, aldehydes, alkanes, ketones) and can include secondary metabolites such as triterpenoids.[50] The triterpenoid acids (TA) contribute to the plant's survival since they can protect the plant against dehydration and further against herbivores.[38]

TAs are frequent components of various plants with concentrations of maximal 2–3% of the dried weight, e.g., BA in plane tree bark, OA in olive leaves and UA in rosemary leaves, as shown in Table 2.1.[3] It should be noted that the TA content varies depending on the plant species and the specific plant part. The multifunctional mixed amyrin synthase is believed to contribute to the co-occurrence of OA and UA in plants.[51] In contrast, BA has a different distribution pattern and is more concentrated in bark.

Table 2.1. Distribution[3] of TAs in common plants

	Dried content in wt.%		
Plant part	**UA**	**OA**	**BA**
Birch bark	-	0.1-1.1	0.5-1.3 *
Eucalyptus leaves	1.17	0.31	0.84
Lavender leaves	1.59	0.45	0.13
Apple fruit peel	1.43	0.28	<0.10
Apple pomace	0.80	0.16	-
Lemon balm leaves	0.67	0.16	-
Olive leaves	0.18	3.10	-
Planes bark	-	<0.10	2.44
Rosemary leaves	2.95	1.23	1.53
Thyme leaves	0.94	0.37	-

*betulin has a significantly higher content than BA in birch bark of 10.5-18.3% [52]

TAs have diverse beneficial pharmacological activities like anti-inflammatory,[53] antibacterial,[54] anti-HIV,[55] and anticancer[56] activities. However, the low concentrations in

plants and the purification are hindering their commercial use.[39] The quantity of betulin can reach up to 30% dry weight of the white outer bark of birches, which is a byproduct from the forest industry.[57] Betulin can be extracted in large quantities by various methods, but it still remains an underutilized natural resource.[57] Another resource discovered for UA is apple pomace, a solid mixture of peel, seeds, and pulp, which is accumulated by the apple processing industry.[58] The total biomass availability of rosemary leaves with a higher content of UA is much lower compared to apple pomace. Since the pomace is available in substantial amounts, extraction and purification methods for UA have been developed.[59,60]

Regarding the production of olive oil, a large amount of olive leaves is discarded with a content of OA up to 3.1 wt%, offering a resource for extraction.[61] The pharmacological effects of OA are limited by its low water solubility and permeability; therefore, synthetic derivatives with increased therapeutic properties are of high interest.[62,63] Structural modifications can be made by C-28 esterification or amidation, C-3 esterification or etherification. Oxidizing the hydroxyl group at C-3 to a ketone is a key strategy to activate the C-2 position or alternatively form oximes from the ketone. The internal double bond allows further modification, e.g., oxidation to a ketone or allylic oxidation to an enone.[64]

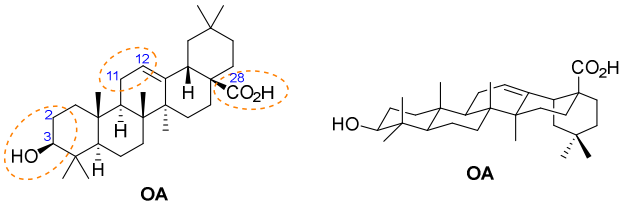

Figure 2.3. Modification sites of OA and its chair conformation.

2.4. Radical Polymerization

2.4.1. Free-Radical Polymerization (FRP)

Conventional FRP remains a widely utilized process for the commercial production of high molecular weight polymers due to its simplicity and scalability.[65] This is conditioned by a wide range of polymerizable monomers, possible solvents, different techniques, and tolerance of unprotected functional groups.[65] Nearly all compounds with C=C bonds can be either homopolymerized or copolymerized via radical polymerization[66] (e.g., terminal alkenes or dienes, vinyl electron-deficient compounds such as (meth)acrylates or halogenated species, styrene derivatives, or *N*-vinyl monomers). FRP has a tolerance for

trace impurities like stabilizers and is furthermore suitable for polar solvents like alcohols or water, providing a sustainable process.[67] Common materials produced by FRP are low-density PE, polystyrene, and poly(vinyl chloride).[68]

FRP follows a chain-growth process, where high molecular weight is reached in the early stages of conversion. It consists of initiation, propagation, termination, and transfer. Initiation starts with the generation of radicals from the initiator (diazo, peroxide, photolabile, organometallic, or redox systems), whereby these primary radicals react with the monomer. For thermal initiators, radical formation is much slower compared to the chain initiation, as can be seen by the rate constants in Scheme 2.5. In an ideal FRP, each formed initiator radical should produce a growing polymer chain. Therefore, a higher initiator concentration might lead to an increased rate of polymerization by consuming monomer faster, but simultaneously lead to shorter chains and vice versa.[67]

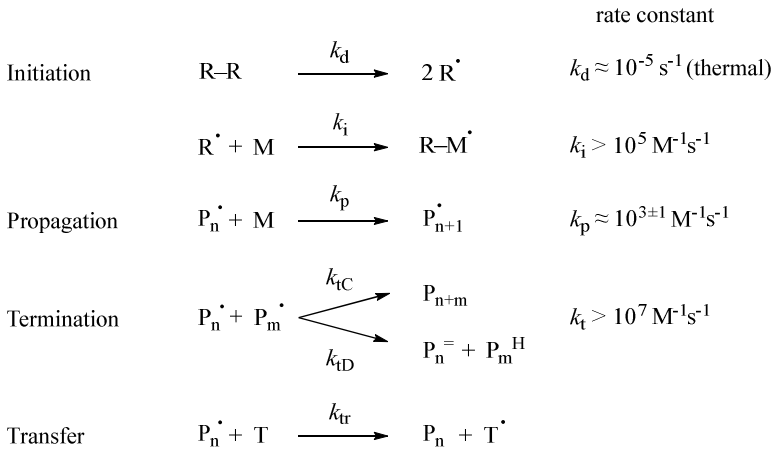

Scheme 2.5. Main mechanistic steps of free-radical polymerization (R–R : initiator, $P_n^{\bullet}$: radical of chain length n, T : chain transfer species, P_n : polymer).[67]

Chain propagation proceeds sequentially, adding monomer units roughly every millisecond, in most cases head-to-tail, where the less sterically hindered carbon atom gets attacked and forms the more stable radical.[67] In rare cases, head-to-head addition can occur, leading to structural irregularities.[67] The propagating carbon radicals are sp^2 hybridized, generally forming atactic polymers.[66] Furthermore, the propagation step is a reversible process determined by the Gibbs free energy ($\Delta G = \Delta H - T\,\Delta S$). The change in reaction enthalpy (ΔH) and entropy (ΔS) are both negative values for FRP; therefore, the ceiling temperature (T_c) of the monomer determines whether ΔG is negative and propagation is favored above depropagation.[69]

The lifetime of a radical is less than a second before termination.[66] Due to the minimal energy barrier for reactions between two radicals, termination in a polymerizing system is primarily determined by diffusion, meaning radicals terminate almost immediately upon collision with each other.[70] Growing radical chains can terminate head-to-head via combination or disproportionation, the latter one producing a polymer with a new terminal double bond and a saturated polymer chain via hydrogen abstraction. For example, the termination of methacrylate monomers mainly occurs by disproportionation, due to steric hindrance around the radical center.[71]

Chain transfer occurs between the growing chain and a nonradical species (T = monomer, polymer, solvent or chain transfer agents such as thiols), mainly by hydrogen abstraction in FRP, deactivating the growing chain and creating another radical species ($T^{\bullet}$) for reinitiation.[67] The transfer to a polymeric species can be either intermolecular, typically generating radicals near the chain end, or intramolecular (backbiting), leading to mid-chain radicals.[69] Both cases can result in branching or β-scission, depending on monomer type and temperature.

Dispersity in FRP can exceed 2.0, and M_n tends to decrease at high conversions (Figure 2.4, left) for several reasons. The monomer concentration decreases, and propagation slows down, contributing to the formation of shorter chains. Additionally, longer polymer chains diffuse more slowly, reducing the frequency of termination and chain transfer events become more significant. A control over the molecular structure (block copolymer, end-group functionality, precise chain-length) and the polymeric architecture is not possible in the conventional method, due to the short lifetime of radicals (< 1 s).[66] To minimize the unavoidable radical termination and enhance their lifetime, different methods of chain polymerization have been developed, belonging to the category of reversible-deactivation radical polymerizations (RDRP).[72] As shown in Figure 2.4 (right), this is achieved with the aid of control agents establishing a dynamic equilibrium between the propagating chain ($P_n^{\bullet}$) and dormant species (P_n-X), which are reversibly deactivated and cannot propagate or terminate.[73,74] RDRP allows a controlled polymerization with first-order kinetic behavior, pre-determinable molecular weight, and low dispersity, as well as the formation of block copolymers and polymer architectures.[73,74] A variety of RDRP techniques are available, including nitroxide-mediated polymerization (NMP), atom-transfer radical polymerization (ATRP), and reversible addition-fragmentation chain transfer (RAFT).

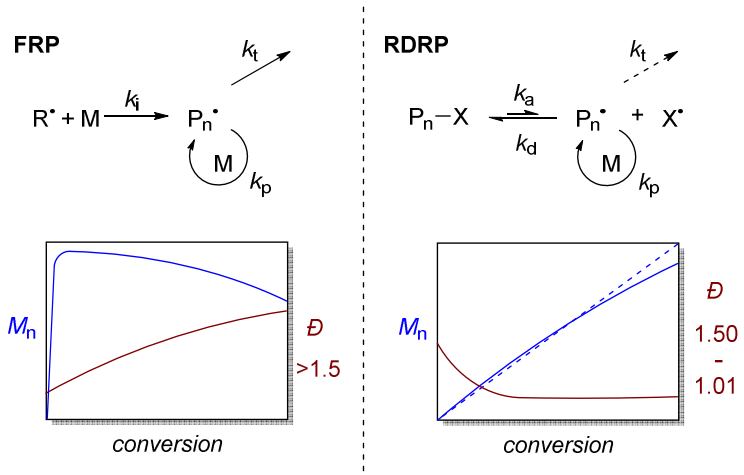

Figure 2.4. Principal pathway and molecular evolution of FRP and RDRP in comparison (curves of M_n and $Đ$ are a generalization and not accurate for specific polymerization systems).[73]

2.4.2. Reversible Addition-Fragmentation Chain Transfer (RAFT)

RAFT is one of the most robust and versatile RDRP techniques because of its ability to polymerize a broad range of monomer classes.[75] Key components are the chain-transfer agents (CTA), typical thiocarbonylthio compounds with a reactive C=S double bond, a radical stabilizing group Z, and a homolytic leaving group R.[76] The Z group further modifies the reactivity of the C=S bond. Importantly, the latter is more reactive to radical addition than the C=C bond of the monomer.[77] The lone electron pairs of sulfur facilitate a radical addition, while the attack on the carbon atom is prevented by an energy barrier.[78] The overall process can be seen as an insertion of monomers between the R- and the Z-CS_2-group, forming a polymeric macroRAFT agent with the corresponding α- and ω-end groups.[77]

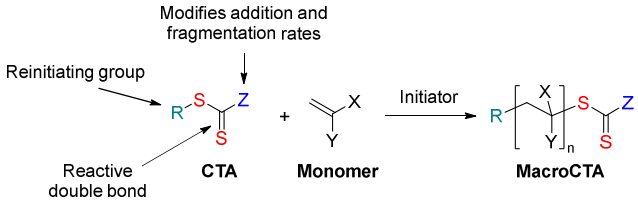

Scheme 2.6. Simplified RAFT polymerization reaction scheme with the chain-transfer agent (CTA).

RAFT requires a radical source to generate propagating radicals. Usually, a thermal initiator is used, leading possibly to the undesired formation of initiator-derived chain ends as terminating or chain-transfer events.[79] As illustrated in Scheme 2.7, a reversible chain transfer of the propagating chain to the CTA (also known as pre-equilibrium) should ideally

take place with a high chain transfer constant and a rapid formation of the macroRAFT agent (**22**).[76] This proceeds by radical addition to the sulfur atom of C=S, forming the carbon-centered radical intermediate **21**, which should favor the fast fragmentation via β-scission into **22** and the leaving radical (R•).[80] R• needs to efficiently reinitiate the polymerization with a rate greater than the propagation rate.[81] In the main equilibrium, a propagating chain (P_m•) adds to the macroRAFT agent **22**, forming the intermediate radical **23**, which fragments into **24** and P_n•. This process is described as a degenerative chain transfer, since the species retain the same reactivity on both sides of the equilibrium.[82] The population of dormant species (**22**, **24**) and the intermediate radical **23**, which is not reactive enough for the monomer, are much higher than the number of possible propagating radicals.[83] The rapid equilibrium between propagating chains and dormant species furthermore transfers the radical in such a way that all chains have the same probability to grow and ensure a simultaneous development.[84] The chain-transfer constant is higher than the rate of propagation and termination, meaning that across several activation/deactivation cycles the chain grows by one monomer while termination is avoided.[77,85] For ideal chain-transfer reactions, RAFT is supposed to have no influence on the rate of polymerization and should show similar kinetics to the conventional FRP.[86]

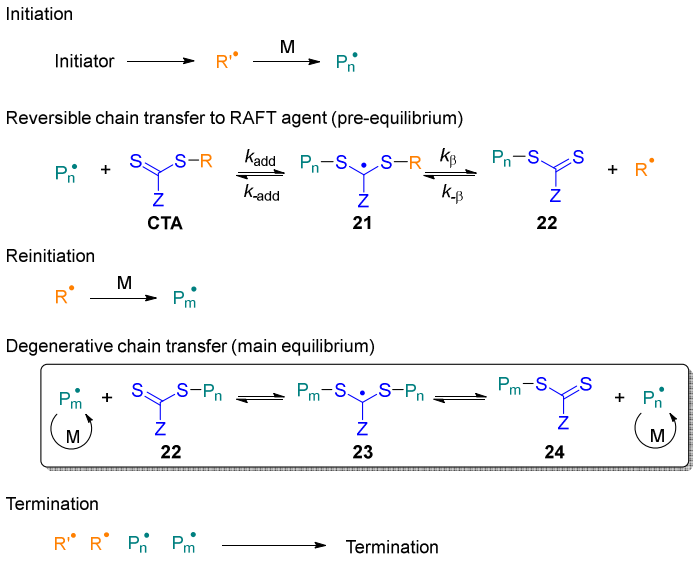

Scheme 2.7. Mechanistic steps of the RAFT polymerization.[77]

Vinyl monomers are divided into two groups regarding their reactivity for radical polymerization: more activated monomers (MAM) and less activated monomers (LAM). The first one includes butadiene, isoprene, styrene, (meth)acrylates, (meth)acrylamides, and acrylonitrile either activated by the electron-deficient double bond or by conjugation

lowering the activation energy.[77] In general, this high reactivity is reversed in the corresponding radical species, leading to more stabilized propagating radicals.[77,87] LAMs such as vinyl acetates, vinyl amides (*N*-vinylpyrrolidone), *N*-vinylimidazole, and *N*-vinylcarbazole have a double bond adjacent to a heteroatom, donating electron density by the mesomeric effect. Their corresponding radicals are unstable and highly reactive.[86,87]

CTAs can be dithioesters, trithiocarbonates, dithiocarbamates, and xanthates with different Z-groups to activate or deactivate towards radical addition. Hereby, the Z-substituent modifies the rate of addition as well as the fragmentation of the intermediate radical by a stabilizing or destabilizing effect.[86] Dithiobenzoates are the most used RAFT agents for methacrylates and methacrylamides, since they offer better control compared to other classes of CTAs.[88] They carry a high stabilizing Z-group, since the aromatic ring allows delocalization of the radical, leading to fast addition and slower fragmentation.[89] In the past, there were numerous investigations about the possible termination of the intermediate radical formed with dithiobenzoates and the resulting retardation in polymerization kinetics compared to FRP.[90,91] Konkolewicz and coworkers showed, that retardation is a phenomenon among all RAFT polymerizations systems, leading to a reduced polymerization rate with increasing CTA concentrations.[89,92]

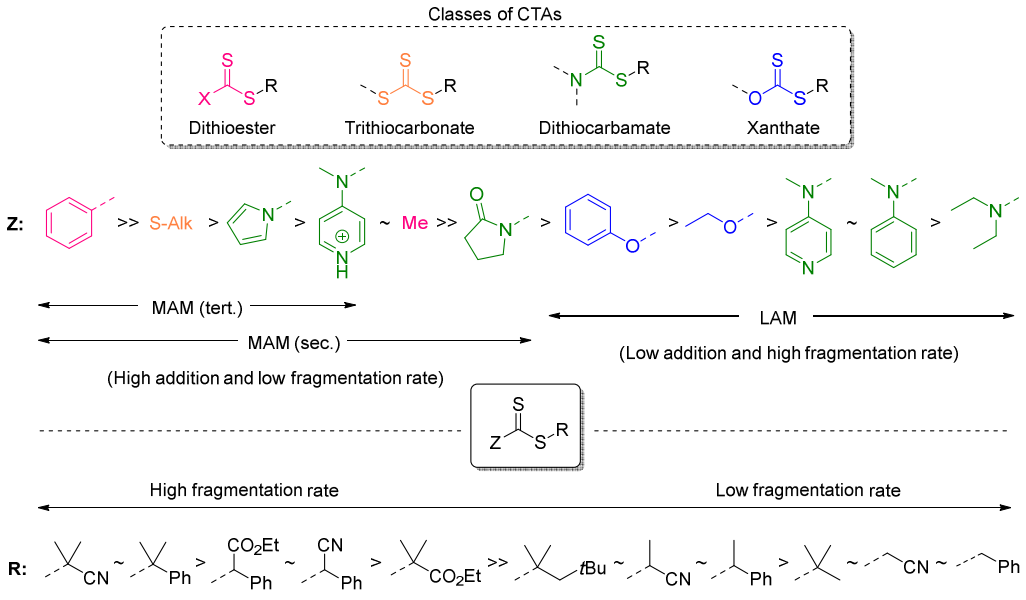

Scheme 2.8. RAFT agent classes with various Z- and R-groups.

Trithiocarbonates (TTC) are less active than dithiobenzoates, but still provide control over the polymerization of MAMs, since the sulfur in the Z-group does not allow a mesomeric effect with the C=S bond of the CTA. In contrast, N- and O-atoms in dithiocarbamates and

xanthates provide the mesomeric effect with the thiocarbonyl group and strongly deactivate the C=S bond towards radical addition, which is beneficial for less activated monomers.[77,78,86] Different dithiocarbamates, shown in Scheme 2.8, cover a wide range of reactivity, since the conjugation of the lone pair with the C=S bond can be influenced (pyrrole-, pyrrolidone-, *N*-(4-pyridinyl)-*N*-methyl-residues).[78,86]

Regarding the R-group of the CTA, the leaving ability and fast fragmentation need to be balanced with the ability to reinitiate the polymerization (R•), as these properties are conflicting. In general, the fragmentation rate increases with steric hindrance, by electron-withdrawing and radical-stabilizing groups.[80] 1,1-disubstituted monomers, creating stabilized tertiary propagating radicals, require R to be tertiary (2-cyano-2-propyl or cumyl) or a secondary cyanobenzyl residue to fragment efficiently.[93] However, tertiary radicals R• are inefficient in the reinitiation and can lead to an inhibition period for less-activated monomers that require R• to be secondary or primary.[86]

RAFT can be performed in heterogeneous media (emulsion, miniemulsion, dispersion) for the formation of homopolymers or block copolymers.[93] Further, RAFT can be used to create complex polymeric architecture like star, graft, branched, and network polymers on the basis of the thiocarbonylthio group, as illustrated in Figure 2.5.[92]

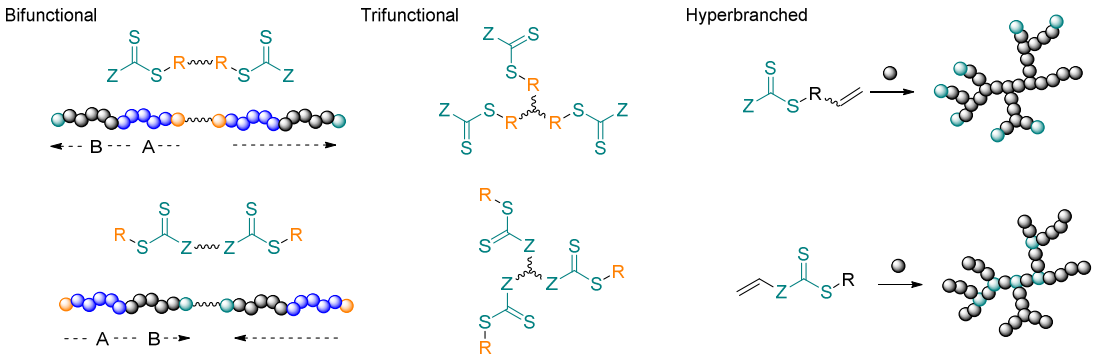

Figure 2.5. Schematic representation of the formation of complex polymeric architectures via the CTA.

The number of chains carrying the RAFT ω-end group defines the degree of livingness and is essential for the synthesis of block copolymers.[94] Thereby, the previously formed polymer serves as a macroCTA, and the polymer chain has to be a good leaving group (R•) compared to the new monomer, else homopolymerization of the second monomer can occur.[95] Termination cannot be fully avoided, since the number of dead chains arises from the amount of initiator decomposing during the polymerization.[94] To maintain a high livingness, polymerizations might be stopped at moderate conversions or the initiator

concentration is kept low at the cost of a decreased polymerization rate. In the latter case, it is possible to achieve full monomer conversion and high livingness by polymerizing monomers with a high propagation rate at high concentrations with a polar solvent facilitating the propagation.[96] Perrier and co-workers prepared different acrylamide block copolymers using a trithiocarbonate as CTA with up to 12 blocks by sequentially adding new aliquots of monomer and initiator (Figure 2.6, left).[97]

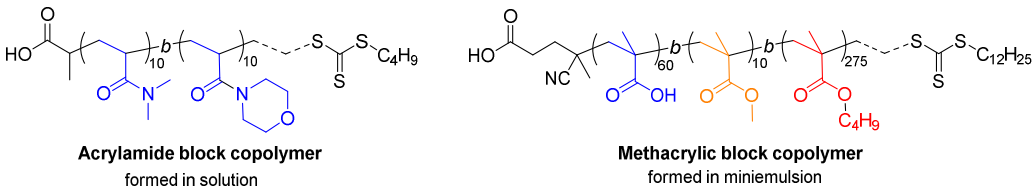

Figure 2.6. Multiblock copolymers by sequential RAFT polymerizations with acrylamides[97] (high propagation rate in solution) or by miniemulsion polymerization of methacrylates[98] starting from the amphiphilic PMAA-*b*-PMMA.

In contrast, multiblocks with low propagation rate monomers such as methacrylates cannot be formed in the same approach. Performing RAFT in miniemulsion leads to a physical separation of radicals (segregation effect), whereby termination is suppressed, and the local concentration of propagating radicals is higher, increasing the polymerization rate.[99] Zetterlund and coworkers synthesized a amphiphilic poly(methacrylic acid)-*b*-poly(methyl methacrylate)-TTC block copolymer, which aggregates in water.[98] Without the addition of new initiator, they could chain-extend the copolymer by different methacrylates diffusing into the micelle cores, forming a heptablock copolymer with each block having a high polymerization degree, high conversion, and livingness in short reaction time (Figure 2.6, right).[98]

Besides the traditional RAFT polymerization with a thermal initiator, novel activation strategies exist that can increase the livingness.[100] The CTA can be activated by a photo-mediated process, either by an additional photocatalyst in photo-electron/energy transfer (PET) RAFT polymerization or by direct interaction of the CTA with light in the photo-iniferter (PI) RAFT process.[101] In the latter, the CTA acts as an initiator, as well as a transfer and termination agent, whereby the initial bond cleavage and radical generation is triggered by a π–π* or n–π* transition by UV or visible light (Scheme 2.9).[95] The chain growth of the reactive carbon-based radical (R$^{\bullet}$) is controlled via the RAFT main equilibrium, while the thio-based persistent radical is preferentially reversibly deactivated by propagating radicals. Irreversible termination is reduced compared to the usage of thermal initiators and

the pre-equilibrium is circumvented, but photo-degradation of the CTA might occur.[101] Yet, the PI-RAFT polymerization of methacrylates is not fully controlled in the presence of dithioesters, as explained by their poor photoreactivity and the inefficient deactivation of the propagating radical by the persistent dithioester radical.[101]

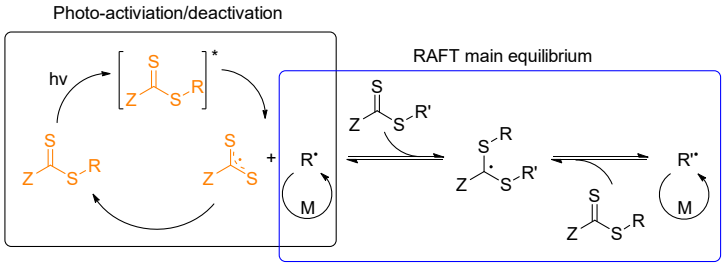

Scheme 2.9. PI-RAFT: photo-iniferter mechanism coupled with the main equilibrium.

2.5. Polyurethanes (PU)

PUs take a leading position in polymer materials because of their outstanding mechanical properties such as high elongation capacity, high resistance, as well as their thermal and chemical stability.[102] Their applications range from rigid and flexible foams to thermoplastics, thermosets, coatings, adhesives, and elastomers.[102] PUs carry the polar urethane group in their backbone, formed through the polyaddition of diol (or polyol) and diisocyanate (or polyisocyanate), as shown in Scheme 2.10. Polyols and polyisocyanates are multifunctional monomers ($f \geq 2$) that can lead to branching or even three-dimensional cross-linking ($f \geq 3$), whereby the latter results in thermoset formation.[103]

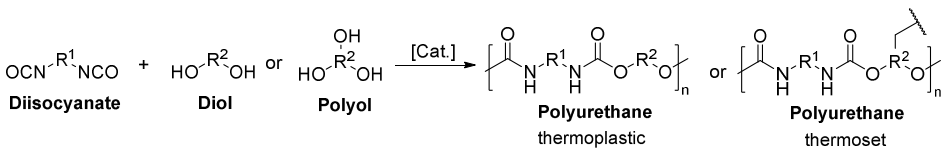

Scheme 2.10. Formation of thermoplastic or thermoset PUs via polyaddition (exemplarily shown with a diisocyanate and a di- or trifunctional alcohol).

PUs can be prepared in a one-step or two-step approach, whereby in the latter a prepolymer with a long-chain diol and an excess of NCO is formed, followed by the addition of a chain-extender, typically a low molecular weight (MW) diol, to promote further polyaddition.[103] For elasticity, segmented PUs with hard and soft segments are synthesized.[104] The soft segment typically consists of the long chain diol, while diisocyanate and chain-extender form hard segments. The mechanical properties can be varied by the phase separation of

these segments as well as the hydrogen bonding between the urethane bonds.[105] For flexible PUs, high MW polyols with a polyether, polyester, polycarbonate, or polyolefin backbone are used, while for rigid PUs low MW polyols with a high functionality are important.[106]

Diisocyanates are industrially produced by the gas-phase or, more commonly, by the liquid-phase phosgene method from the corresponding amines, despite the high toxicity of the gas.[107] Alternative synthesis routes on a small scale can be established by bis(trichloromethyl) carbonate (BTC, triphosgene), di-*tert*-butyl dicarbonate (Boc_2O), or the Curtius, Hofmann, and Lossen rearrangements (Scheme 2.11).[108] However, these pathways still include toxic or explosive reagents. Several other synthetic approaches exist, such as the reductive carbonylation of nitroaromatics with CO to yield isocyanates.[107,109] The formation of carbamates, for instance via the eco-friendly dimethyl carbonate (DMC) is attractive, since they can be decomposed into the corresponding isocyanates or transurethanization with diols can lead to PUs.[107,109]

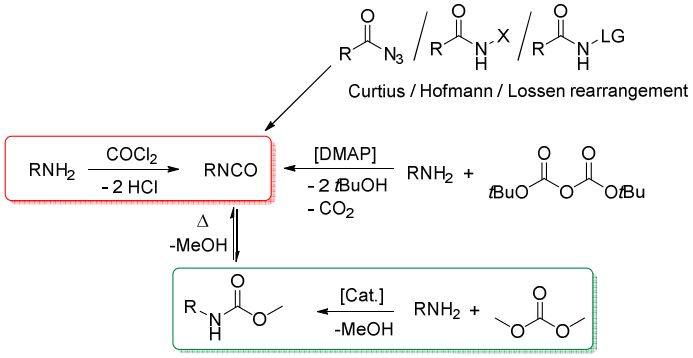

Scheme 2.11. Selected synthesis routes to isocyanates.

The most frequently used diisocyanates are the highly reactive aromatic methylene diphenyl diisocyanate (MDI) and toluene diisocyanate (TDI) to produce flexible or rigid foams, whereby the aromatic core is prone to photo-oxidation, leading to discoloration.[106] Important aliphatic compounds used for coatings are hexamethylene and pentamethylene diisocyanate (HDI, PDI), isophorone diisocyanate (IPDI), as well as 4,4′-dicyclohexylmethane diisocyanate (H_{12}MDI).[110]

The reactivity of isocyanates is not limited solely to amines and alcohols. Despite lower reaction rates, isocyanates in excess can react with urethanes or ureas, forming allophanates or biurets at high temperatures between 100–150 °C, potentially leading to crosslinking during PU synthesis (Scheme 2.12).[111] Uretdione is a dimerized species of (di)isocyanate, formed through a reversible reaction of two NCO groups cyclizing into a stable, blocked

structure, either at elevated temperatures or with a catalyst.[105] The trimerization of (di)isocyanates by a variety of catalysts leads to the six-membered isocyanurate ring, whereby these compounds are known for their exceptionally high thermal and chemical stability.[112] Allophanates, biurets, and isocyanurates are decreasing the NCO content as well as the toxicity and are used in coating raw materials, to create subsequently dense networks with polyols.[110]

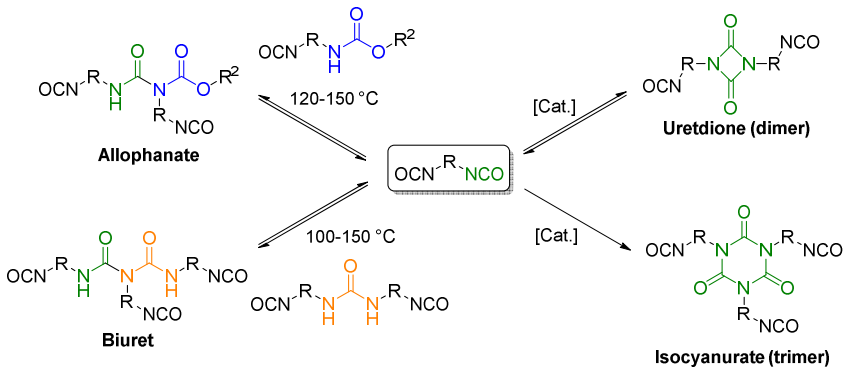

Scheme 2.12. Formation of polyisocyanates.

Since the use of petrochemical resources needs to be decreased, a variety of biobased polyols and diisocyanates were developed. In addition, due to the highly toxic phosgene, as well as the allergic and inflammatory reactions from isocyanates, research towards non-isocyanate polyurethanes (NIPUs) has intensified in the academic and industrial sectors.[113] One approach is the polyaddition of two functional cyclic carbonates with diamines to form linear poly(hydroxy urethanes) (PHU), carrying primary and secondary alcohols, as illustrated in Scheme 2.13. The insertion of CO_2 in epoxides allows the synthesis of a large variety of 5-membered cyclic carbonate monomers (5-CC), which have a high thermal and chemical stability in comparison to the polyisocyanates.[114] In contrast, relatively low reactivity arises from the low ring strain.[115] Side reactions occurring at high temperatures and hydrogen bonding by the additional hydroxyl function hinder the formation of high molecular weight PHUs.[116] Nevertheless, a wide range of PHUs from 5-CC were synthesized, showing their versatility and possible range of application as coatings,[117] adhesives,[118] or elastomers.[119] Sardon and coworkers[120] prepared an 8-membered cyclic carbonate from a diethanolamine, which has more ring strain and higher reactivity compared to 5- and 6-membered cyclic carbonates. As a bifunctional monomer, it can yield high molecular weight PHUs ($M_n \geq 20$ kg/mol) by polyaddition with primary diamines at ambient temperatures.

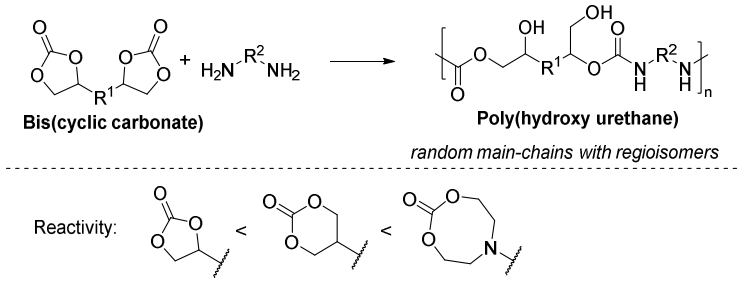

Scheme 2.13. Polyaddition of bis(cyclic carbonate)s with diamines yielding NIPUs.

Further, NIPUs can be formed by polycondensation. That is either possible by transurethanization of bis(alkyl) bis(carbamate)s with a diol or by the reaction of an electron-deficient bis(carbonate) with a diamine (Scheme 2.14). Normally, the polymerization by transurethanization requires high temperatures in the presence of organic bases or metal-based catalysts.[121] The group of Burel[122] transformed aliphatic diamines (C6 or C10) into the corresponding methyl carbamates with DMC and could subsequently prepare NIPU elastomers in bulk polycondensation (140 °C, TBD catalysis) with PEG and 1,4-butanediol, forming soft and hard segments, respectively.

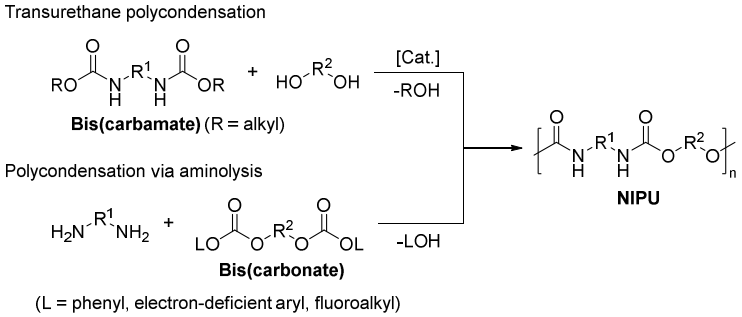

Scheme 2.14. Synthetic pathways for NIPUs by polycondensation.

The group of Tsuda[121] synthesized bis(fluoroalkyl) bis(carbonate)s that increase the electrophilicity of the carbonyl group and the leaving ability of the corresponding alcohol. By polycondensation with various aliphatic diamines, they could achieve high MW polymers in solvent or solvent-free conditions without a catalyst. Varela and coworkers[123] showed the polycondensation of diamines with a D-mannitol-derived 1,6-bis(phenyl carbonate) in solution, facilitated by the base *N*,*N*-diisopropylethylamine (DIPEA), which neutralized the phenol by-product. Since isocyanates and cyclic carbonates are not stable in aqueous solutions, the polymerizations are to that extent limited. Pentafluorophenyl carbonates are highly electrophilic but do not hydrolyze under neutral conditions, allowing those difunctional monomers to react with PEG-based diamines and form water-soluble NIPUs in aqueous media.[124]

PU foams, accounting for 60% of the PU products, are traditionally produced by exploiting the reaction of isocyanate with water, whereby the resulting carbamic acid decomposes into CO_2 and amine, forming additional urea linkages.[125] For the synthesis of NIPU foams, physical or chemical blowing agents are required – for instance, hydrofluorocarbons[126] evaporating or $NaHCO_3$ [127] decomposing at 150 °C and releasing CO_2. The group of Detrembleur[128] produced water-induced self-blown foams by the polyaddition of trimethylpropanol tricyclocarbonate (TMPTC) and diamines (Scheme 2.15). Hereby the trifunctional carbonate is partially hydrolyzed under DBU catalysis, producing CO_2 and vicinal diols that are not further involved in cross-linking.

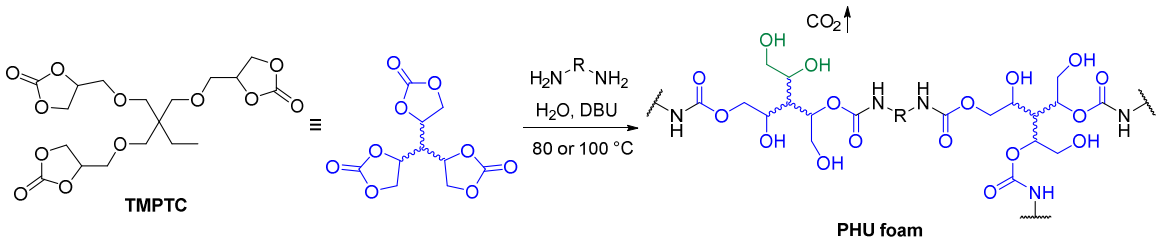

Scheme 2.15. Water-induced self-blown PHU foam on the basis of TMPTC.[128]

2.6. Polycarbonates (PC)

Poly(bisphenol A carbonate) (BPA-PC) has applications in electronics, vehicles, building materials, medical devices, and protective equipment owing to its outstanding properties, including transparency, thermal stability, mechanical strength, and flame resistance.[129] The conventional industrial production of polycarbonate relies on the interfacial phosgene process, in which BPA is deprotonated by aqueous sodium hydroxide and reacts at the water-organic interface with phosgene dissolved in dichloromethane (Scheme 2.16).[130] Hereby, the phosgene does not undergo rapid hydrolysis. An alternative industrial method involves the catalyzed transesterification of BPA with diphenyl carbonate (DPC) in the molten state via a two-step process, carried out under a gradually increasing temperature and decreasing pressure, removing the by-product phenol.[131]

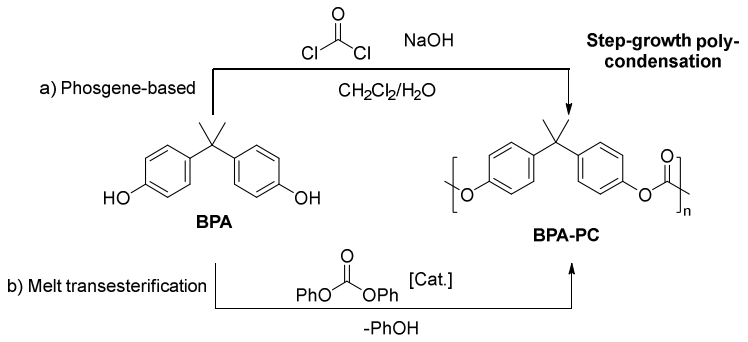

Scheme 2.16. Industrial production of BPA-PC by phosgene (a) or melt transesterification using DPC (b) via polycondensation.

DPC and DMC, both derived from CO_2, can replace phosgene as a carbonyl source.[132] DPC can be formed by transesterification of DMC with phenol. Since the catalytic synthesis of DMC from methanol and CO_2 with the aid of dehydrating agents is actively being researched, it appears to be the more promising reactant for polycarbonate production.[133] However, obtaining high molecular weight BPA-PC with DMC is challenging due to its low boiling point and the inefficient transesterification between the phenolic hydroxyl group and the methyl carbonate group, which is hindered by the poor leaving ability and high basicity of methoxide compared to phenoxide.[132,134] Alternative synthetic procedures of the aromatic polycarbonate arise from *in situ* generated $COCl_2$, either by decomposition of triphosgene or by the UV-irradiation of $CHCl_3$ under O_2 in the concept of the interfacial polycondensation (photo-on-demand phosgenation).[135]

Growing concerns about the release of hormonally active BPA from food-contact materials, either through the diffusion of residual monomers or the hydrolysis of polycarbonate, have driven the search for alternative materials.[136] Most of the aliphatic polycarbonates (aPC), in contrast to BPA-PC, have relatively low thermomechanical properties, limiting their industrial applications in the past and were therefore used as low-molecular-weight macrodiols in polyurethanes.[137,138] In recent years, aPCs have become a promising class of materials since they are biodegradable, biocompatible, as well as non-toxic, and can be obtained using renewable resources via phosgene-free synthesis.[139] They can be degraded into carbon dioxide and neutral diols by microorganisms.[140] High-molecular-weight polycarbonates, such as poly(1,4-butylene carbonate) (PBC) and poly(hexamethylene carbonate) (PHC), can be synthesized via the catalyzed melt polycondensation with DMC. These materials exhibit high tensile strength and elongation at break, presenting valuable

opportunities for use as biodegradable plastics.[140] To alter the thermomechanical properties, copolymers can be formed by mixing different diols for the polymerization.

The sugar-derived isosorbide is a rigid, renewable building block extensively studied for polyesters, polyurethanes, and polycarbonates.[141] Isosorbide has a low melting point suitable for the DMC-based melt polycondensation with strong alkali metal bases[142] or ionic liquids[143] as catalysts, yielding a polycarbonate with high thermal stability and elevated glass-transition temperature (T_g), rendering it a candidate to replace BPA-PC (Scheme 2.17). The catalysts can lower the difference in reactivity between the *exo*- and *endo*-OH of isosorbide and further inhibit the methylation side reaction of DMC, forming methyl ether end-groups that are inactive for the polycondensation.[143]

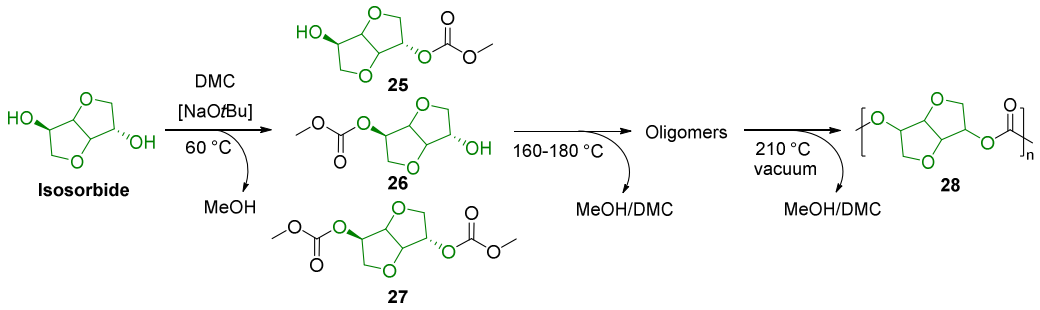

Scheme 2.17. Poly(isosorbide carbonate) (**28**) synthesized via melt polycondensation.

Other polymerization techniques for aPCs exist, like ring-opening polymerization (ROP) of cyclic carbonates, alternating copolymerization of epoxides or oxetanes with CO_2 or the direct polycondensation with CO_2, as illustrated in Scheme 2.18.

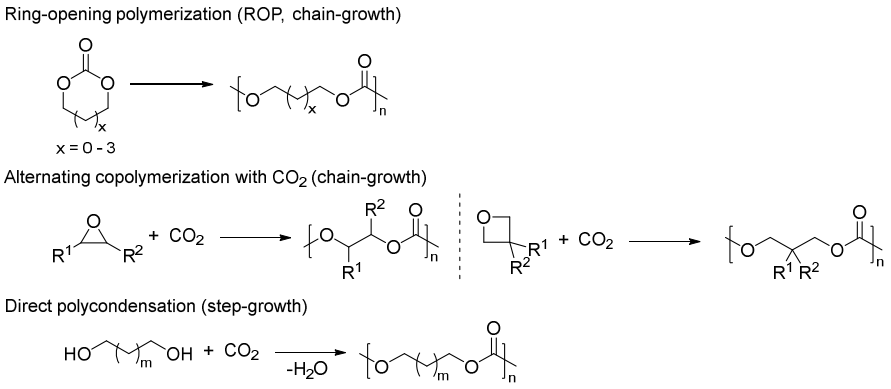

Scheme 2.18. Synthetic methods for polycarbonates via ROP, alternating copolymerization, or direct polycondensation.

ROP of cyclic carbonates can be performed through cationic, anionic, coordination-insertion (metal-based), organocatalytic, and enzymatic methods.[137] It is an outstanding method for the introduction of functional groups into the polycarbonate backbone.[144] In

general, 6–8 membered cyclic carbonates are more prone to polymerization in comparison with the 5-membered species, since they provide higher ring strain,[144] likely due to deviations from the ideal planar geometry of the carbonate group. ROP of monocyclic trimethylene carbonate (TMC) derivatives results in aPCs with low T_g values.[145] In contrast, cyclic carbonates formed from sugars like glucose[145] or D-mannose[146] show elevated T_g values arising from the cyclic sugar structure in the main chain. Buchard and coworkers[146] prepared **29** in a three-step synthesis starting from 1-O-methyl-α-D-mannose, whereby **29** could be polymerized using organocatalytic ROP with TBD and 4-methylbenzyl alcohol as initiator, whereby the chain length could be controlled in the living polymerization by the monomer to initiator ratio (Scheme 2.19).

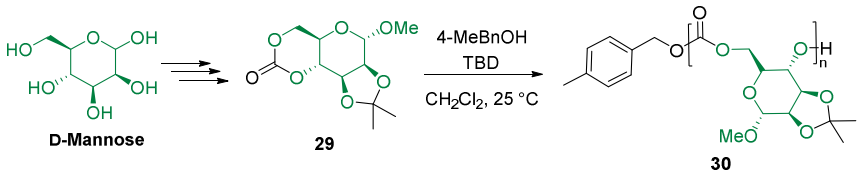

Scheme 2.19. Organocatalytic ROP of protected and functionalized monomer **29** derived from D-mannose.[146]

An alternative route for the synthesis of aPCs is the reaction of epoxides with CO_2, which follows a coordination-insertion polymerization mechanism. It is initiated by the opening of the epoxide by a metal catalyst, followed by CO_2 insertion into the metal-oxygen bond, creating a carbonate linkage.[147] Undesired side reactions can be reduced by certain catalysts, in particular the successive epoxide opening without CO_2 insertion, which leads to a polyether backbone, or intramolecular back-biting reactions that cause the loss of cyclic carbonate from the growing polymer chain.[147] Monomers can be classified as terminal epoxides (e.g., propylene oxide, styrene oxide) and internal epoxides (e.g., cyclohexene oxide, limonene oxide, indene oxide).[148] Regioselective catalysts promote head-to-tail incorporation of terminal epoxides, whereas uncontrolled polymerization yields a mixture due to ring-opening at either the methylene or methine carbon.[148] Limonene is one of the most frequently occurring natural monoterpenes, mainly extracted from the peel of citrus fruits.[148] Greiner and coworkers[149] managed to form a mixture rich in *trans*-limonene oxide (**31**) from (*R*)-limonene via the corresponding bromohydrin, following alkaline epoxide formation and further purification (Scheme 2.20). The utilized β-diiminate zinc catalyst (BDI)Zn(OAc) is selective for the *trans*-isomer **31** and allows the alternating polymerization with CO_2, yielding poly(limonene carbonate) (**32**) with low dispersity, as well as high transparency and hardness, rendering it a promising green coating material.[149]

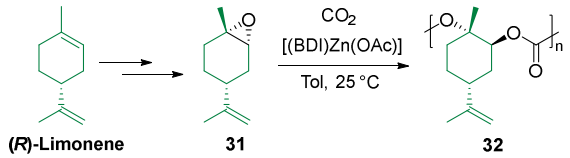

Scheme 2.20. Alternating copolymerization of *trans*-limonene oxide (**31**) and CO_2.[149]

2.7. Betulin-Based Polymers

Betulin, a triterpenoid structurally similar to erythrodiol, has already been used as a building block for various polymeric materials, as will be shown in the following (Scheme 2.21). The group of Zhu[150] synthesized betulin-based methacrylate **33** via esterification with methacrylic anhydride and subsequently prepared both random and block copolymers with a galactose-based methacrylate through thermal RAFT polymerization, using a trithiocarbonate as CTA. Both copolymers had a low content of **33** (3–6%) and could form micelles in water by self-assembly.

Weber and coworkers[151] synthesized a microporous polyurethane network (**34**) via the polyaddition of betulin with triphenylmethane triisocyanate. Furthermore, mixtures of betulin and castor oil (a triglyceride rich in ricinoleic acid) could be polymerized with TDI by the group of Chen[57], yielding PUs with reduced crosslinking density due to betulin and thereby resulting in elastomeric properties.

Betulin-based polyesters **35** were formed by the group of Stanzione[152] by tin-catalyzed melt polycondensation with linear aliphatic diacids. Polyesters with a comparable structural backbone could be obtained from Tabata and coworkers[153] by polycondensation of betulin with aliphatic acid dichlorides in the presence of pyridine. As a final example, polyolefins based on betulin were prepared by the group of Zhu[154]. They synthesized α,ω-diene monomers **36** by Steglich esterification of betulin with either 4-pentenoic acid or 10-undecenoic acid, followed by polymerization through acyclic diene metathesis (ADMET).

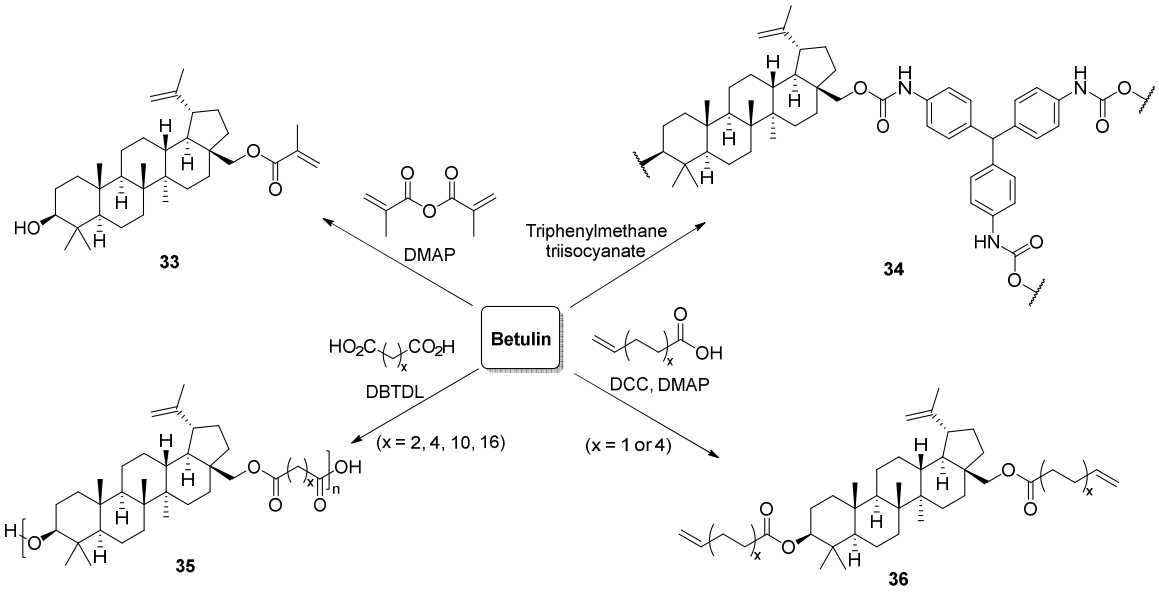

Scheme 2.21. Betulin-based monomers (methacrylate **33**, α,ω-diene **36**) and polymers (polyurethane **34**, polyester **35**).

3. Oleanolic Acid-Derived High-Glass-Transition-Temperature Methacrylic Polymers

Four new monomers based on the naturally occurring pentacyclic triterpenoid oleanolic acid (OA) were synthesized by introducing a methacrylate group at either the hydroxyl or the carboxylic acid positions. After establishing their (in)solubility in a range of solvents, three monomers could notably be polymerized in the green solvent *N*-butyl-2-pyrrolidone (NBP), in which soluble polymers were obtained. Dithiobenzoate-mediated radical polymerization of all four monomers led to polymethacrylates with theoretical number-average molecular weights (M_n) of up to 45 kg/mol and single-detection size-exclusion chromatography M_n values of up to 24 kg/mol. The purified polymers show thermal stabilities in the range of 300–350 °C and high glass-transition temperatures, up to 220 °C.

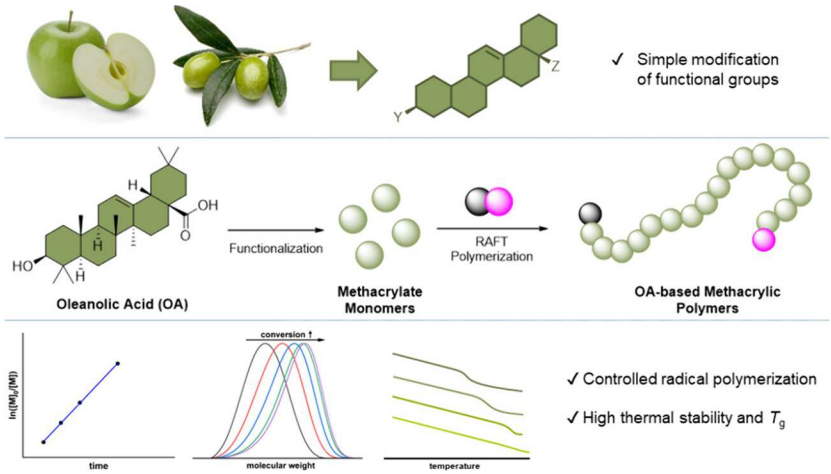

Reprinted (adapted) with permission from: Jessewitsch, T.; Saou, N.; Steinlein, L.; Bensberg, K.; Kirsch, S. F.; Delaittre, G. Oleanolic Acid-Derived High-Glass-Transition-Temperature Methacrylic Polymers. *ACS Sustainable Chem. Eng.* **2024**, *12* (52), 18499–18507. Copyright 2024 American Chemical Society.

Author contributions: T.J., N.S., and L.S. synthesized all monomers except M3 and carried out all polymer reactions and most characterizations. K.B. synthesized M3. S.F.K. contributed ideas and supervision on small-molecule synthesis. G.D. originated the concept and supervised the polymer synthesis and characterization. T.J. and G.D. wrote the manuscript, with all co-authors providing input.

3.1. Introduction

Cyclic triterpenoids consist of six rearranged isoprene units, resulting in a rigid structural skeleton of 30 carbon atoms. They are synthesized in plants by cyclization of squalene[155] and serve as nonessential plant metabolites,[156] allowing them to be competitive in their environment.[157] More than 20 thousand triterpenoids are known to occur in medicinal plants, reflecting their large diversity. Pentacyclic triterpenoids derived from oleanane, ursane, and lupane structures show unique pharmacological activities[156] such as anti-microbial,[158] anti-inflammatory,[159] and anticancer effects.[160] The related hydroxy acid derivative oleanolic acid (3β-hydroxyolean-12-en-28-oic acid, OA) can be found in more than 1600 plant species, including fruits, leaves, and even olive oil.[161,162] Despite its antitumor and anti-inflammatory properties,[162,163] the pharmaceutical use of OA is limited by its low aqueous solubility (< 1 µg/mL) and low bioavailability.[164] An alternative valorization of OA in materials science would therefore appear reasonable. With the aim of more sustainable production and fate of materials, renewable feedstocks are key components, although their implementation in synthetic materials has so far been limited by complexity and efficiency in their production.[152,165,166] The target is thereby to synthesize bioderived plastics having good processability and fulfilling material property requirements such as mechanical stiffness or high glass-transition temperatures (T_g) for amorphous polymers.[167–169] Importantly, one approach to achieve high-T_g polymers is to incorporate rigid components into the polymer structure.[168]

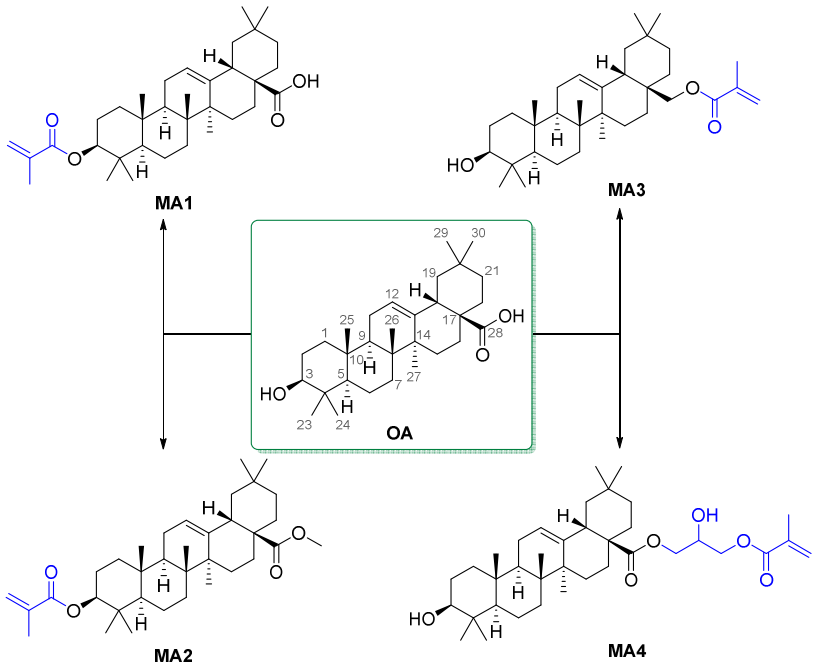

Scheme 3.1. Oleanolic acid (OA) and the corresponding methacrylates **MA1**–**4** reported in this study.

In the present work, we combine the chiral, rigid structure of OA with a methacrylate moiety to obtain four different monomers, **MA1**–**4**, as displayed in Scheme 3.1. Biobased (meth)acrylates are currently important targets in the academic realm[170,171] as well as in the industry.[172–174] The reversible addition−fragmentation chain-transfer (RAFT) polymerization of **MA1**–**4** yielded new biobased polymers with tunable molar masses, moderate dispersities, as well as high thermal stability and high T_g.

3.2. Results and Discussion

3.2.1. Monomer Synthesis

Monomers **MA1**–**4** were obtained in one- to five-step syntheses, which are disclosed in Scheme 3.2 (see also experimental procedures in Section 3.4). The methacrylate functionality, which is amenable to radical polymerization, was incorporated via either the native hydroxyl group (**MA1** and **MA2**) or the reduced or native carboxyl function (**MA3** and **MA4**, respectively).

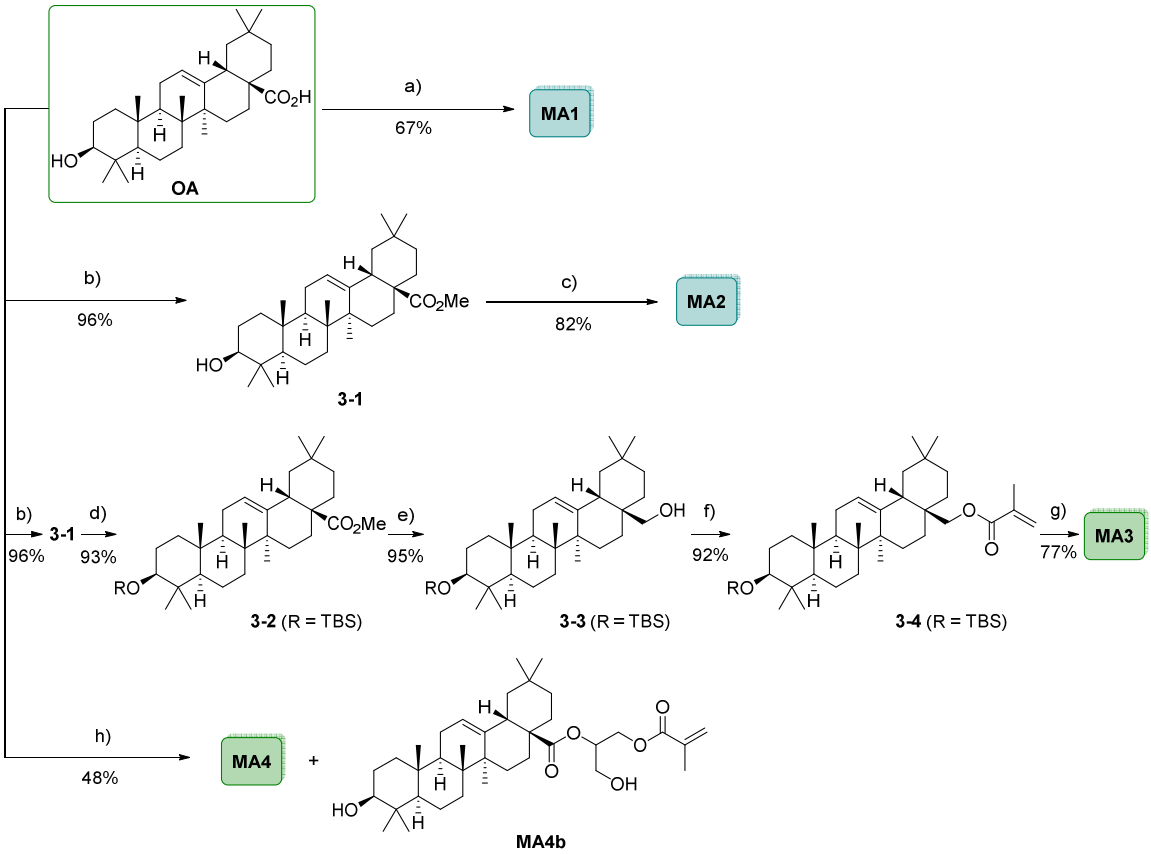

Scheme 3.2. Synthesis of **MA1–4**. (a) Methacrylic anhydride, DMAP, NEt_3, THF, 0 °C to rt, 16 h. (b) MeI, K_2CO_3, DMAc, rt, 16 h. (c) MAC, NEt_3, DCM, 0 °C to rt, 16 h. (d) TBSOTf, 2,6-lutidine, DCM, 0 °C, 3 h. (e) DIBAL-H, DCM, −78 °C, 2 h. (f) MAC, NEt_3, DMF, 0 °C to rt, 16 h. (g) *p*TsOH·H_2O, DCM/MeOH, 40 °C, 5 h. (h) GMA, K_2CO_3, 4-methoxyphenol, DMAc, 80 °C, 8 h.

MA1 was synthesized by simple esterification with methacrylic anhydride and 4-(dimethylamino)pyridine (DMAP) (Scheme 3.2a). In our hands, the previously reported reaction of OA with methacryloyl chloride (MAC)[159] yielded the mixed methacrylic anhydride **MA1′**, which could not be subsequently polymerized in a controlled manner (see following paragraph on polymerization kinetics and Figure S3.2). The synthesis of **MA2** does not pose the same issue because the free carboxylic acid is first converted to oleanolic acid methyl ester (**3-1**) by using methyl iodide (Scheme 3.2b). **MA3** is prepared in five steps with an overall yield of 60%, whereby each of the first four modifications could be established with independent yields of at least 92%. First, **3-1** is synthesized to allow the reduction with diisobutylaluminum hydride (DIBAL-H) in the following steps. Subsequently, the hydroxyl group is protected by reacting with *tert*-butyldimethylsilyl trifluoromethanesulfonate (TBSOTf) in the presence of 2,6-lutidine, providing compound **3-2** (Scheme 3.2d). Lithium aluminum hydride ($LiAlH_4$) could reduce the carboxylic acid without the requirement of esterification, but this approach would cleave the protecting group required for further steps. Instead, methyl ester **3-2** is then directly reduced to the corresponding primary alcohol **3-3** with excess DIBAL-H at −78 °C (Scheme 3.2e). Thanks to the previous silyl ether protection, an esterification to **3-4** was accessible with high yield using MAC (Scheme 3.2f). Lastly, the silyl ether protecting group was removed in mild acidic conditions with *p*-toluenesulfonic acid (*p*TsOH), providing monomer **MA3** (Scheme 3.2g). During our investigations, we noted that tetrabutylammonium fluoride would not only cleave the silylether but also the ester of the targeted methacrylate. With *p*TsOH, the latter could be preserved using mild heating and a short reaction time. Introducing a methacrylate moiety at the carboxyl site of OA was further possible in a one-step reaction using glycidyl methacrylate (GMA) and the radical inhibitor 4-methoxyphenol (Scheme 3.2h). The ring-opening of the epoxide by the carboxylate is not regiospecific and leads to a binary mixture of linear and branched isomers (**MA4** and **MA4b**, respectively), the former being the major product.[175] In this study, the major isomer **MA4** was isolated and further examined.

Subsequently, the solubility of the new monomers in a range of solvents with various polarities[176] was established (Table 3.1). The OA-based methacrylates are practically insoluble in very polar solvents such as methanol and ethanol, as well as in nonpolar solvents like toluene or cyclohexane. DMAc, which is the eluent for one of our size-

exclusion chromatography (SEC) systems, sufficiently solubilizes **MA1** and **MA4**, but not **MA2** and **MA3**. Importantly, **MA1**, **MA3**, and **MA4** are soluble in NBP at ambient temperature up to at least 0.3 mol/L. NBP is a polar aprotic green solvent that is structurally related to *N*-methyl-2-pyrrolidone (NMP) and shows similar characteristics. Yet, as opposed to NMP, it is nonmutagenic, nonreprotoxic, and biodegradable and is proposed as a future universal replacement for DMF.[176,177] It was also recently shown as one of the green solvents with the lowest impact values for solvent emission.[178] Therefore, whenever possible, it was employed in the present study. Counterintuitively, the solubility of the methyl ester-based **MA2** decreases compared to the free carboxylic acid **MA1** and further investigations, such as polymerization kinetics, could only be performed in 1,1,2,2-tetrachloroethane (TeCA).

Table 3.1. Solubility of **MA1**–**4** in solvents of increasing polarity (from top to bottom) at room temperature (0.3 mol/L)[a]

Solvent	Polarity	Non-toxic	MA1	MA2	MA3	MA4
Toluene	0.10	✓	x	x	x	x
1,4-Dioxane	0.16	x	x	x	x	x
Ph-Cl	0.19	x	x	x	x	x
Anisole	0.20	✓	x	x	x	x
TeCA	0.26	x	✓	✓	✓	✓
PC	0.30	✓	x	x	x	x
CPME	0.31	✓	x	x	x	x
NBP	0.32	✓	✓	x	✓	✓
DMAc	0.38	x	✓	x	x	✓
DMSO	0.44	✓	x	x	x	✓

[a] Ph-Cl = chlorobenzene; TeCA = 1,1,2,2-tetrachloroethane; PC = propylene carbonate, CPME= cyclopentyl methyl ether; NBP = *N*-butyl-2-pyrrolidone; DMAc = *N*,*N*-dimethylacetamide; DMSO = dimethyl sulfoxide.

3.2.2. Polymerization Kinetics

The enhanced stability of methacrylate monomers leads to a reduced reactivity in radical polymerization.[86] Therefore, for efficient RAFT polymerization, a dithiobenzoate as a member of one of the most active chain-transfer agent classes was chosen, namely 2-cyano-2-propyl benzodithioate (CPBD), in combination with azobis(isobutyronitrile) (AIBN) as thermal initiator. A ternary ratio [MA]:[CPBD]:[AIBN] = 200/4/1 was set as standard conditions, resulting in a targeted degree of polymerization (DP) of 50 at full conversion. While **MA1** and **MA4** could be polymerized in a classical solvent such as DMAc, considering environmental aspects, we chose to focus on NBP whenever possible. The

polymerizations were therefore conducted at 70 °C in either NBP (**MA1**, **MA3**, and **MA4**) or TeCA (**MA2**), at a concentration of 0.3 M. Besides the methacrylates, the peculiar – and initially not targeted – mixed anhydride **MA1′** could be polymerized, up to ca. 90% in DMAc and ca. 80% in NBP after 15 and 24 h, respectively (Figure S3.2). However, SEC analysis during the polymerization in the presence of CPBD showed no evolution in molecular weight with time. Various M_n values could still be reached by varying the stoichiometry. Note that such mixed methacrylic anhydrides are rare and that the closest polymerized derivative that has been reported is possibly itaconic anhydride, yet under RAFT conditions only in copolymerization.[179,180]

MA1 possessing the methacrylate ester at the C-3 position together with the unmodified carboxylic acid underwent a controlled polymerization, reaching a conversion of 81% after 7 h (Figure 3.1A). The semilogarithmic plot of conversion (Figure 3.1B) suggests a pseudo-first-order reaction with a constant radical concentration. The molecular weight distributions determined by SEC with DMAc as eluent are displayed in Figure 3.1C and

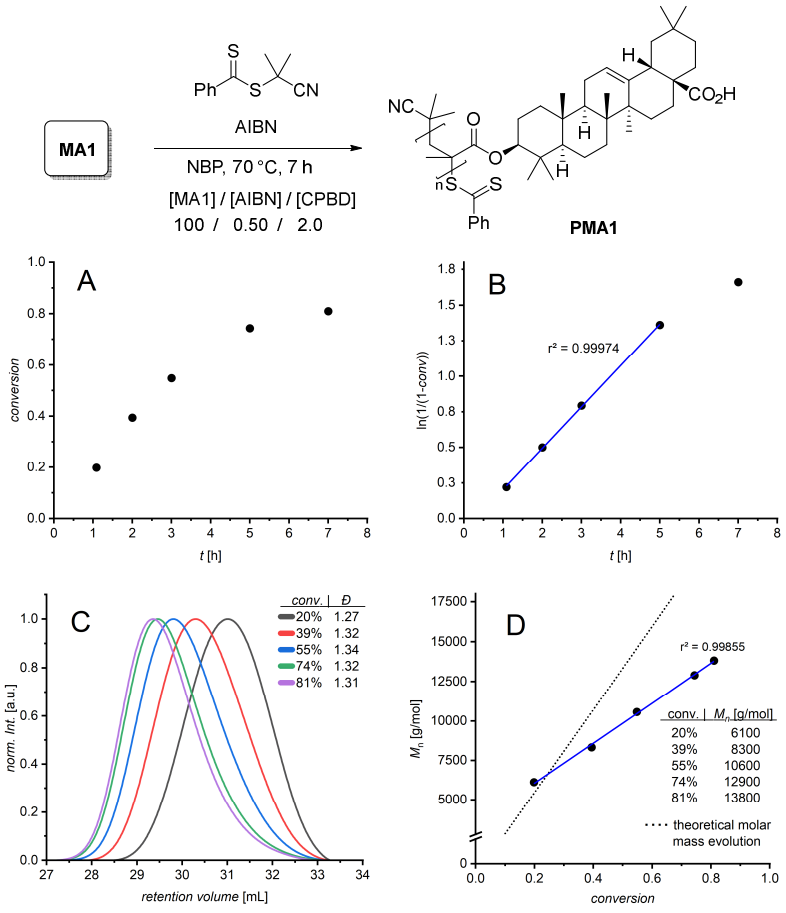

Figure 3.1. Kinetic and macromolecular data for the CPBD-mediated radical polymerization of **MA1** in NBP at 70 °C in standard conditions (A: monomer conversion vs. time; B: semi-logarithmic kinetic plot; C: SEC traces at various conversions, D: M_n evolution with conversion).

appear to quantitatively shift with increasing reaction time, with dispersity barely fluctuating. Figure 3.1D confirms the controlled character of the chain growth with an excellent correlation between the number-average molar masses (derived from a PMMA calibration) and the monomer conversion values. M_n values are nevertheless lower than expected, which is ascribed to the poor match between the hydrodynamic behaviors of the PMMA standards and polymers of **MA1**. This observation is valid for all further polymers.

As mentioned earlier, TeCA is the only suitable solvent for **MA2** to set up the reaction at a reasonable concentration of ca. 10 wt% (0.3 mol/L) at ambient temperature. The polymerization of **MA2** in this less polar solvent is, as expected, significantly slower and could only reach about 60% in 16 h (Figure 3.2A), yet proceeding with first-order kinetics (Figure 3.2B). Polymers of **MA2** could not be sufficiently well dissolved in DMAc. Therefore, SEC was performed in THF (calibrated with polystyrene standards), revealing good control (Figure 3.2, C and D).

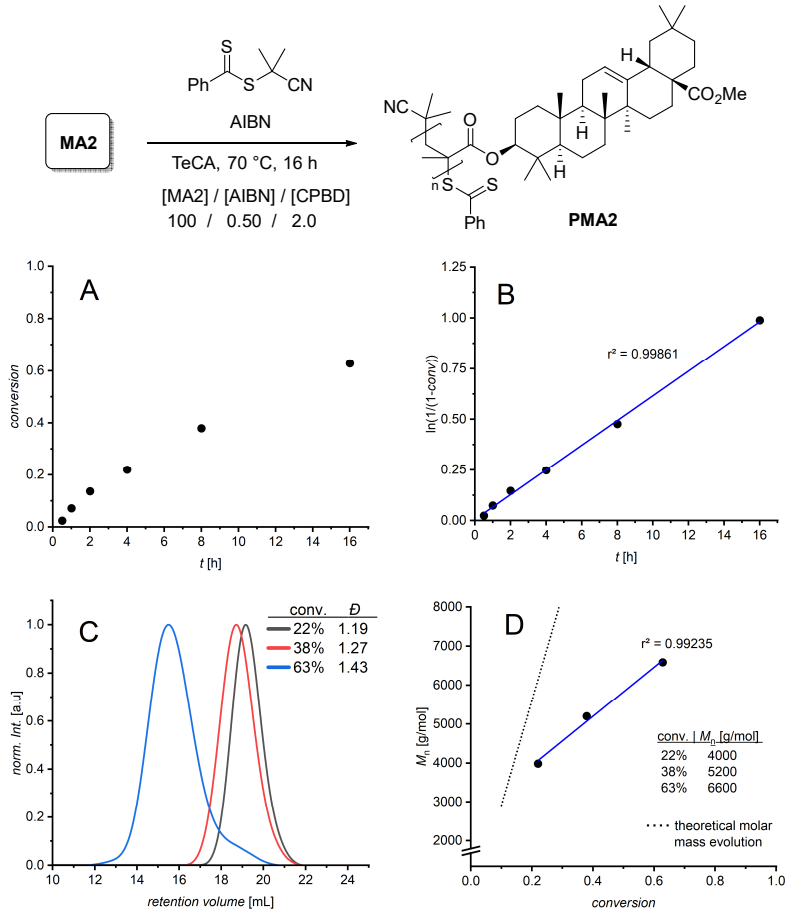

Figure 3.2. Kinetic and macromolecular data for the CPBD-mediated radical polymerization of **MA2** in TeCA at 70 °C in standard conditions (A: monomer conversion vs. time; B: semi-logarithmic kinetic plot; C: SEC traces at various conversions, D: M_n evolution with conversion).

MA3, carrying the methacrylate ester on the reduced C-28 position and the intact hydroxyl group at the C-3 site, allowed to return to NBP as a solvent for polymerization, only requiring mild heating for full dissolution before the initiator was introduced. In analogue conditions, **MA3** clearly propagates faster than **MA1** and reaches 92% conversion only after 3 h (Figure 3.3A), again in a controlled manner before the conversion plateau was reached (Figure 3.3B). As for **MA2** polymers, due to insufficient solubility in DMAc, polystyrene-calibrated SEC in THF was required for polymers of **MA3** (Figure 3.3C). The SEC-based M_n values correlated linearly with the conversion calculated by ^{1}H NMR (Figure 3.3D), thus confirming a controlled radical polymerization of **MA3**.

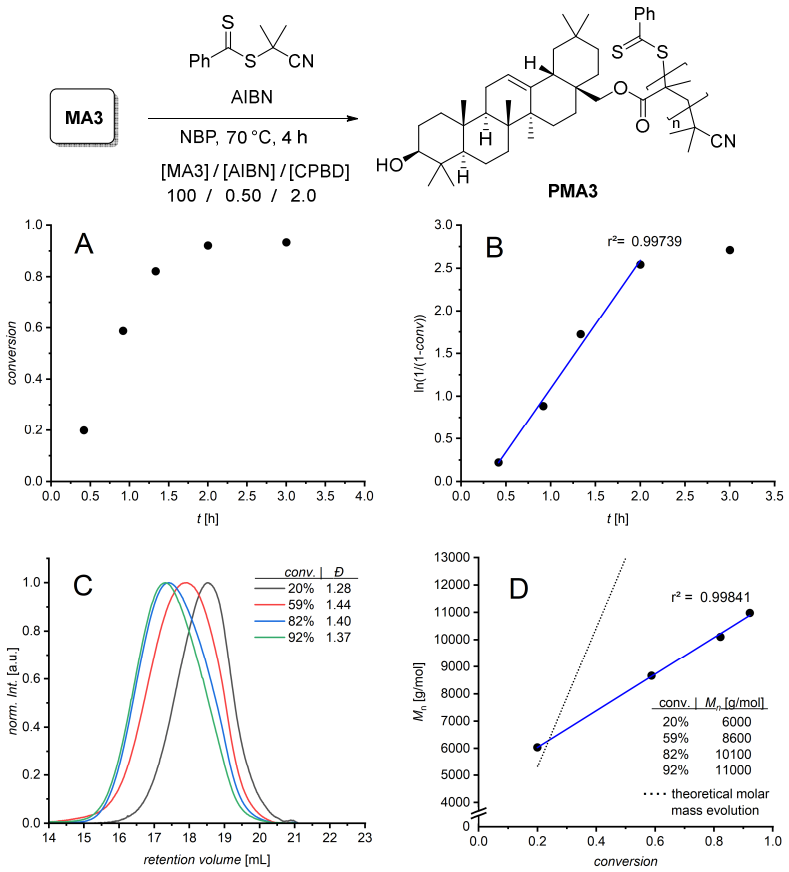

Figure 3.3. Kinetic and macromolecular data for the CPBD-mediated radical polymerization of **MA3** in NBP at 70 °C in standard conditions (A: monomer conversion vs. time; B: semi-logarithmic kinetic plot; C: SEC traces at various conversions, D: M_n evolution with conversion).

Maybe unexpectedly (lower steric hindrance around the methacrylate moiety), under the exact same conditions, **MA4** exhibited a reduced propagation rate compared to **MA3**, only reaching 76% conversion in about 6 h (Figure 3.4A). The semi-logarithmic time-dependent plot once more evidenced a constant radical concentration (Figure 3.4B). The molar mass distributions measured by SEC in DMAc for different polymerization times showed the

expected shift to lower retention volumes with increasing conversion (Figure 3.4C), again following a linear trend (Figure 3.4D).

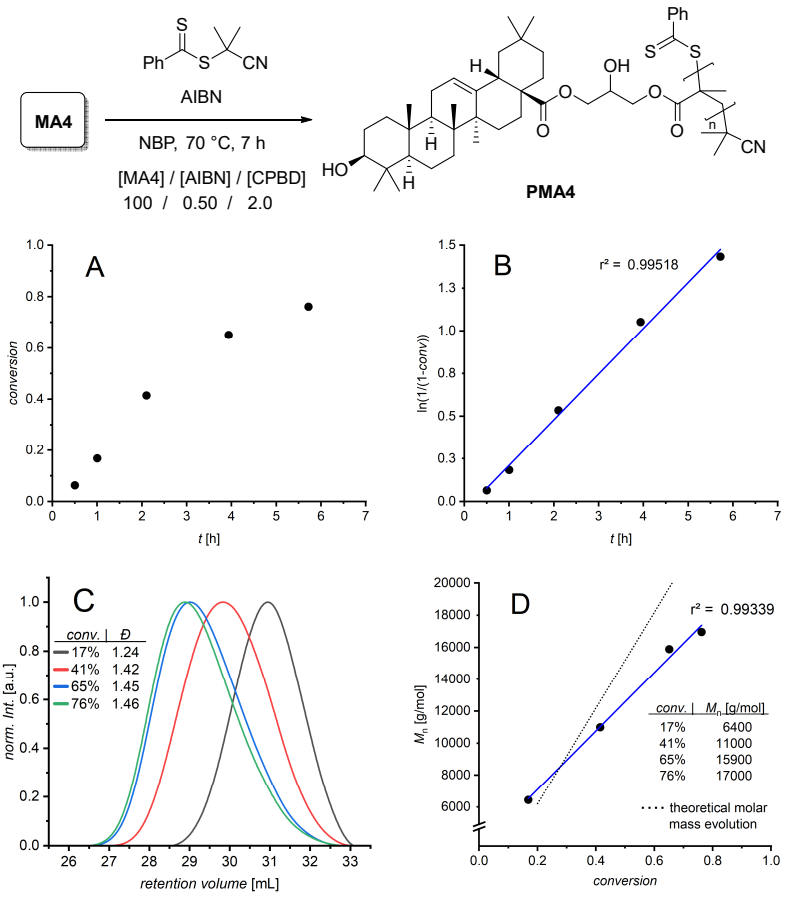

Figure 3.4. Kinetic and macromolecular data for the CPBD-mediated radical polymerization of **MA4** in NBP at 70 °C in standard conditions (A: monomer conversion vs. time; B: semi-logarithmic kinetic plot; C: SEC traces at various conversions, D: M_n evolution with conversion).

3.2.3. Polymer Synthesis with Varied Chain Length

To further assess the CPBD-controlled polymerization of **MA1**–**4** in the investigated conditions, polymerizations with varying targeted molar masses at full conversion were performed at a fixed reaction duration for each monomer. The results for experiments with [monomer]:[CPBD] ratios of 25, 50, and 100, along with reasonably comparable conversions, are displayed in Figure 3.5.

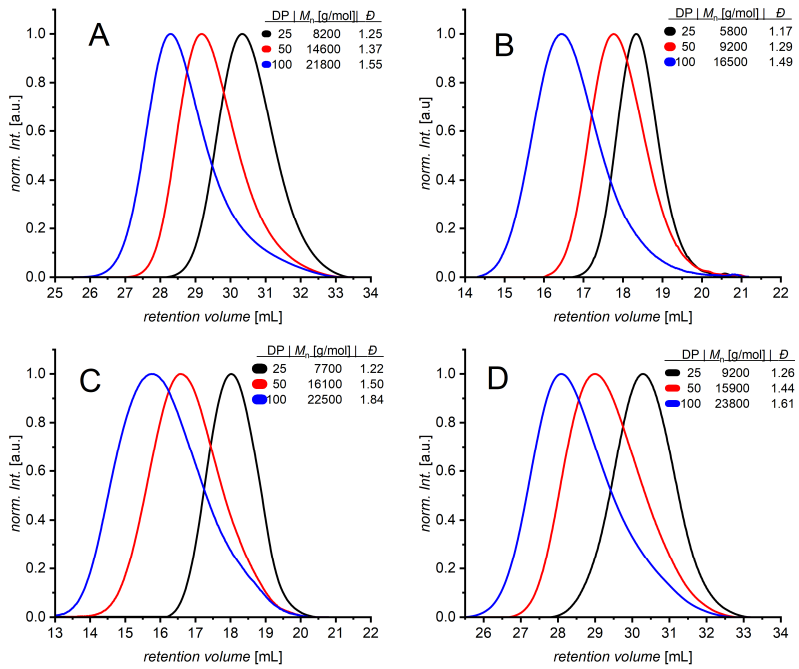

Figure 3.5. SEC traces of polymers synthesized with varying [MA]:[CPBD] ratios (DP). (A) **MA1**, NBP, 7 h, 83–86% conv. (B) **MA2**, TeCA, 24 h, 75–82% conv. (C) **MA3**, NBP, 2 h, 81–93% conv. (D) **MA4**, NBP, 8 h, 74–80% conv.

As an example, polymerizations with **MA1** reached nearly the same conversion after 7 h, i.e., 83–86%. The SEC traces displayed in Figure 3.5A revealed a significant shift toward lower retention volumes with increasing [**MA1**]:[CPBD] ratios (denoted as DP in the graphs). Concomitantly, the dispersity values increased with higher molar masses, revealing a partial loss of control over the polymerization. Especially, polymers with the highest DP showed a tailing toward lower molar masses, which may correspond to the progressive loss of the dithiobenzoate end group, arising from initiator decomposition. Similar outcomes were uncovered for all three further monomers (Figure 3.5, parts B–D). For **MA2** polymerizations, following the observation made during the aforementioned kinetic investigation in TeCA, the [CPBD]:[AIBN] ratio was reduced from 4:1 to 3:1 for DP 100 in order to induce faster kinetics (69 vs. 81% conversion after 24 h) and reach a higher molar mass. Intermonomer comparison is only strictly possible between **MA1** and **MA4**, as they were all polymerized and analyzed in the same solvent (NBP) and SEC eluent (DMAc), respectively. While they polymerized at relatively similar rates (see Figures 3.1B and 3.4B), they led to similar dispersity values (Figure 3.5A and D). In contrast, **MA3** polymerizes significantly faster in the same conditions, which may explain the higher dispersity values obtained with this monomer, but this time with SEC in THF (Figure 3.5C).

The observed significantly slower polymerization of **MA2** may explain the lowest dispersity values (Figure 3.5B).

As a summary of the polymerization investigations, it can be stated that despite their bulky nature, all monomers could be polymerized in a reasonably controlled manner, that is, with ideal kinetics, targetable degrees of polymerization, and moderate dispersity values. Experiments performed with conventional free-radical polymerization (FRP, ratio [MA]:[AIBN] = 100/0.5) show comparable conversions and underline the fundamental polymerizability of the monomers (see §3.5.1 in Supporting Information). For instance, FRP of **MA2** in TeCA shows high molecular weight polymer (M_n = 115 kg/mol, $Đ$ = 1.81, 43% conv.) is formed at low conversion and dispersity broadens significantly at high conversion (M_n = 57 kg/mol, $Đ$ = 2.86, 73% conv.).

3.2.4. Characterization

After proving the controlled polymerization of **MA1**–**4**, the monomers were polymerized on a larger scale using the conditions used for kinetic investigations (i.e., targeted DP of 50), until a conversion of at least approximately 80%. The polymers were precipitated in cold methanol and further purified by Soxhlet extraction with hot methanol to remove residuals of both the monomer and the high-boiling polymerization solvent (bp_{NBP} = 241 °C; bp_{TeCA} = 147 °C).

Table 3.2. Average molecular weight of **PMA1**–**4** determined by SEC and ^{1}H NMR used for further characterization.

	t [h]	conversion [%]	DP_{th}	DP_{NMR}	$M_{n,NMR}$ [g/mol]	$M_{n,SEC}$ [g/mol]	$Đ_{SEC}$
PMA1	7	81	41	47	24 900	14 800 [a]	1.32
PMA2	13	77	39	45	24 500	9400 [b]	1.49
PMA3	2	91	45	50	25 800	16 300 [b]	1.43
PMA4	8	83	42	48	29 000	18 100 [a]	1.41

[a] SEC with DMAc as eluent, calibrated with PMMA. [b] SEC with THF as eluent, calibrated with PS.

Table 3.2 summarizes the reaction time, conversion, and average molecular weights of the synthesized polymers named after their respective constitutive monomers, that is, **PMA1–4**. Both ^{1}H NMR spectroscopy and SEC were employed for (macro)molecular characterization. Prior to this, solubility in various organic solvents for concentrations ranging from 50 to 150 g/L was established (Table S3.1).

NMR spectra for all purified polymers are displayed in Figure 3.6. Several signals are of interest. First, integral comparison of the signals of the internal double bond proton H-12 (5.44–5.09 ppm) and of the methine proton H-3 confirmed that the former functional group essentially remained intact during the polymerization, which is of interest for potential post-polymerization modifications aiming at a variation of physical properties. Second, in this degree of polymerization regime, the signals arising from the aromatic protons of the terminal dithiobenzoate moiety are clearly visible and reliably integrable (see inset of Figure 3.6, with *o*, *m*, and *p* standing for ortho, meta, and para, respectively), which allows for an alternative determination of M_n values by neglecting termination reactions and comparing with the H-12 signal integral. An exception is **PMA1′**, where the signals in the aromatic region are not clearly resolved, which can be linked to the lack of control of **MA1′** polymerization. While the NMR-based DP values (DP_{NMR}) are found to fall in the expected range, they systematically exceed the theoretical values based on conversion (DP_{th}). Comparing $M_{n,NMR}$ (DP_{NMR} multiplied by monomer molecular weight, plus CPBD molecular weight) to $M_{n,SEC}$, it is rather likely that SEC underestimates the real values, be it in PS-calibrated THF-SEC (for **PMA2**) or PMMA-calibrated DMAc-SEC (for all others), as discussed earlier in the kinetic studies.

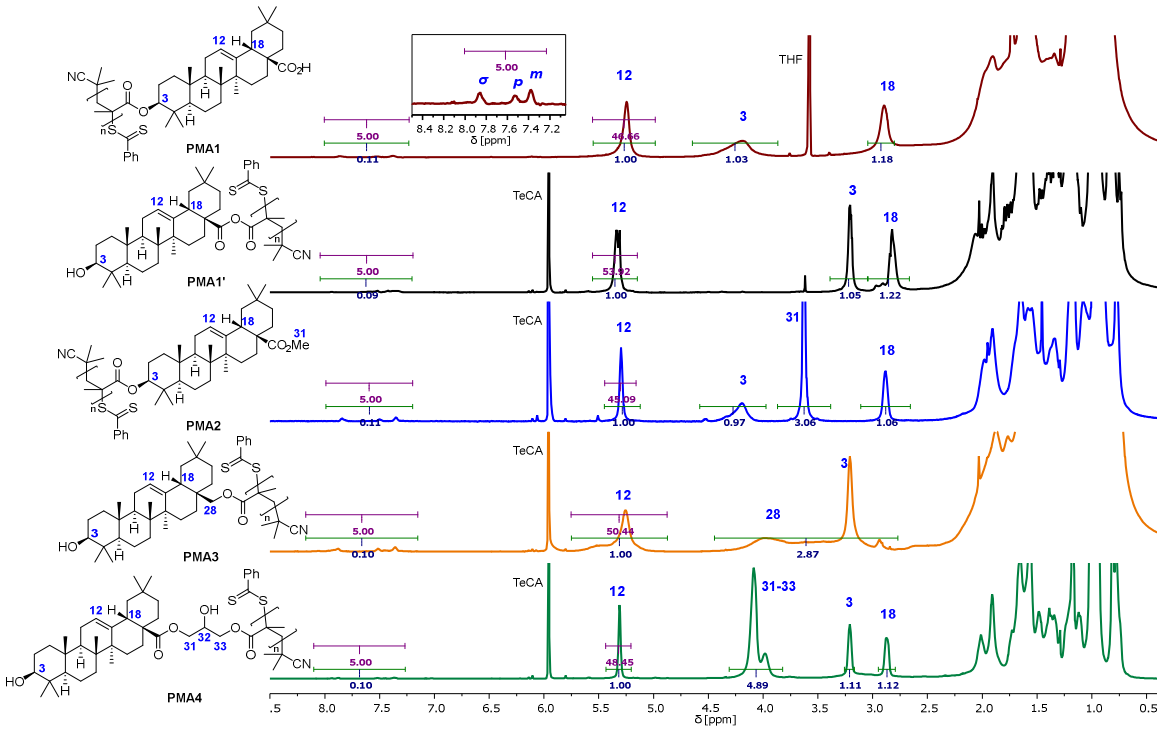

Figure 3.6. Structures of **PMA1**, **PMA1′**, and **PMA2–4**, and the corresponding ^{1}H NMR spectra (TeCA-d_2, 80 °C, except for **PMA1**: THF-d_8, 25 °C).

Additionally, NMR investigations gave information on the purity of the polymers and particularly confirmed the near-quantitative removal of the residual monomer. The remaining monomer content in **PMA2** lies at 3%, while this remained in the range of 0.3–2% for the other polymers. To further prove the controlled/living radical polymerization and the high end-group fidelity, a second polymer batch of **PMA2** (M_n = 9.3 kg/mol, $Đ$ = 1.27, conv. 82%, 0.7% **MA2** remaining) that dissolves, in contrast to **MA2**, in *n*-butyl acetate, was chain-extended with benzyl methacrylate using a ratio [BzMA]/[AIBN]/[macroRAFT] of 200/0.25/1.0. Analysis by ^{1}H NMR (conv. 72% of BzMA) and THF-SEC (M_n = 28 kg/mol, $Đ$ = 1.12) after purification revealed the successful formation of a block copolymer, indicating only a marginal amount of inactive **PMA2** chains present as shown in detail in SI (Figure S3.3). The homopolymers could be further analyzed by thermogravimetric analysis (TGA) and differential scanning calorimetry (DSC) to establish their thermal stability and possible physical state transition, respectively.

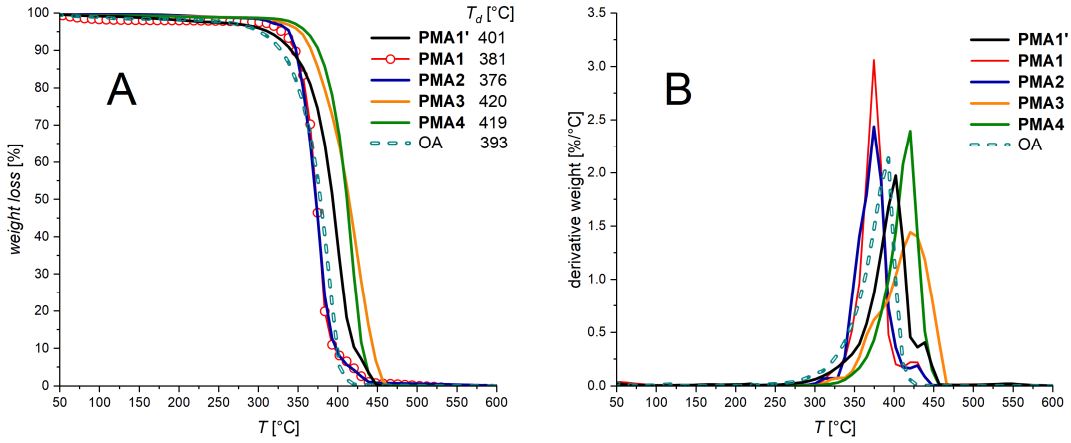

Figure 3.7. TGA (A) and DTG (B) profiles of OA and OA-based polymers. T_d refers to the point of inflection.

The degradation temperature (T_d) of OA, corresponding to the point of inflection of the main mass loss step in the TGA curve, was measured at approximately 390 °C, with an onset at approximately 280 °C (Figure 3.7A). Alternative representations of the data, also including degradation profiles of the monomers, are provided in the SI (Figures S3.4 and S3.5). There is a clear behavior difference between the (poly)methacrylates having the ester connected to the original secondary alcohol of OA (**MA1**/**PMA1** and **MA2**/**PMA2**) on the one hand and those in which the side chain is connected via a primary ester (**MA3**/**PMA3** and **MA4**/**PMA4**) on the other hand. **PMA1** and **PMA2** exhibit T_d values close to that of OA (381 and 376 °C, respectively), suggesting that the first degradation step could take place in the side chain, followed by backbone degradation (second maxima visible in

differential thermogravimetry (DTG) profiles in Figure 3.7B). **PMA3** and **PMA4** degrade about 40 °C higher, which suggests a different mechanism or simply a higher thermal stability of the OA motif in these modified versions. While **PMA4** appears to degrade in one step, probably with side-chain and main-chain degradations occurring coincidentally at the same time, **PMA3** clearly undergoes two nonsimultaneous degradation processes (Figure 3.7B). Furthermore, the mixed anhydride polymer **PMA1′** possesses an intermediate degradation temperature at approximately 400 °C. While the degradation mechanism of such polyanhydride was not documented, it is established that poly(meth)acrylates can undergo chain depolymerization and/or ester cleavage (possibly followed by anhydride formation), the extent of each respective mechanism strongly depending on the structure of the alkyl side chain.[181] We note that two hydrogens are present in *β*-position in the ester side chain in **MA1**/**PMA1** and **MA2**/**PMA2**, while **MA3**/**PMA3** possess none and **MA4**/**PMA4** only one. *β*-Hydrogens are essential for the intramolecular elimination-based pyrolysis of esters through a 6-membered transition state.[182] Furthermore, the product of ester cleavage, namely poly(methacrylic acid) (PMAA), is known to degrade via a two-step mechanism: minor mass loss through anhydride ring formation between neighboring repeating units at approximately 220–230 °C, followed by major and quantitative mass loss at 400 °C.[183]

Finally, the OA-based polymers were further investigated by DSC to give further insights into the thermal behavior before degradation as well as validate their potential use as thermoplastics (Figure 3.8). The polyanhydride **PMA1′** exhibited a glass transition at 192 °C. **PMA2** shows a glass transition at 222 °C, which is considerably higher compared to the common atactic PMMA (105 °C)[184] or even its syndiotactic version (126 °C),[185] as well as other biobased polymethacrylates such as polyisobornyl methacrylate (up to 200 °C, depending on tacticity)[186] and isosorbide-based counterparts (up to 167 °C).[167,168,187] A glass transition temperature could be detected for **PMA4** as well, at 166 °C. However, **PMA1**, the free carboxylic acid version of **PMA2**, and **PMA3** did not show any thermally induced transition below 290 °C. In the case of **PMA1**, the already very high T_g value obtained for **PMA2** is most certainly raised through additional H-bonding. And when comparing **PMA3** to **PMA4**, both linked via the C17–C28 bond to the pentacyclic scaffold, the absence of the flexible segment arising from the ring-opening of the glycidyl motif plausibly leads to a stiffening. Through simple heating to 290 °C on a

heating plate, **PMA1** and **PMA3** remained in their powder form and were only discolored. The synthesized polymers show furthermore no melting point.

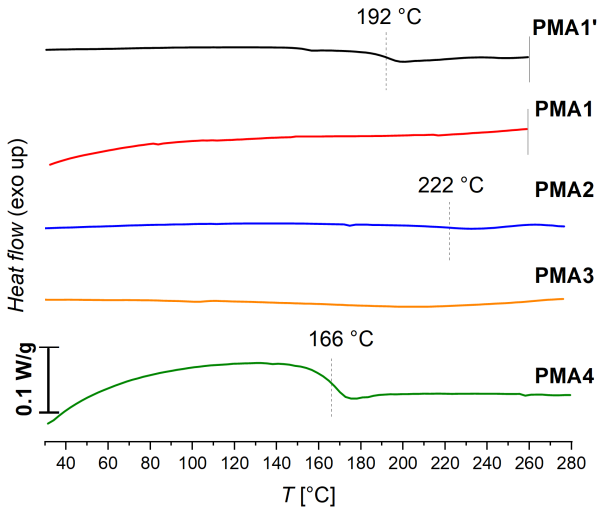

Figure 3.8. Overlay of DSC heating curves from **PMA1**−**4**.

3.3. Conclusion

In this contribution, oleanolic acid was converted into four novel methacrylates as well as a mixed anhydride, using synthetic pathways comprising 1-5 steps (for **MA1** and **MA4** on the one hand and **MA3** on the other hand), with overall yields ranging from 50 to 80% (for **MA4** and **MA2**, respectively) and biobased atom contents between 76 and 87% (for **MA4** and **MA1**, respectively). All four methacrylates could be polymerized in a controlled manner by radical RAFT polymerization, that is, with targetable average molar masses and moderate dispersity values. Importantly, while such complex structures exhibit challenging solubilities, three of the monomers could be polymerized in the green solvent *N*-butyl-2-pyrrolidone under homogeneous conditions. All resulting polymers possessed degradation temperatures above 300 °C. For polymers of **MA2** and **MA4** (**PMA2** and **PMA4**), glass-transition temperatures could be measured below their degradation temperatures, thus offering processing windows of at least 100 °C and making these new polymethacrylates plausible candidate bioplastics for high-temperature applications. Particularly, the relative abundance of oleanolic acid in many plant species (e.g., 3.5% of the dry olive tree leaf weight) suggests a potential cost-effective use, particularly considering such an unusually rigid and chiral structure. Future avenues of research include the corresponding acrylic derivatives, as well as copolymerization with other biobased (meth)acrylates (e.g., from

menthol, citronellol, tetrahydrogeraniol)[188] in order to tune polymer properties. Also reported in this study is an oleanolic acid-based mixed methacrylic anhydride, consisting of an underexplored polymerizable unit, which could not be polymerized in a controlled manner. It certainly would be interesting to investigate further structures of the same type – where the OA fragment would possibly be replaced by a simpler substituent – in order to establish a general structure-reactivity relationship. Additionally, the green solvent *N*-butyl-2-pyrrolidone, being introduced for the first time as a solvent for radical polymerizations, should be further investigated for its propensity to chain transfer, especially because constants for transfer to solvent and monomer, respectively, were reported for the related *N*-methyl-2-pyrrolidone[189] and *N*-vinylpyrrolidone.[190]

3.4. Experimental Procedures

Oleanolic acid 3-methacrylate (MA1)

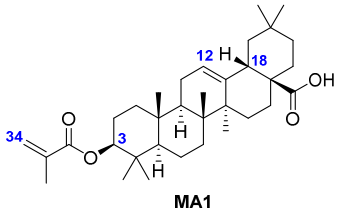

MA1

Oleanolic acid (3.00 g, 6.57 mmol, 1.0 eq) was dissolved in dry THF (33 mL) before adding triethylamine (1.83 mL, 13.1 mmol, 2.0 eq) and DMAP (0.64 g, 5.25 mmol, 0.8 eq). Subsequently, methacrylic anhydride (1.62 mL, 10.5 mmol, 1.6 eq) was added dropwise at 0 °C, and the solution was stirred overnight at ambient temperature. Remaining methacrylic anhydride was deactivated with water. The aqueous phase was separated and extracted with EA. The combined organic layer was washed with water and brine, followed by drying over magnesium sulfate. After removing the solvent *in vacuo*, the crude product was purified by flash chromatography (SiO_2, CH/EA 98/02 → 80/20) to obtain the product **MA1** as a white powder (2.30 g, 4.38 mmol, 67%).

^{1}H NMR (600 MHz, $CDCl_3$): δ [ppm] = 6.09 (s, 1H, H_{34Z}), 5.52 (s, 1H, H_{34E}), 5.27 (t, J = 3.8 Hz, 1H, H_{12}), 4.54 (dd, J = 11.4, 5.0 Hz, 1H, H_3), 2.82 (dd, J = 13.4, 4.7 Hz, 1H, H_{18}), 2.03 – 1.82 (m, 6H), 1.82 – 1.51 (m, 10H), 1.51 – 1.27 (m, 4H), 1.26 – 1.02 (m, 4+3H), 0.96 (s, 3H), 0.93 (s, 3H), 0.90 (s, 3H), 0.90 (s, 3H), 0.89 (s, 3H), 0.87 – 0.84 (m, 1H), 0.75 (s, 3H).

^{13}C{^{1}H} NMR (151 MHz, $CDCl_3$): δ [ppm] = 184.3, 167.3, 143.8, 137.2, 125.0, 122.7, 81.4, 55.5, 47.7, 46.7, 46.0, 41.7, 41.1, 39.5, 38.2, 38.1, 37.2, 34.0, 33.2, 32.7, 32.6, 30.8, 28.3, 27.8, 26.1, 23.7, 23.6, 23.6, 23.0, 18.5, 18.3, 17.3, 16.9, 15.5.

HRMS (ESI): $[M\text{-}H]^-$ *m/z* 523.3794 (calculated for $C_{34}H_{51}O_4^-$: *m/z* 523.3793).

Oleanolic acid 17-methylester (3-1)

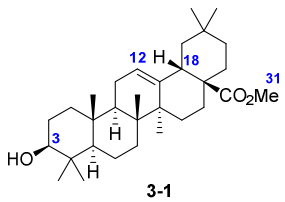

3-1

To a stirred solution of oleanolic acid (2.00 g, 4.38 mmol, 1.0 eq) in DMAc (22 mL) was added potassium carbonate (1.55 g, 11.0 mmol, 2.5 eq). After slow addition of methyl

iodide (0.68 mL, 11.0 mmol, 2.5 eq), the suspension was stirred overnight at ambient temperature. The resulting mixture was diluted with EA and washed with water and saturated aq. $NaHCO_3$ solution. After drying over $MgSO_4$ and filtration, the solvent was evaporated under reduced pressure to give a light-yellow solid, which was purified by flash column chromatography (SiO_2, CH → CH/EA 8:2) to give **3-1** as a white solid (1.99 g, 4.23 mmol, 96%).

^{1}H NMR (600 MHz, $CDCl_3$): δ [ppm] = 5.28 (t, J = 3.7 Hz, 1H, H_{12}), 3.62 (s, 3H, H_{31}), 3.21 (dd, J = 11.3, 4.5 Hz, 1H, H_3), 2.86 (dd, J = 14.0, 4.7 Hz, 1H, H_{18}), 2.01 – 1.91 (m, 1H), 1.91 – 1.82 (m, 2H), 1.74 – 1.48 (m, 10H), 1.48 – 1.22 (m, 5H), 1.21 – 1.11 (m, 2+3H), 1.08 – 1.02 (m, 1H), 0.98 (s, 3H), 0.97 – 0.93 (m, 1H), 0.92 (s, 3H), 0.90 (s, 3H), 0.89 (s, 3H), 0.78 (s, 3H), 0.74 – 0.71 (m, 1+3H).

^{13}C{^{1}H} NMR (151 MHz, $CDCl_3$): δ [ppm] = 178.4, 144.0, 122.5, 79.2, 55.4, 51.7, 47.8, 46.9, 46.1, 41.8, 41.5, 39.5, 38.9, 38.6, 37.2, 34.0, 33.3, 32.8, 32.6, 30.8, 28.3, 27.9, 27.4, 26.1, 23.8, 23.6, 23.2, 18.5, 17.0, 15.7, 15.4.

HRMS (APCI): $[M+H]^+$ *m/z* 471.3834 (calculated for $C_{31}H_{51}O_3^+$: *m/z* 471.3833).

Oleanolic acid 3-methacrylate-17-methylester (MA2)

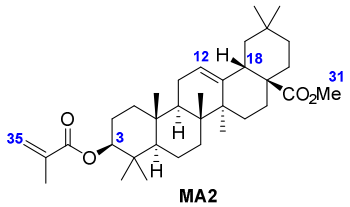

MA2

Oleanolic acid 17-methylester **3-1** (1.56 g, 3.31 mmol, 1.0 eq) was dissolved in dry DCM (33 mL). Subsequently, NEt_3 (1.85 mL, 13.26 mmol, 4.0 eq) was added, followed by dropwise addition of methacryloyl chloride (0.74 mL, 7.62 mmol, 2.3 eq) at 0 °C. After stirring overnight at ambient temperature, the remaining methacryloyl chloride was quenched by the addition of H_2O. The two phases were separated, and the aqueous phase was extracted with DCM. The combined organic phase was washed with brine and dried over $MgSO_4$. After filtration, the solvent was removed *in vacuo*. The resulting raw product was purified by flash chromatography (SiO_2, CH → CH/EA 9:1) to yield **MA2** as a white solid (1.45 g, 2.70 mmol, 81%).

^{1}H NMR (600 MHz, $CDCl_3$): δ [ppm] = 6.08 (s, 1H, H_{35Z}), 5.52 (s, 1H, H_{35E}), 5.28 (t, J = 3.7 Hz, 1H, H_{12}), 4.53 (dd, J = 11.3, 5.0 Hz, 1H, H_3), 3.62 (s, 3H, H_{31}), 2.86 (dd, J = 13.9,

4.6 Hz, 1H, H_{18}), 2.02 – 1.95 (m, 1H), 1.94 (s, 3H), 1.92 – 1.83 (m, 2H), 1.73 – 1.25 (m, 14H), 1.22 – 1.11 (m, 5H), 1.11 – 1.01 (m, 2H), 0.95 (s, 3H), 0.92 (s, 3H), 0.90 (s, 3H), 0.90 (s, 3H), 0.88 (s, 3H), 0.87 – 0.84 (m, 1H), 0.73 (s, 3H).

$^{13}C\{^1H\}$ NMR (151 MHz, $CDCl_3$): δ [ppm] = 178.4, 167.3, 144.0, 137.2, 125.0, 122.4, 81.4, 55.5, 51.6, 47.7, 46.9, 46.0, 41.8, 41.5, 39.5, 38.2, 38.1, 37.1, 34.0, 33.3, 32.8, 32.5, 30.8, 28.3, 27.9, 26.1, 23.8, 23.6, 23.6, 23.2, 18.5, 18.4, 17.0, 17.0, 15.5

HRMS (APCI): $[M+H]^+$ *m/z* 539.4094 (calculated for $C_{35}H_{55}O_4^+$: *m/z* 539.4095).

Oleanolic acid 3-*tert*-butyldimethylsilyl-17-methylester (3-2)

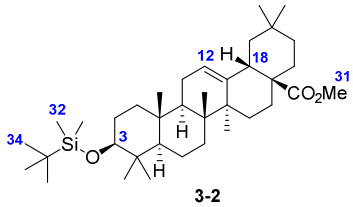

3-2

Oleanolic acid 17-methylester **3-1** (1.56 mg, 3.31 mmol, 1.0 eq) was dissolved in dry DCM (87.2 mL, 0.04 M). The mixture was cooled down to 0 °C, and 2,6-lutidine (1.97 mL, 16.6 mmol, 5.0 eq) was added. After stirring for 5 min, TBSOTf (1.18 mL, 5.02 mmol, 1.5 eq) was added dropwise. The solution was then warmed to room temperature and stirred for 3 h, before being poured into ice-cold saturated aq. $NaHCO_3$ solution. The product was extracted with DCM. The combined organic layer was washed with aq. 1 M HCl solution to remove excess 2,6-lutidine, dried over Na_2SO_4, filtered, and concentrated *in vacuo*. Purification of the residue by flash chromatography (SiO_2, CH/EA 95:5) gave **3-2** as a colorless solid (1.80 g, 3.08 mmol, 93%).

^1H NMR (600 MHz, $CDCl_3$): δ [ppm] = 5.28 (t, *J* = 3.7 Hz, 1H, H_{12}), 3.62 (s, 3H, H_{31}), 3.18 (dd, *J* = 11.4, 4.4 Hz, 1H, H_3), 2.86 (dd, *J* = 13.9, 4.6 Hz, 1H, H_{18}), 2.00 – 1.93 (m, 1H), 1.93 – 1.80 (m, 2H), 1.73 – 1.65 (m, 1H), 1.64 – 1.49 (m, 7H), 1.48 – 1.38 (m, 2H), 1.38 – 1.29 (m, 2H), 1.29 – 1.24 (m, 1H), 1.22 – 1.15 (m, 1H), 1.12 (s, 3H), 1.07 – 1.02 (m, 1H), 0.92 (s, 3H), 0.90 (s, 8H), 0.88 (s, 10H), 0.74 (s, 3H), 0.71 (s, 3H), 0.70 – 0.68 (m, 1H), 0.03 (s, 6H, H_{32}).

$^{13}C\{^1H\}$ NMR (151 MHz, $CDCl_3$): δ [ppm] = 178.4, 143.9, 122.6, 79.7, 55.5, 51.7, 47.9, 46.9, 46.1, 41.8, 41.5, 39.5, 39.5, 38.6, 37.1, 34.1, 33.3, 32.9, 32.6, 30.9, 28.7, 27.9, 27.8, 26.1, 26.1, 23.8, 23.6, 23.3, 18.7, 18.3, 17.0, 16.3, 15.5, -3.6, -4.7.

HRMS (ESI): $[M+Na]^+$ *m/z* 607.4517 (calculated for $C_{37}H_{64}O_3SiNa^+$: *m/z* 607.4517).

Oleanolic acid 3-*tert*-butyldimethylsilyl-17-methanol (3-3)

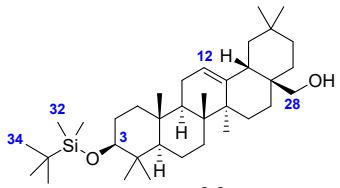

3-3

3-2 (1.80 g, 3.08 mmol, 1.0 eq) was dissolved in dry DCM (61.7 mL, 0.05 M) under argon in a flame-dried round-bottom flask. The mixture was cooled down to −78 °C. DIBAL-H (1.2 M solution in toluene, 15.4 mL, 18.5 mmol, 6.0 eq) was added dropwise during 5 min. The reaction was stirred for 1.5 h before full conversion was observed via TLC. The cooling bath was removed, and the reaction mixture was carefully quenched with an aq. potassium sodium tartrate solution. The mixture was transferred into a separating funnel, and the organic layer was removed. The aqueous layer was washed with DCM twice. The organic layers were combined and dried over Na_2SO_4, filtered, and concentrated *in vacuo*. Purification of the residue by flash chromatography (SiO_2, CH/EA 98:2) yielded **3-3** as a colorless solid (1.64 g, 2.94 mmol, 95%).

^{1}H NMR (400 MHz, $CDCl_3$): δ [ppm] = 5.14 (t, J = 3.7 Hz, 1H, H_{12}), 3.53 (d, J = 10.9 Hz, 1H, H_{28}), 3.20 (d, J = 11.0 Hz, 1H, H_{28}), 3.23 – 3.15 (m, 1H, H_3), 1.99 – 1.87 (m, 3H), 1.78 (td, J = 13.7, 4.8 Hz, 1H), 1.64 – 1.45 (m, 5H), 1.41 – 1.28 (m, 3H), 1.27 – 1.14 (m, 1H), 1.10 (s, 3H), 0.99 (s, 3H), 0.94 (d, J = 6.0 Hz, 6H), 0.91 (s, 3H), 0.89 (s, 12H), 0.81 (d, J = 5.8 Hz, 3H), 0.76 (s, 3H), 0.73 – 0.66 (m, 1H), 0.04 (s, 6H, H_{32}).

^{13}C{^{1}H} NMR (101 MHz, $CDCl_3$): δ [ppm] = 144.3, 122.6, 79.6, 69.8, 55.4, 47.8, 46.6, 42.5, 41.8, 39.9, 39.5, 38.7, 37.1, 37.0, 34.2, 33.4, 32.8, 31.2, 31.1, 28.7, 27.8, 27.1, 26.1, 26.1, 25.7, 23.7, 23.7, 22.2, 18.7, 18.3, 16.9, 16.3, 15.7, -3.6, -4.7.

HRMS (ESI): $[M+Na]^+$ *m/z* 579.4567 (calculated for $C_{36}H_{64}O_2SiNa^+$: *m/z* 579.4568).

Oleanolic acid 3-*tert*-butyldimethylsilyl-17-methyl methacrylate (3-4)

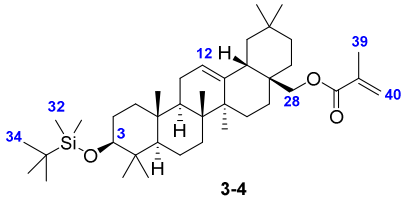

3-4

The reduced species **3-3** (323 mg, 580 µmol, 1.0 eq) was dissolved in dry DMF (3.87 mL, 0.15 M) under argon in a flame-dried round-bottom flask. The mixture was cooled to 0 °C.

NEt_3 (0.322 mL, 2.32 mmol, 4.0 eq) was added. Methacryloyl chloride (0.135 mL, 1.28 mmol, 2.2 eq) was then added dropwise. The reaction mixture was warmed to room temperature and stirred for 2 h. After TLC indicated full conversion, water and DCM were added. The phases were separated, and the aqueous phase was extracted two more times with DCM. The organic phase was dried with brine and Na_2SO_4. The solvent was removed under reduced pressure, and the crude product was purified by column chromatography (SiO_2, CH/EA 95:5), yielding **3-4** as a colorless solid (333 mg, 534 µmol, 92%).

^{1}H NMR (400 MHz, $CDCl_3$): δ [ppm] = 6.10 (dq, J = 2.0, 1.0 Hz, 1H, H_{40Z}), 5.54 (t, J = 1.6 Hz, 1H, H_{40E}), 5.21 (t, J = 3.7 Hz, 1H, H_{12}), 4.09 (d, J = 11.0 Hz, 1H, H_{28}), 3.79 (d, J = 11.0 Hz, 1H, H_{28}), 3.19 (dd, J = 11.2, 4.7 Hz, 1H, H_3), 2.11 (dd, J = 13.7, 4.5 Hz, 1H), 2.05 – 2.00 (m, 1H), 1.96 (t, J = 1.3 Hz, 3H, H_{39}), 1.95 – 1.82 (m, 2H), 1.82 – 1.66 (m, 2H), 1.65 – 1.46 (m, 6H), 1.41 – 1.24 (m, 3H), 1.24 – 1.15 (m, 2+3H), 1.09 (ddd, J = 13.5, 4.7, 2.5 Hz, 1H), 1.04 – 0.98 (m, 1H), 0.96 (s, 3H), 0.92 (s, 3H), 0.91 (s, 3H), 0.90 (s, 3H), 0.89 (s, 12H), 0.75 (s, 3H), 0.73 – 0.65 (m, 1H), 0.04 (s, 6H, H_{32}).

^{13}C{^{1}H} NMR (101 MHz, $CDCl_3$): δ [ppm] = 167.6, 143.7, 136.8, 125.2, 123.2, 79.7, 71.0, 55.5, 47.8, 46.5, 42.7, 41.83, 40.0, 39.5, 38.8, 37.0, 36.3, 34.2, 33.3, 32.8, 31.7, 31.1, 28.7, 27.8, 27.1, 26.2, 26.1, 25.8, 23.8, 23.7, 22.7, 18.7, 18.6, 18.3, 16.9, 16.3, 15.7, -3.6, -4.7.

HRMS (ESI): $[M+Na]^+$ *m/z* 647.4828 (calculated for $C_{40}H_{68}O_3SiNa^+$: *m/z* 647.4830).

Oleanolic acid 17-methyl methacrylate (MA3)

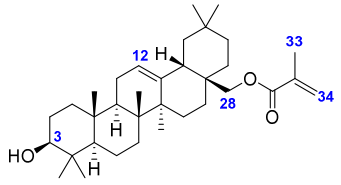

MA3

Methacrylated species **3-4** (333 mg, 534 µmol, 1.0 eq) and *p*-toluenesulfonic acid monohydrate (13.0 mg, 69.4 µmol, 0.13 eq) were dissolved in methanol/DCM (6:1, 6.40 mL, 0.08 M) and stirred for 5 h at 40 °C. To the reaction solution, saturated aq. $NaHCO_3$ solution was added, and the aqueous layer was extracted three times with DCM. The organic phases were combined, dried with Na_2SO_4, and filtered. The solvent was removed *in vacuo*. The residue was purified by column chromatography (SiO_2, CH/EA 9:1), yielding **MA3** as a colorless solid (215 mg, 411 µmol, 77%).

^{1}H NMR (400 MHz, $CDCl_3$): δ [ppm] = 6.10 (dq, J = 2.0, 1.0 Hz, 1H, H_{34Z}), 5.53 (t, J = 1.6 Hz, 1H, H_{34E}), 5.21 (t, J = 3.7 Hz, 1H, H_{12}), 4.09 (d, J = 11.0 Hz, 1H, H_{28}), 3.78 (d, J = 11.1 Hz, 1H, H_{28}), 3.21 (dd, J = 11.0, 4.9 Hz, 1H, H_3), 2.17 – 2.06 (m, 1H), 2.01 – 1.91 (m, 1H), 1.95 (t, J = 1.3 Hz, 3H, H_{33}), 1.92 – 1.82 (m, 2H), 1.82 – 1.69 (m, 2H), 1.65 – 1.49 (m, 6H), 1.41 – 1.24 (m, 5H), 1.21 – 1.13 (m, 2+3H), 1.09 (ddd, J = 13.5, 4.7, 2.5 Hz, 1H), 0.99 (s, 3H), 0.96 (s, 3H), 0.93 (s, 3H), 0.89 (s, 3H), 0.88 (s, 3H), 0.78 (s, 3H), 0.75 – 0.69 (m, 1H).

^{13}C{^{1}H} NMR (101 MHz, $CDCl_3$): δ [ppm] = 167.6, 143.7, 136.8, 125.2, 123.1, 79.1, 7.0, 55.4, 47.8, 46.4, 42.7, 41.8, 40.0, 38.9, 38.8, 37.1, 36.2, 34.2, 33.3, 32.7, 31.6, 31.1, 28.3, 27.4, 26.2, 25.8, 23.7, 23.7, 22.7, 18.5, 18.5, 16.9, 15.7, 15.7.

HRMS (ESI): $[M+Na]^+$ *m/z* 533.3962 (calculated for $C_{34}H_{54}O_3Na^+$: *m/z* 533.3965).

Oleanolic acid 17-(2-hydroxy-3-(methacryloyloxy)propyl) ester (MA4)

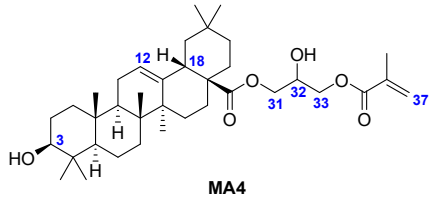

MA4

Oleanolic acid (3.50 g, 7.66 mmol, 1.0 eq) was dissolved in DMAc (48.0 mL, 0.16 M) following the addition of K_2CO_3 (1.59 g, 11.5 mmol, 1.5 eq) and 4-methoxyphenol (9.5 mg, 77 µmol, 0.1 eq). Subsequently, glycidyl methacrylate (1.22 mL, 9.20 mmol, 1.2 eq) was added, and the mixture was stirred at 80 °C for 6 h. After the reaction was complete, the mixture was diluted with EA and washed with water. The organic layer was washed with saturated aq. NaCl solution and dried over $MgSO_4$. The solution was concentrated *in vacuo,* and the crude product was purified by column chromatography (SiO_2, CH → CH/EA 7:3) to afford **MA4** as a white solid (2.18 g, 3.64 mmol, 48%).

^{1}H NMR (600 MHz, $CDCl_3$): δ [ppm] = 6.14 (s, 1H, H_{37Z}), 5.61 (s, 1H, H_{37E}), 5.30 (t, J = 3.8 Hz, 1H, H_{12}), 4.29 – 4.05 (m, 5H, $H_{31\text{-}33}$), 3.23 – 3.18 (m, 1H, H_3), 2.86 (dd, J = 13.9, 4.6 Hz, 1H, H_{18}), 2.48 – 2.44 (m, 1H, OH), 2.04 – 1.92 (m, 1+3H), 1.91 – 1.83 (m, 2H), 1.77 – 1.51 (m, 10H), 1.51 – 1.25 (m, 5H), 1.24 – 1.12 (m, 2+3H), 1.12 – 1.05 (m, 1H), 0.98 (s, 3H), 0.97 – 0.94 (m, 1H), 0.92 (s, 3H), 0.90 (s, 3H), 0.89 (s, 3H), 0.78 (s, 3H), 0.74 – 0.70 (m, 1+3H).

$^{13}C\{^{1}H\}$ NMR (151 MHz, $CDCl_3$): δ [ppm] = 177.9, 167.4, 144.1, 136.0, 126.4, 122.7, 79.2, 68.5, 65.5, 65.3, 55.4, 47.8, 47.2, 45.9, 41.9, 41.6, 39.5, 38.9, 38.6, 37.2, 34.0, 33.2, 32.9, 32.7, 30.8, 28.3, 27.8, 27.4, 26.0, 23.8, 23.6, 23.2, 18.5, 18.4, 17.2, 15.7, 15.4.

HRMS (ESI): $[M+Na]^+$ *m/z* 621.4123 (calculated for $C_{37}H_{58}O_6Na^+$: *m/z* 621.4126).

Oleanolic acid 17-methacrylic anhydride (MA1')

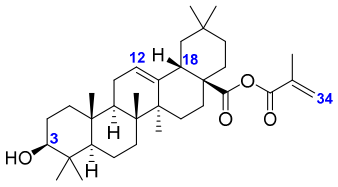

MA1'

Oleanolic acid (1.00 g, 2.19 mmol, 1.0 eq) was dissolved in dry DCM (33 mL) with triethylamine (0.67 mL, 4.82 mmol, 2.2 eq). Subsequently, methacryloyl chloride (0.33 mL, 3.29 mmol, 1.5 eq) was added dropwise at 0 °C, and the solution was stirred overnight at room temperature. Remaining methacryloyl chloride was deactivated by the addition of water. The aqueous phase was separated and extracted with EA. The combined organic layer was washed with water and brine. After drying over magnesium sulfate and removing the solvent *in vacuo*, the crude product was purified by flash chromatography (SiO_2, CH/EA 98/02 → 70/30) to obtain the product **MA1'** as a white powder (782 mg, 1.49 mmol, 68%).

^{1}H NMR (600 MHz, $CDCl_3$): δ [ppm] = 6.17 (s, 1H, H_{34Z}), 5.78 (s, 1H, H_{34E}), 5.33 (t, J = 3.7 Hz, 1H, H_{12}), 3.21 (dd, J = 11.3, 4.4 Hz, 1H, H_3), 2.85 (dd, J = 13.8, 4.7 Hz, 1H, H_{18}), 2.09 – 2.00 (m, 1H), 1.97 (s, 3H), 1.93 – 1.73 (m, 4H), 1.71 – 1.22 (m, 14H), 1.22 – 1.11 (m, 2+3H), 0.99 (s, 3H), 0.98 – 0.94 (m, 1H), 0.93 (s, 3H), 0.92 (s, 3H), 0.91 (s, 3H), 0.82 (s, 3H), 0.78 (s, 3H), 0.75 – 0.71 (m, 1H).

$^{13}C\{^{1}H\}$ NMR (151 MHz, $CDCl_3$): δ [ppm] = 173.1, 163.4, 143.1, 136.4, 128.7, 123.2, 79.1, 55.4, 48.3, 47.7, 45.9, 41.9, 41.4, 39.5, 38.9, 38.6, 37.1, 33.8, 33.1, 32.9, 31.6, 30.7, 28.2, 27.7, 27.3, 25.9, 23.6, 23.6, 23.3, 18.4, 18.0, 17.1, 15.7, 15.5.

HRMS (ESI): $[M+Na]^+$ *m/z* 547.3759 (calculated for $C_{34}H_{52}O_4Na^+$: *m/z* 547.3758).

General procedure for polymerization

One of the monomers among **MA1**, **MA1'**, **MA3**, and **MA4** (100 eq) was mixed with a solution of 2-cyano-2-propyl benzodithioate (CPBD, 2.0 eq) in NBP and a solution of 2,2′-azobis(2-methylpropionitrile) (AIBN, 0.50 eq) in NBP. After the addition of anisole (0.7 eq) as an internal standard, the mixture was further diluted with NBP, giving a clear pink solution with a total concentration of 0.3 M as a reference for conversion (t = 0, ^{1}H NMR). The solution was deoxygenated by sparging with argon for 40 min and stirred at 70 °C for a given time.

MA2 (374 mg, 684 µmol) was polymerized using the same protocol, except that the solvent NBP had to be replaced by TeCA. After sparging with argon, the solution was stirred at 70 °C for 24 h.

For kinetic experiments, **MA1**–**4** (350–586 mg) were polymerized following the general procedure, while samples were regularly taken for ^{1}H NMR and SEC analysis with a syringe.

To obtain polymers with varying the chain length, **MA1**–**4** (50–170 mg, 100 eq) were polymerized in a similar manner to the general procedure, whereby the ratios [MA]/[AIBN]/[CPBD] = 100:1.00:4.00, 100:0.50:2.00, and 100:0.25:1.00 were utilized, and ^{1}H NMR as well as SEC analysis were performed after the reaction. As an exception, for **MA2**, the ratio [MA2]/[AIBN]/[CPBD] = 100:0.34:1.00 for DP 100 was chosen to reach a higher conversion.

For the synthesis of polymers for structural and thermal characterizations after verification via ^{1}H NMR, a conversion of nearly 80% was reached. The polymer was precipitated in cold methanol (−20 °C), filtered, and purified by Soxhlet extraction overnight with hot methanol. Subsequently, the remaining polymer in the filter was dried *in vacuo*.

Polymer of oleanolic acid 3-methacrylate MA1 (PMA1)

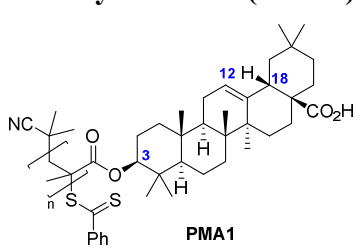

PMA1

PMA1 was prepared from **MA1** (432 mg, 824 µmol), CPBD (3.75 mg, 17.0 µmol), and AIBN (0.676 mg, 4.12 µmol) in NBP (2.75 mL) at 70 °C (7 h) according to the general

procedure and obtained as a pink powder (325 mg, 619 µmol, conversion 81%, isolated yield 75%).

^{1}H NMR (400 MHz, THF-d_8): δ [ppm] = 5.24 (s, 1H, H_{12}), 4.68 – 3.86 (m, 1H, H_3), 2.90 (s, 1H, H_{18}), 2.47 – 0.32 (m, 48H).

SEC: M_n = 14800 g/mol, M_w = 19500 g/mol, $Đ$ = 1.32.

Polymer of oleanolic acid 3-methacrylate-17-methylester MA2 (PMA2)

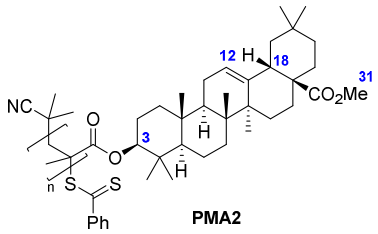

PMA2

PMA2 was prepared from **MA2** (661 mg, 1230 µmol), CPBD (5.43 mg, 24.5 µmol), and AIBN (1.01 mg, 6.13 µmol) in TeCA (4.10 mL) at 70 °C (13 h) according to the general procedure and obtained as a pink powder (474 mg, 880 µmol, conversion 77%, isolated yield 72%).

^{1}H NMR (600 MHz, $C_2D_2Cl_4$): δ [ppm] = 5.24 (s, 1H, H_{12}), 4.48 – 3.95 (m, 1H, H_3), 3.63 (s, 3H, H_{31}), 2.88 (s, 1H, H_{18}), 2.31 – 0.55 (m, 48H).

SEC: M_n = 9400 g/mol, M_w = 14000 g/mol, $Đ$ = 1.49.

Polymer of oleanolic acid 17-methyl methacrylate MA3 (PMA3)

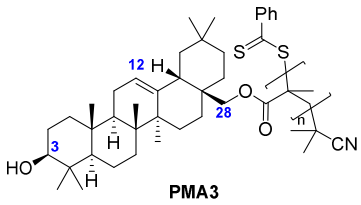

PMA3

PMA3 was prepared from **MA3** (500 mg, 979 µmol), CPBD (4.33 mg, 19.6 µmol), and AIBN (0.804 mg, 4.89 µmol) in NBP (3.26 mL) at 70 °C (2 h) according to the general procedure and obtained as a pink powder (329 mg, 644 µmol, conversion 91%, isolated yield 66%).

^{1}H NMR (600 MHz, $C_2D_2Cl_4$): δ [ppm] = 5.69 – 4.96 (m, 1H, H_{12}), 4.41 – 2.80 (m, 3H, H_{28}+H_3), 2.67 – 0.20 (m, 52H).

SEC: M_n = 16300 g/mol, M_w = 24100 g/mol, $Đ$ = 1.48.

Polymer of oleanolic acid 17-(2-hydroxy-3-(methacryloyloxy)propyl) ester MA4 (PMA4)

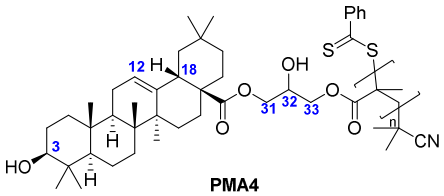

PMA4

PMA4 was prepared from **MA4** (351 mg, 586 µmol), CPBD (2.60 mg, 11.7 µmol), and AIBN (0.481 mg, 2.93 µmol) in NBP (1.95 mL) at 70 °C (8 h) according to the general procedure and obtained as a pink powder (220 mg, 367 µmol, conversion 83%, isolated yield 63%).

^{1}H NMR (600 MHz, $C_2D_2Cl_4$): δ [ppm] = 5.31 (s, 1H, H_{12}), 4.31 – 3.82 (m, 5H, $H_{31\text{-}33}$), 3.20 (s, 1H, H_3), 2.87 (s, 1H, H_{18}), 2.25 – 0.61 (m, 49H).

SEC: M_n = 18100 g/mol, M_w = 25500 g/mol, $Đ$ = 1.41.

Polymer of oleanolic acid 17-methacrylic anhydride MA1' (PMA1')

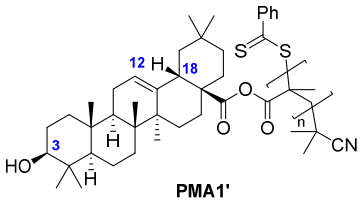

PMA1'

PMA1' was prepared from **MA1'** (380 mg, 724 µmol), CPBD (3.30 mg, 14.9 µmol), and AIBN (0.595 mg, 3.62 µmol) in DMAc (2.40 mL) at 70 °C (8 h) according to the general procedure and obtained as a pink solid (124 mg, 236 µmol, conversion 83%, isolated yield 33%).

^{1}H NMR (600 MHz, $C_2D_2Cl_4$): δ [ppm] = 5.46 – 5.21 (m, 1H, H_{12}), 3.29 – 3.12 (m, 1H, H_3), 2.89 – 2.73 (m, 1H, H_{18}), 2.51 – 0.33 (m, 49H).

SEC: M_n = 16100 g/mol, M_w = 26600 g/mol, $Đ$ = 1.65.

Block copolymer of MA2 and BzMA (PMA2-Bz)

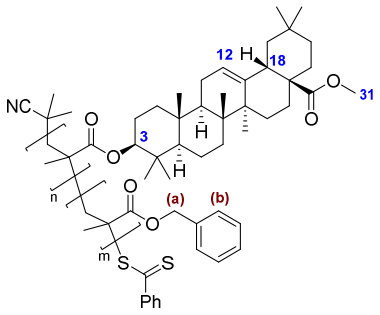

PMA2-Bz

Benzyl methacrylate (BzMA) was removed from its stabilizer by filtering through neutral aluminum oxide. BzMA (200 mg, 1140 µmol, 200 eq), AIBN (0.233 mg, 1.42 µmol, 0.25 eq), macroRAFT agent **PMA2** (133 mg, 5.68 µmol, 1.0 eq, M_{theo} = 23390 g/mol, M_n = 9300 g/mol, M_w = 11800 g/mol, $Đ$ = 1.27), and anisole (30 µL) were dissolved in *n*-butyl acetate (3.78 mL, 0.3 M). The solution was deoxygenated by sparging with argon before stirring at 70 °C for 24 h. The raw mixture was precipitated in cold diethyl ether, filtered, and dried *in vacuo*, yielding **PMA2-Bz** as a pink powder (167 mg, 3.50 µmol, conversion 72%, isolated yield 62%).

^{1}H NMR (600 MHz, $C_2D_2Cl_4$): δ [ppm] = 7.38 – 7.20 (m, 5H, H_a), 5.31 (s, 0.17H, H_{12}), 5.03 – 4.82 (m, 2H, H_b), 4.42 – 4.12 (m, 0.16H, H_3), 3.64 (s, 0.52H, H_{31}), 2.90 (s, 0.17H, H_{18}), 2.20 – 0.61 (m, 15H).

SEC: M_n = 27800 g/mol, M_w = 31000 g/mol, $Đ$ = 1.12.

3.5. Supplementary Information

3.5.1. Conventional Free-Radical Polymerization (FRP)

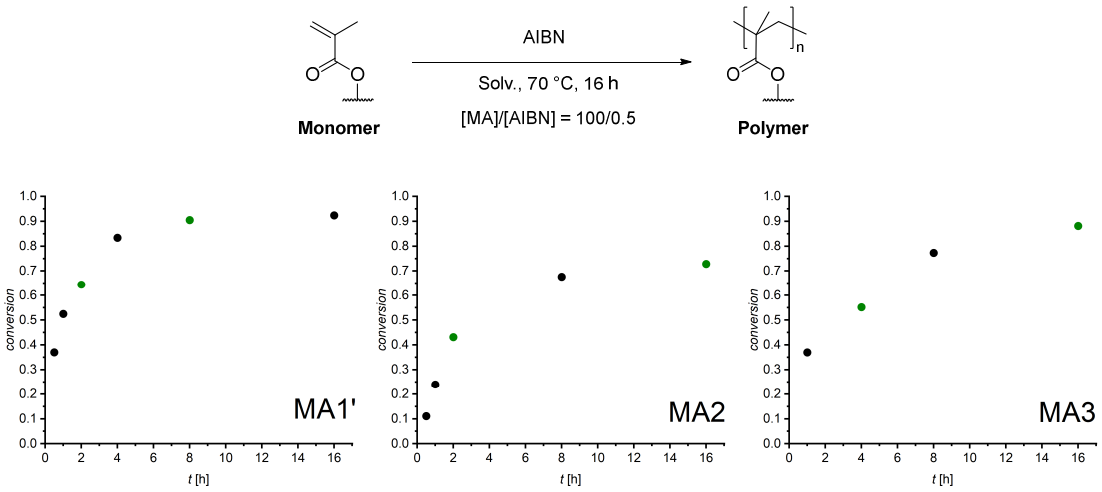

Monomer	Solvent	*t* [h]	*Conv.* [%]	M_n [kg/mol]	M_w [kg/mol]	*Đ*
MA1'	DMAc	2	64	96	214	2.21
		8	91	65	233	3.60
MA2	TeCA	2	43	115	209	1.81
		16	73	57	162	2.86
MA3	TeCA	4	55	52	97	1.86
		16	88	41	106	2.56

Figure S3.1. Kinetic and macromolecular data for the free-radical polymerization of **MA1'**, **MA2**, and **MA3** with [MA]/[AIBN] = 100/0.5 in DMAc or TeCA (**PMA1'** and **PMA3** raw mixtures measured in DMAc-SEC relative to PMMA, **PMA2** accordingly analyzed in THF-SEC relative to PS).

The kinetics of FRP were investigated to evaluate the general polymerizability of the novel monomers. **MA1'**, **MA2**, and **MA3** were polymerized under similar conditions (70 °C, 0.3 M in DMAc or TeCA) and a monomer-to-AIBN ratio of 100:0.5, which is comparable to RAFT experiments with targeted DP 50. The monomers reached high conversions after 16 h (73% to 92%). The polymers reached high molecular weights (M_n = 52–115 kg/mol) with moderate (*Đ* < 2.3) to high (*Đ* > 2.5) dispersity values at semi-quantitative (43–64%) and high (73–91%) conversions, respectively, typical of an FRP.

3.5.2. Polymerization of Oleanolic Acid 17-Methacrylic Anhydride (MA1')

MA1' belongs to a peculiar monomer class, that is, a mixed methacrylic anhydride, whose only studied related compound would be the cyclic itaconic anhydride. The CPBD-mediated radical polymerization of **MA1'** was investigated in conditions similar to monomers **MA1**–**4**, in both DMAc and NBP. While polymerization in the former was faster (Figure S3.2A), as expected in more polar solvents, the semi-logarithmic plots were both linear for the first 7–8 hours, up to conversions of ca. 85% and 55%, respectively (Figure S3.2B).

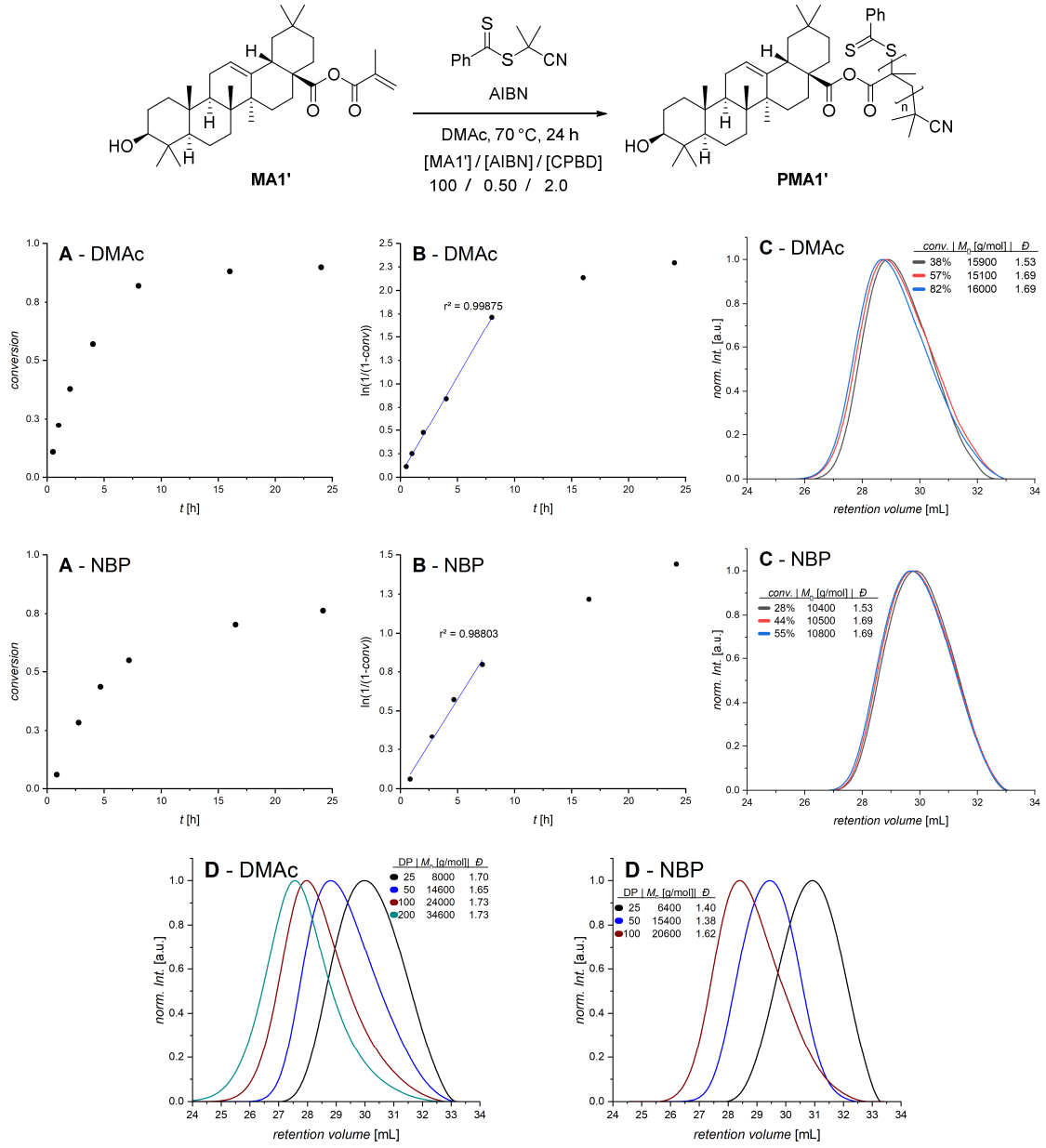

Figure S3.2. Kinetic (A, B) and macromolecular data (C, D) for the polymerization of **MA1'** in the presence of CPBD in DMAc (top row) and NBP (middle row), SEC profiles (D, bottom row) show further experiments with different polymerization degrees.

However, as seen in Figure S3.2C, the molar mass distributions barely evolved and were broader than for **PMA1**–**4**. It was nevertheless possible to obtain **PMA1'** with different molar masses by varying the [**MA1'**]:[CPBD] ratio (DP) from 25 to 200 (Figure S3.2D). Note that the [AIBN]:[CPBD] ratio was kept constant, leading [**MA1'**]:[AIBN] to also vary, which can also explain the variation of average molar mass, as in a traditional free-radical polymerization. Nevertheless, according to Figure 8.25 (in the Appendix), **PMA1'** seems to bear a dithiobenzoate end group (at least partially). It could therefore be assumed that the transfer rate constant for CPBD might be too low in the case of such mixed methacrylic anhydrides and that fragmentation is also difficult. This unexplored topic (i.e., the RAFT-mediated radical polymerization of methacrylic anhydrides) is certainly of interest but beyond the scope of the current paper.

3.5.3. Formation of Block Copolymer Using PMA2 as MacroRAFT Agent

To fulfill all criteria for a controlled/living radical polymerization, the ability to perform chain extension must be investigated. This was done on another batch of **PMA2** dissolved in *n*-butyl acetate (BA), where the polymer acts as a macroRAFT agent. Chain extension was performed with benzyl methacrylate (BzMA) using AIBN as thermal initiator to reach a theoretical DP value of 200 ([BzMA]/[AIBN]/[macroRAFT] = 200/0.25/1.0). After a reaction time of 24 h at 70 °C, a conversion of 72% BzMA could be determined by ^{1}H NMR, providing the possibility of purifying the copolymer by precipitation for SEC analysis as displayed in Figure S3.3.

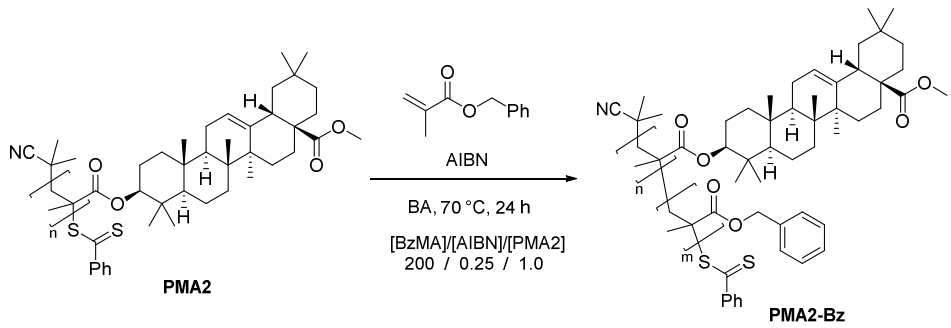

Scheme S3.1. Synthesis of **PMA2-Bz** by chain extension of **PMA2** with BzMA.

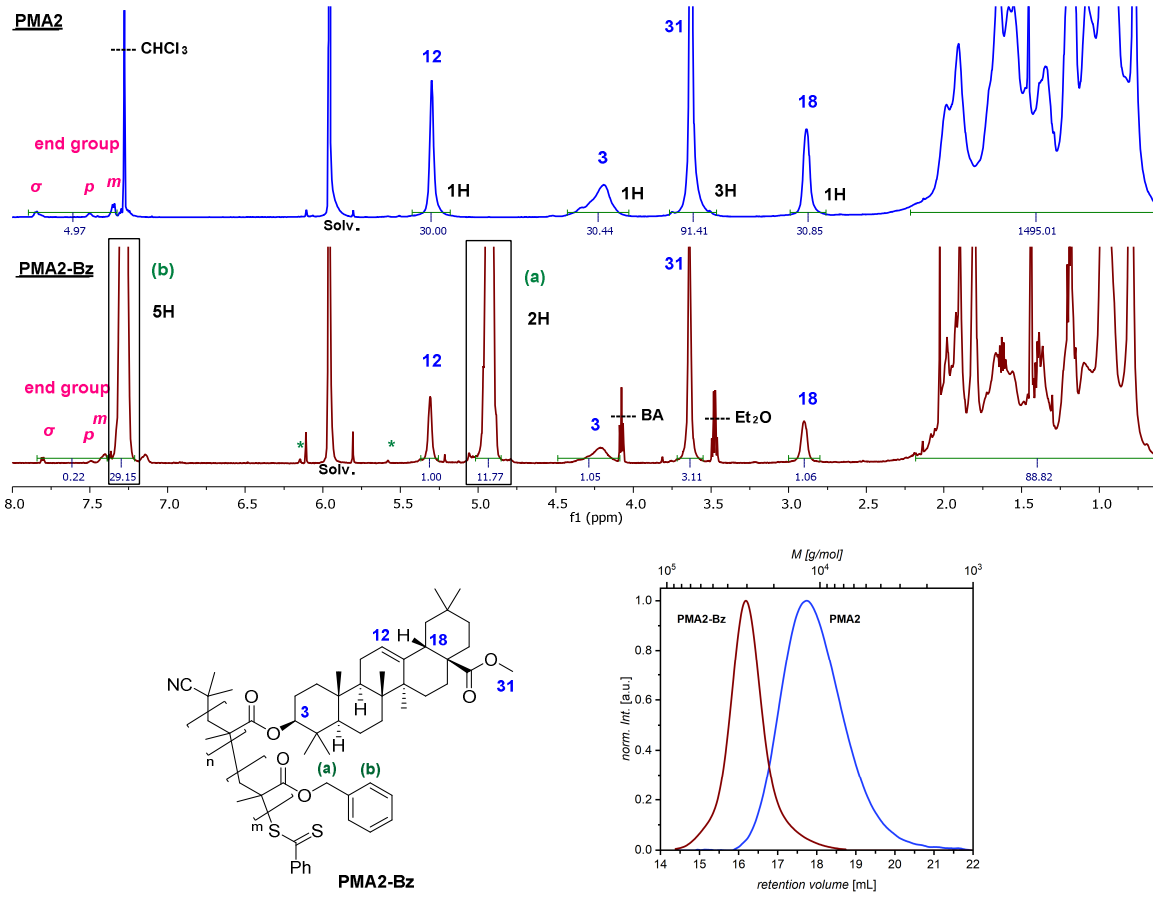

	Conv. [%]	DP_{target}	$DP_{n,NMR}$	M_n [kg/mol]	M_w [kg/mol]	$Đ$
PMA2	82	50	30	9.3	11.9	1.27
PMA2-Bz	72	200	176	27.8	31.0	1.12

Figure S3.3. ^{1}H NMR spectra (TeCA-d_2, 80 °C) and SEC data (THF eluent, calibrated by PS) of **PMA2** and **PMA2-Bz** after chain extension (* remaining BzMA content 0.4%).

According to SEC, M_n of **PMA2** could be increased from 9.3 to 27.8 kg/mol by chain extension, while the dispersity decreases significantly to 1.12.

Considering ^{1}H NMR results, **PMA2** shows a calculated DP value of 30 (aromatic end groups relative to H-12 signal at 5.30 ppm). By dividing the integrals of the new signals H-(b) (7.28 ppm, 29.15/5H) and H-(a) (4.92 ppm, 11.7/2H) in the spectrum of **PMA2-Bz** by its number of protons, an average equivalent of 5.86 BzMA results per **MA2** unit is obtained. With 30 **MA2** units, the second BzMA block therefore consists of 176 units, relatively close to the theoretical 144 (200 x 0.72). Combining the results of NMR and SEC, this demonstrates that the chain ends of **PMA2** remained active and can initiate further polymerization.

3.5.4. Solubility of OA-Based Polymethacrylates

Table S3.1. Solubility of OA-based polymethacrylates, as visually determined for various concentrations and solvents.

		DMAc		THF		$CHCl_3$		TeCA		NBP	
	c [g/L]	25°C	50°C	25°C	50°C	25°C	50°C	25°C	50°C	25°C	50°C
PMA1'	150										
	100										
	50										
PMA1	150										
	100										
	50										
PMA2	150										
	100										
	50										
	25										
	16										
PMA3	150										
	100										
	50										
	25										
	16										
PMA4	150										
	100										
	50										

3.5.5. Thermogravimetric Analysis of the Monomers

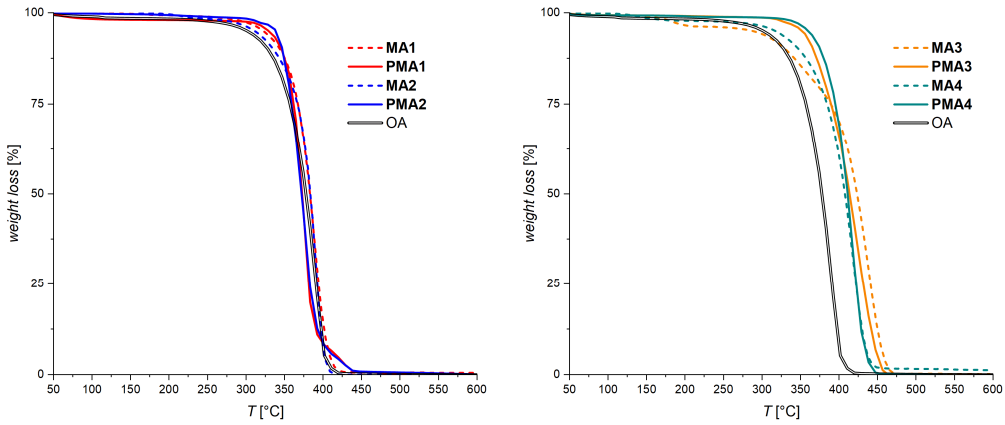

Figure S3.4. TGA weight loss profiles of OA, OA-based monomers, and OA-based polymers (10 °C/min, Ar 50 mL/min).

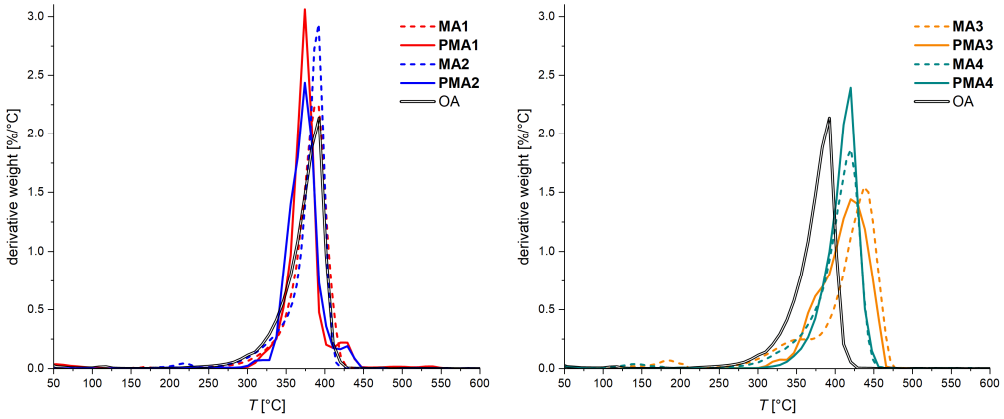

Figure S3.5. DTG profiles of OA, OA-based monomers, and OA-based polymers.

4. Novel Bio-Based Thermoplastic Polyurethanes Derived from Oleanolic Acid

A series of novel polyurethanes (PU) were synthesized by incorporation of erythrodiol (ErDO), produced by direct reduction of the naturally occurring pentacyclic triterpenoid oleanolic acid (OA). Polyaddition was performed with four different diisocyanates, including the bio-based 1,5-pentamethylene diisocyanate (PDI). PUs were obtained with M_n values up to 43 kg/mol (from size-exclusion chromatography), thermal stability up to 310 °C, and high glass-transition temperatures (T_g) up to approximately 250 °C. Copolymerization with 1,6-hexanediol produced a series of fully biobased, ternary ErDO/PDI-containing PUs with T_g ranging from 206 to 81 °C, without compromising thermal stability.

Jessewitsch, T.; Demeler, A. K..; Delaittre, G. submitted for publication.

Author contributions: T.J. contributed ideas, performed all syntheses and most characterization with contribution of A.K.D. in preliminary investigations. G.D. originated the concept. T.J. and G.D. analyzed the data and wrote the manuscript.

4.1. Introduction

Polyurethanes (PUs) represent one of the most important classes of polymeric materials due to their outstanding chemical resistance, toughness, and mechanical strength.[109,191] These properties lead to a large range of applications as bulk materials, films, or foams, in insulating materials, composites, sealants, coatings, and adhesives, for instance.[192,193] Their versatility also originates from the possibility to form materials of opposite properties, such as thermoplastics and thermosets, simply by tuning the functionality of the employed polyols or polyisocyanates, or by using an excess of isocyanate.[193,194] Performance and properties of the polymers are tuned by the chemical nature of the reacting components and the reaction process.[195] Although isocyanate-free protocols are gaining increasing attention, PUs are typically synthesized by reaction of diisocyanates with polyols, specifically diols in the case of thermoplastic PUs.

As for most polymer types, the PU field is in demand for increased sustainability, particularly via biomass feedstocks.[196] Therefore, bio-based diisocyanates have been investigated, e.g., sugar-,[197,198] fatty acid-,[195] and amino acid-based[199] diisocyanates. On the other hand, examples of bio-based polyols based on carbohydrate derivatives[195,200,201] or fatty acids[202,203] are numerous.

In the present study, we explore the incorporation of erythrodiol (olean-12-en-3β,28-diol, **ErDO**) as a diol for thermoplastic PU synthesis. Erythrodiol can be obtained by direct reduction of the related hydroxy acid derivative, oleanolic acid ((3β)-3-hydroxyolean-12-en-28-oic acid, OA). The latter is a pentacyclic triterpenoid found in more than 1600 plant species, including fruits and leaves as well as soya beans, garlic, and olives.[161,162] Despite the numerous pharmacological activities[63] (antitumor[163,204], anti-inflammatory[205], antiviral[206]) of OA, its pharmaceutical use is limited by the low aqueous solubility (< 1 μg/mL) and low bioavailability,[164] therefore rendering the derivatization of OA as an interesting target to achieve novel biologically active molecules.[63] Using OA in materials science would be an alternative utilization, benefiting from its natural availability and eventually from the rigidity of the building block itself. For instance, we recently reported a range of OA-based polymethacrylates exhibiting high glass-transition temperatures.[207] Thermoplastic PUs usually consist of alternating hard and soft segments, whereby hard segments are represented by rigid diisocyanates or short polyols, and soft segments are formed by long polyols or macrodiols providing elasticity.[195] Both segments contribute to

the degree of phase separation, crystallization, and hydrogen bonding of the final polymer.[208] The soft segments commonly used are polyether,[209] polyester,[210] or polycarbonate[211] polyols. The incorporation of erythrodiol in PUs, due to its bulky and chiral pentacyclic structure, should introduce highly rigid segments.

4.2. Results and Discussion

4.2.1. Monomer Synthesis

One of the possible ways to obtain **ErDO** from OA is by esterification with methyl iodide, followed by reduction with diisobutylaluminium hydride (DIBAL-H). For the direct reduction of OA to the diol, DIBAL-H is not suitable, and the use of $LiAlH_4$ is required. The reduction with $LiAlH_4$ proceeds in dry conditions and at elevated temperatures with a yield of 87% after purification (Scheme 4.1). The reaction scale in our study varied from 1 to 4 g of OA. **ErDO** shows high solubility in alcohols such as methanol (MeOH), ethanol (EtOH), and isopropanol (*i*PrOH). It displays, however, moderate solubility in dichloromethane (DCM), ethyl acetate (EtOAc), and aromatic solvents, as well as poor solubility in acetonitrile and cyclohexane.

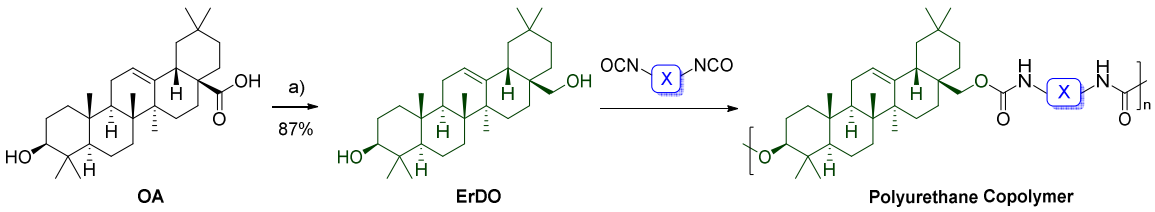

Scheme 4.1. Synthesis of **ErDO** by reduction of OA (a: $LiAlH_4$, THF, 50 °C, 16 h), and its subsequent polymerization with diisocyanates.

4.2.2. Catalyst Selection

For the polyreaction of diols with diisocyanates, elevated temperatures up to 120 °C are favorable to increase conversion. Toluene is often considered as a solvent, yet the solubility of **ErDO** and the corresponding PUs is not sufficient. Consequently, chlorobenzene (PhCl) was first used to avoid precipitation at extended polymerization times, allowing us to

compare the effect of the catalyst on the polyaddition. In the course of this study, the green solvent anisole (PhOMe)[212] was also found to be a good replacement.

Catalysts for the synthesis of PUs reach from metal-based compounds (Sn, Hg, Bi, Al, Zr, Zn) to organic bases (1,4-diazabicyclo[2.2.2]octane, 1,8-diazabicyclo[5.4.0]undec-7-ene) and strong acids (sulfonic acids, phosphonic acids).[213] Since it was observed that very strong acids such as triflic acid (TfOH) and sulfuric acid lead to the dehydration of the secondary alcohol in **ErDO**, the investigated catalysts were the ubiquitous 1,8-diazabicyclo[5.4.0]undec-7-ene (DBU), $Sn(Oct)_2$, as well as zinc diethyldithiocarbamate (ZDTC), which was found to yield high-molecular-weight PUs by polyaddition of hexamethylene diisocyanate (HDI) with polyethylene and polypropylene glycols.[214]

HDI was chosen as the diisocyanate, as it may function as a flexible spacer between the rigid **ErDO** units. After reacting at 110 °C overnight in PhCl, $Sn(Oct)_2$ showed the best catalytic performance leading to a broad polymer distribution (M_n = 8.3 kg/mol, $Đ$ = 2.96; SEC in *N*,*N*-dimethylacetamide (DMAc) with a PMMA calibration, if not stated otherwise) with a low-molecular weight shoulder (M_n = 1.3 kg/mol, V_r = 33.4 mL) (Figure 4.1). This shoulder is most likely resulting from the bulky **ErDO** structure and its less reactive secondary alcohol. Moreover, aliphatic diisocyanates like HDI are less reactive compared to aromatic ones. Catalysis by DBU is less efficient, leading to M_n = 4.0 kg/mol with an intense oligomer-peak at 1.3 kg/mol. Similar behavior was observed for ZDTC (M_n = 3.2 kg/mol), where the SEC trace depicted a typical oligomer distribution. The trace of the Zn-catalyzed polyaddition shows remaining monomer, verified by the single injection of **ErDO** (442.7 g/mol) in the SEC system (M_n = 360 g/mol, V_r = 34.7 mL). It further indicates that the species with M_n = 1.3 kg/mol might be the dimer $[ErDO\text{-}HDI]_2$, rather than the unreacted monomer.

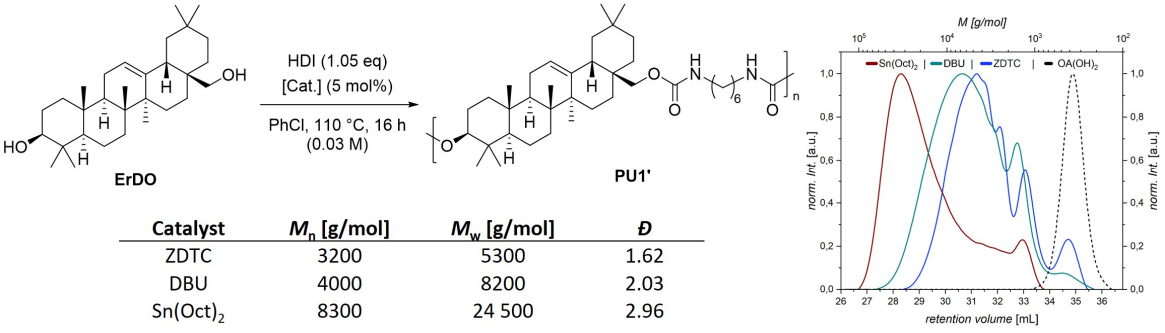

Catalyst	M_n [g/mol]	M_w [g/mol]	$Đ$
ZDTC	3200	5300	1.62
DBU	4000	8200	2.03
$Sn(Oct)_2$	8300	24 500	2.96

Figure 4.1. Experimental conditions and SEC results for the polyaddition of **ErDO** and HDI (dried raw mixtures, redissolved in DMAc + LiBr).

To further increase the conversion with DBU, the polyaddition was performed for 2 days at 110 °C in PhOMe. In Figure 4.2, analysis by SEC shows that molecular weights such as those obtained with $Sn(Oct)_2$ can be achieved with DBU at elongated reaction times. The experiments were repeated with pentamethylene diisocyanate (PDI), a bio-based, glucose-derived diisocyanate, showing almost identical results to those with HDI. P(ErDO-*co*-PDI) could be synthesized with M_n = 10 kg/mol ($Sn(Oct)_2$, 90 °C, 16 h or DBU, 110 °C, 48 h). After evaporating PhOMe, the polymer distributions obtained from SEC were very broad, reaching dispersity values around 5, yet still showing the dimeric species (M_n = 1.3 kg/mol), despite the dry reaction conditions. It is important to highlight that DBU may lead to undesired side products, since it can catalyze the formation of allophanates (by reacting with urethanes) and isocyanurates (by trimerization of isocyanates).[215] The bulkiness and low reactivity of the secondary alcohol of **ErDO** may slow down polyaddition, leading to the accumulation of free isocyanates and favoring side reactions.

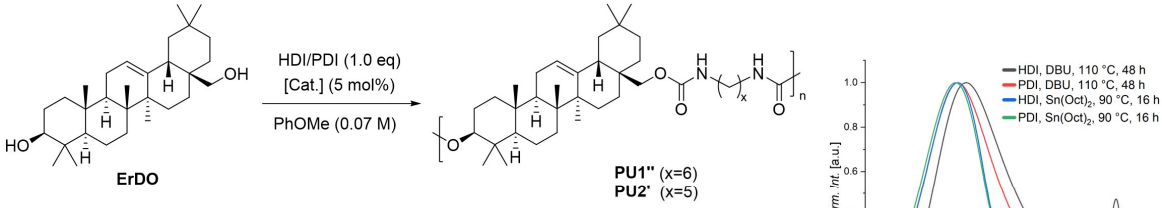

Catalyst	Diisocyanate	Conditions	M_n [g/mol]	M_w [g/mol]	$Đ$
DBU	HDI	110 °C, 48 h	8800	35 400	4.01
	PDI		10 400	50 000	4.76
$Sn(Oct)_2$	HDI	90 °C, 16 h	11 200	53 500	4.77
	PDI		10 000	55 000	5.48

Figure 4.2. Experimental conditions and SEC results for the polyaddition of **ErDO** and HDI or PDI in PhOMe (dried raw mixtures, redissolved in DMAc + LiBr).

4.2.3. Polymer Synthesis

Since $Sn(Oct)_2$ performs best regarding molecular weight and reaction time, it was used to synthesize and purify four different PUs based on **ErDO** with HDI, PDI, H_{12}MDI, and 4,4'-MDI, as shown in Scheme 4.2. Here, 4,4'-diisocyanato dicyclohexylmethane (H_{12}MDI) and 4,4'-methylene diphenyl diisocyanate (MDI) were chosen as diverse aliphatic and aromatic spacer units.

The polyadditions were performed in PhOMe (0.07 M) at 90 °C for 16 h under dry conditions, using an NCO/OH ratio of 1.00:1.00. Notably, when searching for the perfect stoichiometry, ratios of 1.05:1.00 or 0.95:1.00 did not lead to significant differences in

molecular weight. In fact, a larger excess of NCO led to gelation caused by a large reduction of solubility and/or the possibility of crosslinking by forming allophanate/isocyanurate linkages. NCO groups potentially remaining after the polymerization were deactivated with ethanol before solvents were removed under reduced pressure.

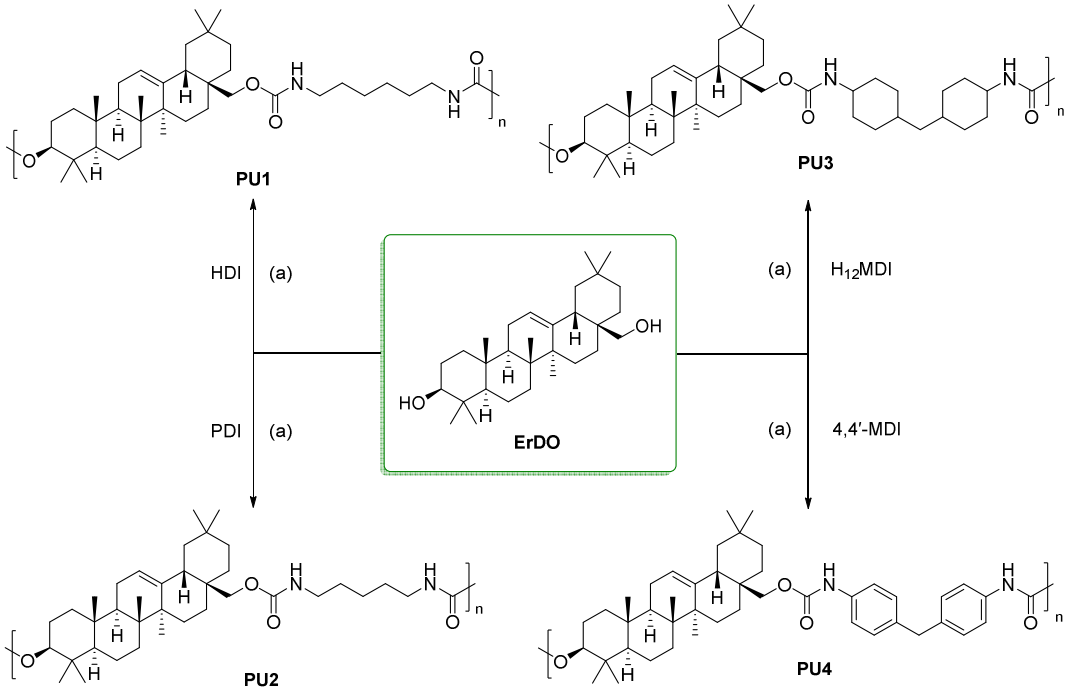

Scheme 4.2. Synthesis of polyurethanes **PU1**–**4**: (a) Diisocyanate (1.0 eq), $Sn(Oct)_2$ (5 mol%), PhOMe (0.07 M), 90 °C, 16 h.

4.2.4. Characterization

SEC analysis (Figure 4.3) revealed anew the presence of dimer species for PUs made from HDI and PDI. Although $H_{12}MDI$ is less reactive, **PU3** shows a more uniform distribution. All polymers were subsequently washed with hot ethanol using Soxhlet extraction to remove the catalyst and remaining PhOMe. The extraction yields PUs essentially free of oligomers, with a uniform distribution and dispersity lying between 1.9–2.5. **PU1**–**4** could be isolated in high yields between (68–97%), suggesting low amounts of oligomers or small molecules at the end of the polymerization. The achieved average molecular weight M_n for **PU1**, **PU2**, and **PU4** measured by SEC in DMAc lies in the range of 21–39 kg/mol. Note that the SEC results are based on a single RI detection with a PMMA calibration and therefore do not correspond to absolute values. **PU3** was unexpectedly insoluble in DMAc but could be dissolved in THF. Single-detection SEC in THF delivered M_n = 43 kg/mol (PS

calibration). Overall, catalysis by $Sn(Oct)_2$ worked efficiently, even with $H_{12}MDI$, the least reactive of the used diisocyanates.

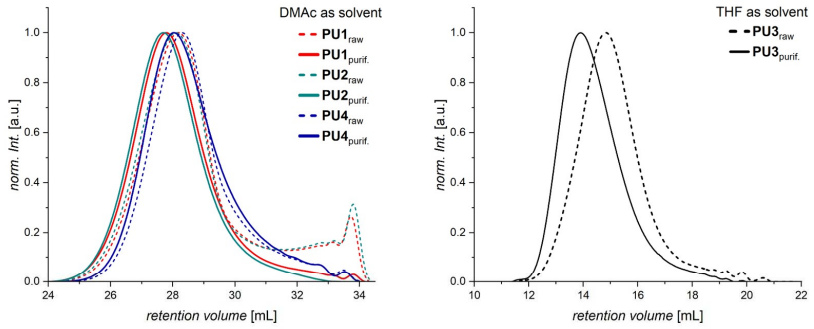

Polymer	Yield	M_n [g/mol]	M_w [g/mol]	$Đ$	DP_n
PU1	85%	27 700	68 500	2.47	45
PU2	68%	38 700	73 300	1.89	65
PU3	92%	43 000*	102 000*	2.38*	61
PU4	97%	21 300	52 900	2.48	31

Figure 4.3. Average molecular weight and SEC profiles of **PU1**–**4** before and after extraction (DMAc as eluent, PMMA calibration; ***PU3**: SEC with THF as eluent, PS calibration).

The polymers have a very low solubility in many common solvents (MeOH, EtOH, acetone, *i*PrOH, DCM, EtOAc, chloroform, diethyl ether) at ambient temperature, likely due to hydrogen bonding, which is characteristic of PUs, combined with the rigid, apolar triterpenoid building block of OA. Therefore, NMR analysis was performed in deuterated 1,1,2,2-tetrachloroethane (TeCA-d_2) at 80 °C to achieve a low signal-to-noise ratio. In Figure 4.4, only signals distinct from those associated with the methyl, methylene, and methine groups of the OA motif (2.20–0.70 ppm) are labeled. The internal double bond (DB) remains intact (5.26−5.23 ppm, H-12) during polymerization and purification, with its associated chemical shift varying only slightly. Signals arising from the urethane proton (N*H*) can be found between 4.60−4.25 ppm for the aliphatic PUs. In contrast, for **PU4**, the adjacent aromatic units generate a uniform NH_{ar} signal shifted downfield at 6.45 ppm. Here, it should be mentioned that all characteristic signals in **PU4** arising from the triterpenoid motif are also shifted downfield due to aromatic electron-withdrawing effects.

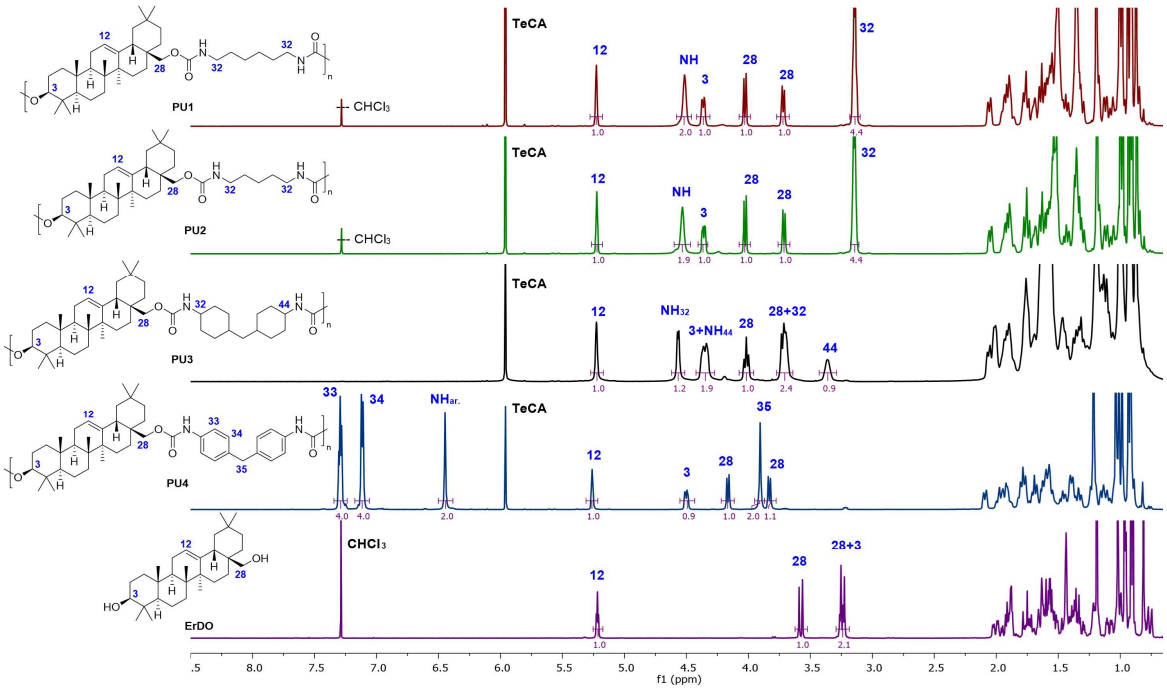

Figure 4.4. Structures of **PU1**–**4** and the corresponding ^{1}H NMR spectra (TeCA-d_2, 80 °C, except for **ErDO**: $CDCl_3$, 25 °C).

The shift of H-3 from 3.22 to 4.20–4.50 ppm evidences the transformation of the secondary alcohol to a urethane. In a similar way, the signals of the methylene group H-28 shift slightly downfield and partially keep their coupling pattern of two separate doublets. Because of the chiral center at C-17, the protons are diastereotopic and one of them is spatially closer to the oxygen atom, and thus more deshielded. **PU3** constitutes a special case: The methine groups neighboring the urethane are not chemically equivalent and yield two separate signals at 3.70 ppm (H-32) and 3.36 ppm (H-44), proving that the three-dimensional structure of the two cyclohexane rings is asymmetrical. The different coupling between each N*H*-C*H*, which can be seen in the ^{1}H-^{1}H COSY spectrum, is illustrated in Figure 8.35 in the Appendix. This behavior is already known for the biscarbamate obtained from H_{12}MDI and two molecules of *n*-butanol.[208] Further, it should be noted that the two different hydroxyl groups of the chiral **ErDO** lead to the formation of urethane linkages with slightly different environments, materializing through the appearance of two urethane signals in the ^{13}C NMR spectra (Figures 8.30, 8.32, and 8.34).

The binary PUs were further analyzed in the solid state by ATR-FTIR spectroscopy, whereby the overlayed spectra are displayed in Figure 4.5. The first noticeable information is the absence of bands in the region of N=C=O vibrations (2270–2200 cm^{-1}). This is expected, as even low-reactive residual NCO end-groups should have been capped during

EtOH quenching at the end of the polymerization or at the latest during Soxhlet extraction. In the region for N-H stretching vibrations (ν), two very small bands at 3455 and 3337 cm^{-1} are assigned to urethane linkages. This can be explained by the formation of H-bonds of varying strength, because strongly H-bonded NH-groups require lower energy to vibrate. This matches with the stronger absorption band at the lower wavenumber of 3337 cm^{-1}, showing that most urethane groups form H-bonds. Consequently, the smaller band at 3455 cm^{-1} arises from weakly H-bonded or even free NH-groups,[216] possibly due to steric hindrance of the OA skeleton as well as the various modes of incorporation (head-to-tail, head-to-head, or tail-to-tail) leading to distinct urethane linkages.

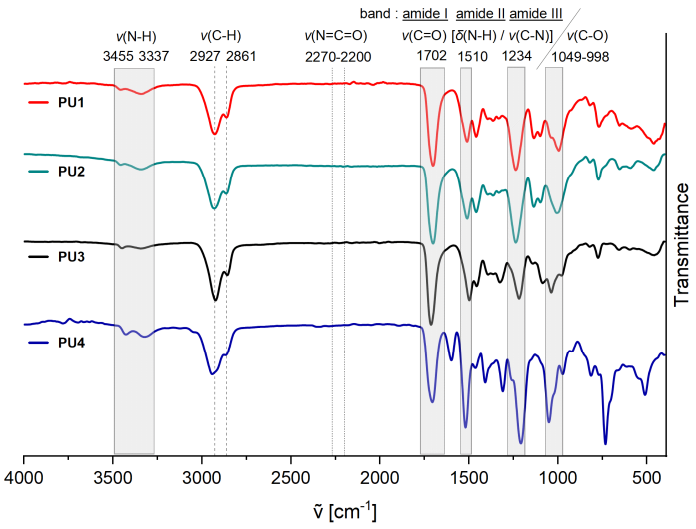

Figure 4.5. ATR-FTIR spectra of **PU1–4**.

PU4 carries MDI as an aromatic urethane spacer, leading to bands with slightly higher or lower wavenumbers depending on the electronic effect of the aromatic core on the specific bond. The N-H stretching vibrations appear slightly shifted to lower wavenumbers, indicating a strengthening of the N-H bonds. The aliphatic C-H vibration shifts to 2948 cm^{-1}, whereas the aromatic vibration is barely detectable at 3049 cm^{-1}. This might originate from the nature of the ATR technique, where bands at higher wavenumbers are less pronounced due to the shorter effective path length compared to transmission IR spectroscopy. Nevertheless, the aromatic ν(C=C) band is visible at 1595 cm^{-1}, next to the ν(C=O) band. The strong absorption from the carbonyl group ν(C=O) (namely amide I band) occurs at 1702 cm^{-1} for **PU1–4**. All polymers exhibit the characteristic amide II and III bands consistent for PUs, highlighted at 1510 and 1234 cm^{-1}, respectively.[208,217] Additionally, the ν(C-O) band is present between 1049 and 998 cm^{-1}, which in combination with the amide bands proves the urethane linkage.

Thermogravimetric analysis of **PU1–4** was performed to establish thermal stability (Figure 4.6). The OA-based PUs are stable until 280 °C and are fully decomposed at temperatures around 500 °C. They all display a similar degradation pattern, with two main processes clearly identifiable in the DTG profiles (Figure 4.6, right). The first event is centered around 332–336 °C and starts around 250–270 °C, as in the case of OA and **ErDO**, suggesting the involvement of the triterpenoidic motif. The second process occurs around 432–444 °C, independently of the used diisocyanate. It is assumed that traces of $Sn(Oct)_2$ are responsible for the degradation behavior, even if the catalyst was expected to be removed after precipitation and Soxhlet extraction with EtOH. This instability caused by the catalyst does not appear when ZDTC was used instead, which most likely could be removed completely (*vide infra*).

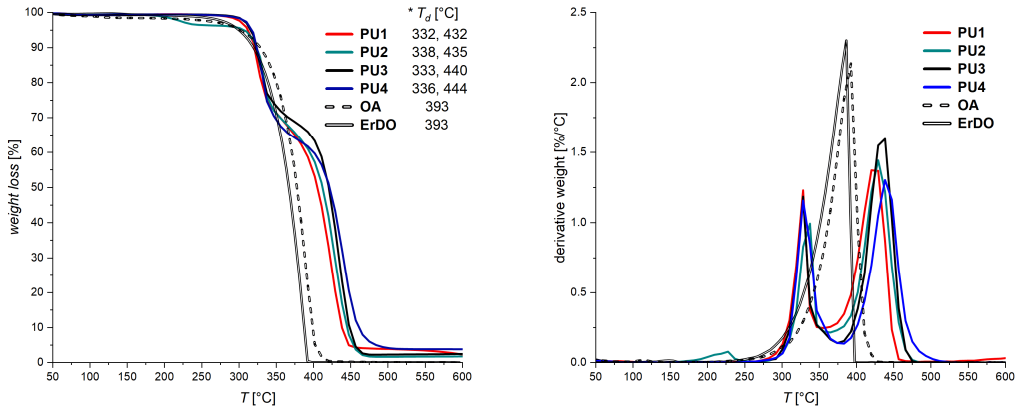

Figure 4.6. TGA and DTG profiles of **PU1–4** (*T_d refers to the point of inflection).

The thermal instability caused by $Sn(Oct)_2$ is also reflected in differential scanning calorimetry (DSC) measurements. Five successive heating-cooling cycles applied to **PU1** in the 25–240 °C range yielded decreasing T_g values (198, 191, 185, 177, and 170 °C – see Figure S4.3, left). To understand this process, **PU1** was first annealed at 240 °C for 4 h. Subsequent SEC analysis revealed a broadening in dispersity from 2.47 to 2.98 with increasing M_w from 69 to 82 kg/mol, while M_n remained constant at 27 kg/mol (Figure S4.3, right). This change in molecular weight was ascribed to transurethanization processes altering the polymer structure and the thermal properties. If DSC analysis of **PU1** is repeatedly performed only until 215 °C, each heating-cooling cycle yields a constant T_g value of 198 °C, which in the context of linear PUs would place it in the upper range. With a slightly smaller linear aliphatic domain, PDI-based **PU2** with five methylene units instead of six shows an increased T_g at 206 °C, arising from slightly reduced chain flexibility. By incorporation of the bulky and rigid H_{12}MDI or MDI in the polymer backbone, T_g was even

increased to 249 °C (**PU3**) and 253 °C (**PU4**). It should be pointed out that the aromatic MDI is indeed more rigid, with less rotational freedom compared to H_{12}MDI with cyclohexane rings. On the one hand, a larger difference in T_g could be expected. On the other hand, **PU4** already starts decomposing at 270–280 °C.

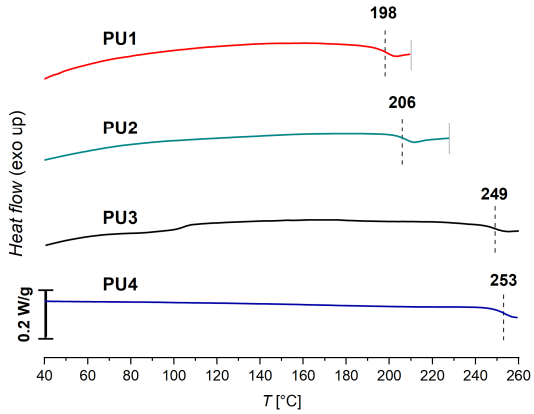

Figure 4.7. DSC heating curves of **PU1–4.**

4.2.5. Tuning Properties by Incorporation of 1,6-Hexanediol

The glass-transition temperatures of **PU1–4** are very high, close to the decomposition temperature. Therefore, the incorporation of another potentially bio-based flexible diol, namely 1,6-hexanediol (HDO), in combination with **ErDO** was envisioned. PDI was selected as the diisocyanate in order to propose a series of fully bio-based ternary PUs (Scheme 4.3).

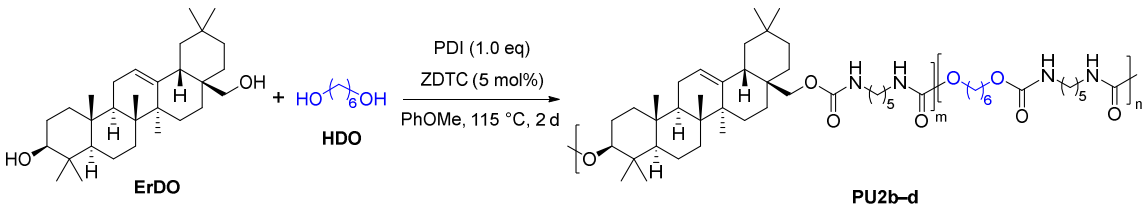

Scheme 4.3. Synthesis of polyurethanes with increasing content of HDO (in PhOMe, 0.1 M).

Since $Sn(Oct)_2$ could not be removed after polymerization of **PU1–4** (*vide infra*), ZDTC was used for further reactions. It needs to be highlighted that the catalytic activity of ZDTC towards the secondary alcohol of **ErDO** is significantly lower compared to that of the tin catalyst. This result seems contrary to some reports, for instance, when the copolymerization of polyether diols with HDI in toluene led to polymers with higher molecular weights using ZDTC instead of a similar tin catalyst.[214] To reach the high

conversions essential for step-growth polymerization, the polyaddition of **ErDO** and HDO with PDI was performed with ZDTC at 115 °C for 2 days in PhOMe (0.1 M). Figure 4.8 shows the ^{1}H NMR spectra corresponding to the copolymer synthesis with a molar ratio **ErDO**:HDO 30:70, after 24 and 48 h revealing a conversion of 90% and > 99%, respectively, according to the C*H*$_2$NCO signal at 3.32 ppm in comparison to the signal at 3.29 ppm of unreacted PDI itself. Simultaneously, SEC analysis reveals an increase in M_n from 7.1 to 23 kg/mol for the unpurified polymer **PU2d**.

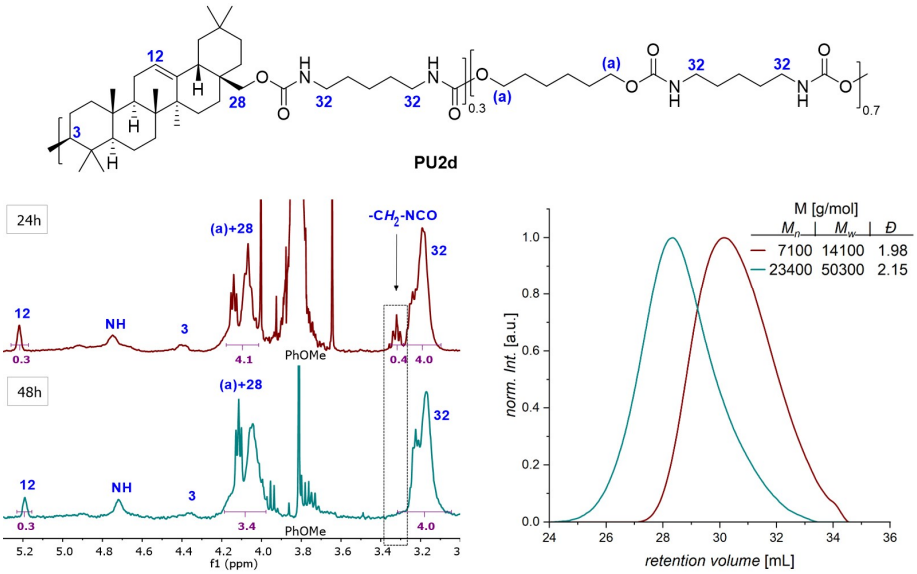

Figure 4.8. (Top) Structure of ternary polyurethane **PU2d** (conditions: ZDTC 5 mol%, PhOMe 0.1 M, 115 °C). (Bottom, left) ^{1}H NMR spectra of the unpurified copolymer at 24 and 48 h. (Bottom, right) Corresponding SEC chromatograms.

A series of experiments with varying **ErDO**:HDO ratios was performed, from 70:30 (**PU2a** and **PU2b**) to 0:100 (**PU2e**, i.e., HDO-PDI binary PU) (Table 4.1). The polymers were precipitated in cold MeOH and washed with hot MeOH using Soxhlet extraction, providing yields between 59 and 98%. A comparison of the ^{1}H NMR spectra can be found in the SI (Figure S4.2). Note that the introduced HDO does not alter the chemical shifts arising from the ErDO-PDI block already displayed in Figure 4.4. ^{1}H NMR peak integration provides the amount of **ErDO** incorporated in the polymer backbone by comparing the alkenyl signal (H-12, 5.22 ppm) to the signal originating from the methylene group of PDI units adjacent to the urethane (H-32, 3.14 ppm). The calculated percentages of **ErDO** lie rather close to the targeted ratios.

SEC analysis in DMAc of the purified polymers showed a uniform distribution with M_n ranging from 14 to 28 kg/mol, except for **PU2e**, exhibiting a small oligomer population (Table 4.1). While the tin-catalyzed polyaddition with 30 mol% HDO led to an increase of

the polymerization degree from 65 (**PU2**) to 196 (**PU2a**), which may be the result of an increased ratio of reactive primary alcohols over secondary alcohols and an increased chain flexibility, this effect was not observed with the zinc catalyst.

Table 4.1. Experimental parameters and results for the synthesis of ternary PDI-based polyurethanes with varying compositions in **ErDO** and HDO.

	[ErDO]:([ErDO]+[HDO])				*M* [g/mol]			
	Target	Exp.	Catalyst [1]	Yield [2]	M_n	M_w	$Đ$	DP_n
PU2	100	100	$Sn(Oct)_2$	68%	38 700	73 300	1.89	65
PU2a	70	65		98%	94 500	236 000	2.50	196
PU2b	70	69	ZDTC	98%	28 400	83 700	2.94	57
PU2c	50	54		59%	23 500	49 300	2.10	53
PU2d	30	33		60%	34 400	65 100	1.89	91
PU2e	0	0		76%	13 500	37 800	2.80	50

[1] $Sn(Oct)_2$ 5 mol%, PhOMe, 90 °C, 16 h; ZDTC 5 mol%, PhOMe, 115 °C, 48 h, except **PU2e**: DMAc, 90 °C, 16 h.
[2] Isolated yield after extraction.

IR analysis revealed that the vibrational band for the free or weakly H-bonded –NH motifs at 3455 cm^{-1} disappears with decreasing **ErDO** content. Concomitantly, the band at 3337 cm^{-1} accounting for stronger H-bonded –NH motifs intensifies, as does the deformation vibration band at 1510 cm^{-1} (Figure 4.9). This increased IR activation arises from an enhanced change of dipole moment and points towards more H-bonding, which is ascribed to increased flexibility through HDO incorporation.

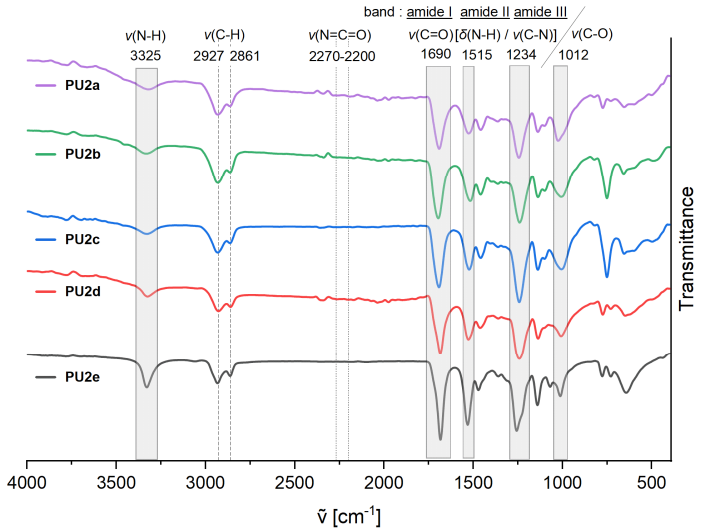

Figure 4.9. ATR-FTIR spectra of **PU2a–e**.

During the investigation of the thermal properties of these terpolyurethanes, the influence of the employed catalyst on the stability was established. TGA and DTG profiles are displayed in Figure 4.10. Only the terpolymer obtained with $Sn(Oct)_2$ (**PU2a**) displays two

separate degradation processes at 314 and 434 °C, respectively, as in the case of the earlier described binary PUs obtained with $Sn(Oct)_2$ (and no HDO). Importantly, **PU2b**, the polymer with the same comonomer composition but obtained with ZDTC, only shows one. Therefore, this different degradation mode must be linked to the remaining catalyst. Additionally, $Sn(Oct)_2$ may favor the creation of HDO-PDI sequences since the first degradation event of **PU2a** clearly overlaps with the only degradation process of **PU2e**, containing no **ErDO** and obtained with ZDTC. Also, while **PU2e** shows a lower thermal stability compared to all ternary ErDO-containing PUs (T_d = 339 °C vs 366–379 °C), the HDO content seems to play a minor role.

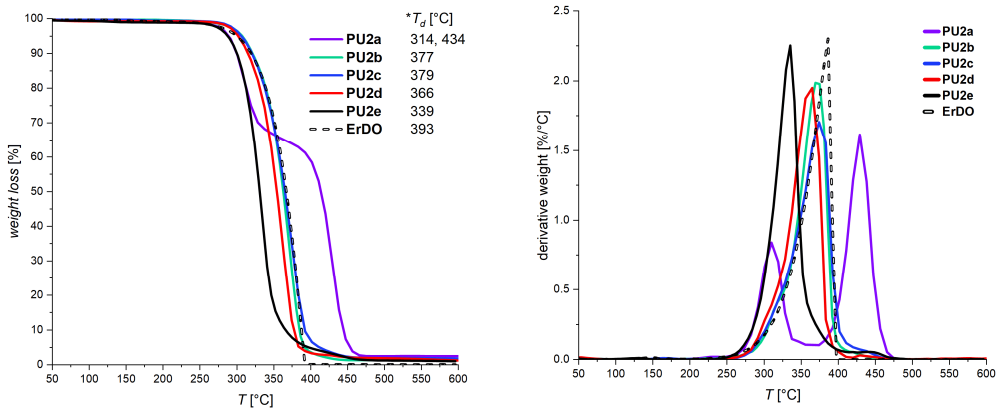

Figure 4.10. TGA and DTG profiles of **P2a**–**e** (*T_d refers to the point of inflection).

In contrast, Figure 4.11 illustrates a clear decreasing trend in T_g with increasing HDO content, as expected. The high T_g of **PU2** (206 °C) could be efficiently reduced to 147, 119, and 81 °C by raising the HDO fraction to 30, 50, and 70 mol%, respectively. As a comparison, **PU2e**, devoid of **ErDO** units, exhibits a low T_g at 18 °C and is semicrystalline, with two melting points (T_{m1} = 131 °C, T_{m2} = 148 °C), suggesting the presence of two crystalline domains. This also implies that if the incorporation of HDO-PDI segments is favored by the tin catalyst, these sequences must be short because **PU2a** is purely amorphous. In summary, the glass transition of the ErDO-PDI bio-based PUs could be tuned in a broad range spanning over 125 °C by introducing various amounts of HDO. Therefore, the occurrence of stronger H-bonding seems to be overcome by the presence of a flexible C_6 spacer.

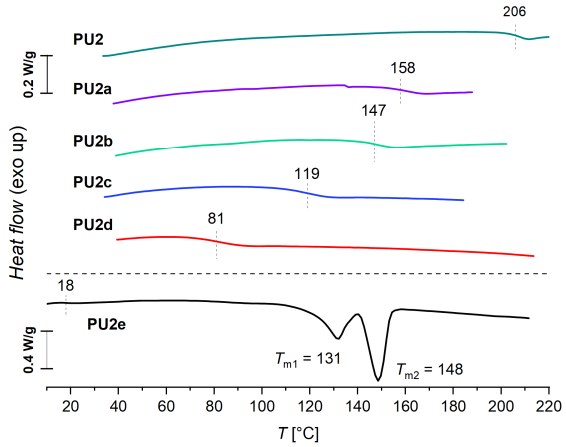

Figure 4.11. DSC heating curves for **PU2a**–**e** (10 °C/min).

4.3. Conclusion

Novel polyurethanes could be synthesized using erythrodiol, a diol obtained by simple reduction of naturally occurring oleanolic acid (OA). The effect of three catalysts (tin octoate, zinc diethyldithiocarbamate, and DBU) on the polymerization of erythrodiol with hexamethylene diisocyanate was investigated, reaching the best outcome with the tin catalyst. The low reactivity of the secondary alcohol of erythrodiol led to the presence of low-molecular-weight products when aliphatic linear diisocyanates were employed. This was not the case with the highly reactive methylene diphenyl diisocyanate and its hydrogenated, non-aromatic counterpart. The corresponding binary polyurethanes possess reasonably high molar masses (M_n = 21–43 kg/mol), good thermal stability (onset of decomposition around 310 °C), and high glass-transition temperatures (T_g ≈ 200–250 °C) arising from the rigid OA motif. The thermal properties could be further tuned by incorporating 1,6-hexanediol (HDO), another potentially bio-based yet flexible diol. Glass-transition temperatures ranging from 206 to 81 °C with increasing HDO content were imparted. Polymers containing HDO were synthesized using zinc diethyldithiocarbamate (ZDTC) as a catalyst. Indeed, while it is assumed that tin octoate traces remain even after Soxhlet extraction and alter the thermal stability, no such issues were observed when using ZDTC. In the future, a comparative study with betulin as an abundant constitutional diol isomer of erythrodiol would be of interest. Functionalization of the OA motif pre- or post-polymerization, particularly via the C=C double bond, should also be envisaged as a way to tune material properties and possibly lead to bio-based PU thermosets.

4.4. Experimental Procedures

Erythrodiol (ErDO)

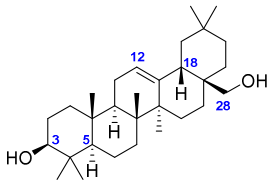

ErDO

Oleanolic acid (4.45 g, 9.74 mmol, 1.0 eq) was dried *in vacuo* prior to dissolution in dry THF (195 mL, 0.05 M). Subsequently, lithium aluminum hydride powder (1.55 g, 40.9 mmol, 4.2 eq) was added through the sleeve in one portion. The reaction mixture was heated to reflux for 1 hour under continuous stirring. Afterwards, the reaction mixture was stirred at 50 °C overnight. While cooling on ice, the reaction mixture was carefully quenched with a saturated aq. potassium sodium tartrate solution. After resolving the emulsion, ethyl acetate was added. The organic phase was separated, washed with water and brine, dried over $MgSO_4$, filtered, and concentrated *in vacuo*. Purification of the resulting raw product by flash chromatography (SiO_2, CH/EA 98/02 → 70/30) yielded **ErDO** as a white powder after solvent evaporation (3.60 g, 8.52 mmol, 87%).

^{1}H NMR (400 MHz, $CDCl_3$): δ [ppm] = 5.19 (t, J = 3.7 Hz, 1H, H_{12}), 3.55 (d, J = 11.0 Hz, 1H, H_{28}), 3.26 – 3.18 (m, 1H, H_3), 3.21 (d, J = 11.1 Hz, 1H, H_{28}), 1.98 (dd, J = 13.7, 4.6 Hz, 1H, H_{18}), 1.94 – 1.83 (m, 3H), 1.78 – 1.24 (m, 14H), 1.22 – 1.13 (m, 2H), 1.16 (s, 3H), 1.06 (ddd, J = 13.4, 4.7, 2.4 Hz, 1H), 0.99 (s, 3H), 1.02 – 0.95 (m, 2H), 0.94 (s, 3H), 0.93 (s, 3H), 0.88 (s, 3H), 0.87 (s, 3H), 0.79 (s, 3H), 0.73 (dd, J = 11.6, 1.9 Hz, 1H, H_5).

^{13}C{^{1}H} NMR (101 MHz, $CDCl_3$): δ [ppm] = 144.4, 122.5, 79.1, 69.8, 55.3, 47.7, 46.6, 42.5, 41.9, 39.9, 38.9, 38.7, 37.1, 37.1, 34.2, 33.3, 32.7, 31.2, 31.1, 28.2, 27.4, 26.1, 25.7, 23.7, 23.7, 22.1, 18.5, 16.9, 15.7, 15.7.

FTIR (ATR): $\tilde{\nu}$ [cm^{-1}] = 3334 (w), 2945 (s), 2930 (s), 2869 (s), 1465 (m), 1361 (m), 1043 (s), 1003 (s).

HRMS (ESI): $[M+H]^+$ *m/z* 443.3881 (calculated for $C_{30}H_{51}O_2^+$: *m/z* 443.3884),
$[M+Na]^+$ *m/z* 465.3701 (calculated for $C_{30}H_{50}O_2Na^+$: *m/z* 465.3703).

TGA (Ar): $T_{d5\%}$ = 299 °C.

Polymers based on erythrodiol and HDI (PU1')

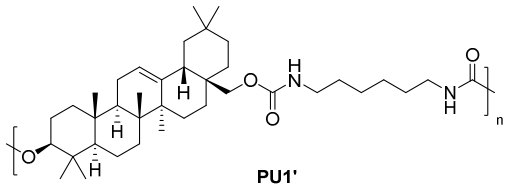

PU1'

ErDO (157 mg, 355 µmol, 1.0 eq) was dissolved in dry PhCl (12 mL, 0.03 M) by moderate heating. Subsequently, one of the catalysts – $Sn(Oct)_2$ (5.7 µL, 17.7 µmol, 0.05 eq), ZDTC (6.4 mg, 17.7 µmol, 0.05 eq), or DBU (2.7 µL, 17.7 µmol, 0.05 eq) – was added as a solution in dry PhCl (0.09 M), followed by the addition of HDI (60 µL, 372 µmol, 1.05 eq). The reaction solution was stirred at 110 °C overnight, whereby remaining NCO groups were end-capped by the addition of 0.3 mL EtOH and further stirring for 20 min. The solvents were removed *in vacuo*, and a sample was collected for SEC analysis in DMAc.

Catalyst	M_n [g/mol]	M_w [g/mol]	$Đ$
ZDTC	3200	5300	1.62
DBU	4000	8200	2.03
$Sn(Oct)_2$	8300	24 500	2.96

Polymers based on erythrodiol and HDI (PU1'') or PDI (PU2')

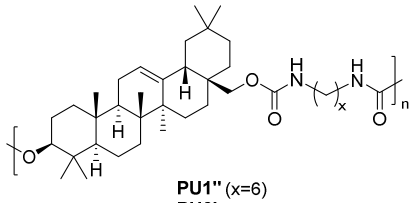

PU1'' (x=6)
PU2' (x=5)

ErDO (1.0 eq) was dissolved in dry anisole (0.07 M) by moderate heating. Subsequently, one of the catalysts – $Sn(Oct)_2$ (0.05 eq) or DBU (0.05 eq) – was added as a solution in dry anisole (0.09 M), followed by the addition of HDI (1.0 eq) resp. PDI (1.0 eq). The two reaction solutions with $Sn(Oct)_2$ were stirred at 90 °C overnight, while the two solutions with DBU were stirred at 110 °C for 2 days. After deactivation of remaining NCO with EtOH (0.3 mL), the solvents were removed *in vacuo*, and a sample was collected for SEC analysis in DMAc.

Catalyst	Diisocyanate	Conditions	M_n [g/mol]	M_w [g/mol]	$Đ$
DBU	HDI	110 °C, 48 h	8800	35 400	4.01
	PDI		10 400	50 000	4.76
$Sn(Oct)_2$	HDI	90 °C, 16 h	11 200	53 500	4.77
	PDI		10 000	55 000	5.48

General procedure for synthesis of PU1–4 (A1)

ErDO (1.0 eq) was dissolved in dry anisole (0.07 M) by moderate heating. $Sn(Oct)_2$ (0.05 eq) was added as a solution in anisole (0.09 M), followed by the addition of diisocyanate (1.0 eq). The reaction solution was stirred at 90 °C overnight. Afterwards, the remaining NCO groups were end-capped with EtOH (0.3 mL) by stirring the solution for a further 20 min. The solvents were removed under reduced pressure, and a sample was collected for SEC analysis prior to purification by procedure B1.

General procedure for synthesis of PU2b–d (A2)

ErDO (X eq), 1,6-hexanediol (1-X eq), and ZDTC (0.05 eq) were dissolved in dry anisole (0.1 M). Followed by the addition of PDI (1.0 eq), the reaction solution was stirred at 115 °C for 2 days. Remaining NCO groups were end-capped by the addition of EtOH (0.3 mL) and subsequent stirring. The solvents were removed under reduced pressure, and a sample was collected for SEC analysis. The polymer was further purified according to procedure B1.

General procedure for purification (B1)

The dried polymer was dissolved in hot chloroform and precipitated in cold methanol (-20 °C). After filtration, the polymers were purified by Soxhlet extraction overnight with hot ethanol (**PU1–4**) or hot methanol (**PU2a–d**) to remove oligomers and the catalyst (traces of $Sn(Oct)_2$ remain in polymer). The polyurethanes were collected as solids from the filter, except **PU1**, **PU2**, **PU2a**, and **PU2b**, which entered the pores of the filter paper. They were therefore redissolved in chloroform from the Soxhlet extractor, concentrated, and dried *in vacuo*.

Poly(1,6-diisocyanatohexane-*alt*-erythrodiol) (PU1)

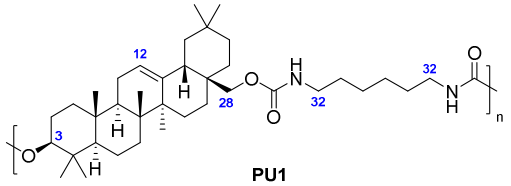

PU1

PU1 was prepared from **ErDO** (247 mg, 558 µmol, 1.0 eq), HDI (89.6 µL, 558 µmol, 1.0 eq), and $Sn(Oct)_2$ (9.0 µL, 27.9 µmol, 0.05 eq) in anisole (8.0 mL, 0.07 M) at 90 °C (16 h) according to procedures A1/B1 and obtained as transparent flakes (290 mg, 475 µmol, isolated yield 85%).

^{1}H NMR (600 MHz, $C_2D_2Cl_4$): δ [ppm] = 5.23 (br. s, 1H, H_{12}), 4.51 (br. s., 2H, N*H*), 4.36 (dd, J = 11.5, 4.5 Hz, 1H, H_3), 4.03 (d, J = 10.7 Hz, 1H, H_{28}), 3.72 (d, J = 10.8 Hz, 1H, H_{28}), 3.19 – 2.31 (m, 4H, H_{32}), 2.15 – 0.71 (m, 52H).

^{13}C{^{1}H} NMR (151 MHz, $C_2D_2Cl_4$): δ [ppm] = 157.1, 156.9, 144.1, 123.0, 81.7, 71.3, 55.9, 48.0, 46.7, 43.0, 42.2, 41.4, 41.3, 40.3, 38.9, 38.3, 37.2, 36.5, 34.5, 33.3, 33.1, 31.8, 31.0, 30.3, 30.3, 28.4, 26.6, 26.6, 26.2, 26.0, 24.3, 24.0, 23.9, 23.0, 18.6, 17.2, 17.0, 15.7.

FTIR (ATR): $\tilde{\nu}$ [cm^{-1}] = 3457 (vw), 3342 (vw), 2926 (m), 2861 (m), 1698 (s), 1511 (m), 1462 (m), 1234 (s), 998 (m).

SEC (DMAc): M_n = 27700 g/mol; M_w = 68500 g/mol; $Đ$ = 2.47.

TGA (Ar): $T_{d5\%}$ = 310 °C. **DSC** (Ar): T_g = 198 °C.

Poly(1,5-diisocyanatopentane-*alt*-erythrodiol) (PU2)

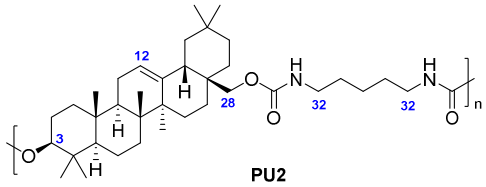

PU2

PU2 was prepared from **ErDO** (233 mg, 527 µmol, 1.0 eq), PDI (75.8 µL, 527 µmol, 1.0 eq) and $Sn(Oct)_2$ (8.5 µL, 26.3 µmol, 0.05 eq) in anisole (7.5 mL, 0.07 M) at 90 °C (16 h) according to procedures A1/B1 and obtained as transparent flakes (215 mg, 360 µmol, isolated yield 68%).

^{1}H NMR (600 MHz, $C_2D_2Cl_4$): δ [ppm] = 5.22 (br. s, 1H, H_{12}), 4.53 (br. s., 2H, N*H*), 4.36 (dd, J = 11.4, 4.7 Hz, 1H, H_3), 4.03 (d, J = 10.7 Hz, 1H, H_{28}), 3.71 (d, J = 10.8 Hz, 1H, H_{28}), 3.20 – 3.10 (m, 4H, H_{32}), 2.10 – 0.77 (m, 50H).

^{13}C{^{1}H} NMR (151 MHz, $C_2D_2Cl_4$): δ [ppm] = 157.0, 156.9, 144.1, 123.0, 81.7, 71.3, 55.9, 48.0, 46.7, 43.0, 42.1, 41.4, 41.3, 40.3, 38.8, 38.3, 37.2, 36.5, 34.5, 33.3, 33.1, 31.8, 31.0, 30.1, 30.1, 28.4, 26.1, 26.0, 24.3, 24.2, 24.0, 23.9, 22.9, 18.6, 17.2, 17.0, 15.7.

FTIR (ATR): $\tilde{\nu}$ [cm^{-1}] = 3457 (vw), 3341 (vw), 2926 (m), 2863 (m), 1700 (s), 1509 (m), 1461 (m), 1237 (s), 1006 (m).

SEC (DMAc): M_n = 38700 g/mol; M_w = 73300 g/mol; $Đ$ = 1.89.

TGA (Ar): $T_{d5\%}$ = 305 °C. **DSC** (Ar): T_g = 206 °C.

Poly(4,4′-methylenebis(cyclohexyl isocyanate)-*alt*-erythrodiol) (PU3)

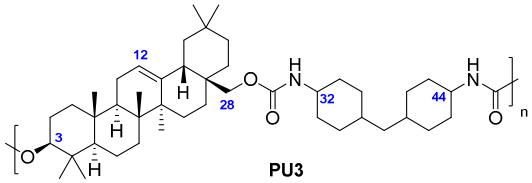

PU3

PU3 was prepared from **ErDO** (237 mg, 535 µmol, 1.0 eq), H_{12}MDI (132 µL, 535 µmol, 1.0 eq) and $Sn(Oct)_2$ (8.7 µL, 26.8 µmol, 0.05 eq) in anisole (7.6 mL, 0.07 M) at 90 °C (16 h) according to procedure A1/B1 and obtained as transparent flakes (347 mg, 492 µmol, isolated yield 92%).

^{1}H NMR (600 MHz, $C_2D_2Cl_4$): δ [ppm] = 5.23 (br. s, 1H, H_{12}), 4.57 (d, J = 7.8 Hz, 1H, NH_{32}), 4.44 – 4.27 (m, 2H NH_{44}+H_3), 4.02 (t, J = 11.2 Hz, 1H, H_{28}), 3.79 – 3.62 (m, 2H, H_{28}+H_{32}), 3.44 – 3.28 (m, 1H, H_{44}), 2.15 – 0.65 (m, 64H).

^{13}C{^{1}H} NMR (151 MHz, $C_2D_2Cl_4$): δ [ppm] = 156.4, 156.2 , 144.1, 123.0, 81.5, 71.2, 55.9, 51.0, 51.0, 48.0, 48.0, 47.8, 46.7, 46.7, 43.1, 43.0, 42.2, 40.3, 38.9, 38.3, 37.2, 36.5, 36.5, 34.5, 33.8, 33.3, 33.1, 33.0, 32.5, 31.8, 31.0, 30.0, 28.6, 28.4, 26.1, 26.0, 24.3, 24.0, 23.9, 23.0, 18.6, 17.2, 17.0, 17.0, 15.7.

FTIR (ATR): $\tilde{\nu}$ [cm^{-1}] = 3449 (vw), 3342 (vw), 2924/2857 (m), 1713 (s), 1498 (m), 1455 (m), 1217 (s), 1039 (m).

SEC (THF): M_n = 43000 g/mol; M_w = 102000 g/mol; $Đ$ = 2.38.

TGA (Ar): $T_{d5\%}$ = 315 °C. **DSC** (Ar): T_g = 249 °C.

Poly(4,4′-methylenebis(phenyl isocyanate)-*alt*-erythrodiol) (PU4)

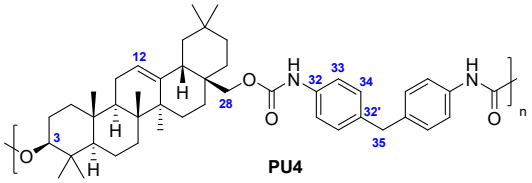

PU4

PU4 was prepared from **ErDO** (236 mg, 533 µmol, 1.0 eq), 4,4′-MDI (133 mg, 533 µmol, 1.0 eq) and $Sn(Oct)_2$ (8.7 µL, 26.6 µmol, 0.05 eq) in anisole (7.6 mL, 0.07 M) at 90 °C (16 h) according to procedure A1/B1 and obtained as a white solid (359 mg, 518 µmol, isolated yield 97%).

^{1}H NMR (600 MHz, $C_2D_2Cl_4$): δ [ppm] = 7.29 (t, J = 7.3 Hz, 4H, H_{33}), 7.12 (d, J = 8.5 Hz, 4H, H_{34}), 6.45 (s, 2H, NH), 5.26 (br. s, 1H, H_{12}), 4.50 (dd, J = 11.4, 4.8 Hz, 1H, H_3), 4.17 (d, J = 10.8 Hz, 1H, H_{28}), 3.91 (s, 2H, H_{35}), 3.83 (d, J = 10.9 Hz, 1H, H_{28}), 2.16 – 0.78 (m, 44H).

^{13}C{^{1}H} NMR (151 MHz, $C_2D_2Cl_4$): δ [ppm] = 154.2, 154.0, 143.9, 136.6 (2C), 136.5 (2C), 129.6 (4C), 123.2, 119.7 (2C), 119.6 (2C), 82.6, 71.9, 55.9, 48.0, 46.7, 43.1, 42.2, 40.8, 40.3, 38.9, 38.3, 37.3, 36.5, 34.4, 33.3, 33.0, 31.8, 31.0, 28.4, 26.2, 26.1, 24.3, 24.0, 23.9, 22.9, 18.6, 17.2, 17.0, 15.7.

FTIR (ATR): $\tilde{\nu}$ [cm^{-1}] = 3429 (vw), 3323 (vw), 2946 (m), 2865 (m), 1704 (s), 1595 (w), 1519 (s), 1459 (w), 1207 (s), 1049 (m).

SEC (DMAc): M_n = 21300 g/mol; M_w = 52900 g/mol; $Đ$ = 2.48.

TGA (Ar): $T_{d5\%}$ = 319 °C. **DSC** (Ar): T_g = 253 °C.

Poly(1,5-diisocyanatopentane-*co*-erythrodiol-*co*-1,6-hexanediol) (PU2a)

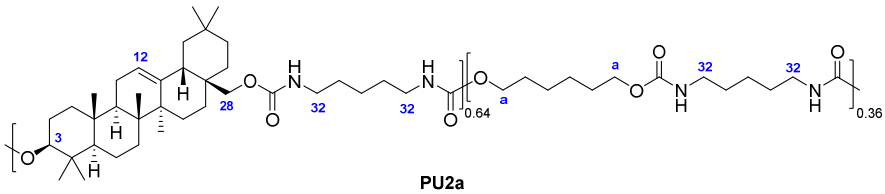

PU2a

PU2a was synthesized by dissolving **ErDO** (195 mg, 440 µmol, 0.7 eq) and 1,6-hexanediol (22.3 mg, 189 µmol, 0.3 eq) in dry anisole (6.3 mL, 0.1 M) by moderate heating. $Sn(Oct)_2$ (10.2 µL, 31.5 µmol, 0.05 eq) was added as a solution in dry anisole (0.09 M) to the reaction mixture, followed by the addition of PDI (90.5 µL, 629 µmol, 1.0 eq). The reaction

solution was stirred at 90 °C overnight, and afterwards remaining NCO groups were end-capped with EtOH (0.3 mL). The solvents were removed under reduced pressure, a sample was collected for SEC analysis, and the polymer was purified following procedure B1, yielding **PU2a** as a transparent solid (298 mg, 617 µmol, isolated yield 98%).

^{1}H NMR (600 MHz, $C_2D_2Cl_4$): δ [ppm] = 5.22 (br s., 0.6H, H_{12}), 4.74 – 4.47 (m, 2H, N*H*), 4.36 (dd, J = 11.5, 4.6 Hz, 0.6H, H_3), 4.10 – 3.97 (m, 1.6H, H_{28}+H_a), 3.71 (d, J = 10.8 Hz, 0.6H, H_{28}), 3.14 (dd, J = 6.3, 6.1 Hz, 4H, H_{32}), 2.11 – 0.70 (m, 37H).

^{13}C{^{1}H} NMR (151 MHz, $C_2D_2Cl_4$): δ [ppm] = 157.1 (2C), 156.9 (2C), 144.1, 123.0, 81.7, 71.3, 65.0, 55.9, 48.0, 46.7, 43.0, 42.1, 41.4, 41.3, 40.3, 38.8, 38.3, 37.2, 36.5, 34.5, 33.3, 33.1, 31.8, 31.0, 30.2, 30.1, 30.1, 30.1, 30.0, 30.0, 30.0, 30.0, 29.2, 28.4, 26.1, 26.0, 25.8, 24.3, 24.2, 24.2, 24.2, 24.0, 23.9, 22.9, 18.6, 17.2, 17.0, 15.7.

FTIR (ATR): $\tilde{\nu}$ [cm^{-1}] = 3321 (w), 2933 (m), 2861 (m), 1691 (s), 1525 (m), 1457 (w), 1243 (s), 1024 (m).

SEC (DMAc): M_n = 94500 g/mol; M_w = 236000 g/mol; $Đ$ = 2.50.

TGA (Ar): $T_{d5\%}$ = 287 °C. **DSC** (Ar): T_g = 158 °C.

Poly(1,5-diisocyanatopentane-*co*-erythrodiol-*co*-1,6-hexanediol) (PU2b)

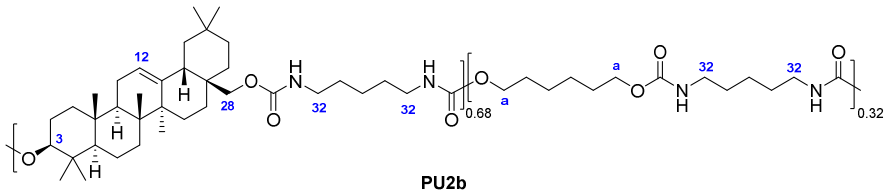

PU2b

PU2b was prepared from **ErDO** (195 mg, 440 µmol, 0.7 eq), 1,6-hexanediol (22.3 mg, 189 µmol, 0.3 eq), PDI (90.5 µL, 629 µmol, 1.0 eq), and ZDTC (11.4 mg, 31.5 µmol, 0.05 eq) in anisole (6.3 mL, 0.1 M) at 115 °C (48 h) according to procedure A2/B1 and obtained as a transparent solid (305 mg, 615 µmol, isolated yield 98%).

^{1}H NMR (600 MHz, $C_2D_2Cl_4$): δ [ppm] = 5.22 (br. s, 0.7H, H_{12}), 4.73 – 4.45 (m, 2H, N*H*), 4.36 (dd, J = 11.4, 4.7 Hz, 0.7H, H_3), 4.09 – 3.98 (m, 1.7H, H_{28}+H_a), 3.71 (d, J = 10.8 Hz, 0.7H, H_{28}), 3.14 (dd, J = 6.4, 6.1 Hz, 4H, H_{32}), 2.10 – 0.77 (m, 38H).

^{13}C{^{1}H} NMR (151 MHz, $C_2D_2Cl_4$): δ [ppm] = 157.1 (2C), 156.9 (2C), 144.1, 123.0, 81.7, 71.3, 65.0, 55.9, 48.0, 46.7, 43.0, 42.1, 41.4, 41.3, 40.3, 38.8, 38.3, 37.2, 36.5, 34.5, 33.3,

33.1, 31.8, 31.0, 30.1, 30.1, 30.1, 30.1, 30.0, 30.0, 30.0, 30.0, 29.2, 28.4, 26.1, 26.0, 25.8, 24.3, 24.2, 24.2, 24.2, 24.0, 23.9, 22.9, 18.6, 17.2, 17.0, 15.7.

FTIR (ATR): $\tilde{\nu}$ [cm^{-1}] = 3331 (w), 2929 (m), 2861 (m), 1694 (s), 1515 (m), 1459 (w), 1240 (s), 1006 (m).

SEC (DMAc): M_n = 28400 g/mol; M_w = 83700 g/mol; $Đ$ = 2.94.

TGA (Ar): $T_{d5\%}$ = 307 °C. **DSC** (Ar): T_g = 147 °C.

Poly(1,5-diisocyanatopentane-*co*-erythrodiol-*co*-1,6-hexanediol) (PU2c)

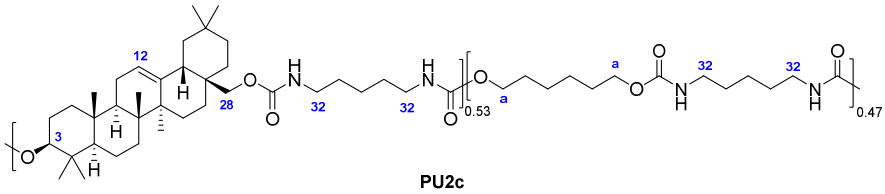

PU2c

PU2c was prepared from **ErDO** (139 mg, 314 µmol, 0.5 eq), 1,6-hexanediol (37.1 mg, 314 µmol, 0.5 eq), PDI (90.3 µL, 628 µmol, 1.0 eq), and ZDTC (11.4 mg, 31.4 µmol, 0.05 eq) in anisole (6.3 mL, 0.1 M) at 115 °C (48 h) according to procedure A2/B1 and obtained as a transparent solid (167 mg, 373 µmol, isolated yield 59%).

^{1}H NMR (600 MHz, $C_2D_2Cl_4$): δ [ppm] = 5.22 (br. s, 0.5H, H_{12}), 4.82 – 4.43 (m, 2H, N*H*), 4.36 (dd, J = 11.4, 4.7 Hz, 0.5H, H_3), 4.11 – 3.96 (m, 2.2H, H_{28}+H_a), 3.71 (d, J = 10.8 Hz, 0.5H, H_{28}), 3.14 (dd, J = 6.9, 6.7 Hz, 4H, H_{32}), 2.10 – 0.78 (m, 33H).

^{13}C{^{1}H} NMR (151 MHz, $C_2D_2Cl_4$): δ [ppm] = 157.1 (2C), 156.9 (2C), 144.1, 123.0, 81.7, 71.3, 65.0, 55.9, 48.0, 46.7, 43.0, 42.1, 41.4, 41.3, 40.3, 38.8, 38.3, 37.2, 36.5, 34.5, 33.3, 33.1, 31.8, 31.0, 30.1, 30.1, 30.0, 30.0, 30.0, 30.0, 30.0, 30.0, 29.2, 28.4, 26.1, 26.0, 25.8, 24.3, 24.2, 24.2, 24.2, 24.0, 23.9, 22.9, 18.6, 17.2, 17.0, 15.7.

FTIR (ATR): $\tilde{\nu}$ [cm^{-1}] = 3329 (w), 2931 (m), 2861 (m), 1691 (s), 1521 (m), 1457 (w), 1242 (s), 1003 (m).

SEC (DMAc): M_n = 23500 g/mol; M_w = 49300 g/mol; $Đ$ = 2.10.

TGA (Ar): $T_{d5\%}$ = 305 °C. **DSC** (Ar): T_g = 119 °C.

Poly(1,5-diisocyanatopentane-*co*-erythrodiol-*co*-1,6-hexanediol) (PU2d)

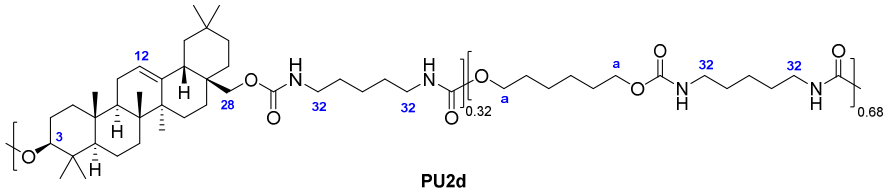

PU2d

PU2d was prepared from **ErDO** (92.0 mg, 208 µmol, 0.3 eq), 1,6-hexanediol (57.3 mg, 485 µmol, 0.7 eq), PDI (100 µL, 693 µmol, 1.0 eq), and ZDTC (12.5 mg, 34.6 µmol, 0.05 eq) in anisole (6.9 mL, 0.1 M) at 115 °C (48 h) according to procedure A2/B1 and obtained as a transparent solid (158 mg, 416 µmol, isolated yield 60%).

^{1}H NMR (600 MHz, $C_2D_2Cl_4$): δ [ppm] = 5.21 (br. s, 0.3H, H_{12}), 4.86 – 4.45 (m, 2H, N*H*), 4.35 (dd, J = 11.5, 4.7 Hz, 0.3H, H_3), 4.12 – 3.95 (m, 2.7H, H_{28}+H_a), 3.71 (d, J = 10.9 Hz, 0.3H, H_{28}), 3.14 (dd, J = 6.9, 6.8 Hz, 4H, H_{32}), 2.12 – 0.76 (m, 26H).

^{13}C{^{1}H} NMR (151 MHz, $C_2D_2Cl_4$): δ [ppm] = 157.1 (2C), 156.9 (2C), 144.1, 123.0, 81.7, 71.3, 65.0, 55.9, 48.0, 46.7, 43.0, 42.1, 41.4, 41.3, 40.3, 38.8, 38.3, 37.2, 36.5, 34.5, 33.3, 33.0, 31.8, 31.0, 30.2, 30.1, 30.1, 30.0, 30.0, 30.0, 29.9, 29.9, 29.2, 28.4, 26.1, 26.0, 25.8, 24.3, 24.2, 24.2, 24.2, 24.0, 23.9, 22.9, 18.6, 17.2, 17.0, 15.7.

FTIR (ATR): $\tilde{\nu}$ [cm^{-1}] = 3325 (w), 2927 (m), 2859 (m), 1684 (s), 1527 (m), 1461 (w), 1243 (s), 1008 (w).

SEC (DMAc): M_n = 34400 g/mol; M_w = 65100 g/mol; $Đ$ = 1.89.

TGA (Ar): $T_{d5\%}$ = 301 °C. **DSC** (Ar): T_g = 81 °C.

Poly(1,5-diisocyanatopentane-*alt*-1,6-hexanediol) (PU2e)

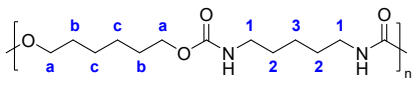

PU2e

1,6-hexanediol (189 mg, 1560 µmol, 1.0 eq) and ZDTC (28.9 mg, 80.0 µmol, 0.05 eq) were dissolved in dry DMAc (8.0 mL, 0.2 M), followed by the addition of PDI (230 µL, 1560 µmol, 1.0 eq). The reaction solution was stirred at 90 °C overnight. Possible remaining NCO groups were end-capped with EtOH (0.3 mL). The solvents were removed under reduced pressure, and a sample was collected for SEC analysis. The polymer was purified according to procedure B1, except that Soxhlet extraction with MeOH was

ineffective and was therefore repeated with isopropanol. After drying, **PU2e** was obtained as a white solid (333 mg, 1220 µmol, isolated yield 76%).

^{1}H NMR (600 MHz, DMSO-d_6): δ [ppm] = 6.57 (s, 2H, N*H*), 3.94 (t, J = 6.7 Hz, 4H, H_a), 2.97 (q, J = 6.7 Hz, 4H, H_1), 1.56 (p, J = 6.7 Hz, 4H, H_b), 1.42 (p, J = 7.3 Hz, 4H, H_2), 1.34 (p, J = 3.6 Hz, 4H, H_c), 1.26 (p, J = 7.6 Hz, 2H, H_3).

^{13}C{^{1}H} NMR (151 MHz, DMSO-d_6): δ [ppm] = 155.8 (2C), 63.1 (2C), 39.9 (2C), 28.6 (2C), 28.2 (2C), 24.6 (2C), 23.1.

FTIR (ATR): $\tilde{\nu}$ [cm^{-1}] = 3331 (m), 2931 (m), 2861 (m), 1682 (s), 1532 (s), 1474 (w), 1258 (s), 1012 (w).

SEC (DMAc): M_n = 13500 g/mol; M_w = 37800 g/mol; $Đ$ = 2.80.

TGA (Ar): $T_{d5\%}$ = 287 °C. **DSC** (Ar): T_g = 18 °C; T_{m1} = 131 °C; T_{m2} = 148 °C.

4.5. Supplementary Information

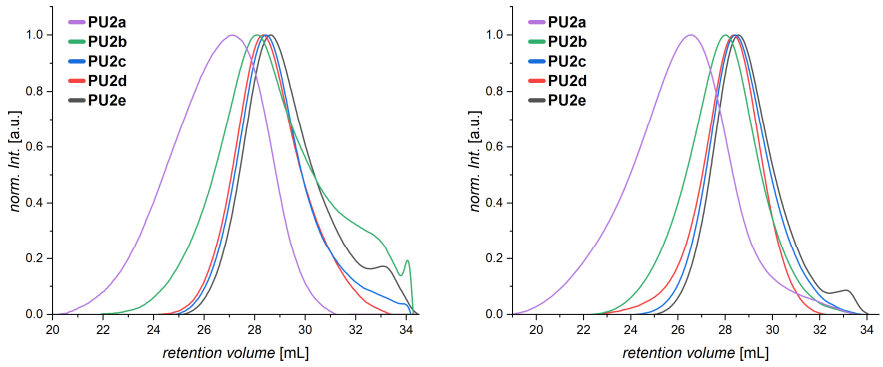

Figure S4.1. SEC profiles of **PU2a**–**e** before (left) and after (right) extraction with MeOH (SEC with DMAc as eluent. **PU2a**: $Sn(Oct)_2$ 5 mol%, PhOMe, 90 °C, 16 h; **PU2b**–**d**: ZDTC 5 mol%, PhOMe, 115 °C, 48 h; **PU2e**: ZDTC 5 mol%, DMAc, 90 °C, 16 h)

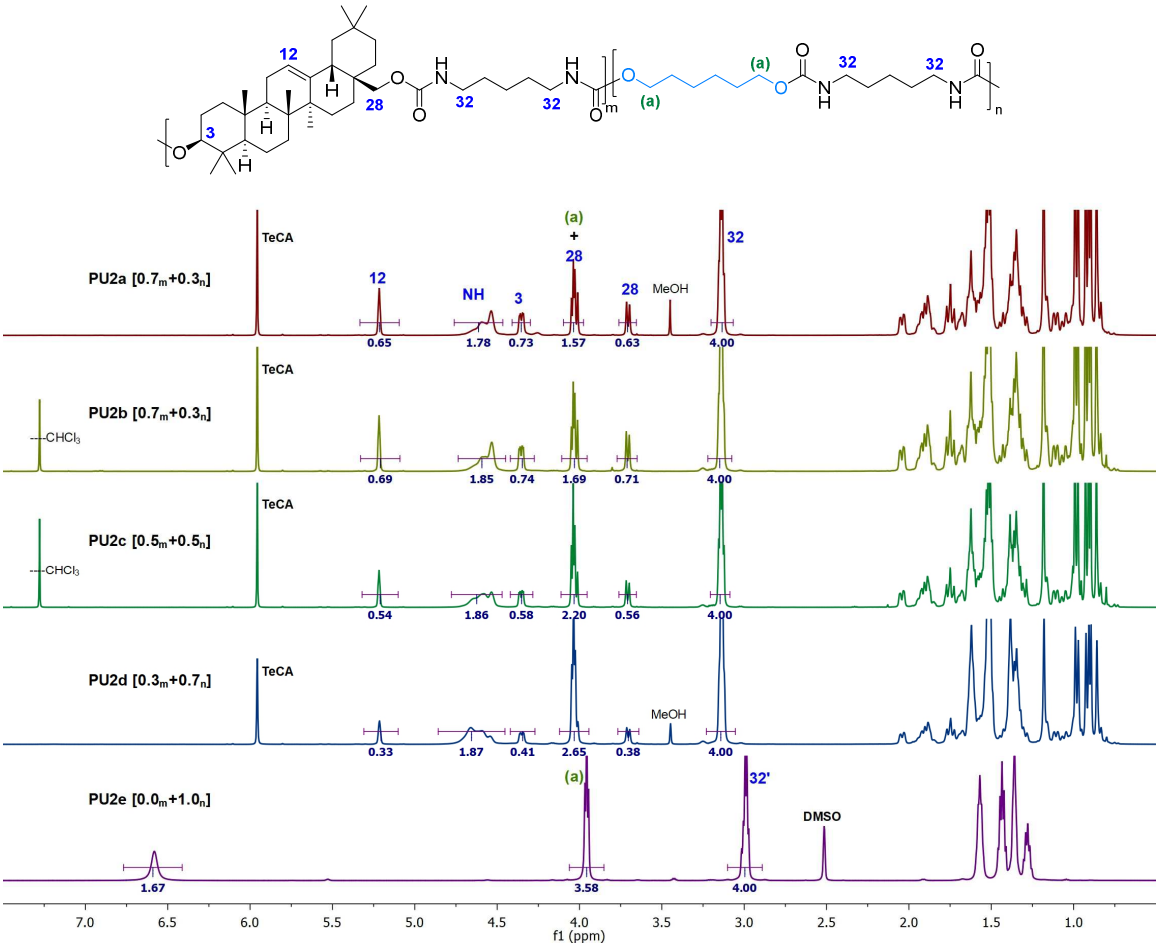

Figure S4.2. General structure of copolymers **PU2a–e** and corresponding ^{1}H NMR spectra (TeCA-d_2, 80 °C, except for **PU2e**: DMSO-d_6, 80 °C)

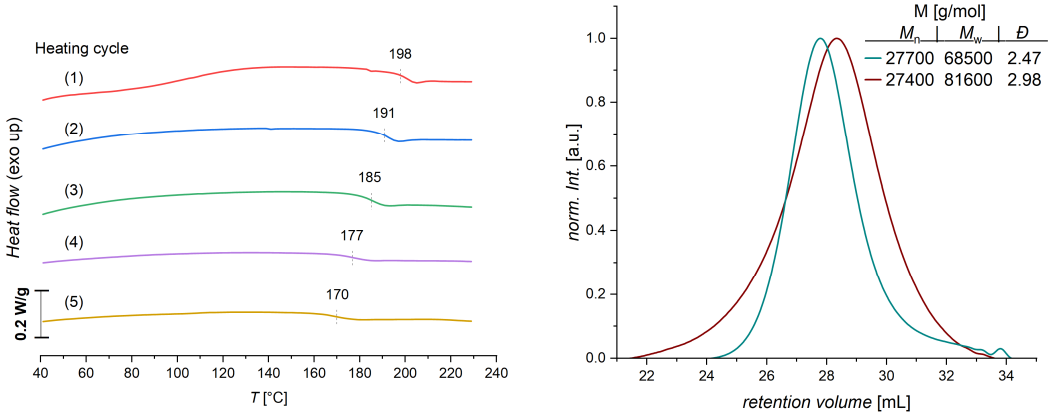

Figure S4.3. (Left) DSC heating curves of **PU1** (25–240 °C). (Right) SEC profile of **PU1** before (—) and after (—) annealing at 240 °C for 4 h (SEC with DMAc as eluent and PMMA calibration).

5. Renewable Polycarbonates Based on Erythrodiol

The naturally occurring pentacyclic triterpenoid oleanolic acid (OA) was reduced to yield erythrodiol (ErDO), a rigid and polychiral diol. Consequently, poly(erythrodiol carbonate), a novel bio-based polycarbonate, could be synthesized by polycondensation with dimethyl carbonate or diphenyl carbonate, yet with low molecular weights (M_w up to 10 kg/mol). Potential explanations are the low reactivity of the secondary alcohol, as well as the bulky structure and the high melting point of ErDO. By introducing 1,6-hexanediol (HDO) as a further bio-based diol comonomer, a copolymer with a content of 37 mol% ErDO showed a significant increase in M_w up to 74 kg/mol. The homopolymer shows a remarkably high glass-transition temperature (T_g) for polycarbonates at 232 °C and could be effectively tuned by copolymerization with HDO (e.g., 109 °C for 37 mol% ErDO). All (co)polymers are thermally stable until at least 300 °C.

Jessewitsch, T.; Delaittre, G. submitted for publication.

Author contributions: T.J. designed the entire study and performed all syntheses and most characterization. G.D. originated the concept. T.J. and G.D. analyzed the data and wrote the manuscript.

5.1. Introduction

Poly(bisphenol A carbonate) is widely known for its exceptional toughness, high transparency, and thermal stability.[218] However, without UV stabilizers or protective coatings, it presents drawbacks such as yellowing (photo-oxidation), a decrease in physical properties that appear during natural weathering, and release of the endocrine disruptor bisphenol A (BPA) by hydrolysis.[219,220] At the same time, rising concerns about human health and the environment arising from the past and present linear, fossil-based economy direct research towards alternative sustainable materials, with the aim of providing comparable physical properties.

For polycarbonates, research expands towards bio-based aromatic BPA derivatives,[221] as well as alternative aliphatic monomers.[222] For example, *o*-methoxylated bisphenols derived from lignin were found to show a strong decrease in estrogenic activity.[221] Apart from the lignin source, polycarbonates formed via chain growth are available from epoxidized species like terpenes (limonene oxide[223]) and vegetable oils[224] by performing ring-opening polymerization (ROP) with CO_2 as a comonomer in the presence of a catalyst. Poly(limonene carbonate) possesses a high glass-transition temperature (T_g) of 130 °C and contains an external double bond in every repeating unit, allowing a range of modifications, e.g., by the thiol-ene reaction or epoxidation to tune the properties.[223,225,226] ROP was also employed with sugar-based cyclic carbonates derived from glucose[227,228] or mannose.[229]

Mitsubishi Chemical has commercialized a UV-resistant copolycarbonate "Durabio" produced from the sugar-derived isosorbide.[230] The literature shows further that poly(isosorbide carbonate) (PIC) can be obtained with high molecular weights by melt polycondensation with dimethyl carbonate (DMC) catalyzed by ionic liquids[143,231] or strong bases[142] via step-growth polymerization. On the one hand, this approach avoids the use of the highly toxic phosgene and, on the other hand, DMC can be produced using CO or CO_2.[232,233] Besides other linear bio-based diols, 2,5-bis(hydroxymethyl)furan can be easily obtained from fructose for the formation of polyesters[234], but due to the low thermal stability of the furan ring, it requires a mild polymerization method with 1,1′-carbonyldiimidazole to obtain polycarbonates.[235]

In the present contribution, we propose the addition of erythrodiol (olean-12-en-3β,28-diol; $C_{30}H_{50}O_2$; **ErDO**) to the repertoire of bio-based diols for polycarbonates. **ErDO** is a rigid building block belonging to the class of pentacyclic triterpenes with the oleanane skeleton

and consisting of 8 chiral centers. It is extractable from olive fruit and leaves and is proposed to be a precursor of oleanolic acid (OA) in plants.[236] **ErDO** shows important diverse bioactivity such as anticancer activity in different cell lines,[237,238] as well as cardioprotective[239] and blood vessel relaxing[240] activities.

5.2. Results and Discussion

5.2.1. Monomer Synthesis

To obtain **ErDO** from OA – the latter currently being far more commercially available than the former – in a single-step synthesis, the use of $LiAlH_4$ was required since the milder reducing agent DIBAL-H is generally not sufficiently active (Scheme 5.1).[207] The reduction with $LiAlH_4$ proceeded in dry conditions with an isolated yield of 87%. **ErDO** shows high solubility in lower alcohols (methanol, ethanol, isopropanol). It has moderate solubility in dichloromethane, ethyl acetate, as well as in aromatic solvents, and poor solubility in acetonitrile or cyclohexane.

The bis(methylcarbonate) **ErDO-BMC** was synthesized as a model compound by reacting **ErDO** with an excess of DMC in the presence of sodium *tert*-butoxide (NaO*t*Bu) at 130 °C (Figure 5.1). All synthetic procedures are described in detail in Section 5.4.

5.2.2. Polymer Synthesis – Homopolymer of ErDO

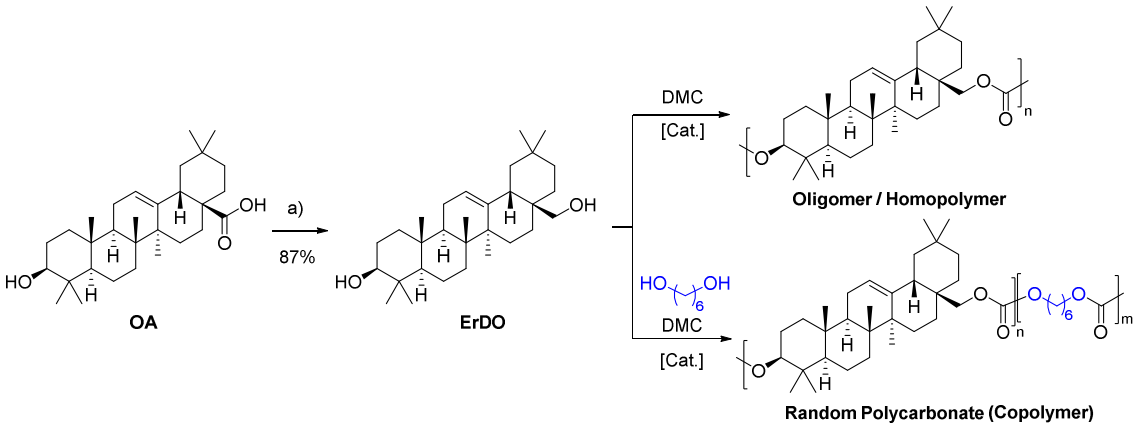

Scheme 5.1. Synthetic route: reduction of OA to **ErDO**, followed by polycondensation to a homopolymer or copolymers with 1,6-hexanediol. (a) $LiAlH_4$, THF, 50 °C, 16 h.

Polycarbonates can be synthesized with high molecular weights by melt polycondensation with DMC or diphenyl carbonate (DPC) under reduced pressure. This method is, however, not suitable for **ErDO** since its high melting point (230–231 °C) is relatively close to its decomposition temperature ($T_{d5\%}$ = 299 °C, Figure 5.1C). Notably, a mass loss is already

observable at 240 °C. **ErDO** shows an almost identical decomposition to OA. In contrast, **ErDO-BMC**, carrying terminal methyl carbonate groups, shows a mass loss of 17% starting from 276 °C, corresponding to the decomposition of the carbonate groups. Since those are essential for the step-growth mechanism, such high temperatures are not suitable.

B

				Conv. of funct. group		
	DMC [eq]	**Solvent**	***T* [°C]**	**CO_3*Me***	***CH*-OH**	**$DP_{n,th}$ (3)**
OC1	10	/	230 (1)	83%	90%	3.9
OC2	1.7	$Ph(OMe)_2$	210	96%	55%	2.1
OC3	2.2			93%	70%	2.9
OC4	2.7			86%	85%	3.7
OC5	10			88%	97%	6.8
OC6		Ph_2O (2)		86%	60%	3.0
OC7			230	89%	95%	6.3
PC1		***n*-$C_{14}H_{30}$** (2)		**93%**	**95%**	**8.6**

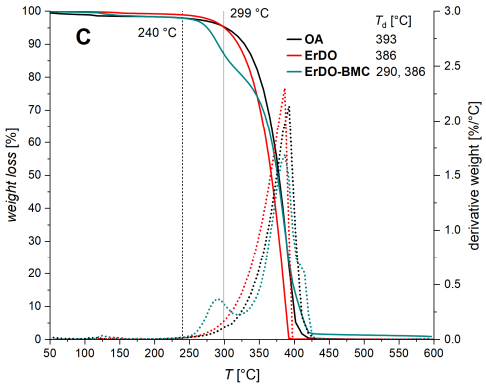

Figure 5.1. [A] Reaction of **ErDO** to **ErDO-BMC** or polycondensation to oligomers and polymer. [B] ^{1}H NMR screening of the reaction between **ErDO** and DMC under varying conditions ((1) stirred at 230 °C, resulting in a solid product after 16 h; (2) Ph_2O and *n*-$C_{14}H_{30}$ were added after distilling of DMC at 180 °C, since they do not dissolve **ErDO**, but **ErDO-BMC** and the corresponding oligomers; (3) $DP_{n,th}$ calculated from the overall conversion using the Carothers equation). [C] TGA (—) and DTG (···) profiles of OA, **ErDO**, and **ErDO-BMC** (T_d refers to the maxima in the DTG curve).

During polycondensation with DMC in the presence of a strong non-nucleophilic base, the formed alcoholate performs a nucleophilic attack on DMC by generating methanol as part of the substitution. Step-growth proceeds via nucleophilic attack on a terminal methyl carbonate of the chain ([DMC]:[diol] < 2) or by transesterification reactions between the two methyl carbonate chain ends, which releases DMC ([DMC]:[diol] ≥ 2).[138,241] Further polycondensation proceeds by increasing temperature and reducing pressure.

Since **ErDO** and **ErDO-BMC** do not melt at temperatures below 230 °C, the polycondensation with an excess of DMC stops at the oligomeric stage with an average of four repeating units (entry **OC1**), with the reaction mixture becoming solid after complete distillation of DMC. The polycondensation could have been envisaged in solution using triphosgene as a reagent, yet its toxicity led us to explore the combination of a high-boiling-point solvent with DMC or DPC. For our initial attempts, the theoretical number-average degree of polymerization ($DP_{n,th}$) was calculated using the Carothers equation and the

product of both conversion values (remaining secondary alcohol and terminal methyl carbonate group). For instance, the synthesis of **ErDO-BMC** corresponds to 100% conversion of the primary and secondary alcohols of **ErDO** to the corresponding methyl carbonate, yet the methyl carbonate end groups are 0% converted to a bridging carbonate group, resulting in a $DP_{n,th}$ value of 1. As indicated in Figure 5.1B, 1,3-dimethoxybenzene ($Ph(OMe)_2$; *bp* = 217 °C) dissolves **ErDO** directly and allows further heating, but a decreasing amount of DMC (2.7 → 1.7 eq) did not promote step growth. With 10 equivalents DMC (210 °C, 3 d), oligomers with $DP_{n,th}$ = 6.8 were formed. By first transforming **ErDO** to **ErDO-BMC** with DMC (10 eq, 120–180 °C) and subsequently heating the mixture in diphenyl ether (Ph_2O; *bp* = 258 °C), a similar $DP_{n,th}$ value of 6.3 could be achieved. The largest $DP_{n,th}$ value was obtained in *n*-tetradecane (*bp* = 253 °C) with the same reaction procedure, yielding a polymer with $DP_{n,th}$ of 8.6.

In Figure 5.2, ^{1}H NMR spectra of **ErDO**, **ErDO-BMC**, and **PC1** (both purified) are displayed. By transforming the secondary alcohol of **ErDO** into the methyl carbonate, the signal of H-3 (3.24–3.20 ppm, m, 1H) experiences a downfield shift to 4.33 ppm (H-3'). The protons of the methylene group C-28 are diastereotopic, therefore producing two separate doublets (3.55 and 3.21 ppm, H-28) in **ErDO** that also undergo a downfield shift in **ErDO-BMC** (H-28'). The peaks of the two corresponding methyl groups appear at 3.77 ppm (s, H-31') and overlap with that of proton H-28', leading to an integral of 7. The proton of the internal double bond (5.19 ppm, H-12) is forming a triplet in both monomeric species, almost decoupled from the end groups, and yields a broader, undefined signal in **PC1**. During polycondensation, the signal of the methine proton (H-3") remains at its position, while the two doublets generated by the methylene protons H-28" become closer to each other (Δδ 0.37 → 0.22 ppm). This behavior might be explained by the restricted conformational flexibility of the formed polymer. The step-growth polymerization of **ErDO** could only be performed until roughly 88% total conversion, which would correspond to $DP_{n,th}$ = 8.6. Considering the absent and weak signals at approx. 3.5 ppm (H-28) and 3.2 ppm (H-28 and H-3), respectively, and their distinct reactivities, it is reasonable to assume that all primary alcohols were consumed and that only secondary alcohols remain. Therefore, the corresponding **PC1** contains two types of end groups, namely secondary alcohols (H-3) or methyl carbonate (H-31"). By comparing signal integrals of H-12" with both end groups (H-3 and H-31"), a $DP_{n,NMR}$ value of 7.9 could be calculated.

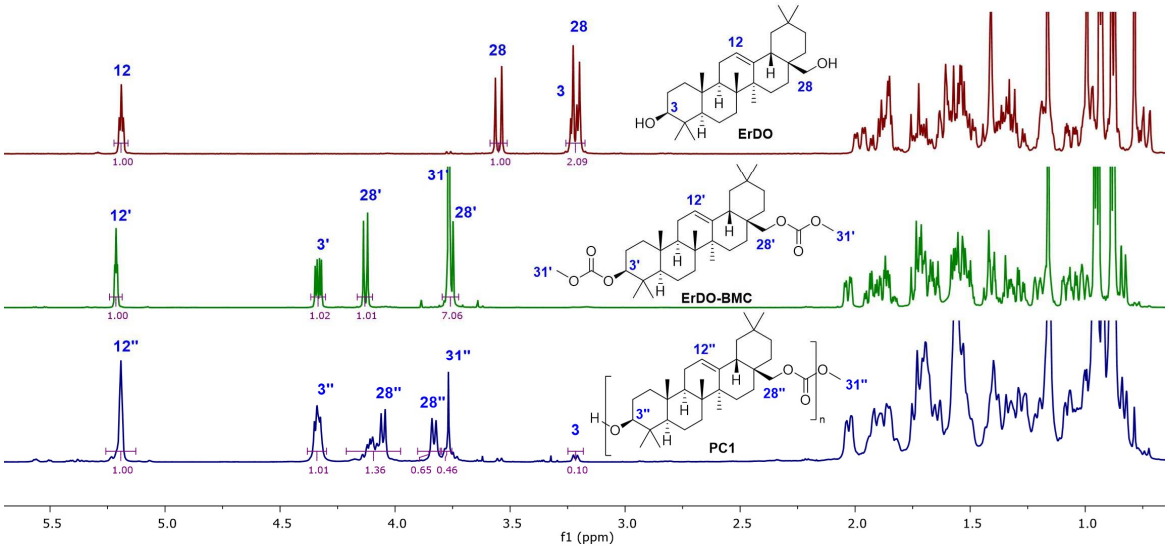

Figure 5.2. ^{1}H NMR spectra of **ErDO**, **ErDO-BMC**, and **PC1** (in $CDCl_3$).

To possibly reach higher molecular weights, DMC was replaced by DPC, which – despite its bulkiness – is a better electrophile, with phenol being a better leaving group compared to methanol. With respect to the polycondensation mechanism, there are two main differences. First, the use of DPC cannot lead to undesired methylation as with DMC, since the transfer of a phenyl group is not favored. Second, oligomers with two terminal methyl carbonate groups can undergo step-growth by transesterification and elimination of the volatile DMC, while oligomers capped with two phenyl carbonate end-groups do not readily release DPC to permit an equilibrium shift. Therefore, the ratio of **ErDO** to DPC was varied between 1.1 and 1.6, leading to different products, as can be seen in Figure 5.3. The reaction was performed in Ph_2O using NaO*t*Bu as catalyst at 190 °C and 200 mbar (3 d). The raw mixture was precipitated in cold methanol to remove residues of the aromatic solvent, revealing the signals of the phenyl carbonate end groups. By using 1.1 equivalents of DPC, close to a theoretical ideal 1:1 ratio, ^{1}H NMR spectroscopic analysis of the purified product **OC8** revealed an oligomer ($DP_{n,NMR}$ = 4.4) with essentially two terminal secondary alcohols, as inferred from (i) the low intensity of aromatic proton signals and H-3' (i.e., minimal traces of the -CO_3*Ph* end group), (ii) the absence of signals arising from the primary alcohol methylene protons (H-28 in Figure 5.2), and (iii) the high intensity of the secondary alcohol methine signal H-3 at 3.19 ppm. **ErDO** was therefore incorporated partially mirror-inverted (head-to-tail vs. head-to-head). This leads to the possibility of various carbonate motifs, including one with a methylene group on each side of the carbonate group, which materializes in the occurrence of two distinct shifts for H-28", each appearing as doublets in the region of 4.10–3.92 and 3.89–3.71 ppm. $DP_{n,NMR}$ values were

calculated by comparing signal integrals of H-12" with those of H-3' and H-3. With 1.5 equivalents of DPC (**O9**), $DP_{n,NMR}$ increased to 6.1, with the two secondary alcohols still representing the major end groups (approx. 80%). In contrast, 1.6 eq. of DPC (**O10**) yielded oligomers with an average of 5.1 repeating units, but instead with two phenyl carbonates as main end groups (approx. 70%), as can be seen from the distinct signals in the aromatic region and the signal at 4.38 ppm originating from the methine group (H-3') connected to the phenyl carbonate. Using DPC did not further advance the polycondensation, but it revealed that **ErDO** can be incorporated mirror-inverted by using the more sterically hindered phenyl carbonate. In ^{13}C NMR spectroscopy, two carbonate signals are observed for the oligomers, which can be attributed to the presence of different carbonate environments arising from the distinctly reactive secondary and primary hydroxyl groups of **ErDO** (Figures S5.1 and S5.3).

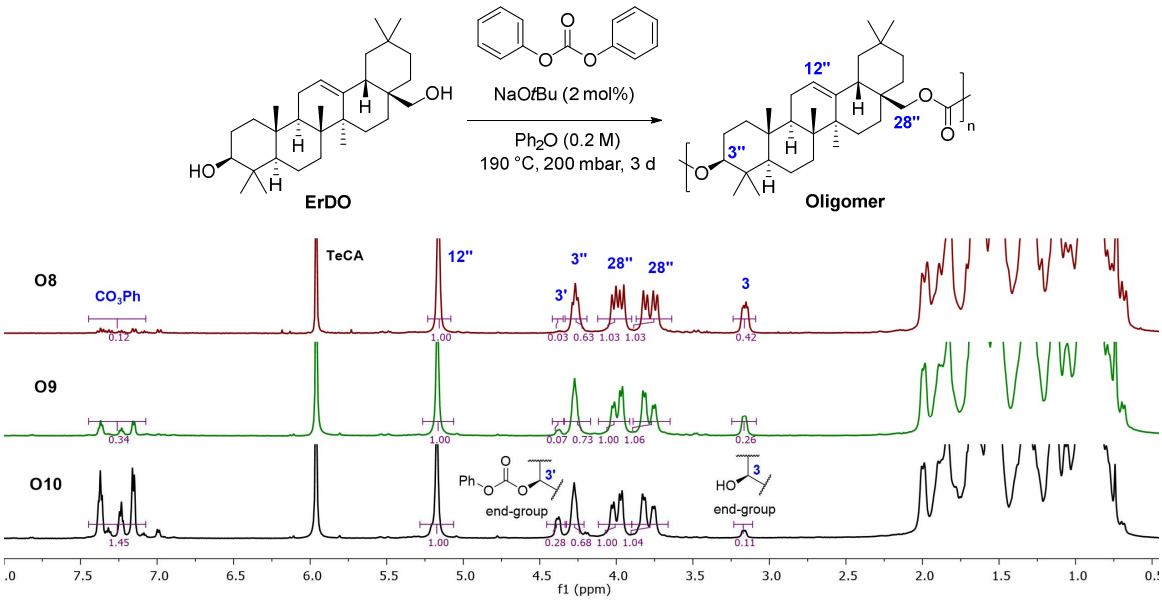

Figure 5.3. (Top) Polycondensation of **ErDO** and DPC catalyzed by NaO*t*Bu in Ph_2O. (Bottom) ^{1}H NMR spectra of **OC8**–**10** in $C_2D_2Cl_4$ (TeCA-d_2).

SEC analysis could be performed in chloroform (polystyrene calibration). The chromatogram of **OC8** (Figure 5.4, right) exhibits a typical low oligomeric distribution, with stationary points attributed to species from dimer to pentamer. **OC9** and **OC10** show very similar SEC profiles with M_w = 5.1–5.4 kg/mol and smoothened stationary points. Purified **PC1**, synthesized by polycondensation with DMC, possesses a broad polymer distribution (M_w = 10 kg/mol, $Đ$ = 1.70), apparently with no trimers or dimers.

	DPC [eq]	Yield*	$DP_{n,NMR}$	M_n [g/mol]	M_w [g/mol]	Đ
OC8	1.1	50%	4.4	2300	3200	1.41
OC9	1.5	63%	6.1	3300	5400	1.66
OC10	1.6	66%	5.1	3200	5100	1.62
PC1	10 eq DMC	83%	7.9	5900	10 000	1.70

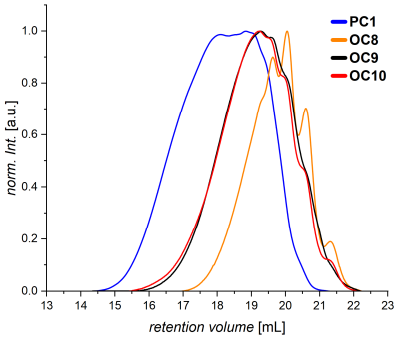

Figure 5.4. (Left) Experimental conditions and results of the corresponding reactions with varying DPC equivalents (*isolated yield, purified by precipitation in cold MeOH). (Right) SEC profiles ($CHCl_3$ as solvent, calibrated with PS).

The TGA profiles (Figure 5.5, left) of **OC9**, **OC10**, and **PC1** show identical degradation patterns. **PC1** has a decomposition temperature of 335 °C ($T_{d5\%}$), potentially allowing a high processing temperature. $T_{d5\%}$ of **PC1** is noticeably higher than **ErDO** itself (299 °C) and slightly higher compared to its oligomers. The triterpenoid structure decomposes most likely starting from its functional groups at C-3 and C-28 before the six-membered rings can break.[242] At these high temperatures, it is likely that aliphatic polycarbonates decarboxylate by releasing CO_2 and reform an ether linkage, which can cleave further.[243] Additionally, scission at the carbonate group via a β-H transfer, forming an unstable carboxylic acid and an alkene, is possible in the triterpene structure starting from C-2 (CH_2, A ring), but might be less favorable due to the rigidity. As a comparison, a series of poly(isosorbide carbonate)s (PIC) with $T_{d5\%}$ between 323–336 °C was reported.[143] Yet, $T_{d5\%}$ of **PC1** is clearly lower compared to that of poly(bisphenol A carbonate) (487 °C).[218] DTG profiles of the oligomers **OC9** and **OC10** reveal two further degradation processes at 337 and 426 °C, which might originate from hydroxyl and phenyl carbonate chain ends.

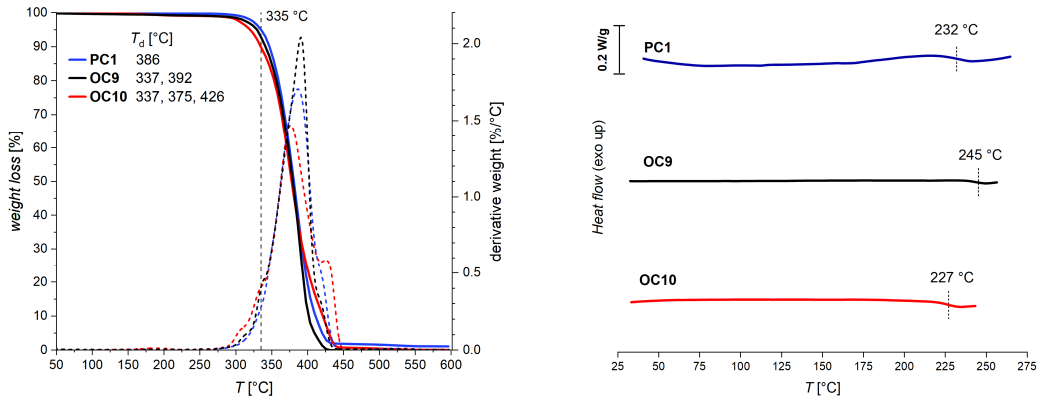

Figure 5.5. (Left) TGA (—) and DTG (···) profiles (10 °C/min, argon, T_d refers to the maxima in the DTG curves), (Right) DSC profiles (10 °C/min, except **PC1** with 20 °C/min) of **PC1**, **OC9**, and **OC10**.

DSC analyses (Figure 5.5, right) evidenced that the samples are entirely amorphous, without any crystalline domains. **PC1** shows a T_g at 232 °C, which could be detected with an increased heating rate of 20 °C/min. It needs to be highlighted that the T_g is very high in comparison to classic polycarbonates, in which the carbonate linkages typically provide flexibility, in contrast to polysulfones, aromatic polyamides, and polyimides. For instance, poly(trimethylene carbonate) (PTMC) is an amorphous polymer used in biomedical applications and has a low T_g of –15 °C.[244] The aforementioned PIC possesses a T_g in the range of 143–163 °C, similar to the aromatic PC (148 °C) depending on its molecular weight and terminal groups.[143] The more bulky and rigid triterpenoid structure in **PC1** is certainly responsible for such a further increase. A polyester of the structurally related diol betulin,[245] with the comonomer succinic acid, shows a high T_g at 214 °C while having a comparable molecular weight, despite the flexibility provided by succinic ester units. In our study on ErDO-based polyurethanes,[246] with the comonomer hexamethylene diisocyanate (HDI) and bio-based pentamethylene diisocyanate (PDI), similarly high T_g values of 198 and 206 °C were measured. Even vinyl polymers with the triterpenoidic structure present as a side chain could reach T_g values above 200 °C.[207]

Oligomers **OC9** and **OC10** prepared with DPC show a glass transition at 245 resp. 227 °C, slightly deviating from **PC1**. We note that, as mentioned before, the use of DPC leads to various carbonate linkages. Particularly, the low degrees of polymerization may give rise to a non-negligible influence of the end groups. **OC9**, carrying mainly two terminal hydroxyl groups, shows the highest glass transition temperature at 245 °C, possibly due to increased hydrogen bonding.

5.2.3. Polymer Synthesis – Copolymers of ErDO/HDO

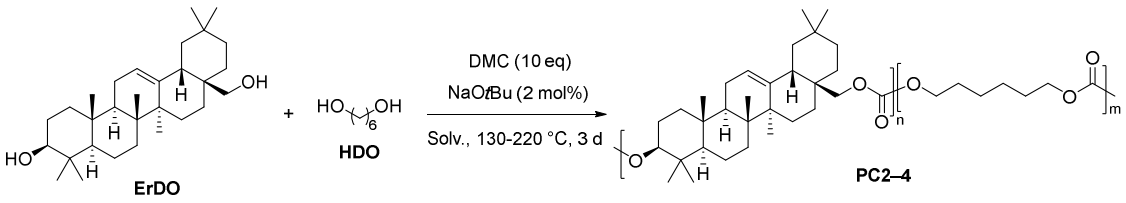

Scheme 5.2. Synthesis for random copolymers with diverse **ErDO**/HDO content.

Since the glass transition of **PC1** is already exceptionally high, but the attainable molecular weights are limited due to the polymerization methodology (polycondensation with DMC in a high-boiling solvent) and the high steric hindrance of **ErDO** itself, another diol was

added as a comonomer (Scheme 5.2). 1,6-hexanediol (HDO) was investigated because it can be bio-based[247] and might function already as a spacing unit facilitating the polymerization and allowing tuning of the T_g over a large temperature range. HDO has a high boiling point of 250 °C and low hygroscopicity, which is also beneficial in the reaction process. In practice, the excess amount of DMC distills off completely at 180 °C, leaving an oligomer mixture containing NaO*t*Bu, which was diluted with 1,3-dimethoxybenzene (for **PC2**) or diphenyl ether (for **PC3**) to allow further stirring at high temperature (220 °C, 3 d). The reaction mixture of **PC4** (63 mol% HDO) remained sufficiently low in viscosity to allow stirring without solvent addition. By precipitating in cold methanol, the purified copolymers **PC2**, **PC3**, and **PC4** could be isolated in yields between 78–81%. For comparison, poly(hexamethylene carbonate) (**PC5**) was synthesized as a reference material by melt polycondensation with reduced pressure using 1,5,7-triazabicyclo[4.4.0]dec-5-ene (TBD). ^{1}H NMR spectra of the copolymers can be found in the SI (Figure S5.2).

	ErDO	HDO	Solvent	Yield	$DP_{n,NMR}$ (ErDO)	$DP_{n,NMR}$ (HDO)
PC2	70%	30%	$Ph(OMe)_2$	78%	11	5
PC3	43%	57%	Ph_2O	81%	9	13
PC4	37%	63%	/	79%	32	54
PC5	0%	100%	/	83%	0	490

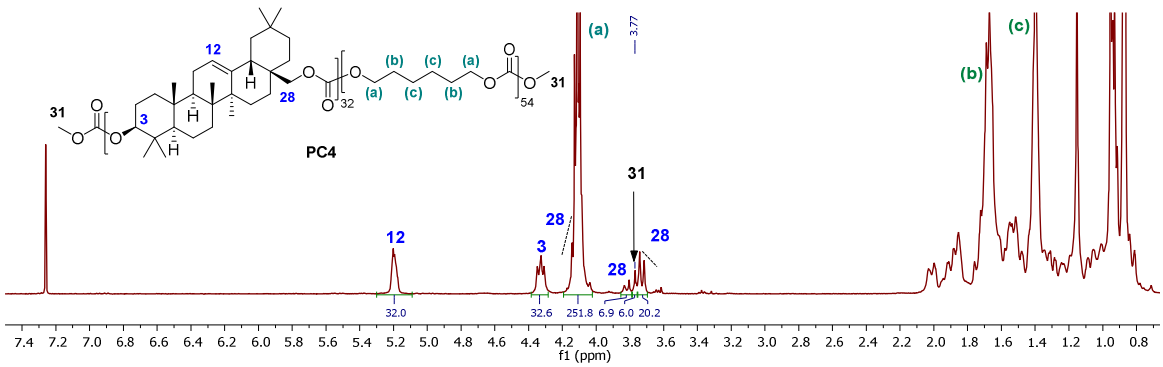

Figure 5.6. (Top) Experimental details and results for the corresponding copolymers with varying ErDO/HDO ratios (**PC2**–**4**: 2 mol% NaO*t*Bu, **PC5**: 2 mol% TBD). (Bottom) ^{1}H NMR spectrum of **PC4** (in $CDCl_3$).

For **PC4**, the spectrum is exemplary shown in Figure 5.6, where signals of the HDO-carbonate block appear additionally at 4.12 ppm (H_a), 1.67 ppm (H_b), and 1.40 ppm (H_c), overlapping with the signals of the **ErDO** unit. The excess of DMC minimizes the presence of terminal hydroxyl groups. Therefore, the methyl carbonate signal at 3.77 ppm (integral 6.0) was used for calculating the number of repeating units. For the **ErDO** units (5.20 ppm, 1H, H-12) a value of 32 can be directly resolved, while for the HDO unit, the integral of the signal (4.12 ppm, 4H, H_a) should be subtracted from the possible underlying H-28

protons (37 remaining), resulting in 54 units. It was expected that the introduction of HDO would significantly enhance the overall polymerization. However, **PC1**, **PC2**, and **PC3** show similar M_n values in both NMR and SEC, even with an HDO fraction as high as 57 mol% for **PC3**. With 63 mol% HDO (**PC4**) under bulk conditions, an overall $DP_{n,NMR}$ of 86 could be reached, including 32 **ErDO** units. Here, it is assumed that the hexyl spacer may be rather short in comparison to the bulky OA unit and that a comonomer with an even longer aliphatic linear chain (e.g., dodecyl) may better facilitate the polymerization. For instance, the group of Stanzione reported that the melt polycondensation of betulin with 1,12-dodecanedioic acid or 1,18-octadecanedioic acid led to polyesters with higher molecular weights compared to the shorter-chain relatives.[245] Nevertheless, all copolymers already display a monomodal polymeric SEC profile. **PC5**, consisting purely of HDO units, remained melted at high temperature and reduced pressure, thus giving access to a high-molecular-weight polycarbonate (M_w = 205 kg/mol, $Đ$ = 3.02).

	$M_{n,NMR}$ [g/mol]	$M_{n,SEC}$ [g/mol]	$M_{w,SEC}$ [g/mol]	$Đ$
PC1	3700	5900	10 000	1.70
PC2	5900	5900	8600	1.46
PC3	6100	6600	13 600	2.06
PC4	22 800	32 800	73 500	2.24
PC5	70 600	68 100	205 000	3.02

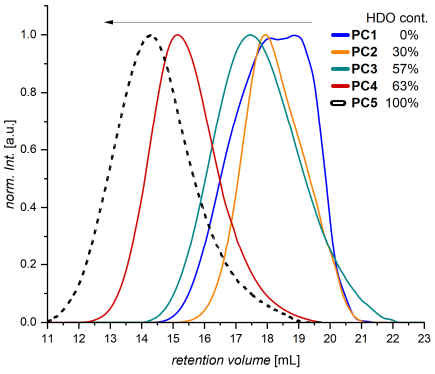

Figure 5.7. (Left) Average molecular weights of **PC1–5** determined by NMR and by SEC ($CHCl_3$ as solvent, calibrated with PS). (Right) SEC profiles of copolymers **PC2–4** in comparison to homopolymers **PC1** and **PC5**.

Analysis by TGA revealed that **PC1** is thermally slightly more stable compared to **PC5**, with a decomposition temperature ($T_{d5\%}$) of 335 °C instead of 310 °C (Figure 5.8). The one-step degradation of **PC5** leads to a rapid decrease in mass by decarboxylation and by β-H transfer, the latter forming terminal alkenes and unstable carboxylic acids.[243] The DTG profile of **PC1** shows a small shoulder towards higher temperatures, indicating a second degradation process that, interestingly, becomes more significant with increasing HDO content (T_{d2} = 420 °C for **PC2–4**). The rigid and bulky triterpenoid structure might suppress (in the case of **PC1**) or delay (in the case of copolymers) the degradation via β-H transfer, while a decomposition via decarboxylation, cleavage of the resulting ether, and radical chain scission might be favored.

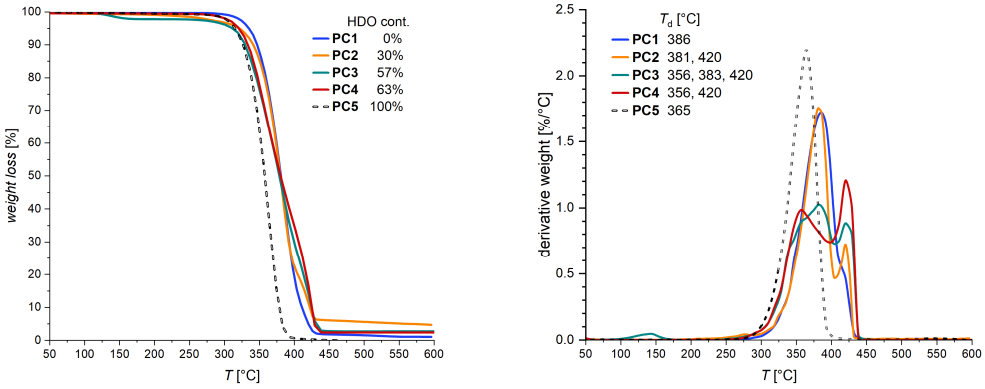

Figure 5.8. (From left to right) TGA profiles (10 °C/min, argon), and DTG profiles (T_d values refer to the maxima) of copolymers **PC2–4** in comparison to ErDO (**PC1**) and HDO (**PC5**) homopolymers.

The results of the DSC analysis are displayed in Figure 5.9. For **PC2** (70 mol% **ErDO**), no T_g could be detected with a heating rate of 10 °C/min and 20 °C/min (not displayed). Since the incorporation of 30 mol% HDO already decreases the thermal stability of the copolymer, the DSC measurement could only be performed until 230 °C. In that case, we assume the T_g is not significantly lowered by 5 HDO units. Therefore, it might lie close to the decomposition temperature, preventing its detection. Lowering the **ErDO** content to 43 mol% in **PC3** resulted in a significant decrease in T_g of roughly 100 °C, from 232 °C (**PC1**) to 128 °C, which is clear evidence for the more flexible polymer backbone. **PC4** (37 mol% **ErDO**) displays a drastic increase in molecular weight accompanied by a further decrease in T_g to 109 °C. The homopolymer **PC5** highlights the low glass-transition temperature of linear aliphatic polycarbonates with a T_g of –44 °C due to high flexibility and weak intermolecular forces. In addition, **PC5** can crystallize because of its long, regular, and flexible aliphatic structure, showing a melting point T_m at 50 °C, while **ErDO** copolymers containing even large amounts of HDO remain amorph, suggesting the absence of block-like microstructural elements.

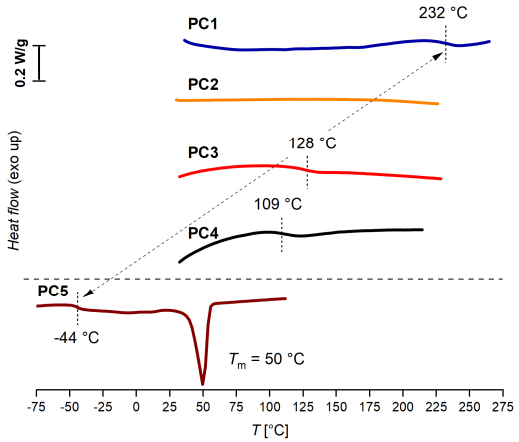

Figure 5.9. DSC profiles of homo- and copolymers (heating rate 10 °C/min, except **PC1**: 20 °C/min).

5.3. Conclusion

To summarize, different conditions were investigated to synthesize poly(erythrodiol carbonate) via polycondensation with dimethyl carbonate (DMC), to avoid the use of toxic triphosgene. Erythrodiol (**ErDO**) could be obtained in high yields of 87% by reduction of oleanolic acid (OA) using $LiAlH_4$. Since the melting point of **ErDO** is very high (230–231 °C) and the corresponding bis(methyl carbonate) model compound **ErDO-BMC** starts decomposing at 276 °C, a conventional melt polycondensation under reduced pressure was not possible. Instead, by using an excess of DMC and the addition of a high-boiling solvent, the step growth could be induced. By using *n*-tetradecane as a solvent, we could synthesize the novel short homopolymer **PC1** that shows good solubility in $CHCl_3$ for analysis by SEC (M_w = 10 kg/mol). The purified polymer has high thermal stability, up to 275 °C without mass loss ($T_{d5\%}$ = 335 °C), and a remarkably high T_g at 232 °C due to the rigid pentacyclic structure, which is unusual for polycarbonates. By using diphenyl carbonate (DPC) as a stronger electrophile and reduced pressure to remove the phenol by-product, the molecular weight could not be increased. Nevertheless, the corresponding oligomers **OC9** and **OC10** show glass transitions at 245 and 227 °C and indicate in ^1H and ^{13}C NMR spectroscopy that **ErDO** is incorporated partly mirror-inverted. Furthermore, copolymers **PC2** (70 mol% ErDO), **PC3** (43 mol%), and **PC4** (37 mol%) were synthesized using DMC and the potentially bio-based diol 1,6-hexanediol (HDO). By lowering the content of **ErDO** to 37 mol%, the molecular weight of **PC4** could be significantly increased, as the SEC and ^1H NMR results highlight. However, the C_6 spacer is likely too short to strongly facilitate the polycondensation of **ErDO** when used in small amounts. The copolymers have a slightly lower thermal stability ($T_{d5\%}$ = 310–320 °C), likely due to the incorporation of HDO, and show a two-step degradation in the DTG profiles. The glass-transition temperature could be lowered to 128 °C (**PC3**) and 109 °C (**PC4**). We could highlight that erythrodiol is a relevant building block for bio-based polycarbonates, extending alternatives to the poly(bisphenol A carbonate). In future work, the pre- or post-polymerization modification of **ErDO** (units) via the internal double bond – such as in the case of poly(limonene carbonate)[223] – could be investigated, as well as the comparison with the structurally related diols betulin and uvaol.

5.4. Experimental Procedures

Analytical data and the procedure of **ErDO** can be found in Section 4.4.

Erythrodiol-3,28-diyl dimethyl bis(carbonate) (ErDO-BMC)

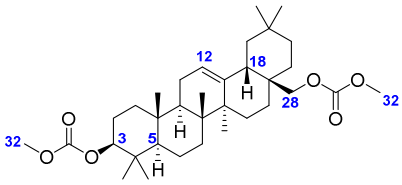

ErDO-BMC

To **ErDO** (50.0 mg, 118 µmol, 1.0 eq) and sodium *tert*-butoxide (0.2 mg, 2.36 µmol, 0.02 eq), DMC (100 µL, 1180 µmol, 10 eq) was added under a dry atmosphere. After heating at 130 °C for 3 h, the temperature was increased stepwise to 160 °C, removing residual DMC by distillation. The product was dried *in vacuo*, yielding **ErDO-BMC** as a white solid (55.0 mg, 117 µmol, 99%) that was used for analysis without any further purification.

^{1}H NMR (600 MHz, $CDCl_3$): δ [ppm] = 5.21 (t, J = 3.7 Hz, 1H, H_{12}), 4.33 (dd, J = 11.3, 5.0 Hz, 1H, H_3), 4.13 (d, J = 10.6 Hz, 1H, H_{28}), 3.79 – 3.73 (m, 7H, H_{28}+H_{32}), 2.03 (dd, J = 13.7, 5.1 Hz, 1H, H_{18}), 1.98 – 1.79 (m, 3H), 1.78 – 1.62 (m, 5H), 1.62 – 1.46 (m, 4H), 1.46 – 1.24 (m, 4H), 1.24 – 1.12 (m, 2+3H), 1.12 – 0.98 (m, 3H), 0.96 (s, 3H), 0.95 (s, 3H), 0.94 (s, 3H), 0.89 (s, 3H), 0.88 (s, 3H), 0.87 (s, 3H), 0.83 (dd, J = 11.8, 1.9 Hz, 1H, H_5).

^{13}C{^{1}H} NMR (151 MHz, $CDCl_3$): δ [ppm] = 156.2, 156.0, 143.7, 123.0, 85.6, 74.6, 55.4, 54.8, 54.6, 47.6, 46.3, 42.6, 41.8, 40.0, 38.4, 38.1, 36.9, 36.2, 34.0, 33.3, 32.6, 31.4, 31.0, 28.1, 26.1, 25.7, 23.7, 23.7, 23.7, 22.1, 18.3, 16.8, 16.7, 15.7.

HRMS (ESI): $[M+Na]^+$ *m/z* 581.3812 (calculated for $C_{34}H_{54}O_6Na^+$: *m/z* 581.3813).

TGA (Ar): $T_{d5\%}$ = 276 °C.

Procedure for the purification of polymers and oligomers

The remaining solvent was removed under reduced pressure and moderate heat. Subsequently, the polymer was redissolved in hot chloroform and precipitated in cold methanol (−20 °C). After filtration, the polymer was dried *in vacuo*.

Poly(erythrodiol carbonate) (PC1)

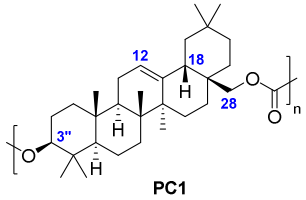

PC1

ErDO (100 mg, 237 µmol, 1.0 eq) and sodium *tert*-butoxide (0.5 mg, 4.73 µmol, 0.02 eq) were dissolved in DMC (200 µL, 2370 µmol, 10 eq) by stirring the mixture at 120 °C. The temperature was increased stepwise to 180 °C, followed by the addition of *n*-tetradecane (0.4 mL, 0.6 M). The reaction mixture was further stirred at 230 °C for 72 h. After removing the solvent and purification via precipitation, **PC1** was obtained as a slight beige powder (92 mg, 196 µmol, 83% yield).

^{1}H NMR (600 MHz, $CDCl_3$): δ [ppm] = 5.26 – 5.15 (m, 1H, H_{12}), 4.39 – 4.29 (m, 1H, $H_{3''}$), 4.16 – 4.01 (m, 1.4H, H_{28}), 3.83 (d, J = 10.9 Hz, 0.6H, H_{28}), 3.80 – 3.75 (m, 0.5H, CO_3Me), 2.07 – 1.98 (m, 1H, H_{18}), 1.98 – 0.75 (m, 43H).

^{13}C{^{1}H} NMR (151 MHz, $CDCl_3$): δ [ppm] = 155.9, 143.8, 122.9, 85.0, 74.0, 55.4, 47.7, 46.4, 42.6, 41.8, 40.0, 38.5, 38.3, 37.0, 36.5, 34.1, 33.3, 32.6, 31.3, 31.0, 28.1, 26.1, 25.8, 23.8, 23.7, 23.7, 22.2, 18.3, 16.9, 16.8, 15.7.

SEC ($CHCl_3$): M_n = 5900 g/mol, M_w = 10000 g/mol, $Đ$ = 1.70.

TGA (Ar): $T_{d5\%}$ = 335 °C. **DSC** (Ar): T_g = 232 °C.

General procedure for synthesis of oligomers (A1)

A solution of **ErDO** (80 mg, 189 µmol, 1.0 eq), diphenyl carbonate (DPC, 1.1–1.6 eq), sodium *tert*-butoxide (0.4 mg, 3.78 µmol, 0.02 eq), and diphenyl ether (1.0 mL, 0.19 M) was heated at 200 °C for 1 h. Afterwards, the pressure was reduced to 200 mbar and the mixture was stirred at 190 °C for 72 h. Purification of the oligomers was achieved by precipitation in cold methanol, similar as mentioned before.

For the reported NMR data, it should be noted that the oligomers have varying end-group compositions. Therefore, integrals are given as decimal values. The proton at C-3, with different adjacent groups, is assigned as follows: H-3 (secondary alcohol), H-3' (phenyl carbonate), and H-3" (bridging carbonate).

Oligo(erythrodiol carbonate) (OC8)

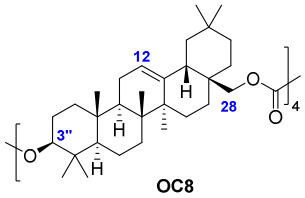

OC8

According to the general procedure A1, **OC8** was synthesized from **ErDO** (80 mg, 189 µmol, 1.0 eq) and diphenyl carbonate (45 mg, 208 µmol, 1.1 eq) in Ph_2O at 190 °C under reduced pressure. The oligomer could be isolated as a white powder (44 mg, 94.7 µmol, 50% yield) after purification.

^{1}H NMR (400 MHz, $C_2D_2Cl_4$): δ [ppm] = 5.22 – 5.09 (m, 1.0H, H_{12}), 4.27 (t, J = 8.0 Hz, 0.6H, $H_{3''}$), 4.10 – 3.91 (m, 1.0H, H_{28}), 3.87 – 3.65 (m, 1.0H, H_{28}), 3.16 (dd, J = 10.7, 5.0 Hz, 0.4H, H_3), 2.06 – 0.61 (m, 50H).

^{13}C{^{1}H} NMR (101 MHz, $C_2D_2Cl_4$): δ [ppm] = 155.9, 155.8, 143.8, 123.2, 85.3, 79.2, 74.1, 55.5, 47.7, 46.4, 42.6, 41.8, 40.0, 38.9, 38.3, 37.0, 36.4, 34.2, 33.5, 32.8, 31.5, 31.1, 28.2, 26.3, 25.8, 23.9, 23.8, 23.8, 22.4, 18.5, 17.0, 16.9, 15.8.

SEC ($CHCl_3$): M_n = 2300 g/mol, M_w = 3200 g/mol, $Đ$ = 1.41.

Oligo(erythrodiol carbonate) (OC9)

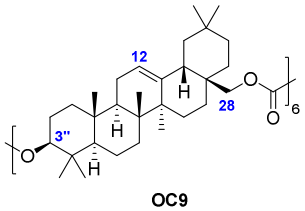

OC9

According to the general procedure A1, **OC9** was prepared from **ErDO** (80 mg, 189 µmol, 1.0 eq) and diphenyl carbonate (61 mg, 284 µmol, 1.5 eq) in Ph_2O at 190 °C under reduced pressure. The oligomer could be obtained as a white powder (56 mg, 120 µmol, 63% yield) after purification.

^{1}H NMR (400 MHz, $C_2D_2Cl_4$): δ [ppm] = 7.41 – 7.12 (m, 0.3H, CO_3Ph), 5.23 – 5.09 (m, 1.0H, H_{12}), 4.42 – 4.32 (m, 0.1H, $H_{3'}$), 4.27 (t, J = 8.0 Hz, 0.7H, $H_{3''}$), 4.07 – 3.89 (m, 1.0H, H_{28}), 3.87 – 3.65 (m, 1.0H, H_{28}), 3.21 – 3.10 (m, 0.3H, H_3), 2.11 – 0.62 (m, 51H).

$^{13}C\{^{1}H\}$ NMR (101 MHz, $C_2D_2Cl_4$): δ [ppm] = 155.9, 155.8, 143.8, 123.1, 85.3, 79.2, 74.1, 55.5, 47.7, 46.4, 42.6, 41.8, 40.0, 38.9, 38.3, 37.0, 36.5, 34.2, 33.5, 32.7, 31.4, 31.1, 28.2, 26.2, 25.8, 23.9, 23.8, 23.8, 22.3, 18.5, 17.0, 16.9, 15.8.

SEC ($CHCl_3$): M_n = 3300 g/mol, M_w = 5400 g/mol, $Đ$ = 1.66.

TGA (Ar): $T_{d5\%}$ = 330 °C. **DSC** (Ar): T_g = 245 °C.

Oligo(erythrodiol carbonate) (OC10)

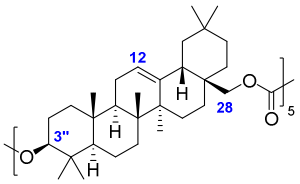

OC10

According to the general procedure A1, **OC10** was formed via the catalyzed reaction between **ErDO** (80 mg, 189 µmol, 1.0 eq) and diphenyl carbonate (65 mg, 303 µmol, 1.6 eq) in Ph_2O at 190 °C under reduced pressure. The oligomer could be obtained as a white powder (58 mg, 124 µmol, 66% yield) after purification.

^{1}H NMR (400 MHz, $C_2D_2Cl_4$): δ [ppm] = 7.41 – 7.12 (m, 1.5H, CO_3Ph), 5.24 – 5.10 (m, 1.0H, H_{12}), 4.38 (dd, J = 10.8, 5.5 Hz, 0.3H, $H_{3'}$), 4.27 (t, J = 8.1 Hz, 0.7H, $H_{3''}$), 4.09 – 3.90 (m, 1.0H, H_{28}), 3.87 – 3.69 (m, 1.0H, H_{28}), 3.20 – 3.12 (m, 0.1H, H_3), 2.10 – 0.65 (m, 51H).

$^{13}C\{^{1}H\}$ NMR (101 MHz, $C_2D_2Cl_4$): δ [ppm] = 155.9, 155.8, 153.9, 151.3, 143.8, 129.8, 126.3, 123.0, 121.6, 86.9, 85.3, 74.0, 55.5, 47.7, 46.4, 42.6, 41.8, 40.0, 38.5, 38.3, 37.0, 36.4, 34.2, 33.5, 32.7, 31.5, 31.1, 28.2, 26.2, 25.8, 23.9, 23.8, 23.8, 22.3, 18.5, 17.0, 16.9, 15.8.

SEC ($CHCl_3$): M_n = 3200 g/mol, M_w = 5100 g/mol, $Đ$ = 1.62.

TGA (Ar): $T_{d5\%}$ = 318 °C. **DSC** (Ar): T_g = 227 °C.

Poly[(1,6-hexanediol)-*co*-(erythrodiol)] (PC2)

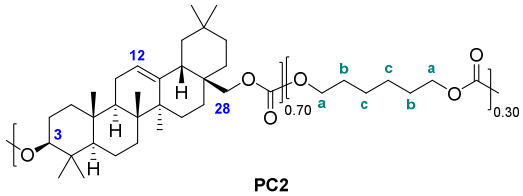

PC2

To **ErDO** (100 mg, 237 µmol, 0.7 eq), 1,6-hexanediol (12.0 mg, 102 µmol, 0.3 eq), sodium *tert*-butoxide (0.7 mg, 6.77 µmol, 0.02 eq), and dimethyl carbonate (290 µL, 3390 µmol, 10 eq) were added, and the mixture was heated at 130 °C for one hour. The temperature was increased further to 180 °C, the mixture was diluted with 1,3-dimethoxybenzene (1.7 mL, 0.2 M), and the solution was stirred at 220 °C for 72 h. The crude product was dried, redissolved in chloroform, and precipitated in cold methanol. After filtration and drying *in vacuo*, **PC2** could be obtained as a white powder (98 mg, 264 µmol, 78% yield).

^{1}H NMR (400 MHz, $CDCl_3$): δ [ppm] = 5.24 – 5.15 (m, 1H, H_{12}), 4.38 – 4.29 (m, 1H, H_3), 4.17 – 4.02 (m, 2.2H, H_a + H_{28}), 3.83 (d, J = 10.8 Hz, 0.5H, H_{28}), 3.80 – 3.76 (m, 0.4H, CO_3Me), 3.76 – 3.71 (m, 0.4H, H_{28}), 2.08 – 0.71 (m, 55H).

^{13}C{^{1}H} NMR (101 MHz, $CDCl_3$): δ [ppm] = 155.9, 155.8, 155.6, 143.8, 122.9, 85.0, 74.0, 67.9, 67.8, 55.4, 47.6, 46.4, 42.6, 41.8, 39.9, 38.2, 38.1, 36.9, 36.4, 34.1, 33.3, 32.6, 31.3, 31.0, 28.7 (2C), 28.1, 26.1, 25.7, 25.5 (2C), 23.8, 23.7, 23.7, 22.2, 18.3, 16.8, 16.8, 15.7.

SEC ($CHCl_3$): M_n = 5900 g/mol, M_w = 8600 g/mol, $Đ$ = 1.46.

TGA (Ar): $T_{d5\%}$ = 321 °C. **DSC** (Ar): T_g not detected.

Poly[(1,6-hexanediol)-*co*-(erythrodiol)] (PC3)

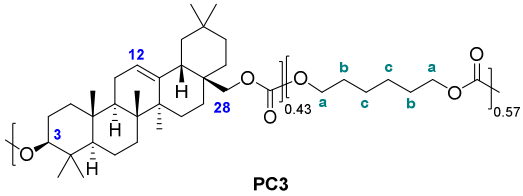

PC3

ErDO (179 mg, 423 µmol, 0.5 eq), 1,6-hexanediol (50.0 mg, 423 µmol, 0.5 eq), and sodium *tert*-butoxide (1.6 mg, 16.9 µmol, 0.02 eq) were dissolved by heating in dimethyl carbonate (500 µL, 5920 µmol, 10 eq) at 130 °C for one hour. At 180 °C, the mixture was diluted with diphenyl ether (1.2 mL, 0.7 M), and the solution was stirred at 220 °C for 72 h. The

crude polymer was dried, redissolved in chloroform, and precipitated in cold methanol. **PC3** was obtained as a white powder (196 mg, 687 µmol, 81% yield).

^{1}H NMR (400 MHz, $CDCl_3$): δ [ppm] = 5.25 – 5.15 (m, 1H, H_{12}), 4.38 – 4.28 (m, 1H, H_3), 4.18 – 4.01 (m, 6H, H_a + H_{28}), 3.82 (d, J = 10.3 Hz, 0.3H, H_{28}), 3.79 – 3.76 (m, 0.4H, CO_3Me), 3.73 (d, J = 10.8 Hz, 0.6H, H_{28}), 2.09 – 0.74 (m, 66H).

^{13}C{^{1}H} NMR (101 MHz, $CDCl_3$): δ [ppm] = 155.8, 155.5, 155.5, 143.7, 123.0, 85.3, 74.4, 67.9 (2C), 55.4, 47.6, 46.3, 42.6, 41.8, 39.9, 38.4, 38.1, 36.9, 36.3, 34.0, 33.3, 32.6, 31.5, 31.0, 28.7 (2C), 28.1, 26.1, 25.7, 25.5 (2C), 23.7, 23.7, 23.7, 22.0, 18.3, 16.8, 16.8, 15.7.

SEC ($CHCl_3$): M_n = 6600 g/mol, M_w = 13600 g/mol, $Đ$ = 2.06.

TGA (Ar): $T_{d5\%}$ = 310 °C. **DSC** (Ar): T_g = 128 °C.

Poly[(1,6-hexanediol)-*co*-(erythrodiol)] (PC4)

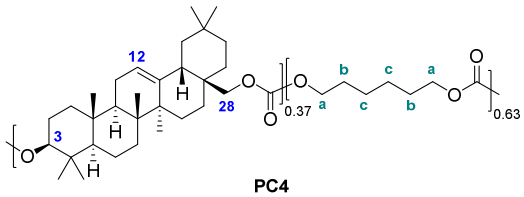

PC4

ErDO (138 mg, 326 µmol, 0.3 eq), 1,6-hexanediol (90.0 mg, 762 µmol, 0.7 eq), and sodium *tert*-butoxide (2.1 mg, 21.8 µmol, 0.02 eq) were dissolved by heating in dimethyl carbonate (920 µL, 10.9 mmol, 10 eq) at 130 °C for one hour. The temperature was increased stepwise to 220 °C and heated further for 72 h. **PC4** was dissolved in chloroform and precipitated in cold methanol, yielding a white solid (229 mg, 856 µmol, 79% yield).

^{1}H NMR (400 MHz, $CDCl_3$): δ [ppm] = 5.25 – 5.14 (m, 1H, H_{12}), 4.39 – 4.27 (m, 1H, H_3), 4.20 – 4.00 (m, 8H, H_a + H_{28}), 3.87 – 3.79 (m, 0.2H, H_{28}), 3.79 – 3.76 (m, 0.2H, CO_3Me), 3.73 (d, J = 10.8 Hz, 0.6H, H_{28}), 2.11 – 0.65 (m, 65H).

^{13}C{^{1}H} NMR (101 MHz, $CDCl_3$): δ [ppm] = 155.8, 155.5, 155.5, 143.7, 123.0, 85.3, 74.4, 67.9 (2C), 55.4, 47.6, 46.3, 42.6, 41.8, 39.9, 38.4, 38.1, 36.9, 36.2, 34.0, 33.3, 32.6, 31.5, 31.0, 28.7 (2C) 28.1, 26.1, 25.7, 25.5 (2C), 23.7, 23.7, 23.7, 22.0, 18.3, 16.8, 16.8, 15.7.

SEC ($CHCl_3$): M_n = 32800 g/mol, M_w = 73500 g/mol, $Đ$ = 2.24.

TGA (Ar): $T_{d5\%}$ = 319 °C. **DSC** (Ar): T_g = 109 °C.

Poly(hexamethylene carbonate) (PC5)

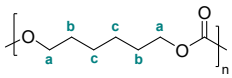

PC5

To 1,6-hexanediol (700 mg, 5.92 mmol, 1.0 eq), TBD (16.5 mg, 118 µmol, 0.02 eq) and dimethyl carbonate (1.0 mL, 11.8 mmol, 2.0 eq) were added, and the mixture was stirred at 130 °C for one hour. The temperature was increased stepwise to 220 °C, the pressure was reduced to 100 mbar, and the mixture was stirred overnight under these conditions. By dissolving in chloroform and precipitating in cold methanol, **PC5** could be obtained as a reddish solid (706 mg, 4.90 mmol, 83% yield), still discolored by the catalyst.

^{1}H NMR (600 MHz, $CDCl_3$): δ [ppm] = 4.11 (t, J = 6.7 Hz, 2H, H_a), 1.72 – 1.63 (m, 2H, H_b), 1.44 – 1.36 (m, 2H, H_c).

^{13}C{^{1}H} NMR (151 MHz, $CDCl_3$): δ [ppm] = 155.5, 67.9 (2C), 28.7 (2C), 25.5 (2C).

SEC ($CHCl_3$): M_n = 68100 g/mol, M_w = 205000 g/mol, $Đ$ = 3.02.

TGA (Ar): $T_{d5\%}$ = 310 °C. **DSC** (Ar): T_g = – 44 °C, T_m = 50 °C.

5.5. Supplementary Information

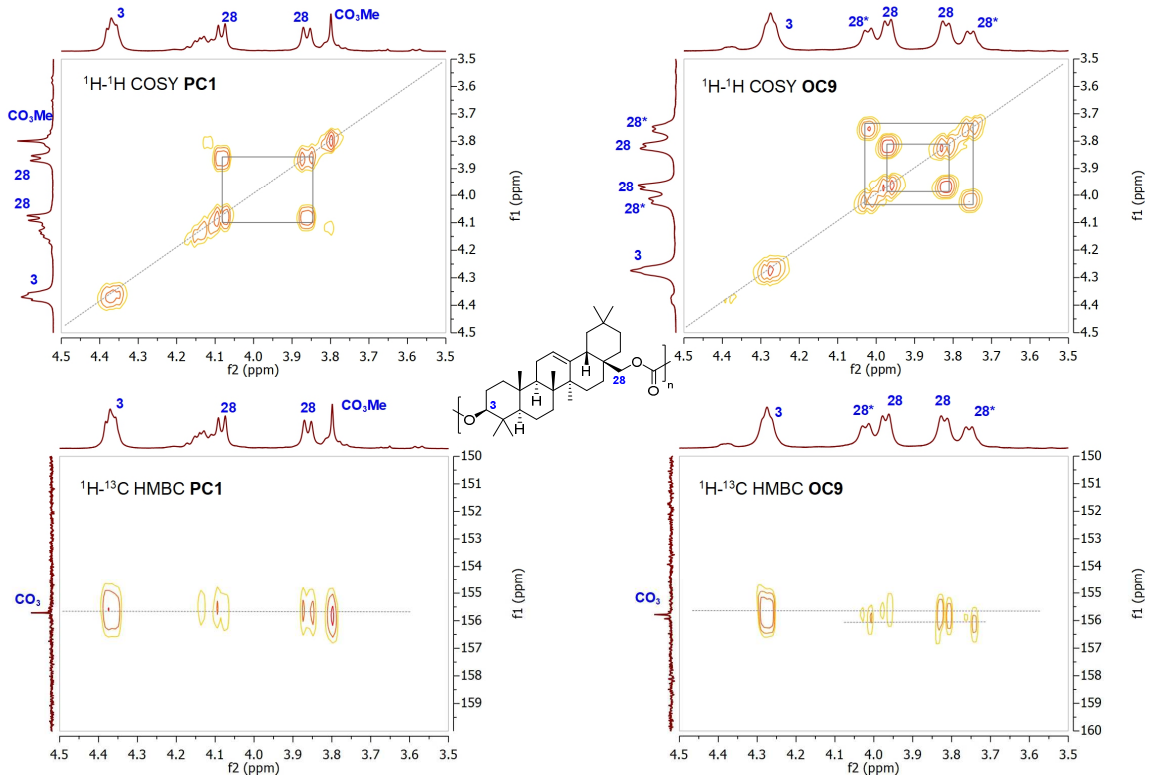

Figure S5.1. ^{1}H-^{1}H COSY and ^{1}H-^{13}C HMBC of **PC1** (reagent DMC, NMR in $CDCl_3$) and **OC9** (reagent DPC, NMR in $C_2D_2Cl_4$).

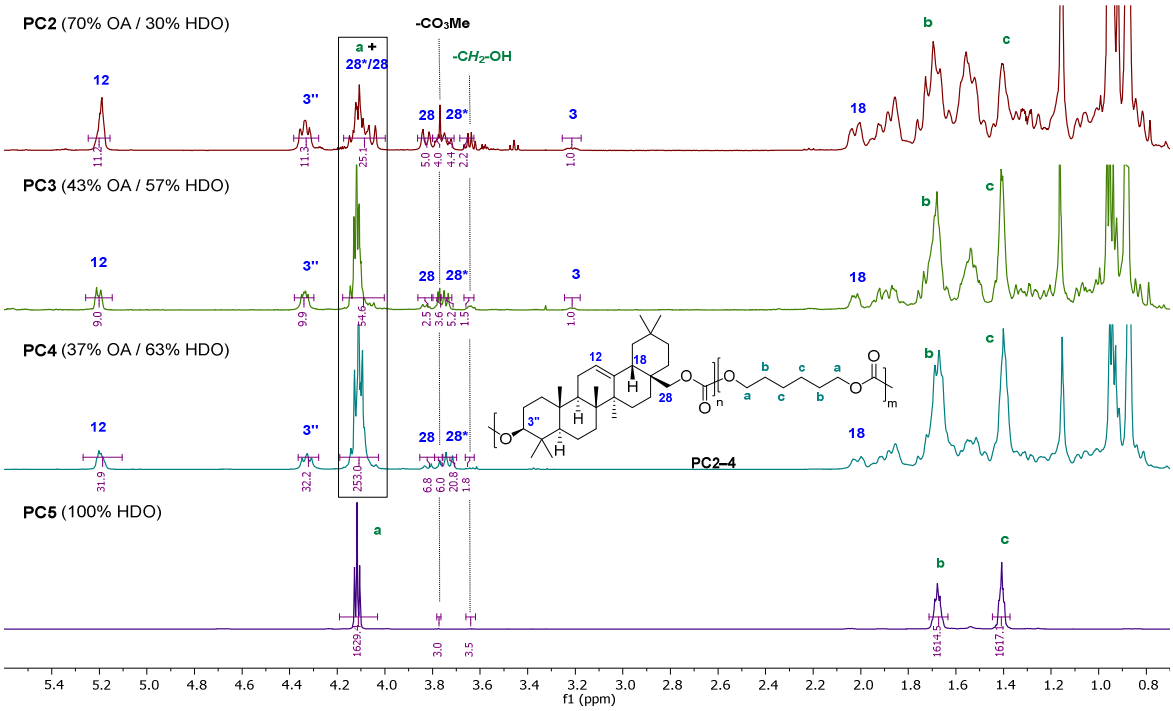

Figure S5.2. ^{1}H NMR spectra of copolymers **PC2**–**4** and homopolymer **PC5** for calculating a theoretical DP value of the ErDO and HDO block, as well as an average molecular weight.

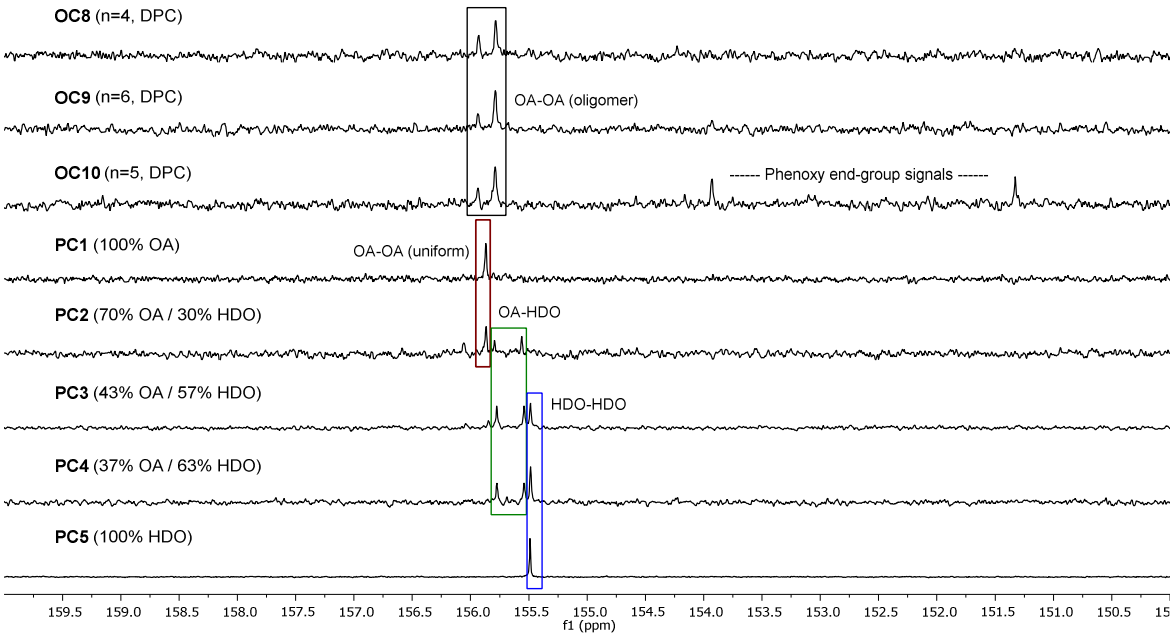

Figure S5.3. ^{13}C NMR segments from 160-150 ppm of all oligomeric and polymeric species, revealing the different environment and chemical shift of the carbonate groups by the adjacent units OA-OA, OA-HDO, and HDO-HDO.

6. Conclusion and Future Perspectives

In the present dissertation, the oleanolic acid (OA) motif was incorporated into polymethacrylates (PMA), polyurethanes (PU), and polycarbonates (PC) either as a pendant group in the side chain (PMA) or as a structural unit within the polymer backbone (PU/PC), highlighting its versatility as a bio-based building block for functional materials.

In the first part of the study (Chapter 3), OA-based methacrylic polymers could be obtained by RAFT polymerization. For this, five monomers were synthesized by modifying either the hydroxy- or carboxyl-function of OA in one to five steps. The monomers show a low solubility in most of the solvents suitable for thermal polymerization. Yet the green solvent *N*-butyl-2-pyrrolidone (NBP) could dissolve four of them (**MA1**, **MA3**, **MA4**, **MA1'**). The fifth one (**MA2**) required 1,1,2,2-tetrachloroethane (TeCA). It should be noted that the required diluted conditions and the bulky monomeric compounds can lead to higher dispersity compared to more soluble monomers like MMA with low steric hindrance. At first, a general polymerizability of the novel monomers by conventional free-radical polymerization (FRP) could be verified. Subsequently, the kinetics of the thermal RAFT polymerizations were studied using 2-cyano-2-propyl benzodithioate, one of the most active chain-transfer agents, adequate for methacrylates.

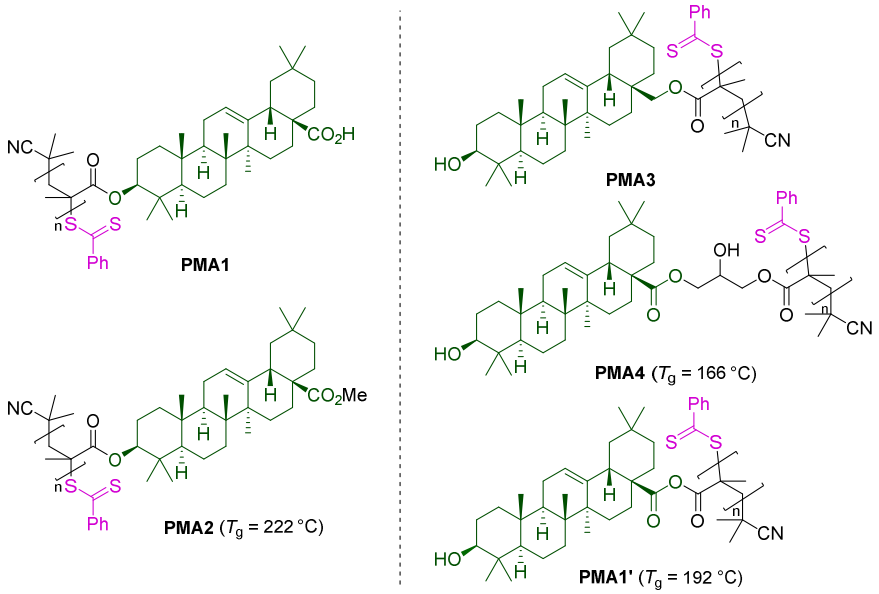

Figure 6.1. Polymethacrylates formed by RAFT polymerization (T_g for polymers with DP 50).

The kinetic investigations revealed a controlled radical polymerization by first-order kinetic behavior, a targetable average molar mass, and moderate dispersity at high conversion (DP 50, $Đ$ = 1.3–1.5) for **MA1–4**. In contrast, in **MA1'**, the polymerizable unit

is present as a mixed methacrylic anhydride that does not provide control in RAFT polymerization, particularly with regard to the evolution of molecular weight with conversion. Yet the polymerization degree (DP) could be influenced by the monomer-to-CTA ratio.

By increasing the targeted DP to 100, SEC revealed a tailing towards lower molar masses caused by a partial loss of control over the polymerization. All purified polymers (DP 50) showed degradation temperatures above 300 °C and T_g values in the range of 166–222 °C, except for **PMA1** and **PMA3**, where decomposition occurs before any thermal transition could be detected by DSC.

For future investigations, interesting monomers are the corresponding acrylates, since they typically exhibit higher propagation rates, and the polyacrylates tend to be more flexible with a lower T_g. This could make them suitable for applications that demand elasticity and strong adhesive properties, such as in glues and sealants. Yet the acrylate monomers might require radical inhibitors as an additive, since the synthesis of **MA3** as acrylate species already yielded insoluble polymerized material during purification.

To prove the preserved end-functionality of the RAFT polymers, **PMA2** was chain-extended in solution with benzyl methacrylate (BzMA). For further reactions, it could be beneficial to form another polymer block first and then chain-extend with the hydrophobic triterpenoid monomers, in order to optimize the use of the latter with high conversions. If the first block consists, for example, of hydrophilic methacrylic acid or oligo(ethylene glycol) methacrylate units, amphiphilic block copolymers can be prepared in solution polymerization, and assembly into nanoparticles might be induced in a second step, for instance, by nanoprecipitation. Dispersion polymerization and polymerization-induced self-assembly (PISA) in alcohols could pose challenges regarding the low solubility of **MA1–4**.

The second part of the study (Chapter 4) continues with the reduction of OA to erythrodiol (**ErDO**), which was utilized for the formation of linear PUs by polyaddition with various aliphatic (HDI, PDI, H_{12}MDI) and aromatic (4,4′-MDI) diisocyanates, catalyzed by $Sn(Oct)_2$. It was initially found that the polyaddition of **ErDO** and HDI, catalyzed by DBU or zinc diethyldithiocarbamate (ZDTC), is less efficient than with $Sn(Oct)_2$.

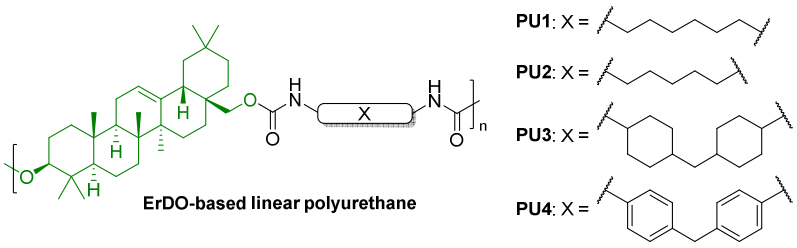

Figure 6.2. Polyurethanes based on **ErDO** and diisocyanates (HDI, PDI, H_{12}MDI, 4,4′-MDI).

All four PUs showed high molecular weight after purification (M_n = 21–43 kg/mol). IR spectroscopy revealed that the incorporation of the bulky OA unit partially disrupts hydrogen bonding interactions between urethane groups. **PU2** contains the bio-based, glucose-derived PDI instead of the fossil-based HDI, leading to a slight increase in T_g from 198 to 206 °C. **PU3** and **PU4**, with the rigid diisocyanates H_{12}MDI and 4,4′-MDI, show higher T_g values at 249 and 253 °C. Initially, decreasing glass transitions were detected at each heating cycle by reaching temperatures close to decomposition. Annealing of **PU1** at 240 °C led to a broadening of the polymer distribution as evidence for remaining $Sn(Oct)_2$, which promotes transurethanization reactions at high temperature in the solid phase. Ternary PUs with **ErDO**, 1,6-hexanediol (HDO), and PDI were obtained by ZDTC-catalyzed polyaddition and showed no signs of this thermal alteration. The **ErDO** content in each polymer was gradually reduced to 69, 54, and 33 mol%, with the effect of a softened polymer backbone represented in the T_g values descending from 147 to 81 °C.

Future work could be directed to the synthesis of NIPUs. Aliphatic diamines can be converted by dimethyl carbonate (DMC) into bis(carbamates), but due to the high melting point of **ErDO**, long-chain comonomers (e.g., C12) might be more suitable candidates for melt polycondensation. Further, a bis(cyclic carbonate) from **ErDO** could be synthesized starting with the ring-opening of epichlorhydrin (ECH) and the alkaline epoxide formation to **6-1** (Scheme 6.1). To avoid the use of the carcinogenic ECH, ether formation with allyl bromide could yield **6-3** in a first step.[248] *m*CPBA cannot be used for subsequent epoxidation to **6-1** since it may also react with the internal double bond of the triterpenoid. Therefore, vanadyl acetylacetonate and *tert*-butyl hydroperoxide might yield the desired product.[249] By the catalytic insertion of CO_2 into the epoxide groups of **6-1**, the difunctional 5-membered cyclic carbonate **6-2** can be obtained and used for polyaddition with diamines. Since this monomer synthesis will be challenging, another approach might be the coupling of **ErDO** with 1,1'-carbonyldiimidazole (CDI) in the presence of a catalyst or base (e.g.,

CsF, TEA, DBU) to obtain **6-4** and produce NIPUs by polycondensation with a diamine in melt[250] or potentially in solution.

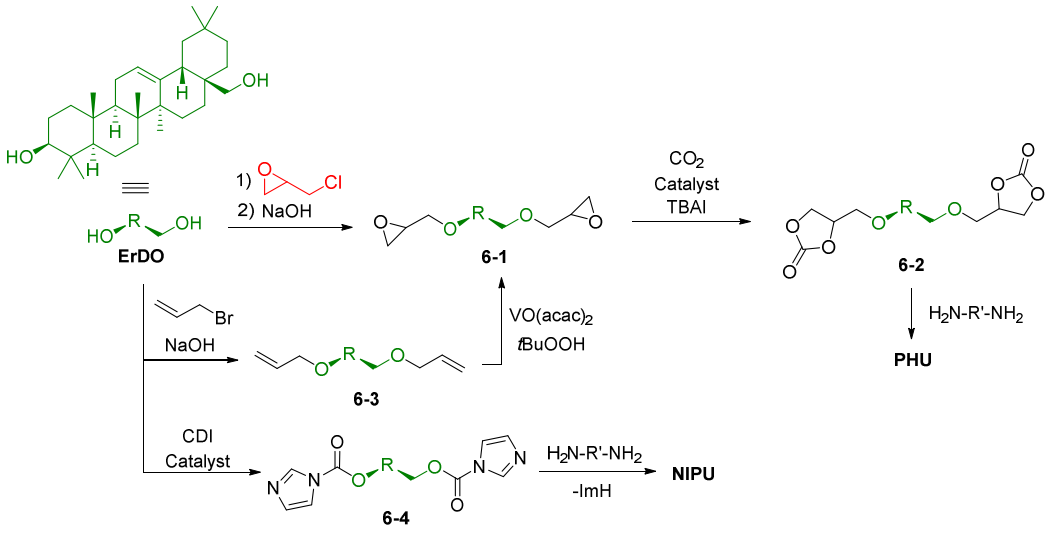

Scheme 6.1. Proposed monomer synthesis for the formation of NIPUs by bis(cyclic carbonate) **6-2** or bis(carbonylimidazole) **6-4**.

In the third part of the study (Chapter 5), **ErDO** was utilized to produce polycarbonates using DMC as a coupling reagent. A melt polycondensation could not be achieved, but an excess of DMC and an additional high-boiling solvent allowed the reaction at high temperature, forming the homopolymer **PC1** with low molecular weight (M_w = 10 kg/mol). This novel fully bio-based polycarbonate is thermally stable up to 300 °C and has a T_g at 232 °C. Since the use of diphenyl carbonate as a more reactive coupling agent did not deliver higher molecular weight species, HDO was used as a comonomer to facilitate the polymerization, owing to its potential impact on chain flexibility. The synthesis of high molecular weight **PC4** (M_w = 74 kg/mol) could be achieved by an **ErDO**/HDO molar ratio of 37:63, which lowered the T_g to 109 °C without significantly influencing the thermal stability.

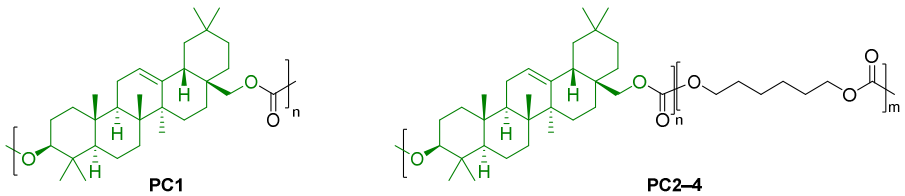

Figure 6.3. Polycarbonates as homopolymer **PC1** or random copolymers **PC2–4** (from **ErDO** and HDO)

Since **PC1** could be obtained with solely **ErDO** in the backbone, further investigations should be made for improvement. Apart from the reaction with triphosgene, Song and coworkers[251] demonstrated a fluoride-catalyzed polycondensation approach, wherein the

thermally labile 2,5-bis(hydroxymethyl)furan was converted with two equivalents of CDI and subsequently reacted with the diol itself. Carbonylimidazole end-groups have a higher reactivity in comparison to methyl carbonate end-groups, as well as the by-product imidazole is a weak nucleophile and does not require continuous removal.[252] Therefore, the direct polycondensation of **ErDO** with CDI as well as the copolymerization of **6-4** with various diols appear to be promising approaches, each promoted by either CsF catalysis or the use of DBU.[253]

Ring-opening polymerization (ROP) of a cyclic carbonate via chain growth produces polycarbonates with narrow dispersity. This technique could be accessible by using 2,2-bis(hydroxymethyl)propionic acid (bis-MPA) as a precursor. Park and coworkers[254] managed to form the ring-strained carbonate **6-5** by reacting bis-MPA with CDI and subsequent ring closure with acetic acid. **6-5** could be coupled to oleanolic acid methyl ester (**3-1**) by Steglich-type esterification, and the corresponding monomer **6-6** might be polymerized by organocatalyzed ROP, whereby the triterpenoid is incorporated as a side chain.

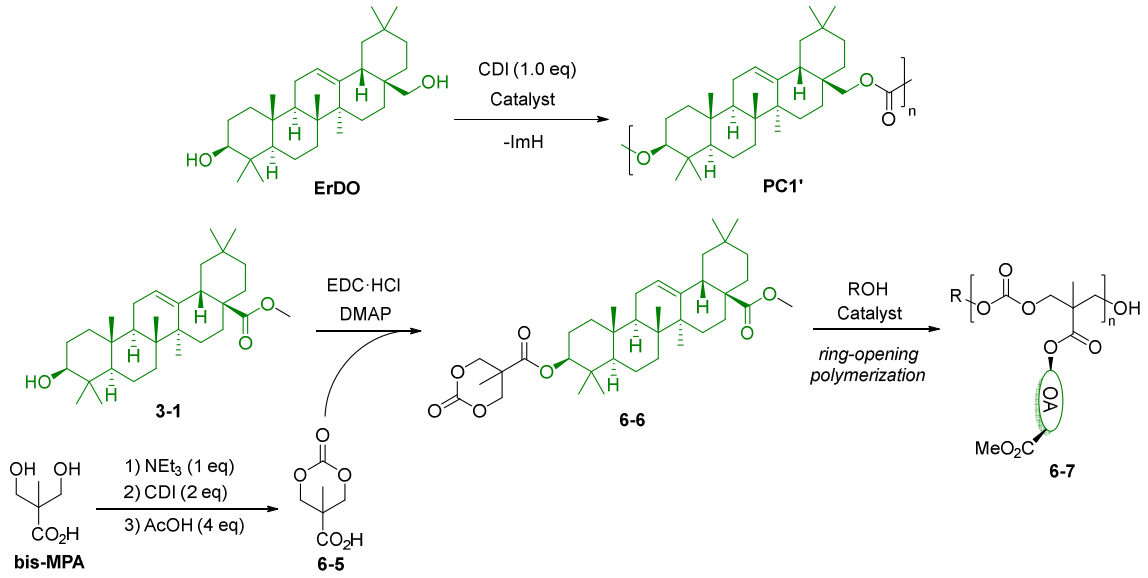

Scheme 6.2. Proposed synthesis of polycarbonates: a) **PC1'** by CDI-based polycondensation of **ErDO**, b) **6-7** by ROP of the OA-functionalized cyclic carbonate **6-6**.

Extract of apple peel containing UA and OA as a mixture could be a resource for further polymerizations, provided that other triterpenoid acids with multiple hydroxyl groups in minor quantity, such as pomolic acid or corosolic acid, can be separated beforehand.[59] The formation of polymers based on BA or betulin is particularly interesting, as they might be modified either pre- or post-polymerization by the thiol-ene reaction.

7. General Experimental Remarks

7.1. Materials

Specific reagents were obtained from the following suppliers with the given purity and used without purification:

Oleanolic acid (98%, abcr GmbH), methacryloyl chloride (MAC, 97%, abcr GmbH), methacrylic anhydride (94%, Sigma-Aldrich), 2-cyano-2-propyl benzodithionate (CPBD, 97%, abcr GmbH), *tert*-butyldimethylsilyl trifluoromethanesulfonate (TBSOTf, 98%, Sigma-Aldrich), 2,2′-azobis(2-methylpropionitrile) (AIBN, 98%, Sigma-Aldrich), 2,6-lutidine (99%, Thermo Scientific), 4-dimethylaminopyridine (DMAP, > 99%, TCI Deutschland GmbH), glycidyl methacrylate (GMA, > 97%, Sigma-Aldrich), *p*-toluenesulfonic acid monohydrate (*p*TsOH·H_2O, > 98%, TCI Deutschland GmbH), iodomethane (MeI, 99%, Thermo Fisher Scientific), 4-methoxyphenol (MeHQ, 99%, Thermo Scientific Chemicals), diisobutylaluminum hydride solution (DIBAL-H, 1.2 M in toluene, Acros Organics), *n*-butyl acetate (BA, > 99%, Thermo Scientific), 1,1,2,2-tetrachloroethane (TeCA, 98%, Thermo Fisher Scientific), *N*,*N*-dimethylacetamide (DMAc, > 99%, Carl Roth GmbH), *N*-butyl-2-pyrrolidone (NBP, > 99.5 %, Carl Roth GmbH).

Lithium aluminum hydride powder ($LiAlH_4$, 95%, Sigma-Aldrich), hexamethylene diisocyanate (HDI, > 99%, Sigma-Aldrich), pentamethylene diisocyanate (PDI, > 99%, Covestro Deutschland AG), 4,4'-methylenebis(cyclohexyl isocyanate) (H_{12}MDI, 90%, mixture of isomers, Thermo Fisher Scientific), 4,4'-methylenebis(phenyl isocyanate) (4,4'-MDI, 98%, Thermo Fisher Scientific), 1,6-hexanediol (HDO, 97%, Thermo Fisher Scientific), 1,8-diazabicyclo[5.4.0]undec-7-ene (DBU, > 99%, Sigma-Aldrich), tin(II) 2-ethylhexanoate ($Sn(Oct)_2$, 92.5–100.0%, Sigma-Aldrich), zinc diethyldithiocarbamate (ZDTC, > 99%, TCI Deutschland GmbH), chlorobenzene (PhCl, 99.8%, extra dry, Thermo Fisher Scientific), anisole (PhOMe, 99%, extra dry, Thermo Fisher Scientific).

Dimethyl carbonate (DMC, > 99%, Sigma-Aldrich), diphenyl carbonate (DPC, 99%, Thermo Fisher), sodium *tert*-butoxide (NaO*t*Bu, 98%, Thermo Scientific), 1,5,7-triazabicyclo[4.4.0]dec-5-ene (TBD, 98%, Sigma-Aldrich), diphenyl ether (Ph_2O, 99%, Acros Organics), *n*-tetradecane (> 99%, TCI Deutschland GmbH), 1,3-dimethoxybenzene (> 99%, TCI Deutschland GmbH)

All other reagents and solvents were obtained from commercial sources and were used without further purification, if not mentioned separately. Air- or water-sensitive reactions were carried out under an argon atmosphere in dry solvents. Benzyl methacrylate (BzMA, 98%, Alfa Aesar) was passed through a short aluminum oxide column to remove inhibitors. AIBN was recrystallized from ethanol and stored at 4 °C. Dry dichloromethane (DCM) and tetrahydrofuran (THF) were obtained from the solvent purification system SPS 800 (MBraun GmbH). Flash column chromatography was performed on silica gel 60 (0.040–0.063 mm, 230–400 mesh, Carl Roth GmbH)**.** Monomer synthesis was monitored by thin-layer chromatography (TLC, SIL G/UV_{254}), with the silica plates being stained with an alkaline $KMnO_4$ solution and subsequent heating. OA and all monomers were stored in a refrigerator (4 °C).

7.2. Analytical Techniques

Nuclear magnetic resonance (NMR) spectroscopy

^{1}H and ^{13}C NMR spectra were recorded on a Bruker Avance III 600 (basis frequencies: ^{1}H: 600 MHz, ^{13}C: 151 MHz) or an Avance 400 spectrometer (basis frequencies: ^{1}H: 400 MHz, ^{13}C: 101 MHz) at 300 K (resp. 353 K). Chemical shifts are reported in ppm, relative to the solvent signal. Coupling constants (*J*) are reported in Hz, and the multiplicity of signals is described as s (singlet), d (doublet), t (triplet), and m (multiplet). The deuterated solvents used are stated in the protocol: $CDCl_3$ (300 K), THF-d_8 (300 K), TeCA-d_2 (300 K, 353 K), DMSO-d_6 (300 K, 353 K). Solvent signals from TeCA-d_2 were referenced to 5.96 ppm (s, ^{1}H NMR) and 74.2 ppm (t, $^{13}C\{^{1}H\}$ NMR).

High-resolution mass spectrometry (HRMS)

HRMS spectra were obtained using ESI or APCI ionization on a Bruker Daltronic micrOTOF.

Infrared spectroscopy (IR)

IR spectra were measured on an FTIR spectrometer ALPHA from Bruker Corporation with an ATR unit. Each band is described with the intensity using the following descriptors (s – strong, m – medium, w – weak, vw – very weak).

Size-exclusion chromatography (SEC)

The average molecular weight of the polymers was determined by analytical size-exclusion chromatography (SEC) with DMAc, THF, or $CHCl_3$ as solvent.

SEC with DMAc was performed on a PSS/Agilent SECurity² system at 50 °C using LiBr (0.28 g/L) as an additive, at an elution rate of 1.0 mL/min. The system was equipped with a PSS PFG precolumn (7 µm, 8 × 50 mm), three separating PFG columns (7 µm, 8 × 300 mm, porosities: 100, 1000, 4000 Å), and an RI detector (P/N 404-2106). The SEC system was calibrated with linear poly(methyl methacrylate) standards.

SEC with THF and $CHCl_3$ was performed on two separate Agilent SECurity SEC systems, equipped each with a diode array (ALS G1329A) and RI detector (G1362A) at an elution rate of 1.0 mL/min (25 °C). Separation proceeded by a pair of SEC columns (PSS Linear M SDV, 5 µm, 8 × 300 mm, mixed porosity) aside from the precolumn (PSS SDV guard column, 5 µm, 8 × 50 mm). Both systems were run with solvents containing the internal stabilizer BHT and were calibrated with polystyrene standards.

Thermogravimetric analysis (TGA)

TGA was performed on a Mettler Toledo TGA/DSC 1 STAR^e System with an SDTA sensor in the range of 35–600 °C or 35–900 °C, a heating rate of 10 K/min, and an argon stream of 50.0 mL/min.

Differential scanning calorimetry (DSC)

DSC measurements were carried out on a Mettler Toledo TGA/DSC 1 STAR^e System (FRS5 400W) with a heating rate of 10 K/min (except **PC1**: 20 K/min) and an argon stream of 30.0 mL/min. As usual, the second or third heating curve was used.

8. Appendix

8.1. Depolymerization

The thermal RAFT depolymerization process has recently shown great promise as a strategy for chemical polymer recycling.[255,256] Upon thermal dissociation, the RAFT end group forms a chain-end radical via homolytic C−S bond cleavage, which allows depolymerization.[257] Since exceeding the ceiling temperature (T_c) in bulk conditions is not feasible for most polymers, conducting the reaction under dilute conditions can favor depropagation over propagation, as it proceeds via a unimolecular rather than a bimolecular mechanism.[257] Due to steric effects, bulkier polymer side chains can result in a lower T_c, making the depolymerization of OA-based polymethacrylates a promising approach.

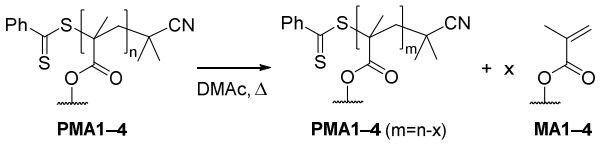

Scheme 8.1. General depolymerization of OA-based polymethacrylates (in DMAc).

The depolymerization experiments of **PMA1** were initially carried out in DMAc, chosen for its high boiling point and favorable solubilization properties for **PMA1**. The conversion of the reaction mixture was determined by ^{1}H NMR, comparing the integrals of the overlapping signals from the double bond of the OA structure in both monomer and polymer with the distinct methacrylate signals (Figure 8.1). In dilute conditions (5 mM), a maximum depolymerization conversion of 12% was detected, while concentrated conditions led to an unexpectedly higher conversion of 34% (at 200 mM). A comparable experiment with **PMA3** resulted in a similar conversion of 28%, whereby **PMA2** required dilution (100 mM) to dissolve at 120 °C. **PMA4** could only be depolymerized to 14%, possibly due to the less rigid glycerol-type linker.

Based on these results, future investigations aimed at depolymerization could explore diluted conditions using an alternative solvent to DMAc, yet non-stabilized 1,4-dioxane or dimethyl sulfoxide did not lead to any significant conversion.

Table 8.1. Depolymerization experiments of **PMA1-4** in DMAc.

Polymer	c [mol/L]	*T* [°C]	*t* [h]	Conv. [%]
PMA1	0.005	100	16	5
		110	16	12
		120	16	4
	0.1	120	4	22
		130	4	23
	0.2	100	16	22
		120	**4**	**34**
		120	8	25
PMA2	0.1	120	4	29
PMA3	0.2	120	4	28
PMA4	0.2	120	4	12

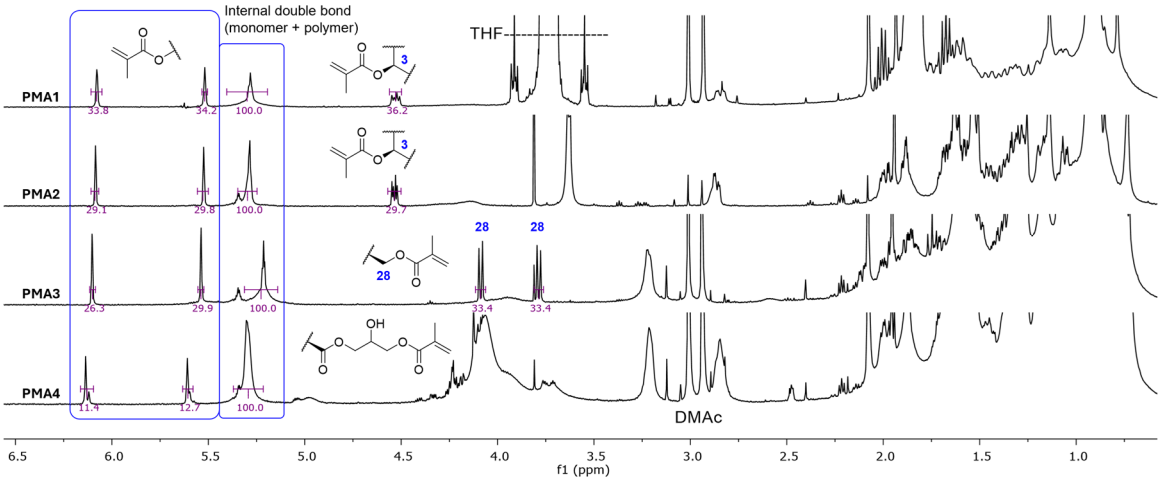

Figure 8.1. ^{1}H NMR spectra from depolymerization experiments of **PMA1-4** (concentrated raw mixtures with DMAc residue, dissolved in $CDCl_3$).

8.2. Double-Bond Modification

The internal double bond in OA presents a potential site for pre- or post-polymerization modification, for instance via the thiol-ene reaction. In the reaction of OA with 2-mercaptoethanol and AIBN, only minor conversion was indicated by ^{1}H NMR spectroscopy. However, this could not be fully confirmed and was not further investigated. Bensberg[258] showed in her dissertation that the double bond of a UA derivative (3-acetoxy-urs-12-en-28-oic acid methyl ester) could not be targeted by catalytic hydrogenation, possibly caused by steric hindrance. In contrast, the epoxidation should be possible, as

proven by Park and coworkers[259] on 3-acetoxy-olean-12-en-28-oic acid methyl ester with *m*CPBA. However, acidic silica in the purification step causes a rearrangement to the corresponding ketone. Therefore, polyurethane **PU1** was treated with *m*CPBA, since purification by precipitation in diethyl ether is sufficient. In the ^{1}H NMR spectrum (Figure 8.2), an upfield shift of the H-12 signal from 5.19 to 2.93 ppm could be observed, indicating the formation of the epoxide. Experiments to ring-open the epoxide with benzylamine showed no significant conversion, potentially due to steric hindrance or prior hydrolysis to an inactive diol at C-12 and C-13.

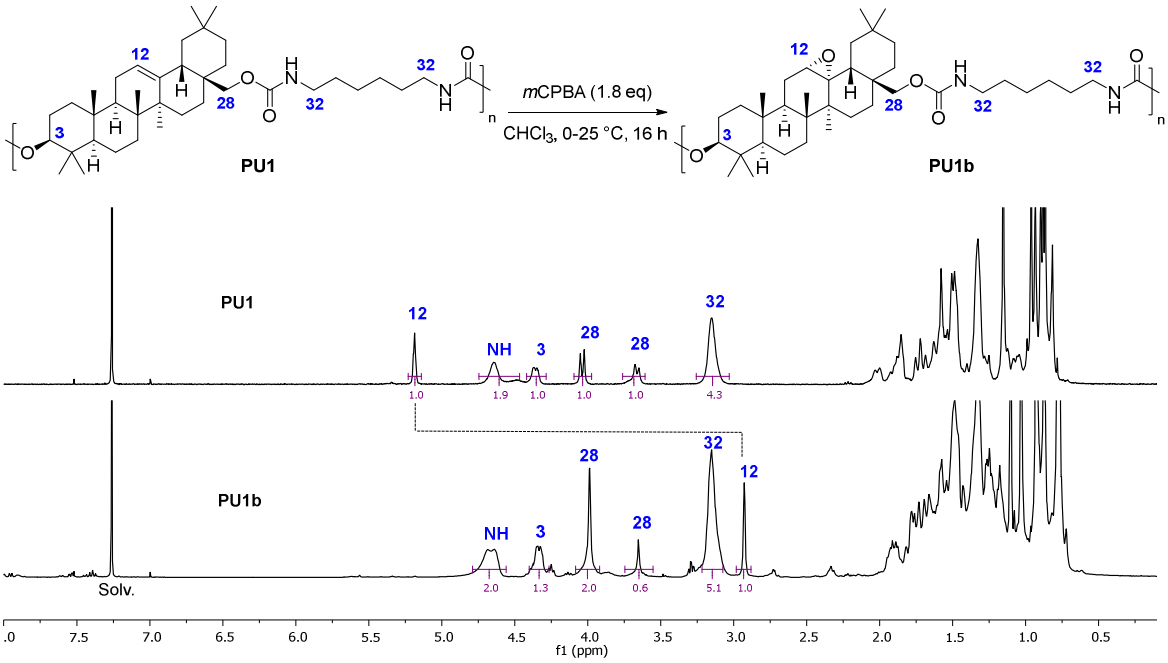

Figure 8.2. (Top) Epoxidation reaction of **PU1**. (Bottom) ^{1}H NMR spectra of **PU1** and the corresponding epoxide (**PU1b**) in $CDCl_3$.

8.3. Abbreviations

4,4′-MDI	4,4′-diphenylmethane diisocyanate
AIBN	azobisisobutyronitrile
aPC	aliphatic polycarbonate
APCI	atmospheric pressure chemical ionization
aq.	aqueous
ATR	attenuated total reflection
BHT	butylated hydroxytoluene
BPA	bisphenol A
BPA-PC	poly(bisphenol A carbonate)
CC	cyclic carbonate
CH	cyclohexane
CPBD	2-cyano-2-propyl benzodithioate
CPME	cyclopentyl methyl ether
CTA	chain-transfer agent
CYP	cytochrome P450
DBU	1,8-diazabicyclo[5.4.0]undec-7-ene
DCM	dichloromethane
DIBAL-H	diisobutylaluminum hydride
DMAc	*N*,*N*-dimethylacetamide
DMAP	4-dimethylaminopyridine
DMC	dimethyl carbonate
DMF	*N*,*N*-dimethylformamide
DPC	diphenyl carbonate
DSC	differential scanning calorimetry
EA	ethyl acetate
ErDO	erythrodiol
ESI	electrospray ionization
FRP	free-radical polymerization
GMA	glycidyl methacrylate
H_{12}MDI	4,4′-dicyclohexylmethane diisocyanate
HDI	hexamethylene diisocyanate
HDO	1,6-hexanediol

$LiAlH_4$	lithium aluminium hydride
MAC	methacryloyl chloride
*m*CPBA	*meta*-chloroperoxybenzoic acid
NBP	*N*-butyl-2-pyrrolidinone
NIPU	non-isocyanate polyurethane
NMR	nuclear magnetic resonance spectroscopy
PC	polycarbonate
PDI	pentamethylene diisocyanate
PISA	polymerization-induced self-assembly
PMA	polymethacrylate
PMMA	polymethylmethacrylate
PS	polystyrene
PU	polyurethane
RAFT	reversible addition−fragmentation chain transfer
RDRP	reversible-deactivation radical polymerization
ROP	ring-opening polymerization
SEC	size exclusion chromatography
$Sn(Oct)_2$	tin(II) 2-ethylhexanoate
TA	triterpenoid acid
TBD	1,5,7-triazabicyclo[4.4.0]dec-5-ene
TBSOTf	*tert*-butyldimethylsilyl trifluoromethanesulfonate
TeCA	1,1,2,2-tetrachloroethane
TGA	thermogravimetric analysis
THF	tetrahydrofuran
ZDTC	zinc diethyldithiocarbamate

8.4. ^{1}H and ^{13}C NMR Spectra

Ch. 3: Oleanolic Acid-Derived High-Glass-Transition-Temperature Methacrylic Polymers

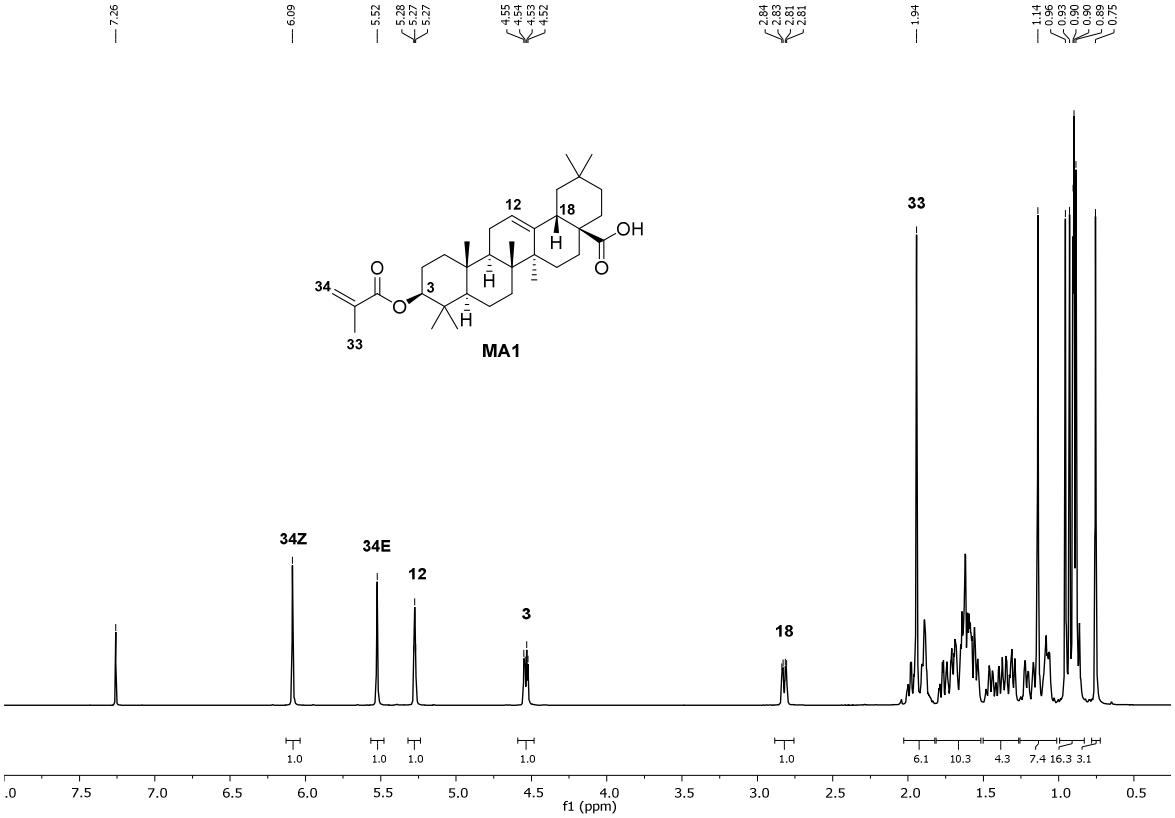

Figure 8.3. ^{1}H NMR spectrum of **MA1** in $CDCl_3$.

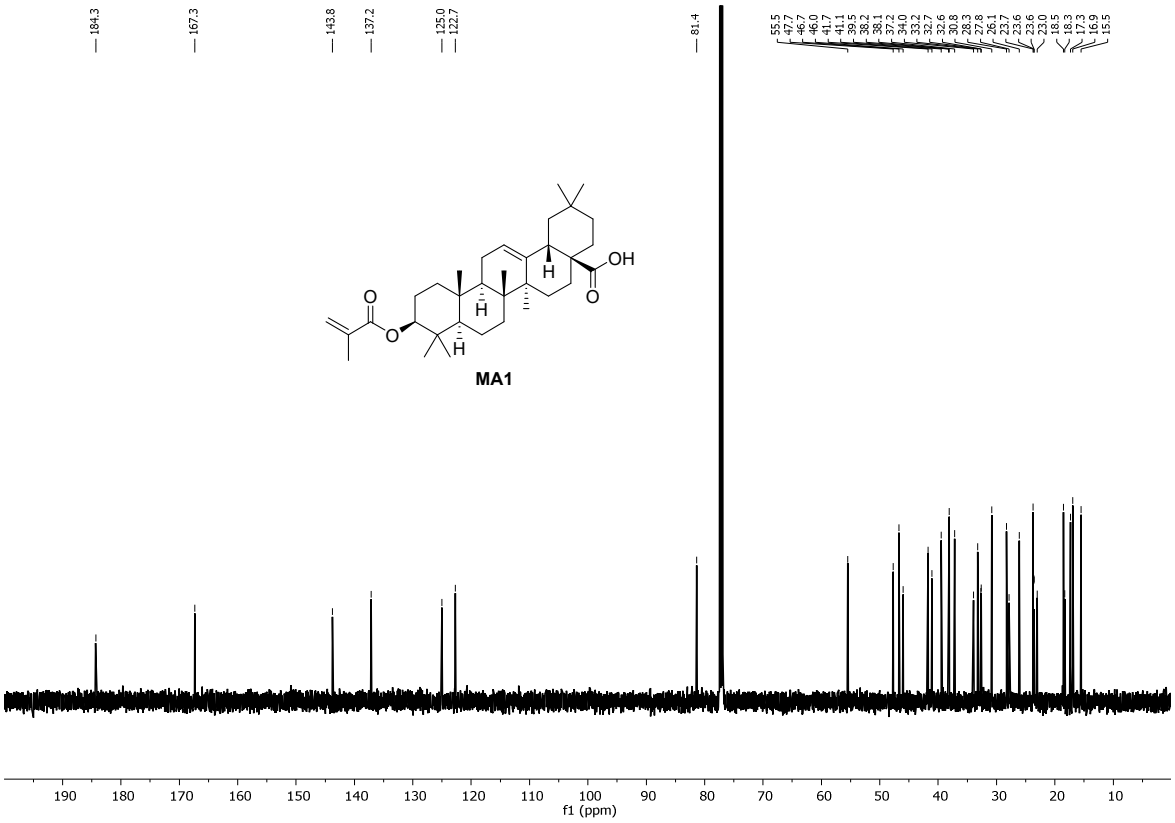

Figure 8.4. ^{13}C NMR spectrum of **MA1** in $CDCl_3$.

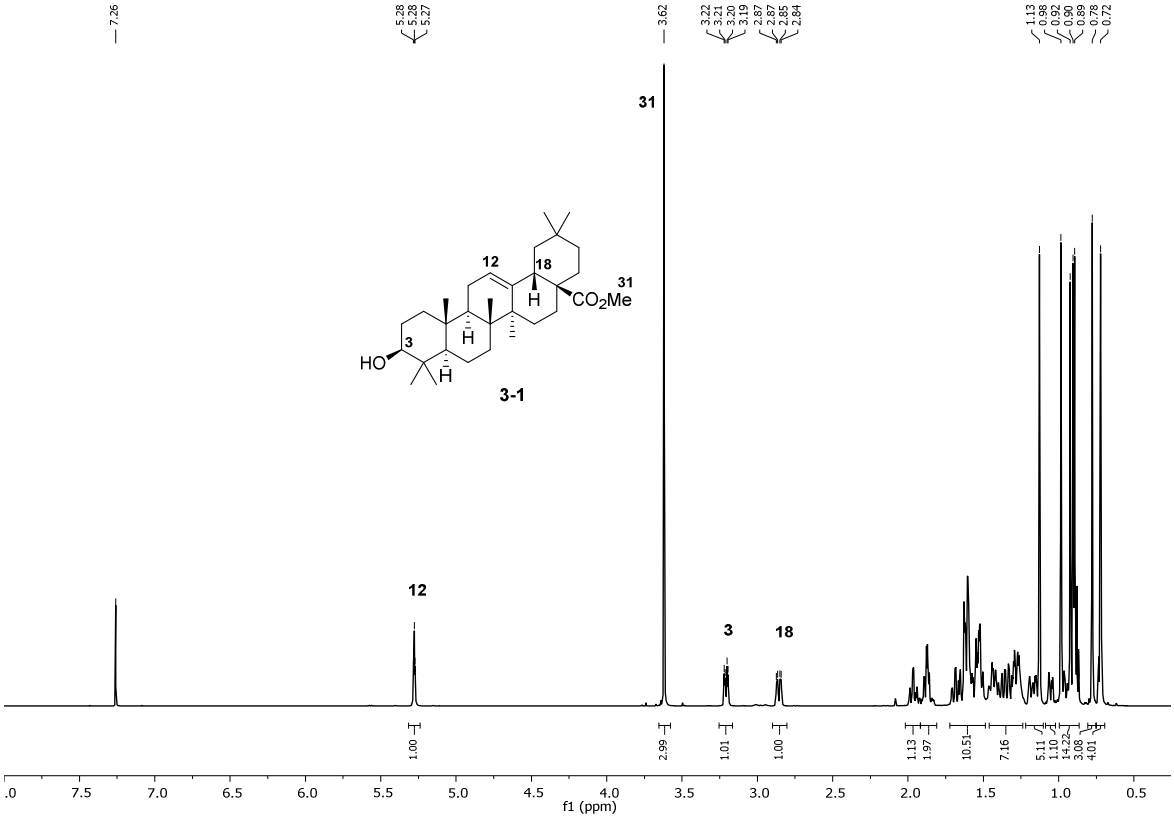

Figure 8.5. ^{1}H NMR spectrum of **3-1** in $CDCl_3$.

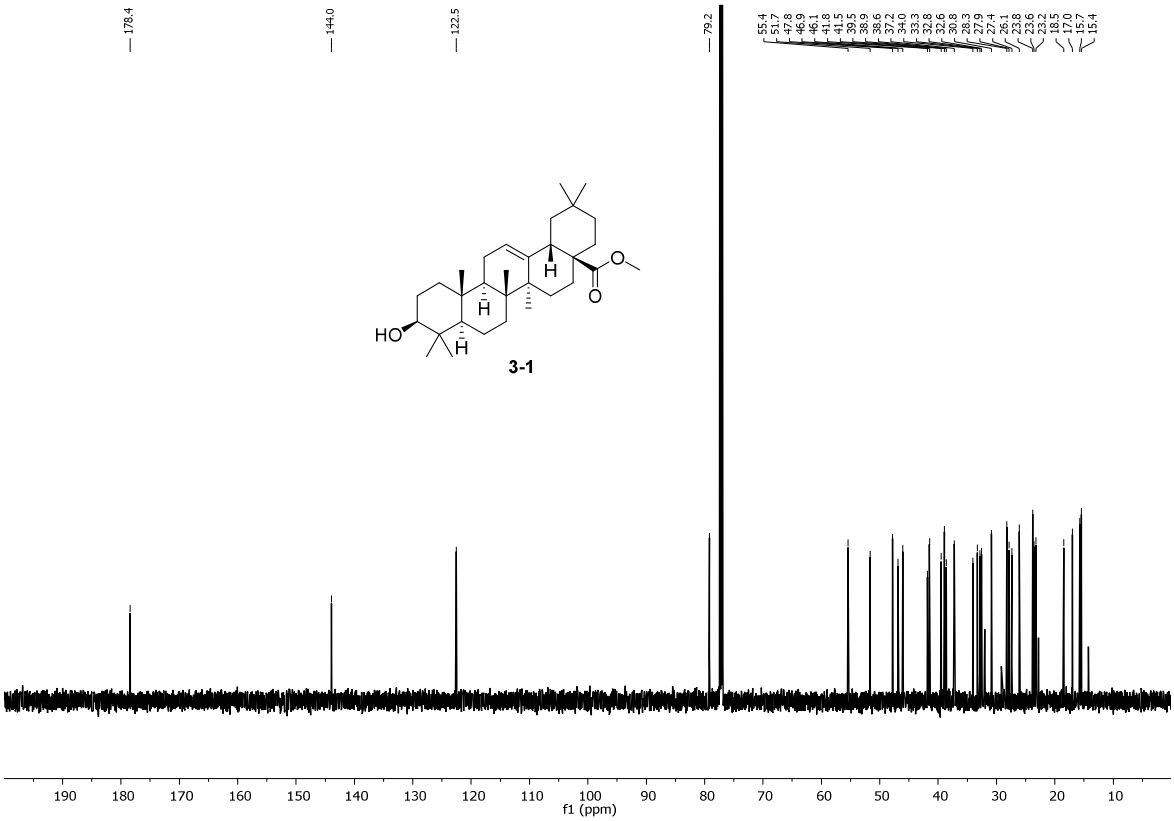

Figure 8.6. ^{13}C NMR spectrum of **3-1** in $CDCl_3$.

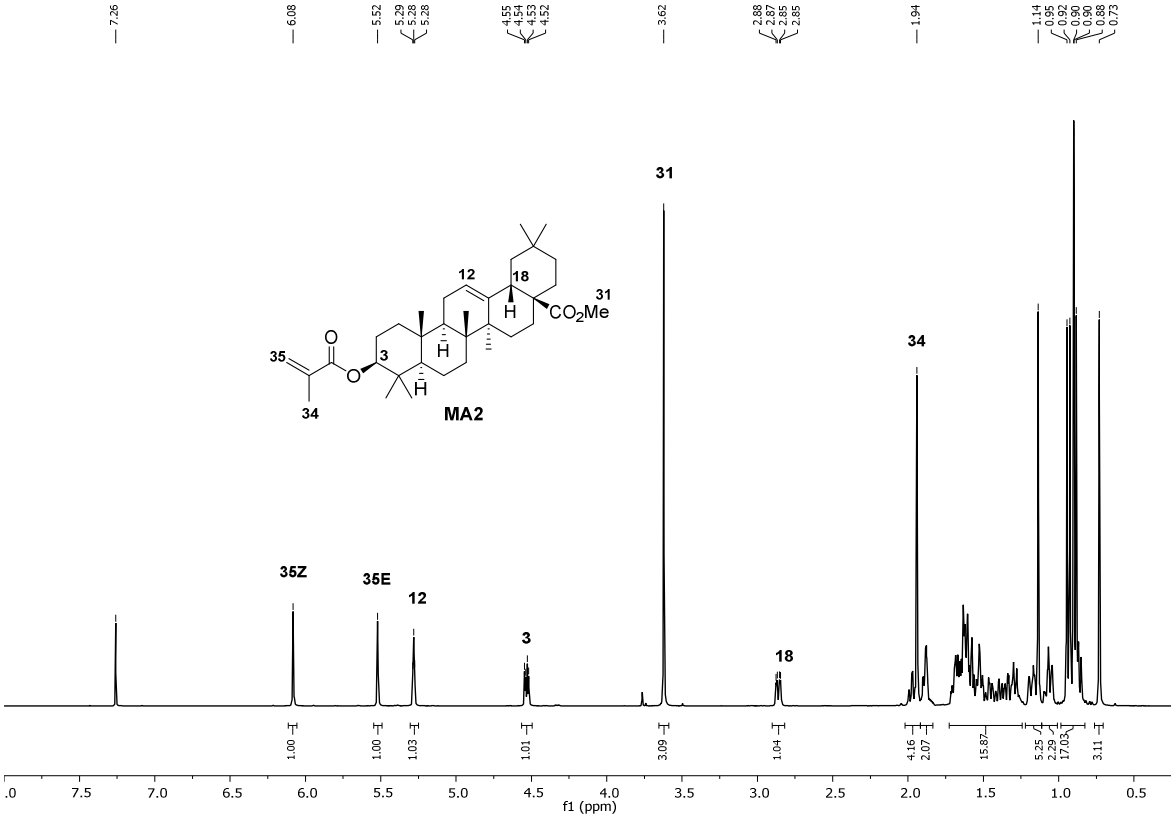

Figure 8.7. ^{1}H NMR spectrum of **MA2** in $CDCl_3$.

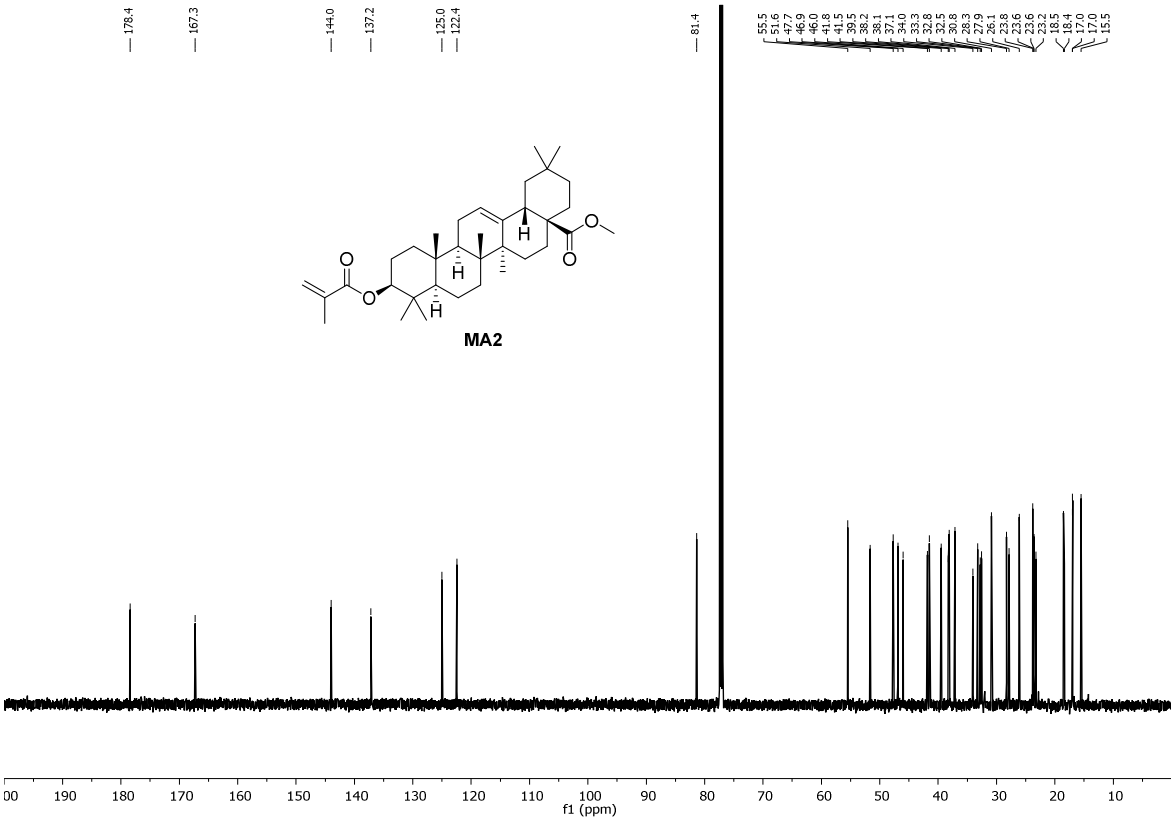

Figure 8.8. ^{13}C NMR spectrum of **MA2** in $CDCl_3$.

Figure 8.9. ^{1}H NMR spectrum of **3-2** in $CDCl_3$.

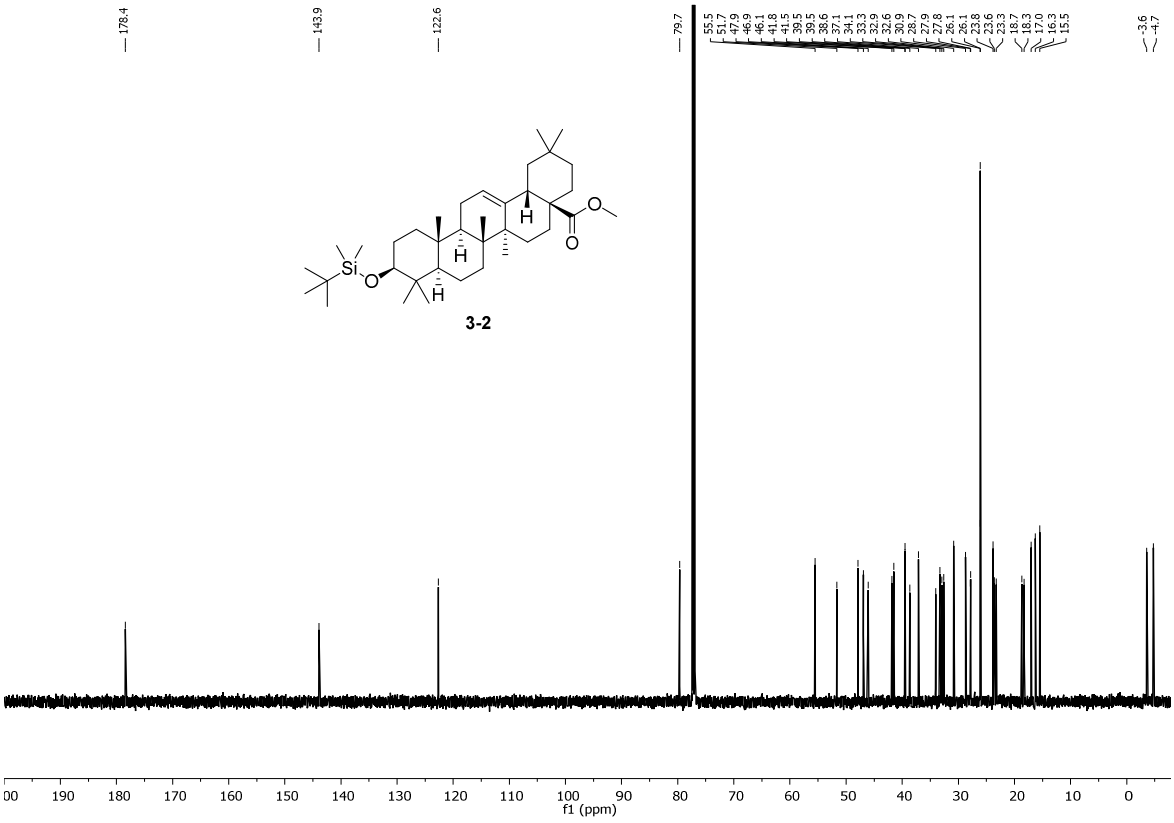

Figure 8.10. ^{13}C NMR spectrum of **3-2** in $CDCl_3$.

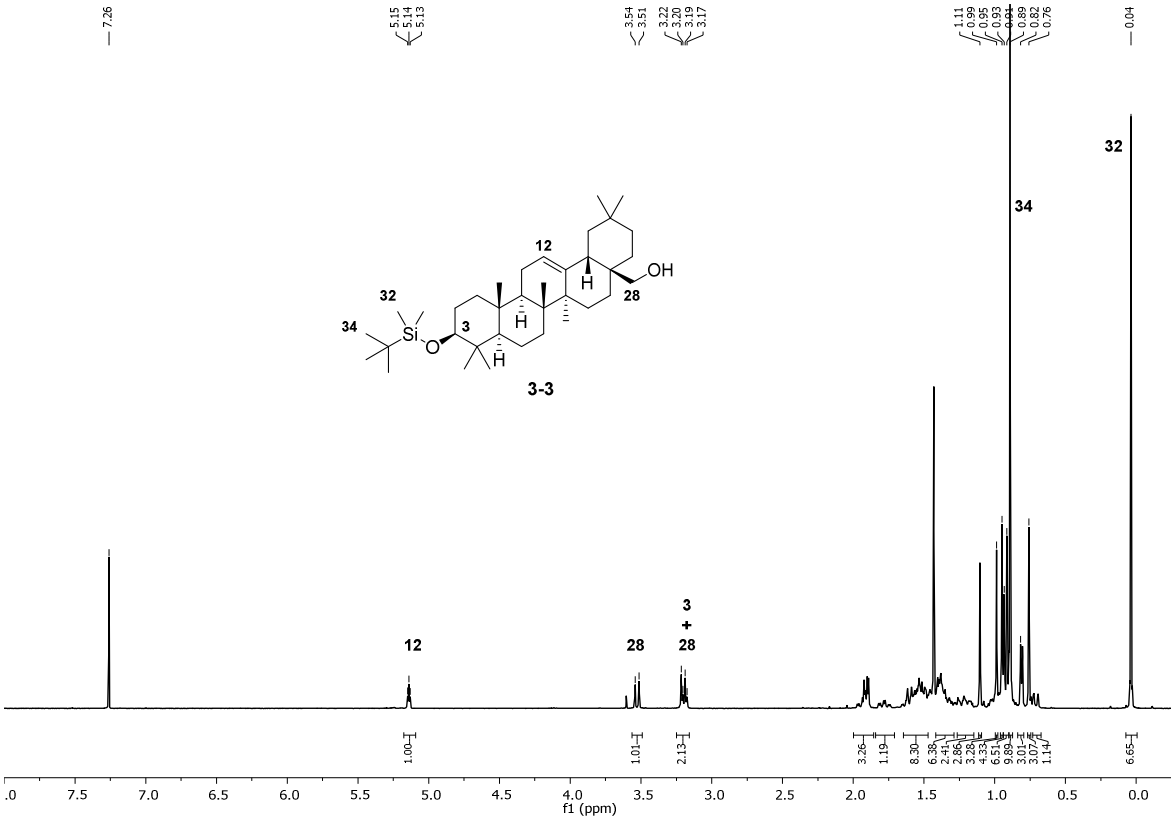

Figure 8.11. ^{1}H NMR spectrum of **3-3** in $CDCl_3$.

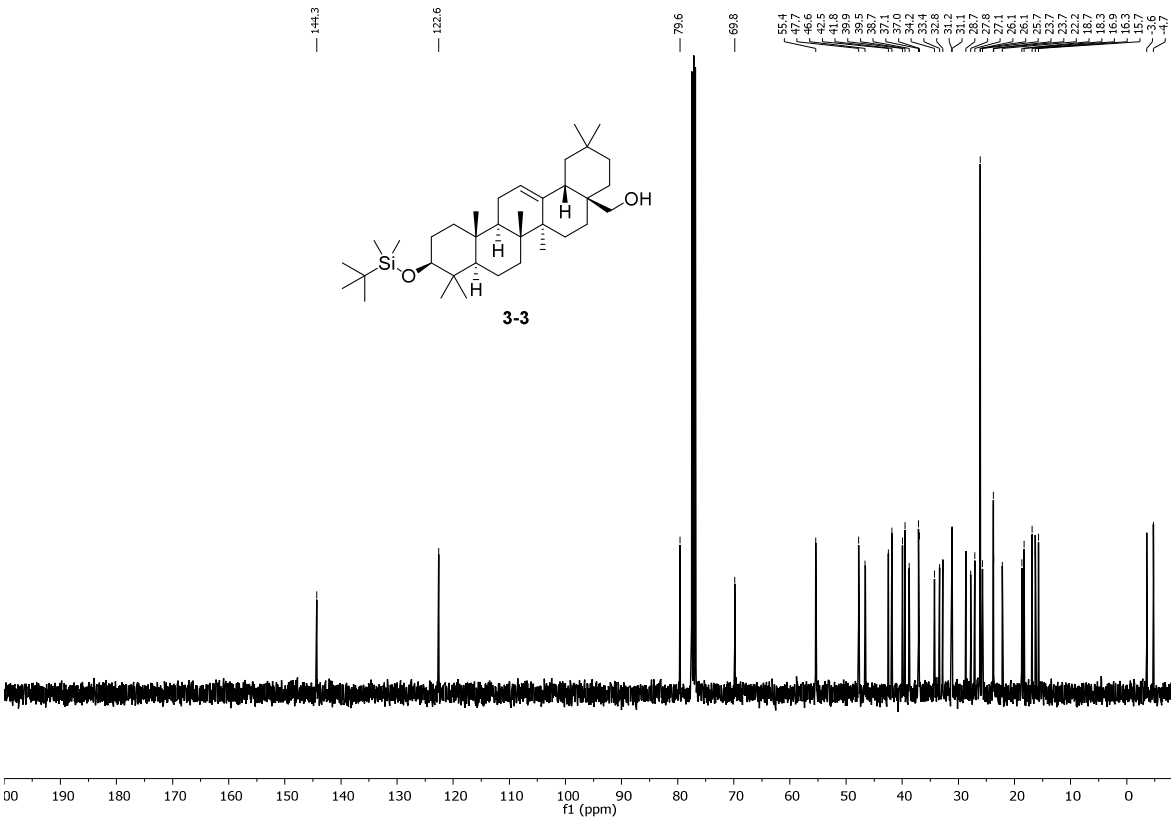

Figure 8.12. ^{13}C NMR spectrum of **3-3** in $CDCl_3$.

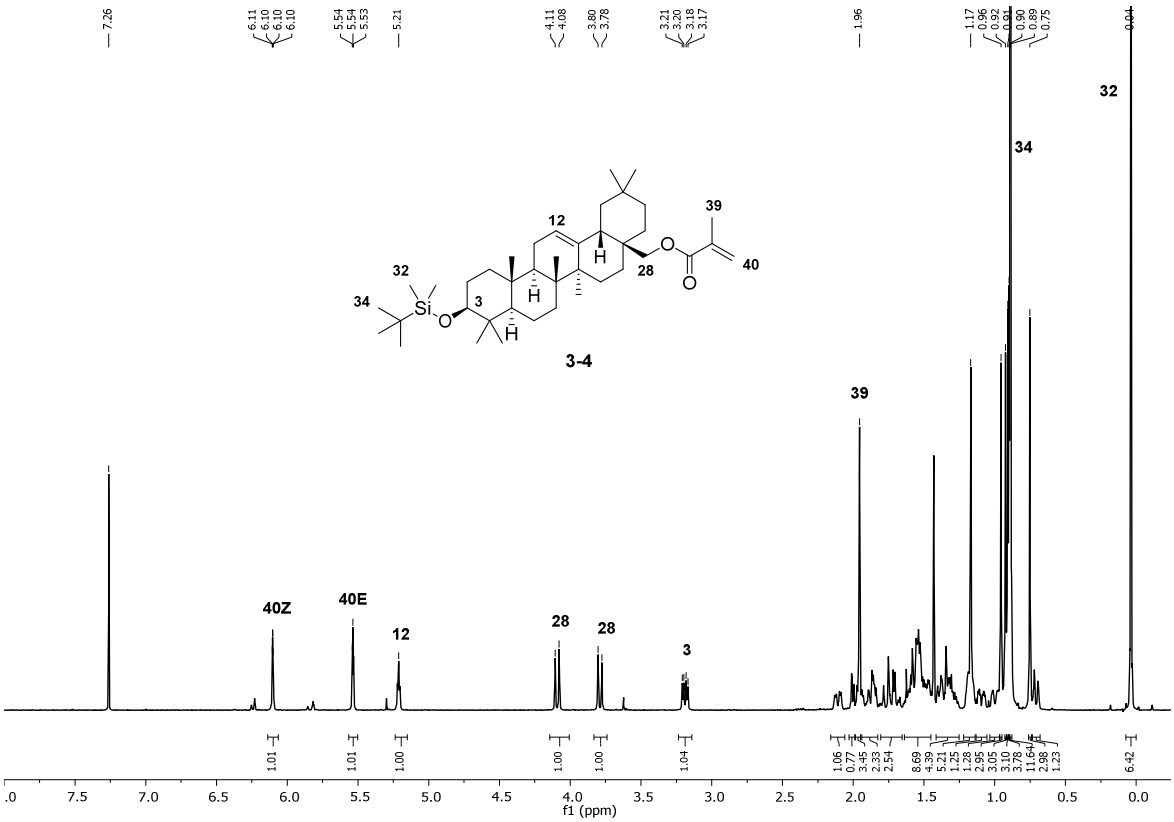

Figure 8.13. ^{1}H NMR spectrum of **3-4** in $CDCl_3$.

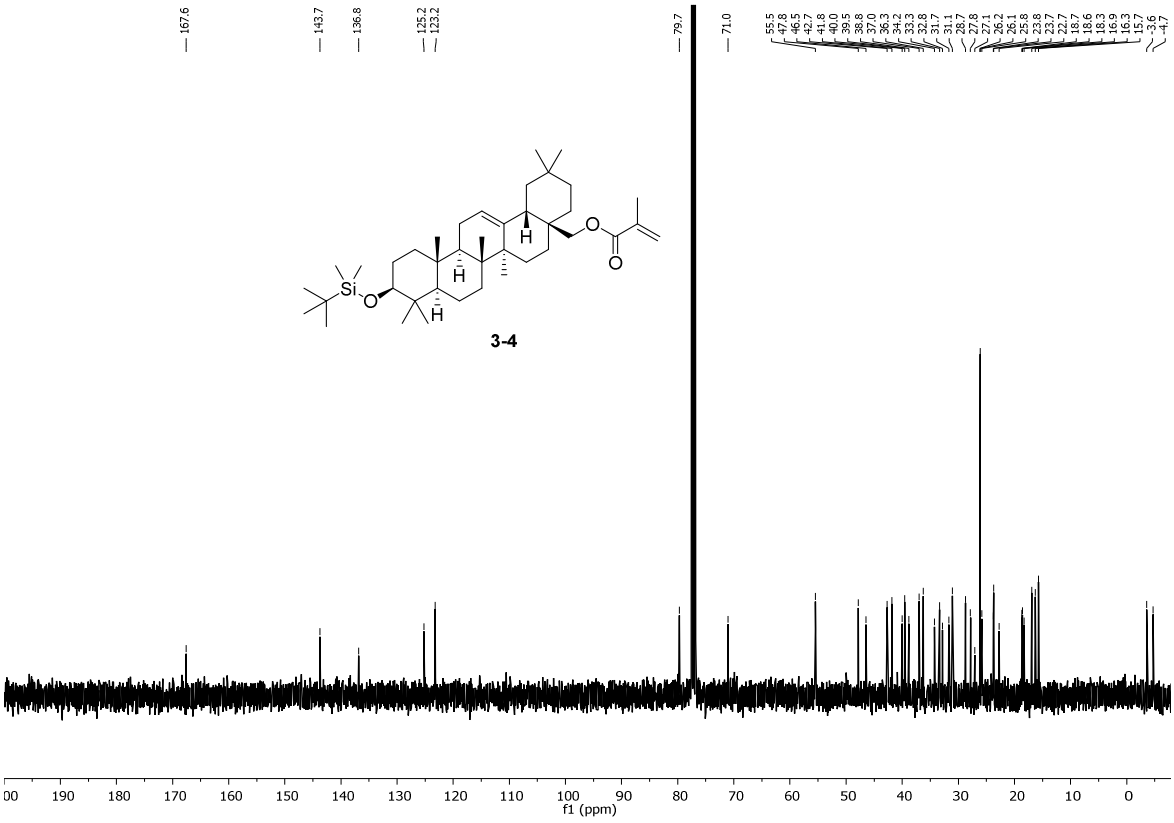

Figure 8.14. ^{13}C NMR spectrum of **3-4** in $CDCl_3$.

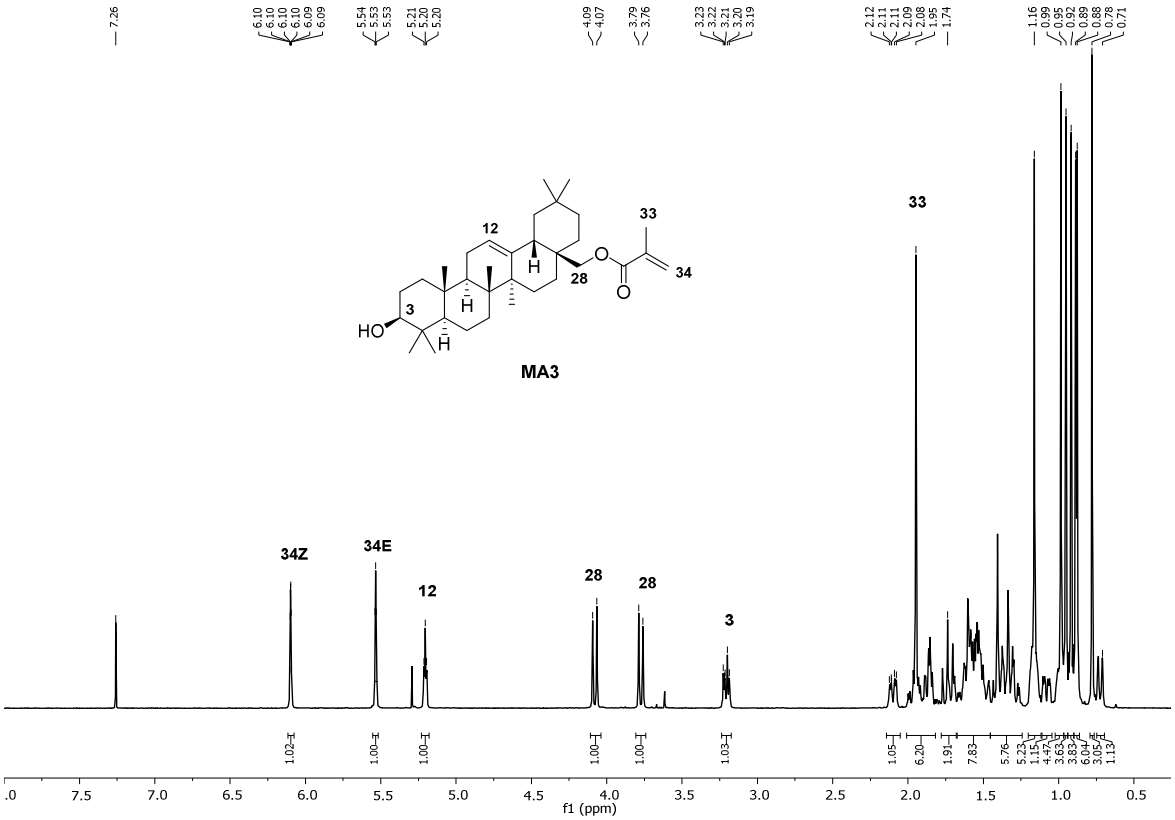

Figure 8.15. ^{1}H NMR spectrum of **MA3** in $CDCl_3$.

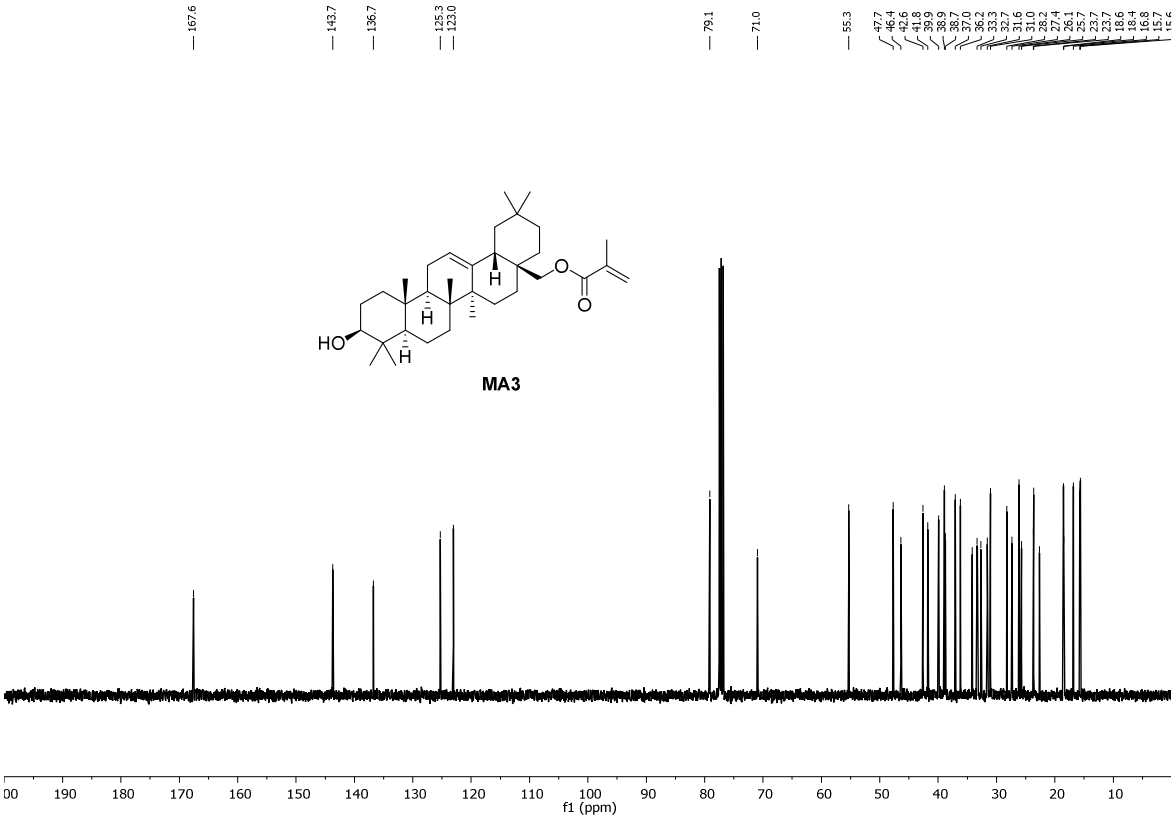

Figure 8.16. ^{13}C NMR spectrum of **MA3** in $CDCl_3$.

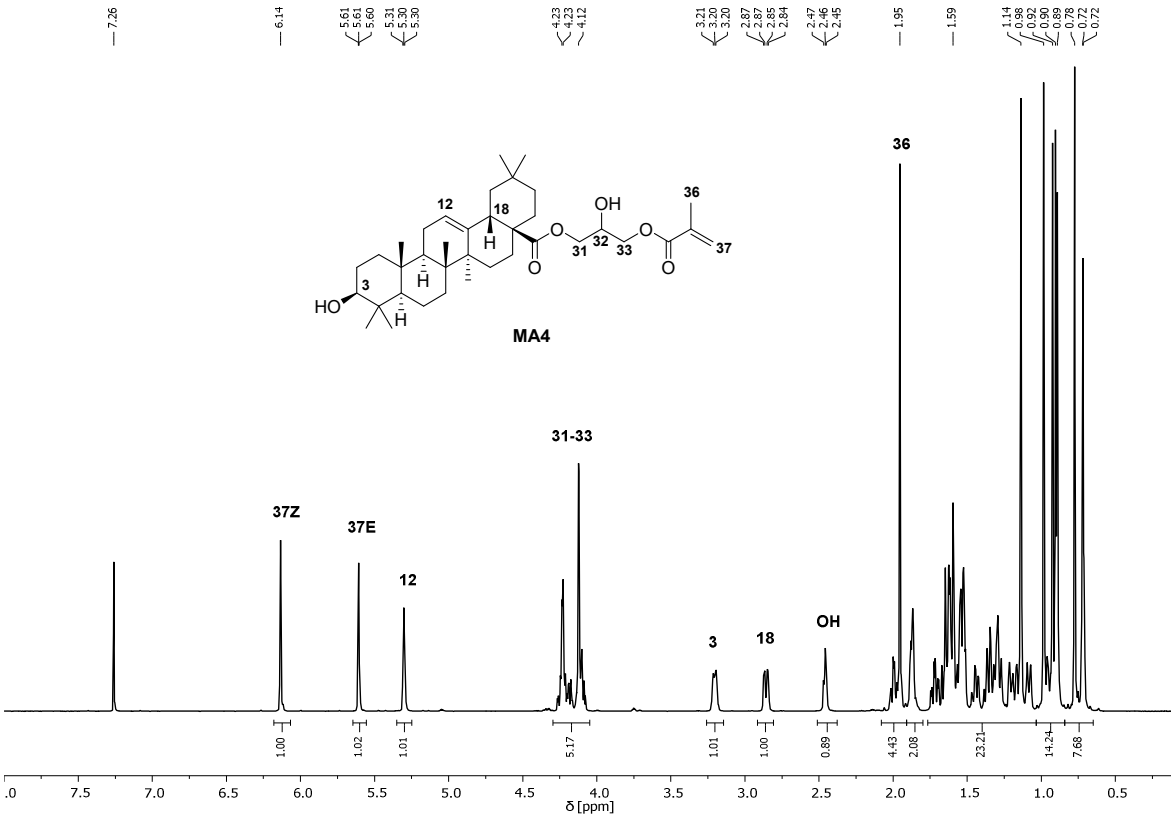

Figure 8.17. ^{1}H NMR spectrum of **MA4** in $CDCl_3$.

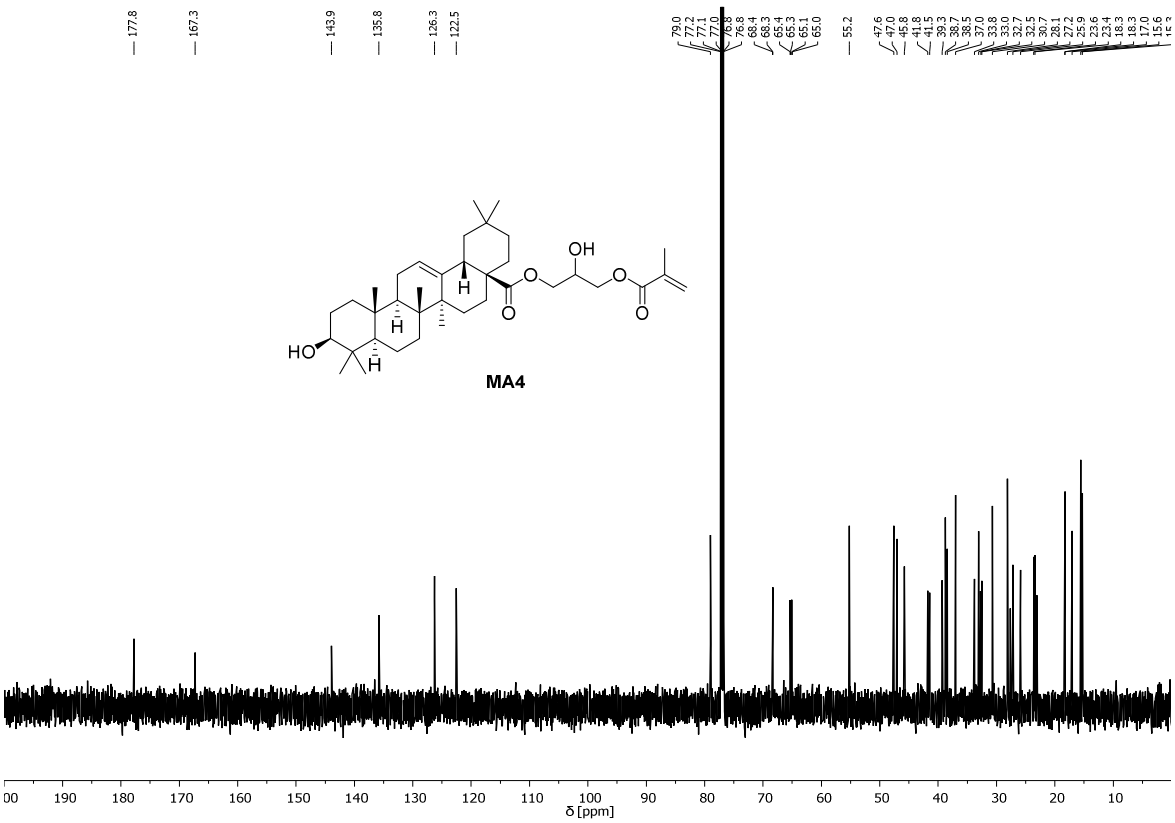

Figure 8.18. ^{13}C NMR spectrum of **MA4** in $CDCl_3$.

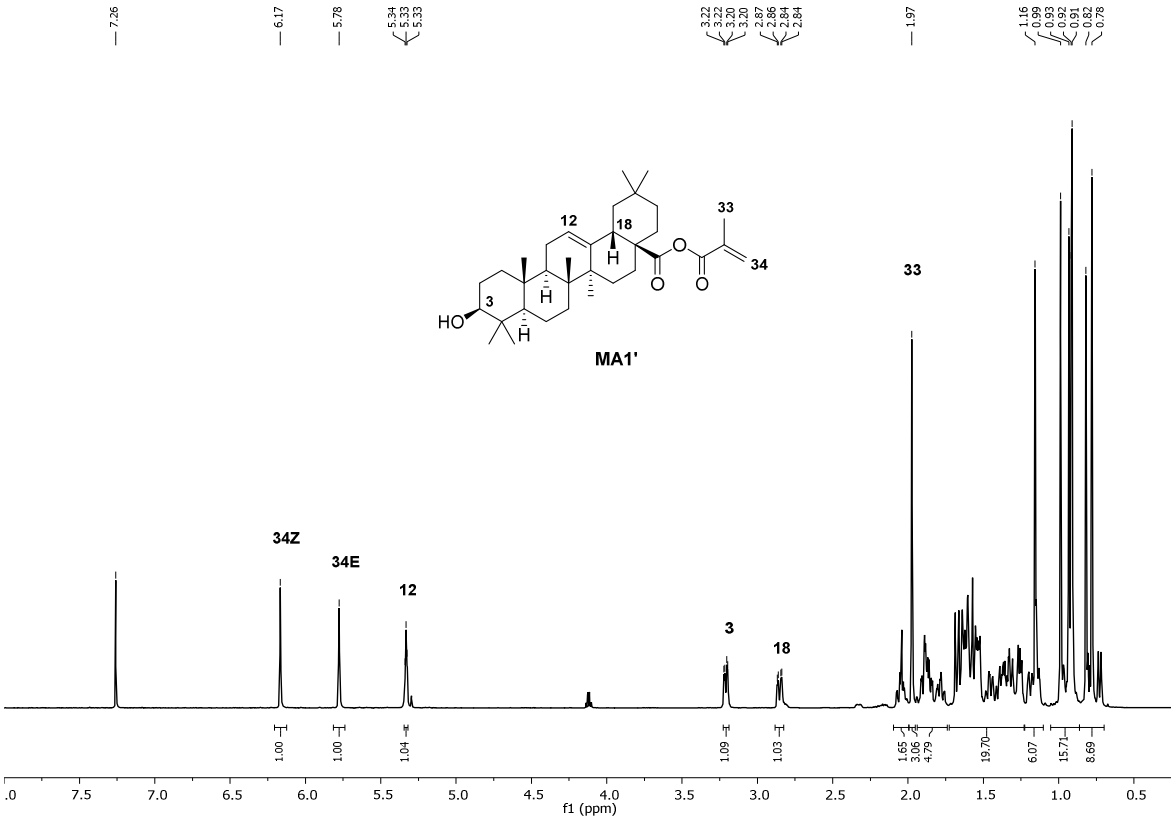

Figure 8.19. ^{1}H NMR spectrum of **MA1'** in $CDCl_3$.

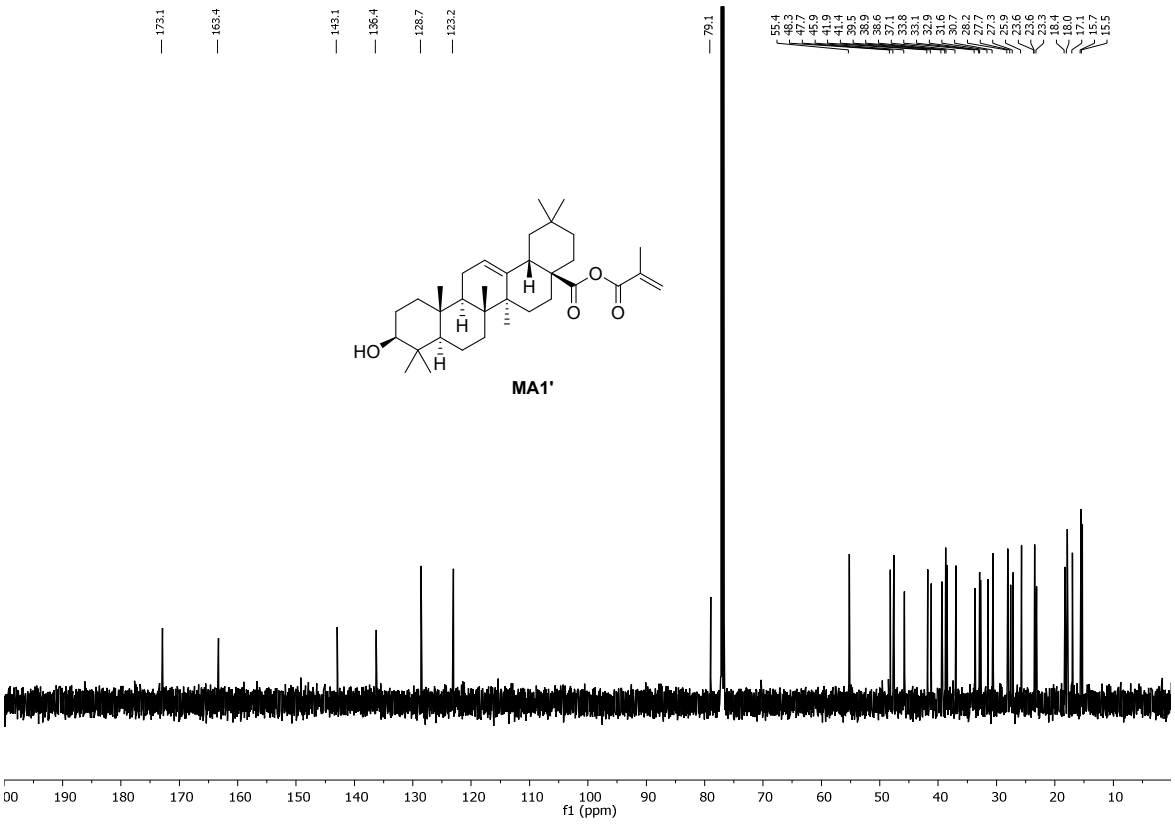

Figure 8.20. ^{13}C NMR spectrum of **MA1'** in $CDCl_3$.

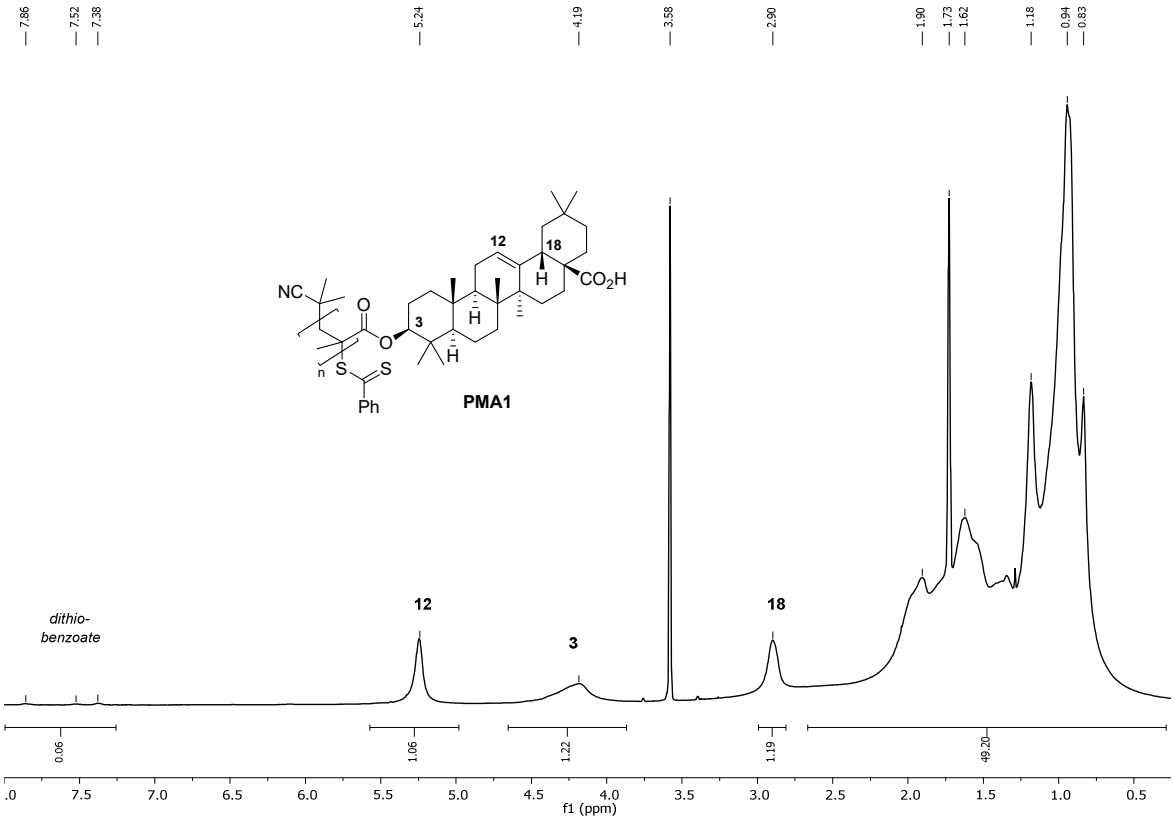

Figure 8.21. ^{1}H NMR spectrum of **PMA1** in THF-d_8.

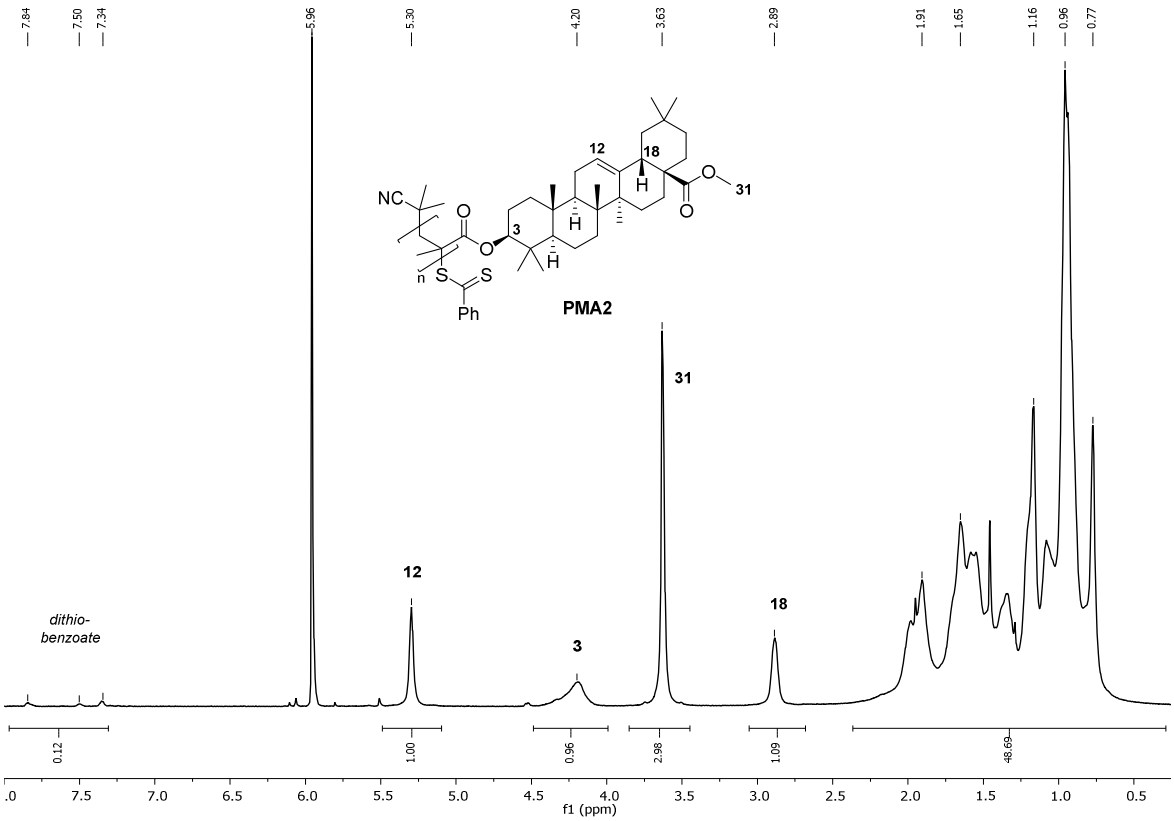

Figure 8.22. ^{1}H NMR spectrum of **PMA2** in TeCA-d_2.

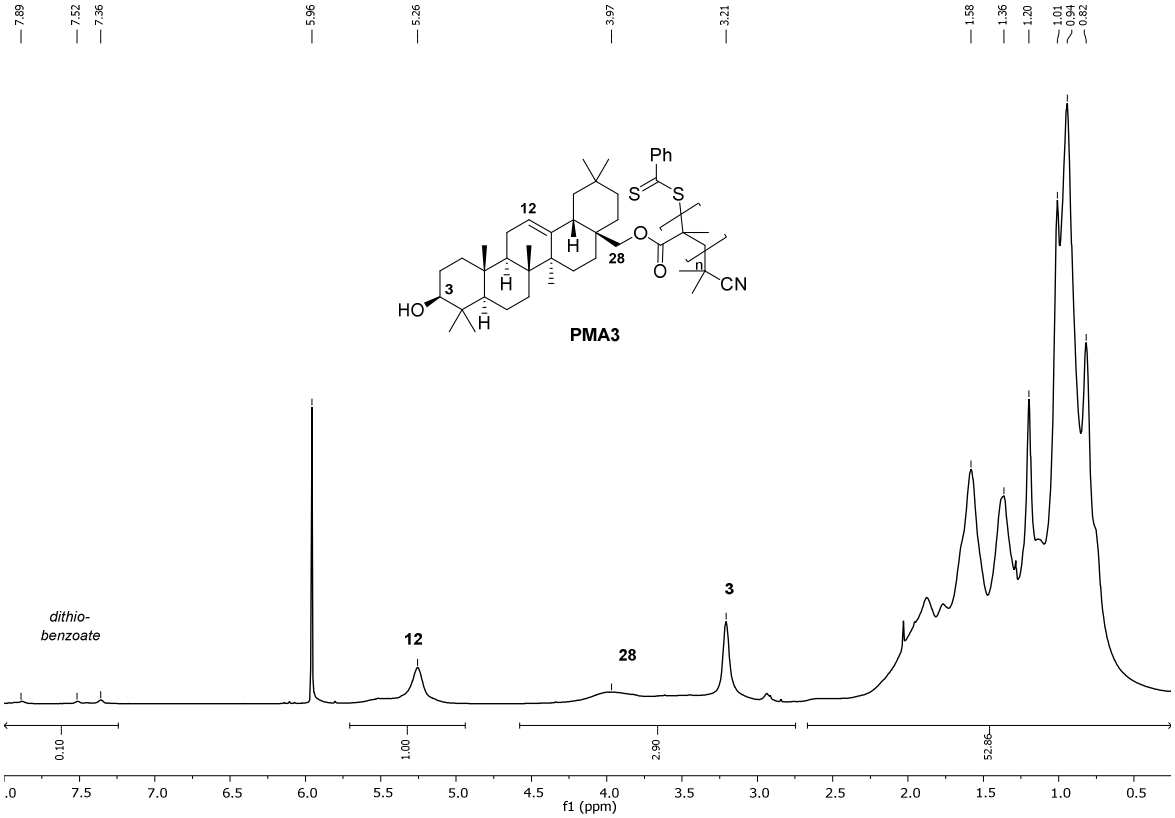

Figure 8.23. ^{1}H NMR spectrum of **PMA3** in TeCA-d_2.

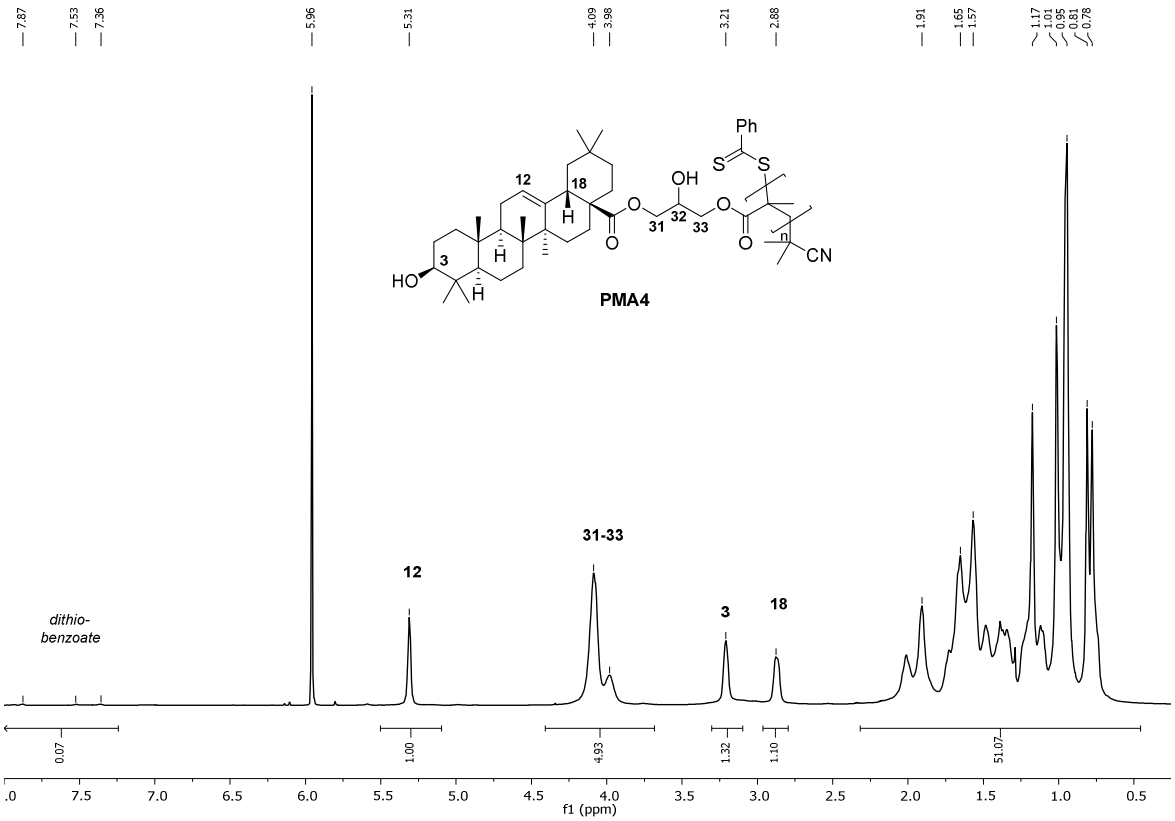

Figure 8.24. ^{1}H NMR spectrum of **PMA4** in TeCA-d_2.

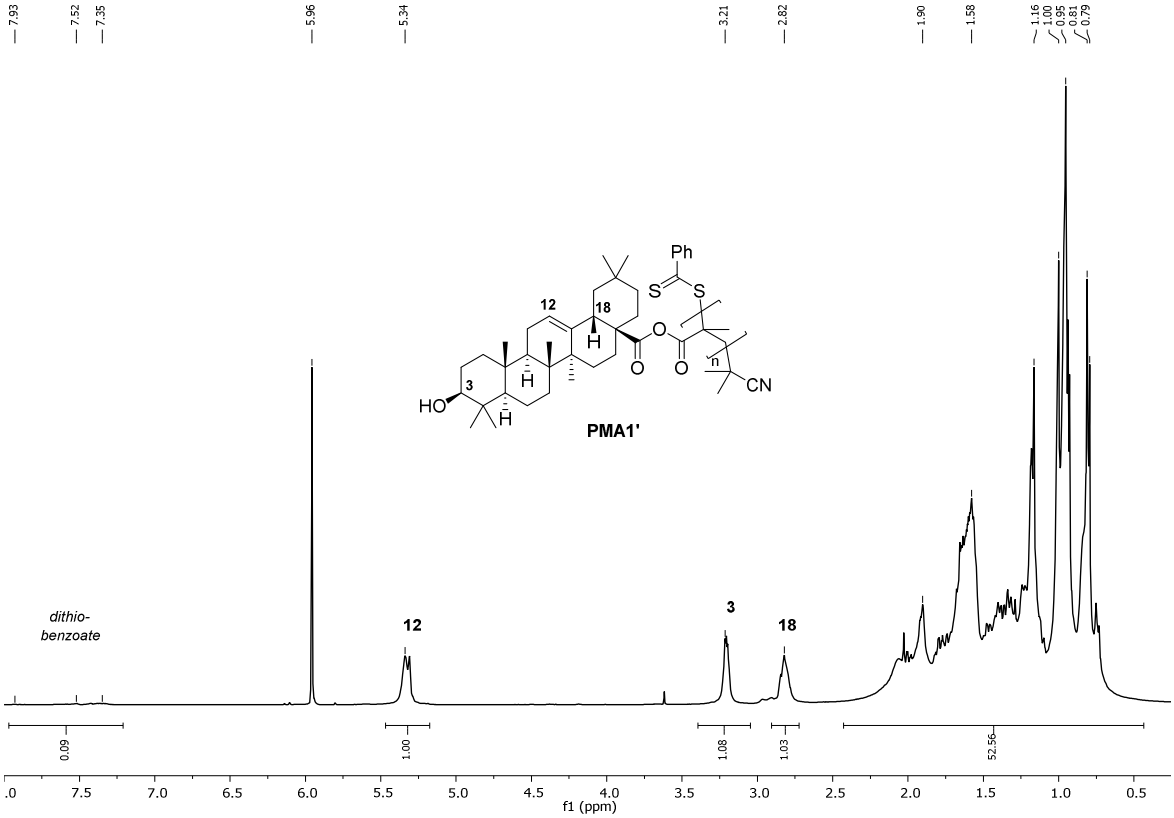

Figure 8.25. ^{1}H NMR spectrum of **PMA1'** in TeCA-d_2.

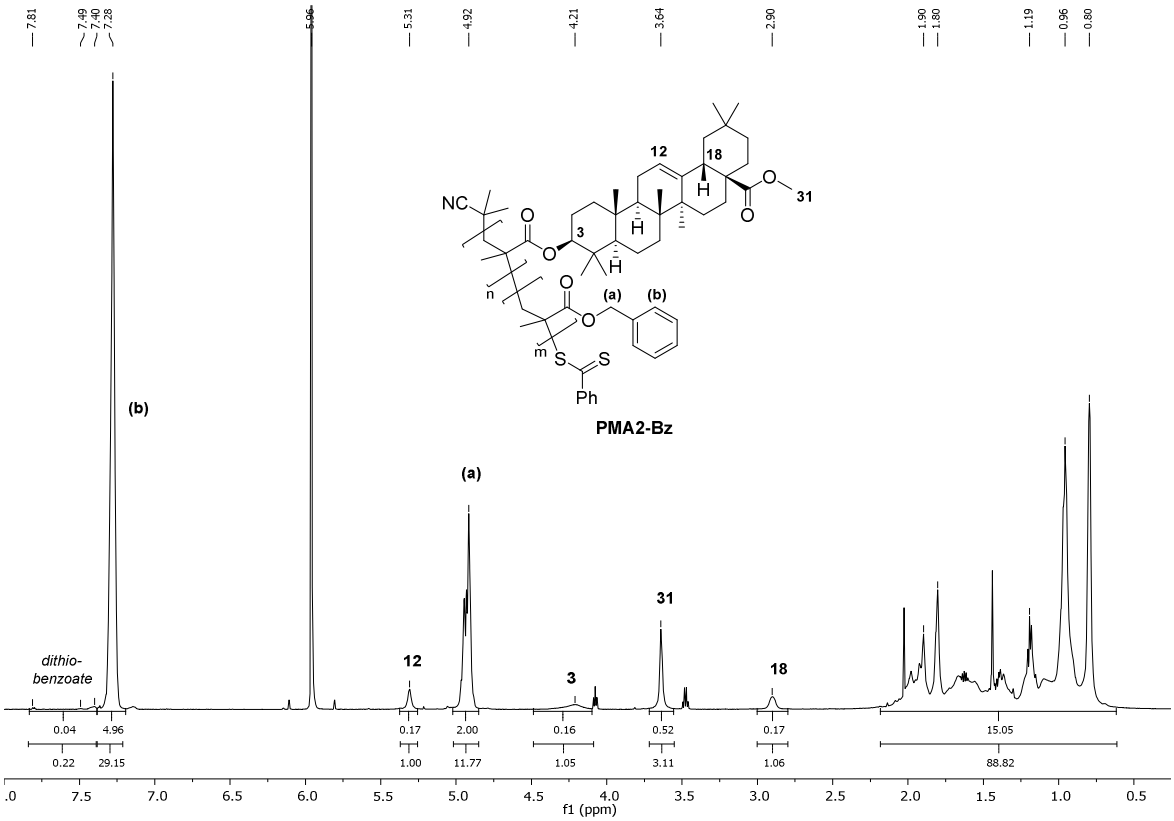

Figure 8.26. ^{1}H NMR spectrum of **PMA2-Bz** in TeCA-d_2.

Ch. 4: Novel Bio-based Thermoplastic Polyurethanes Derived From Oleanolic Acid

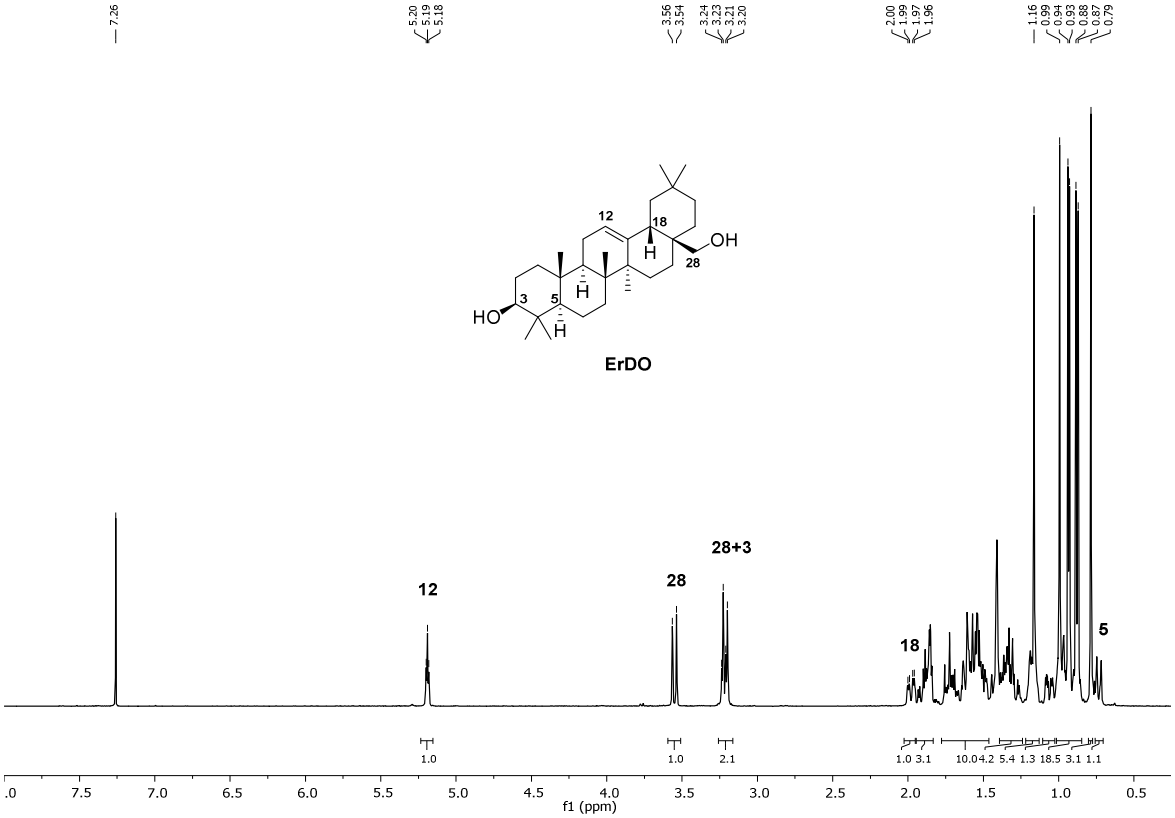

Figure 8.27. ^{1}H NMR spectrum of **ErDO** in $CDCl_3$.

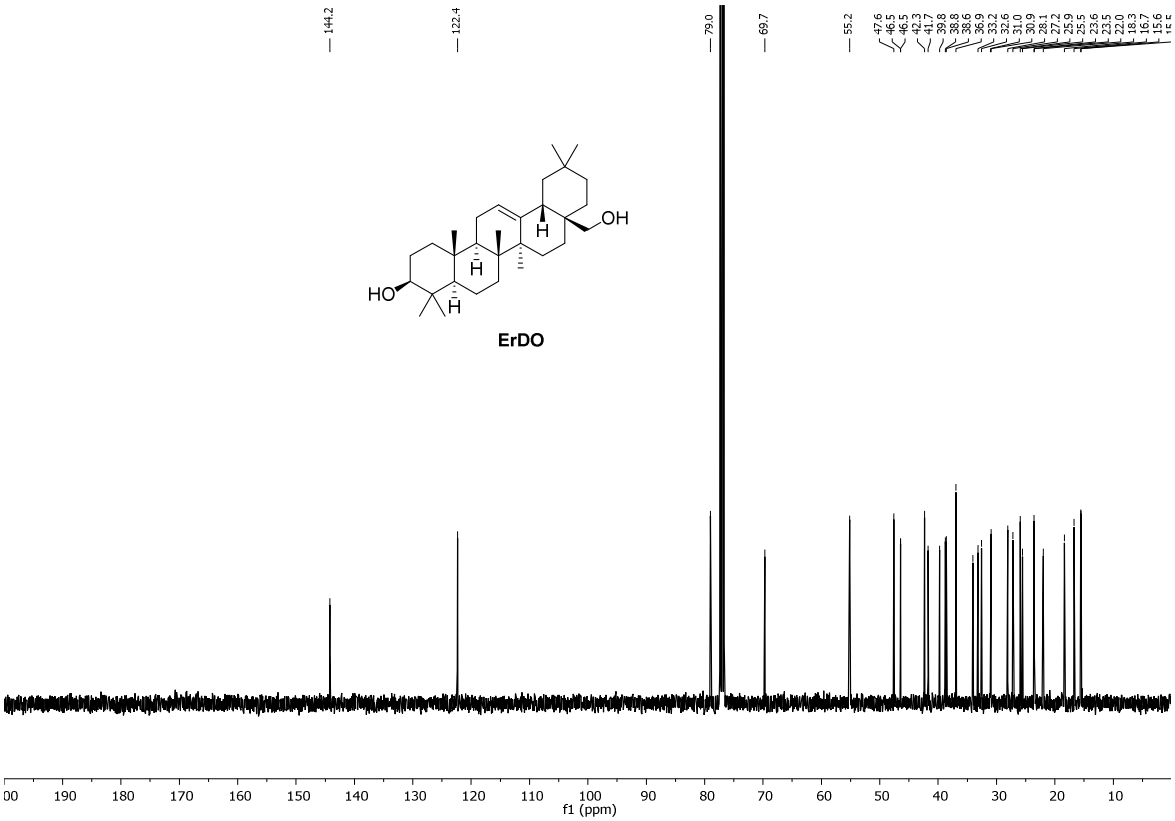

Figure 8.28. ^{13}C NMR spectrum of **ErDO** in $CDCl_3$.

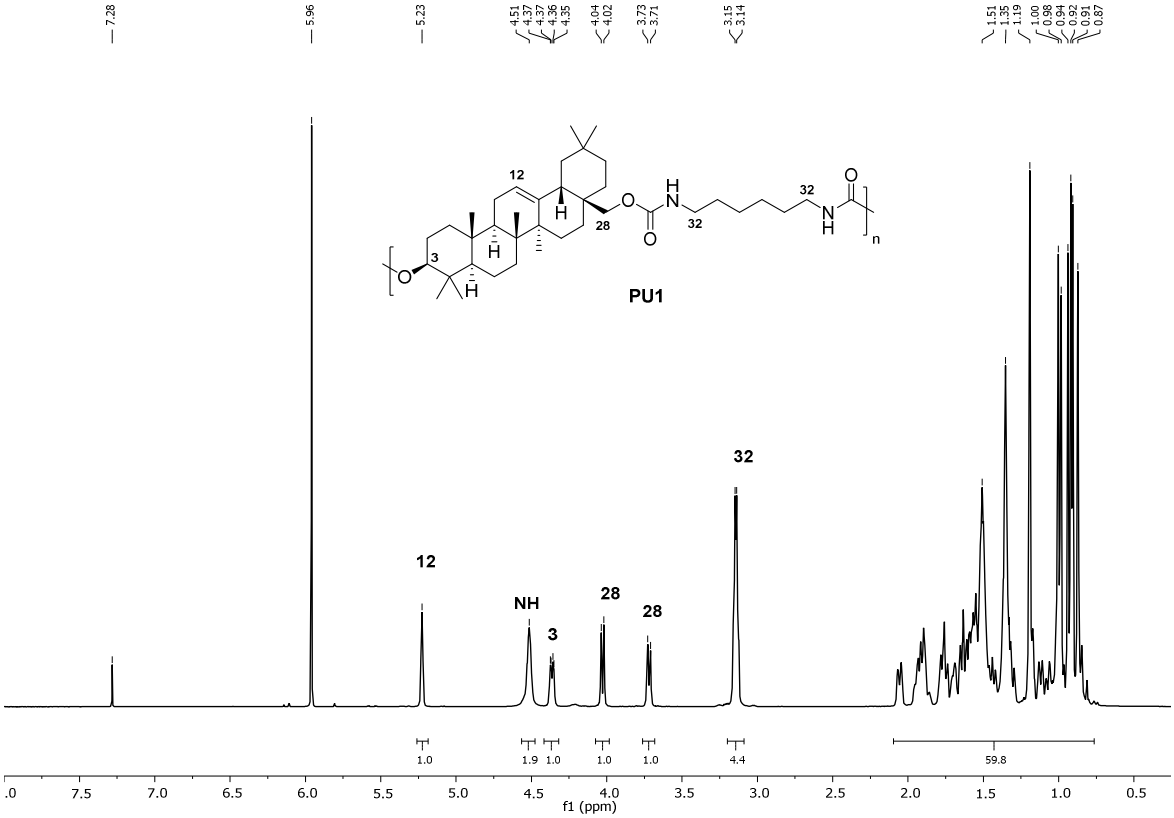

Figure 8.29. ^{1}H NMR spectrum of **PU1** in TeCA-d_2.

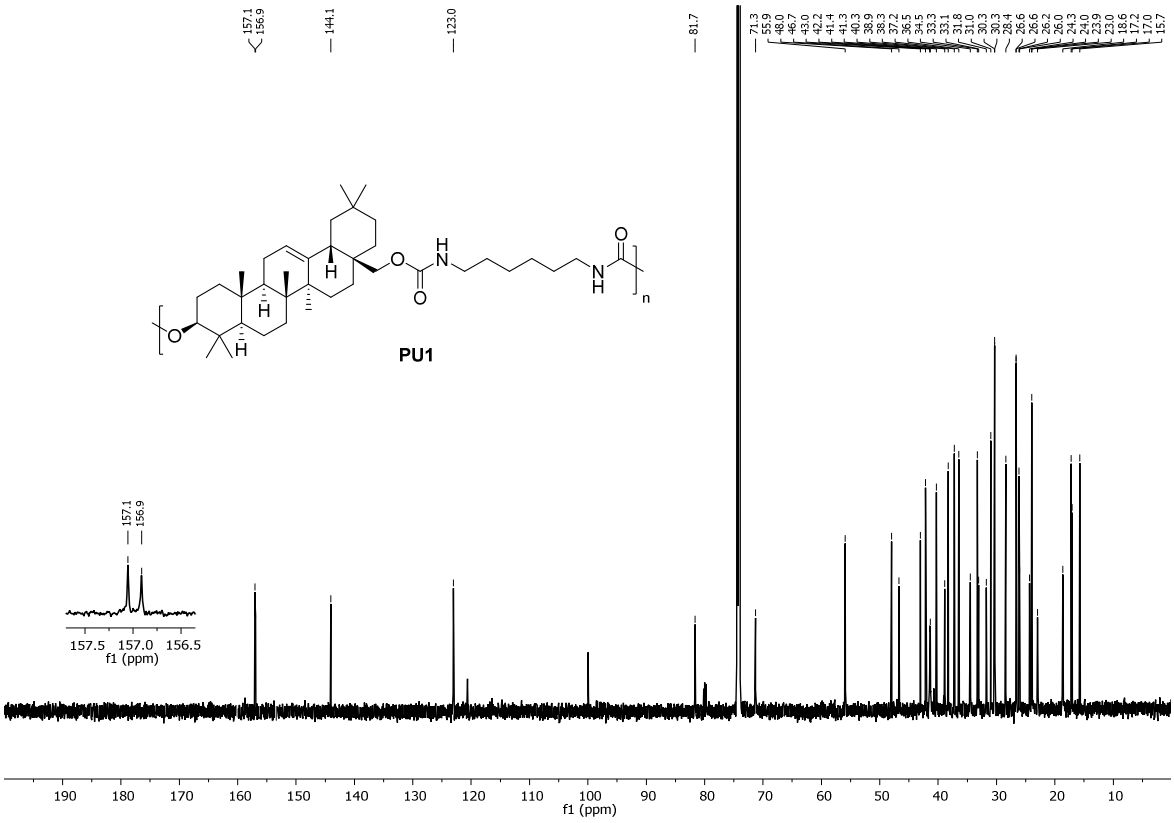

Figure 8.30. ^{13}C NMR spectrum of **PU1** in TeCA-d_2.

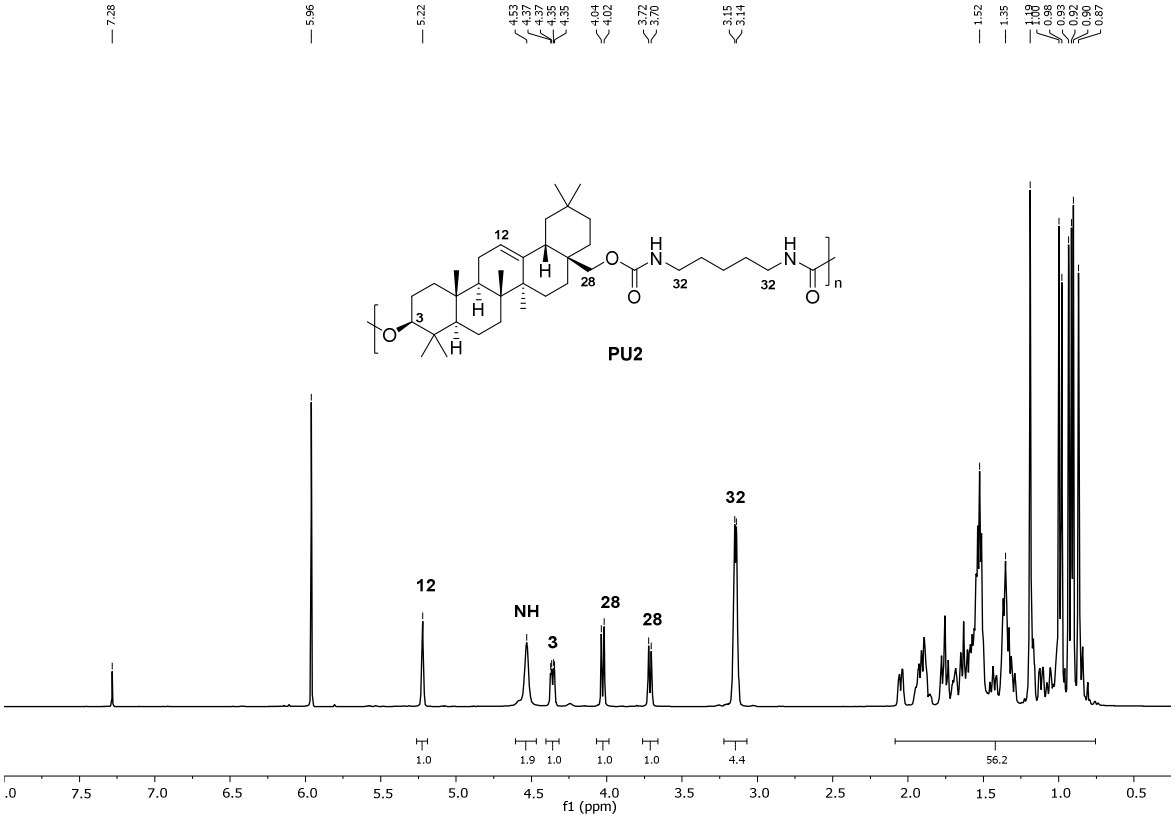

Figure 8.31. ^{1}H NMR spectrum of **PU2** in TeCA-d_2.

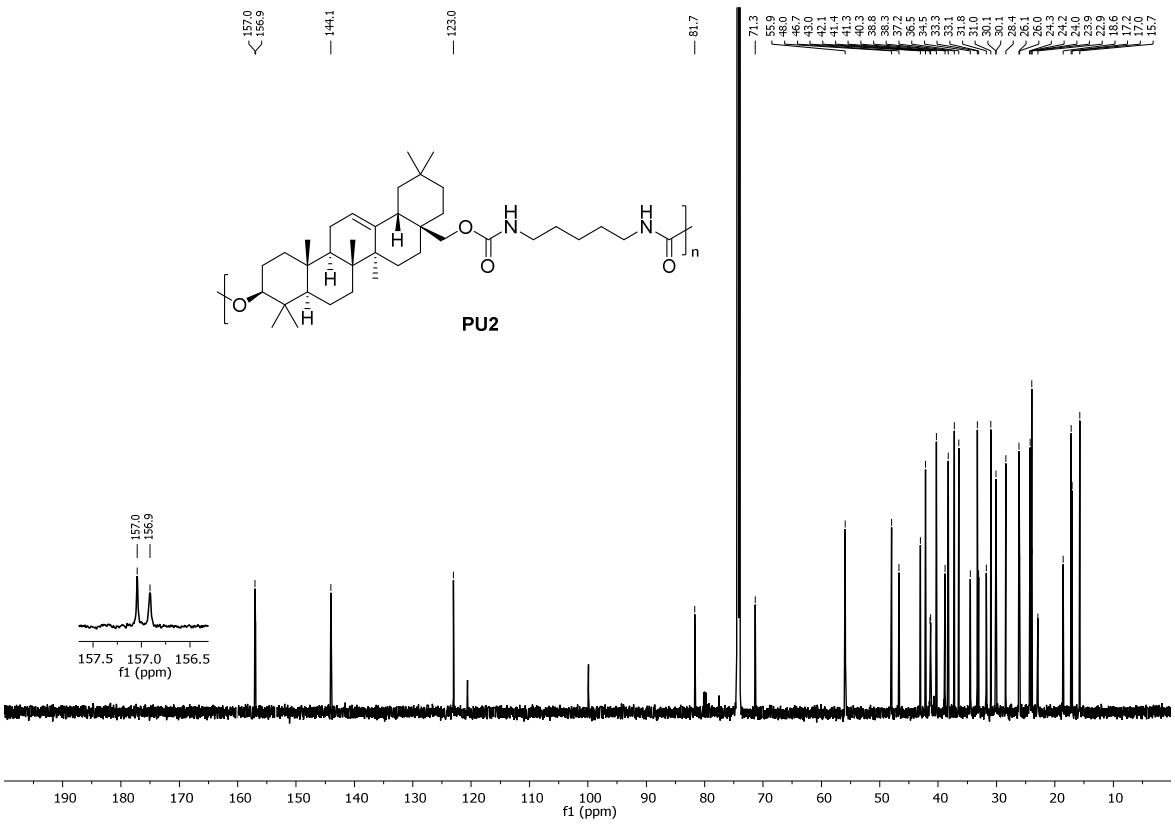

Figure 8.32. ^{13}C NMR spectrum of **PU2** in TeCA-d_2.

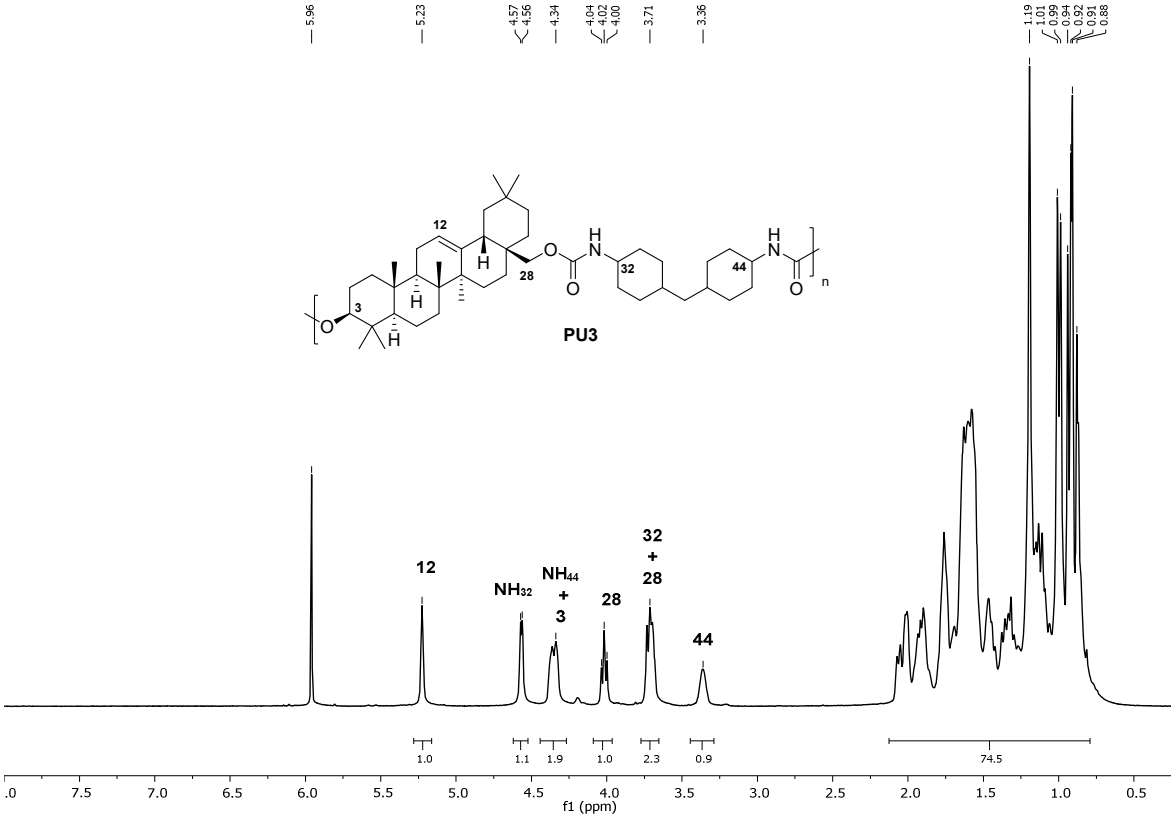

Figure 8.33. ^{1}H NMR spectrum of **PU3** in TeCA-d_2.

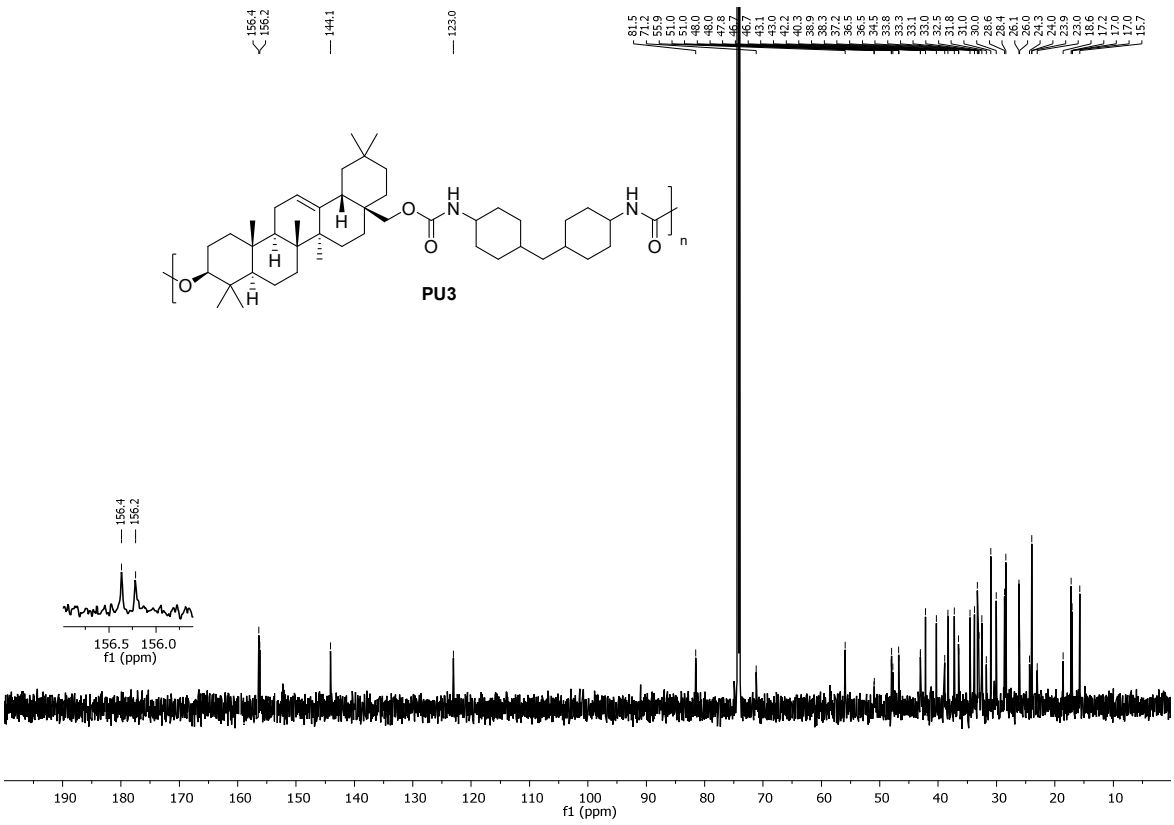

Figure 8.34. ^{13}C NMR spectrum of **PU3** in TeCA-d_2.

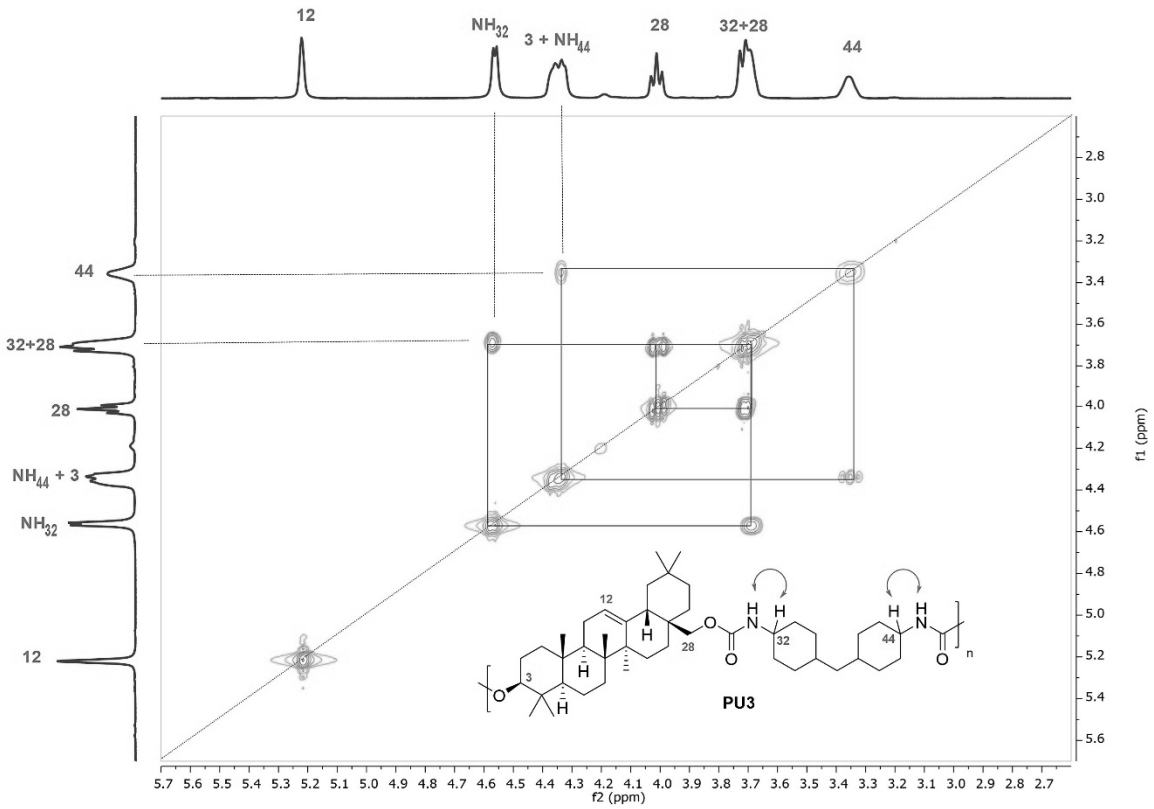

Figure 8.35. ^{1}H-^{1}H COSY NMR spectrum of **PU3** in TeCA-d_2.

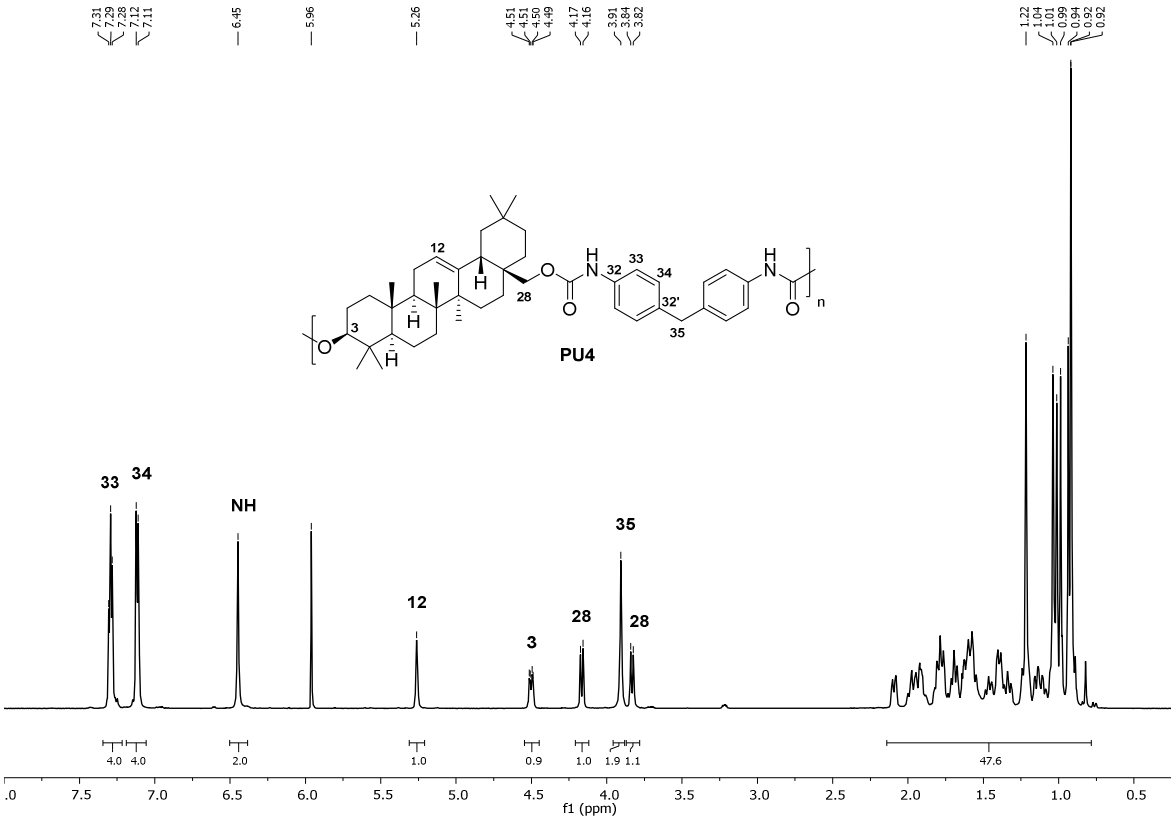

Figure 8.36. ^{1}H NMR spectrum of **PU4** in TeCA-d_2.

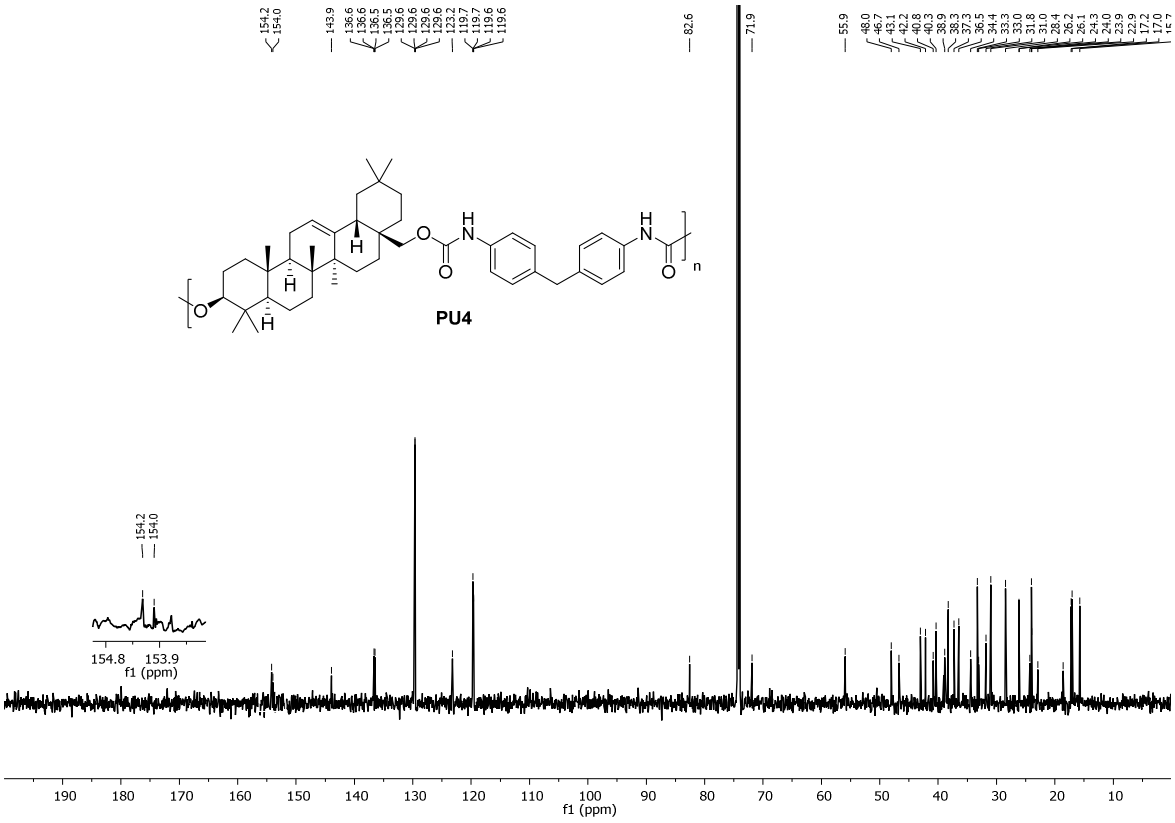

Figure 8.37. ^{13}C NMR spectrum of **PU4** in TeCA-d_2.

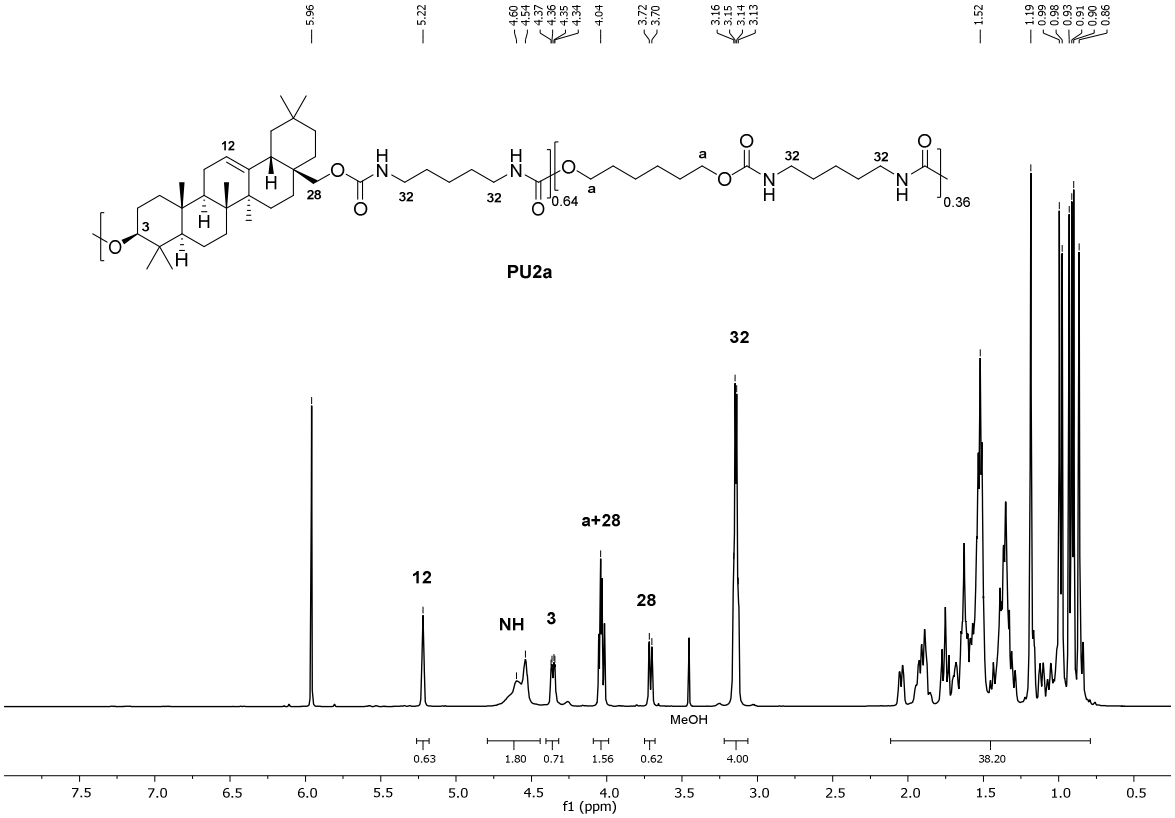

Figure 8.38. ^{1}H NMR spectrum of **PU2a** in TeCA-d_2.

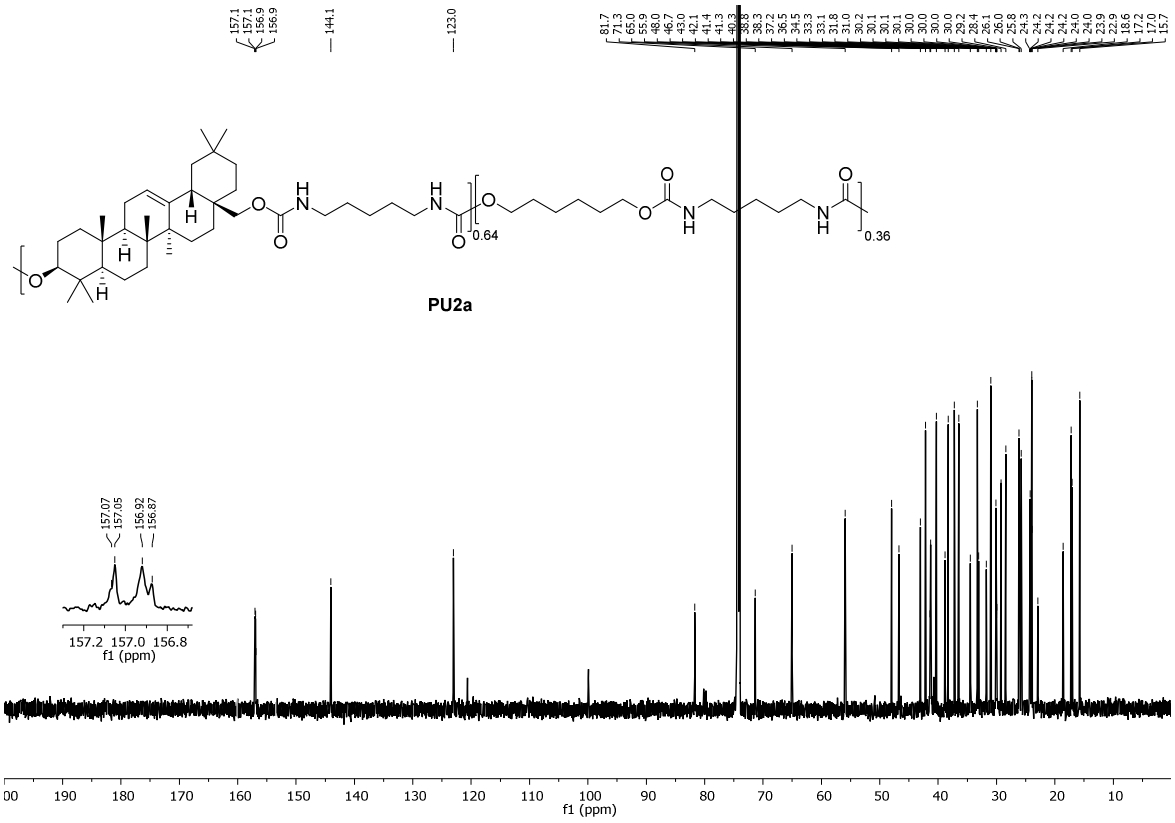

Figure 8.39. ^{13}C NMR spectrum of **PU2a** in TeCA-d_2.

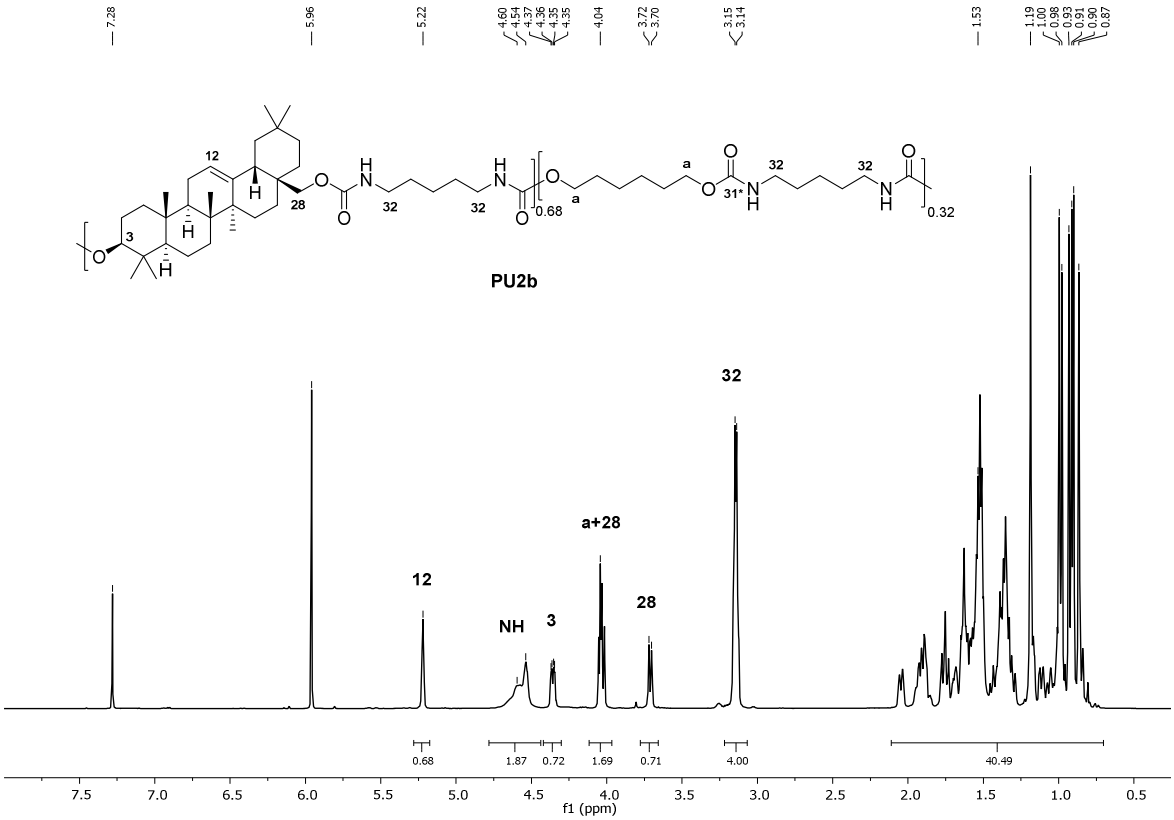

Figure 8.40. [1]H NMR spectrum of **PU2b** in TeCA-d_2.

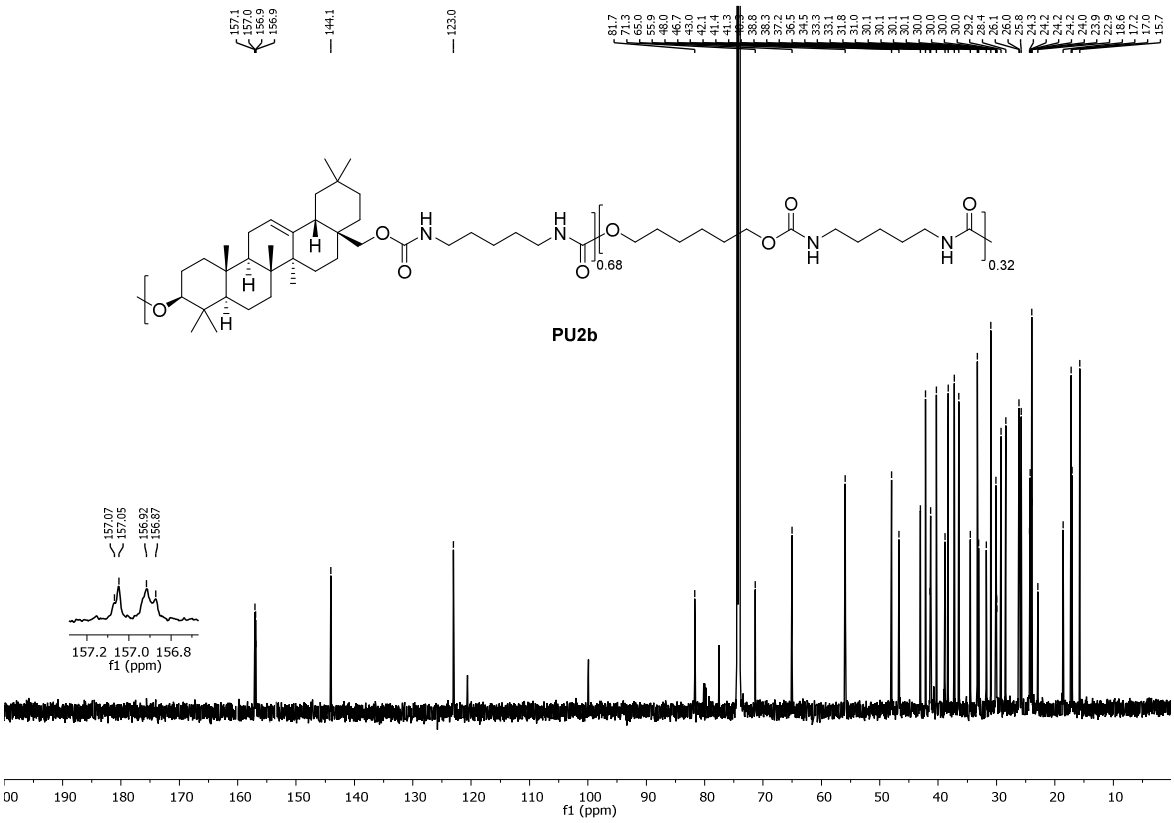

Figure 8.41. [13]C NMR spectrum of **PU2b** in TeCA-d_2.

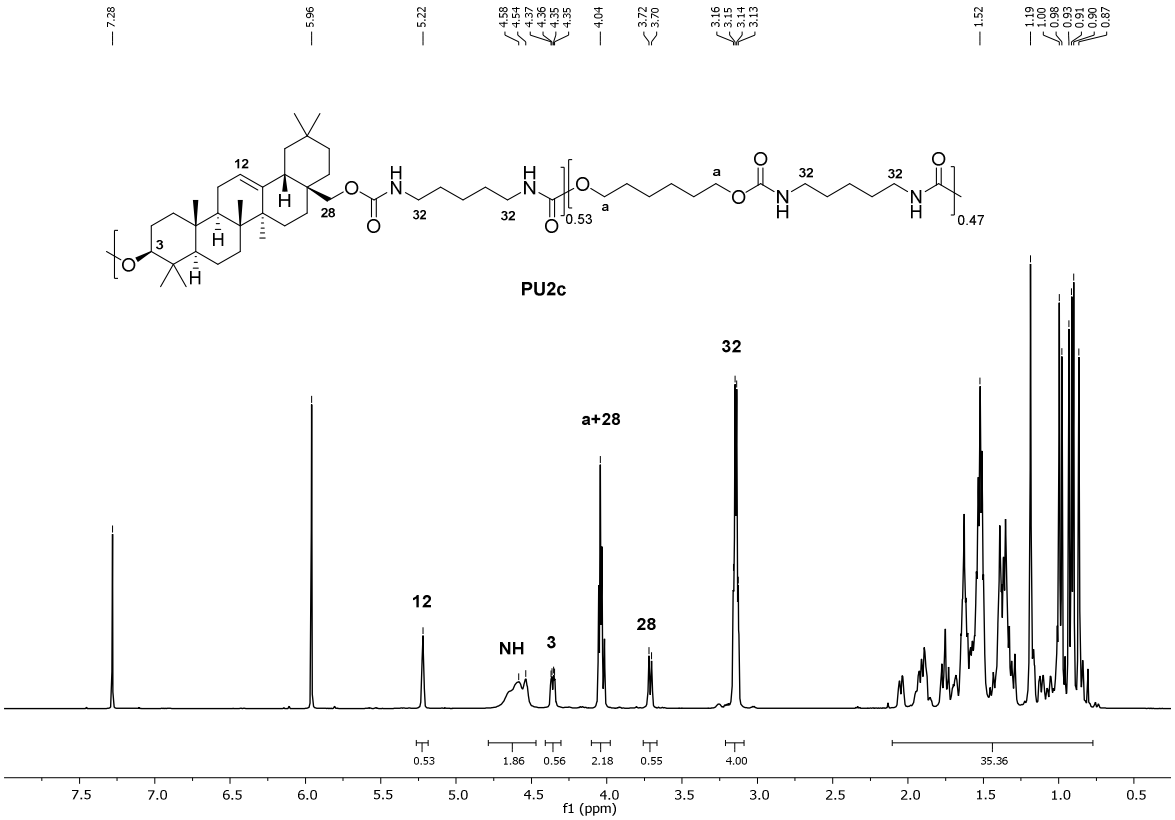

Figure 8.42. ^{1}H NMR spectrum of **PU2c** in TeCA-d_2.

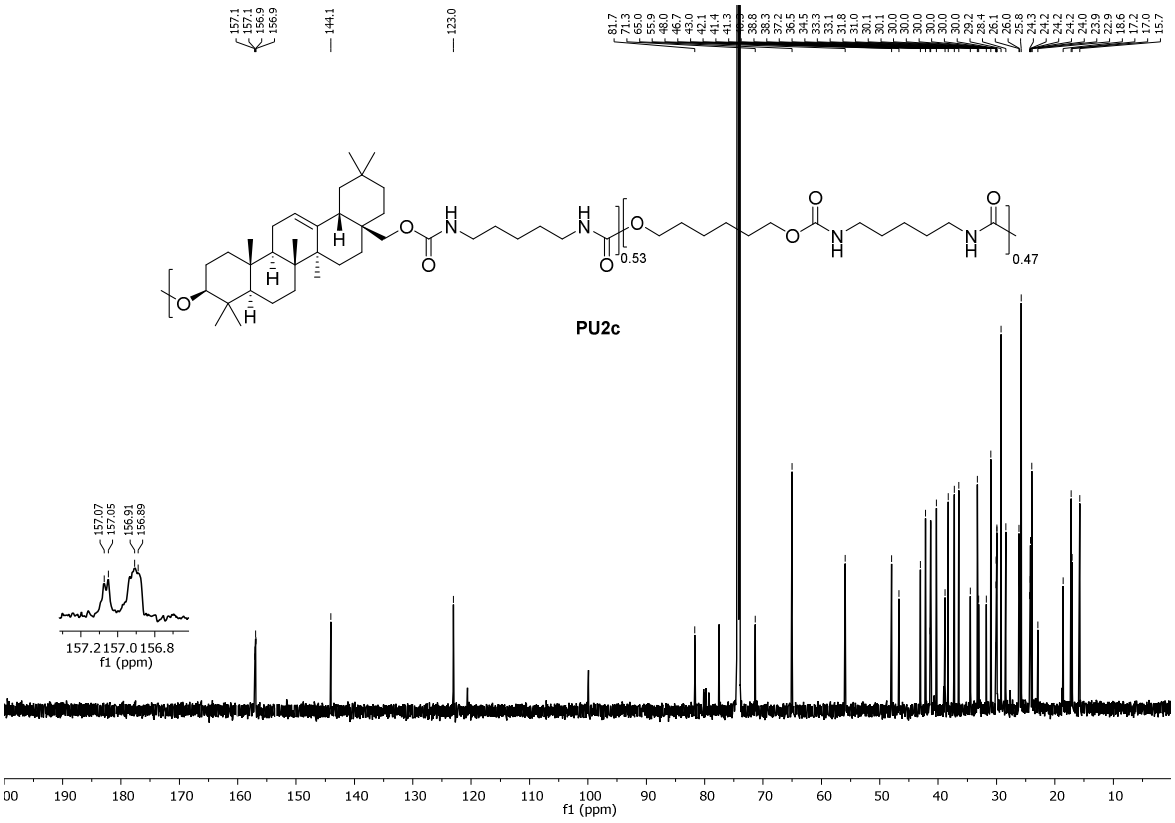

Figure 8.43. ^{13}C NMR spectrum of **PU2c** in TeCA-d_2.

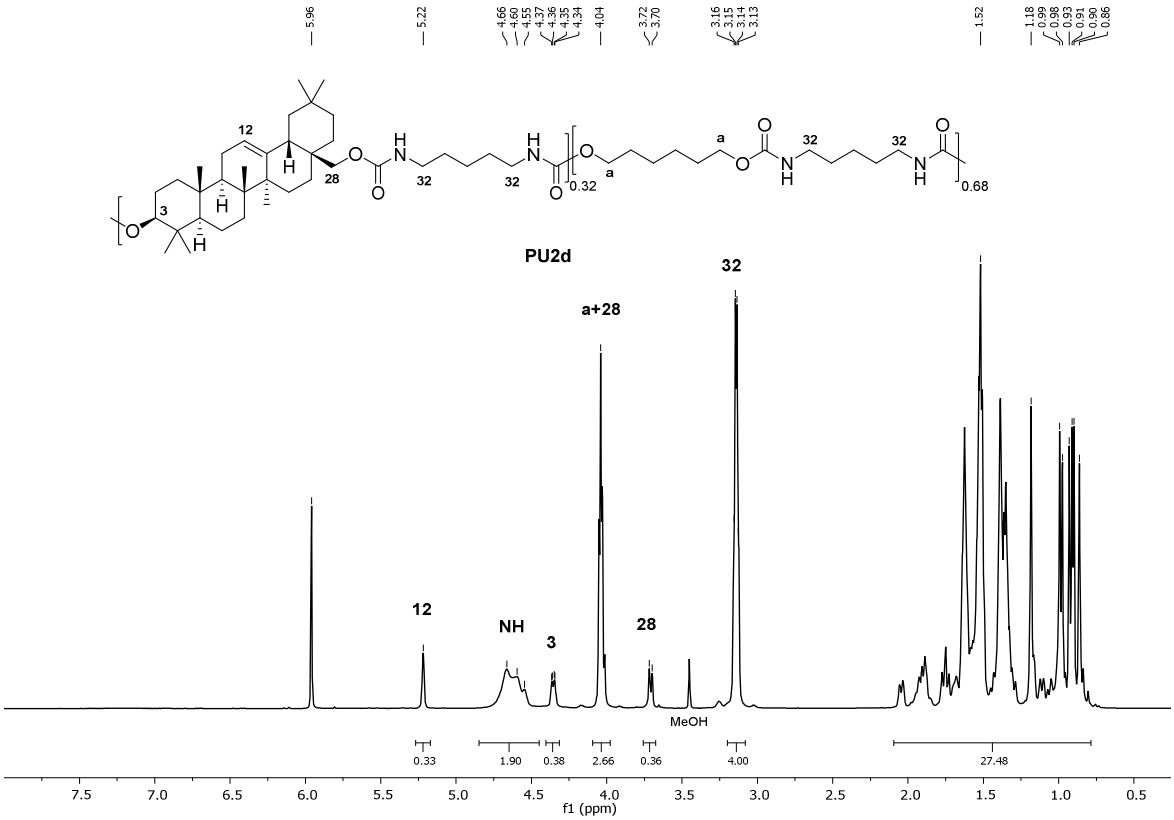

Figure 8.44. [1]H NMR spectrum of **PU2d** in TeCA-d_2.

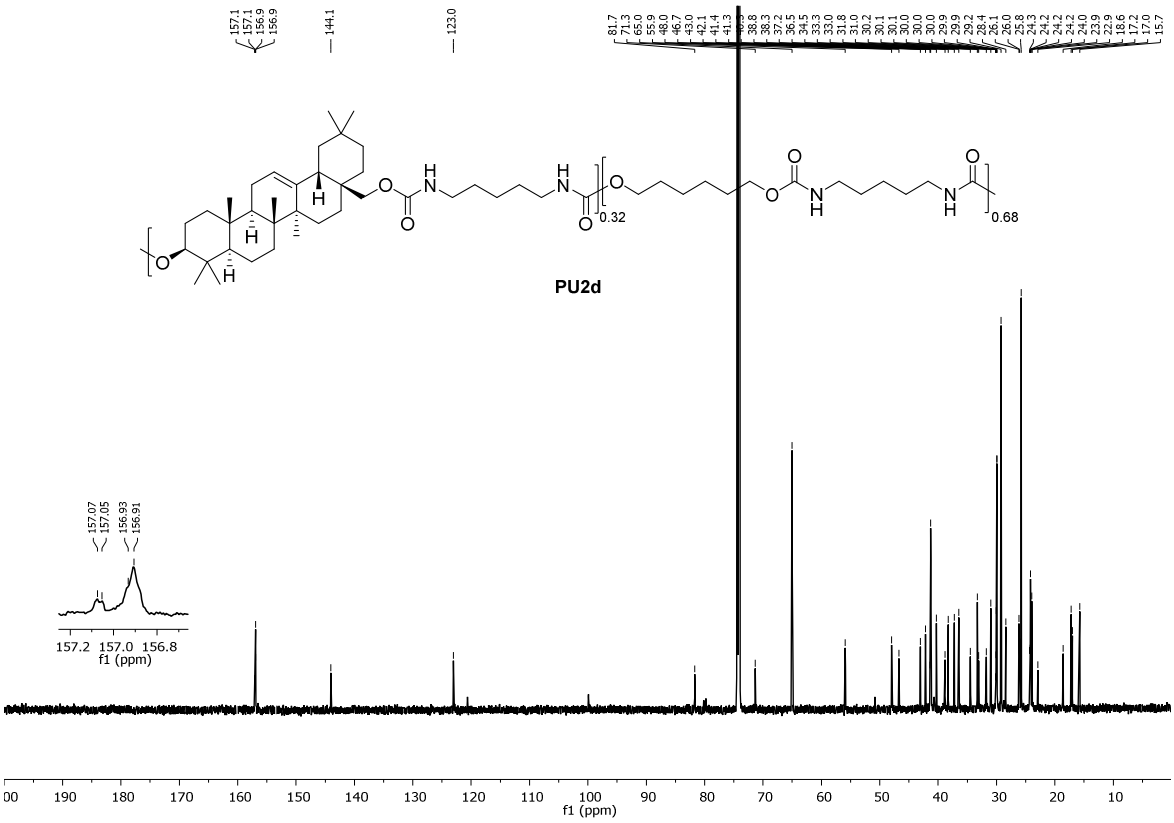

Figure 8.45. [13]C NMR spectrum of **PU2d** in TeCA-d_2.

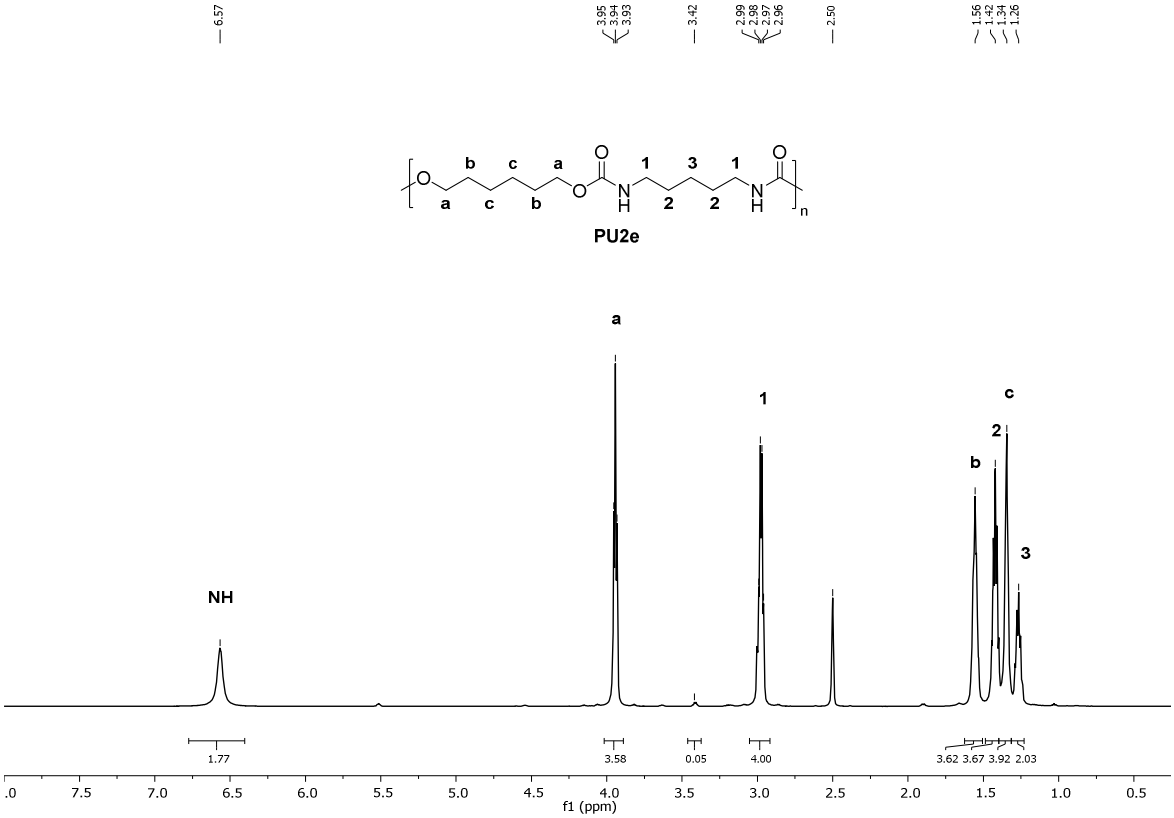

Figure 8.46. ^{1}H NMR spectrum of **PU2e** in DMSO-d_6.

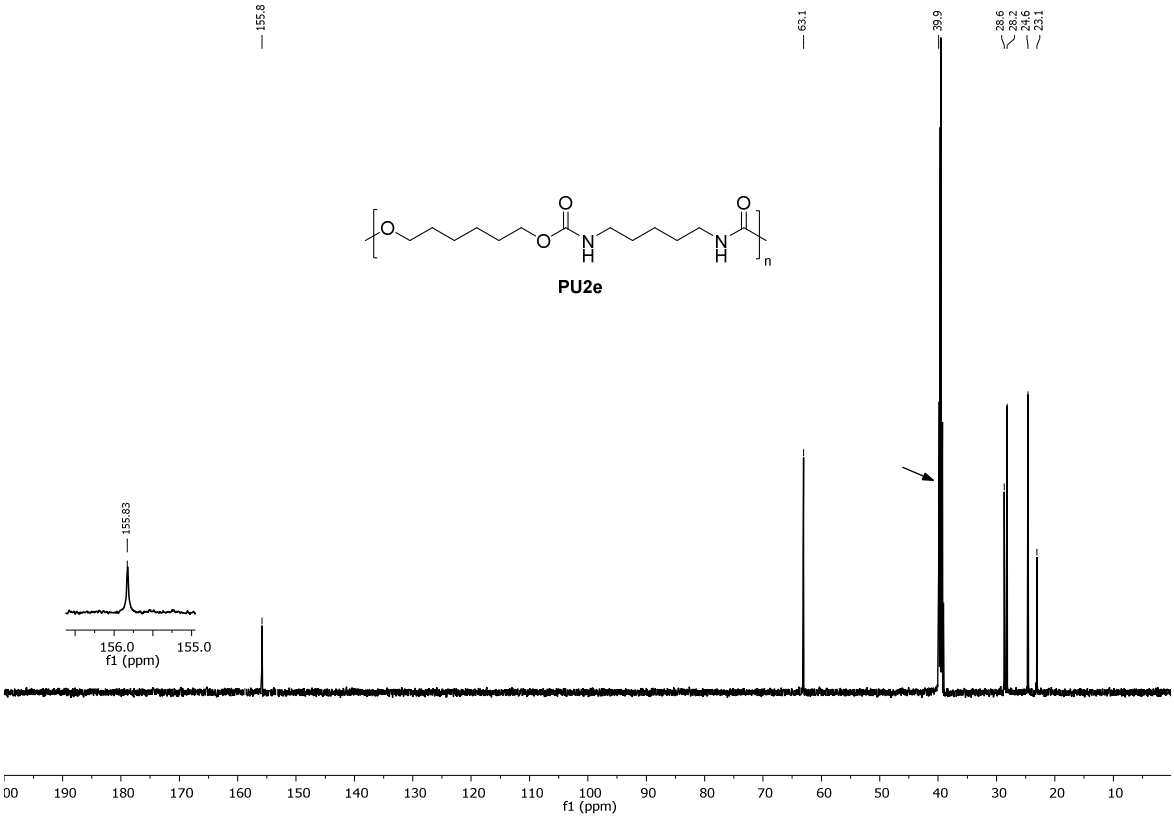

Figure 8.47. ^{13}C NMR spectrum of **PU2e** in DMSO-d_6.

Ch. 5: Renewable Polycarbonates Based On Erythrodiol

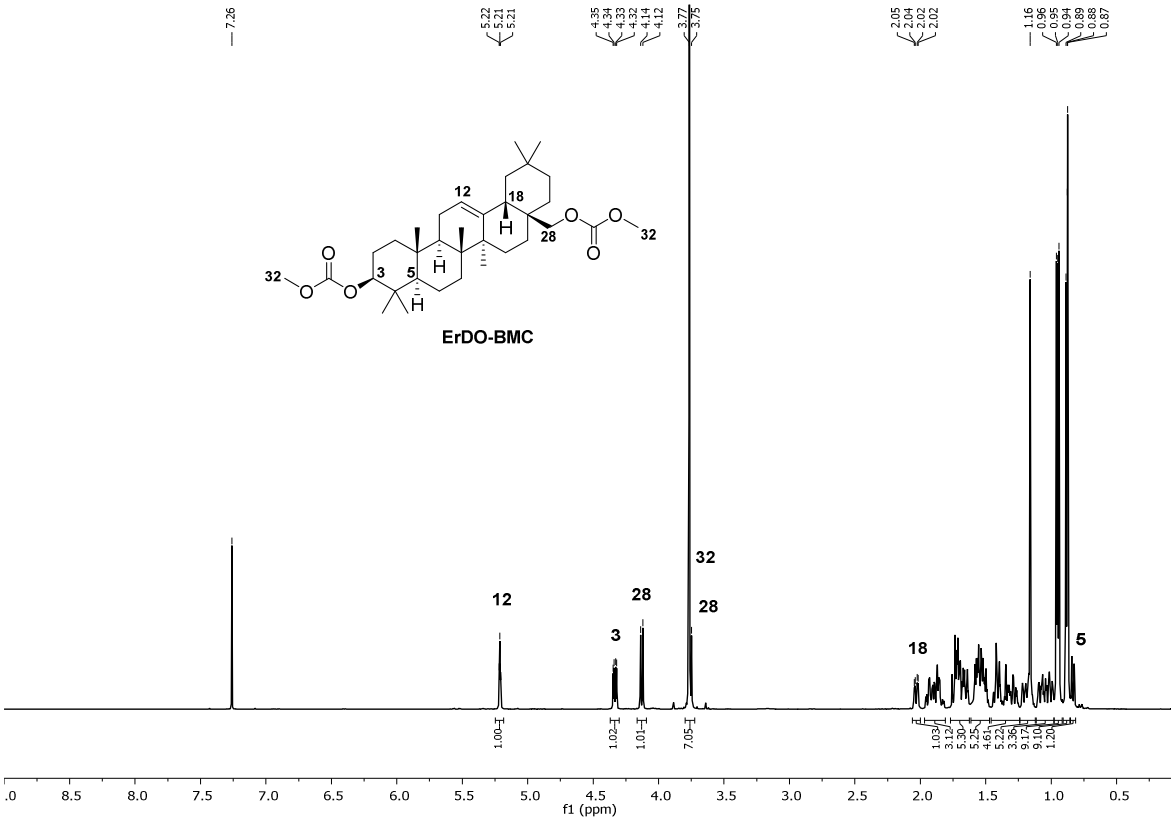

Figure 8.48. ^{1}H NMR spectrum of **ErDO-BMC** in $CDCl_3$.

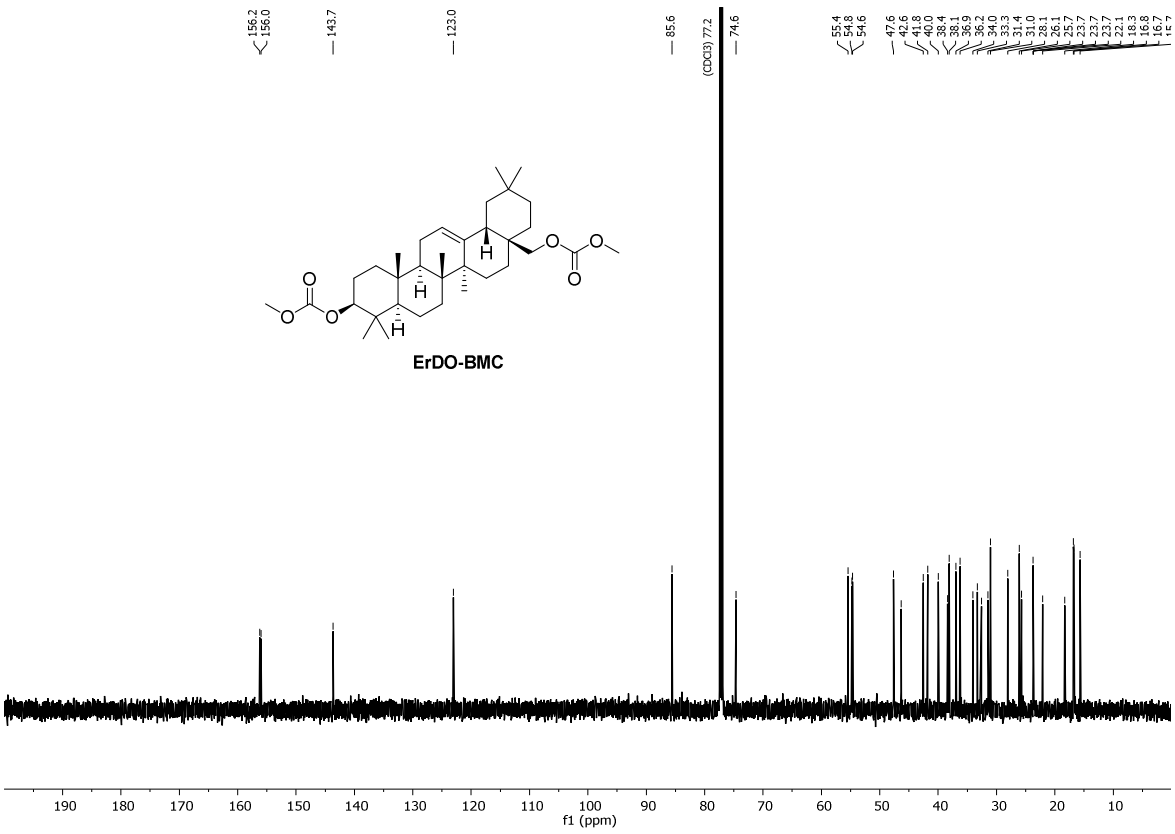

Figure 8.49. ^{13}C NMR spectrum of **ErDO-BMC** in $CDCl_3$.

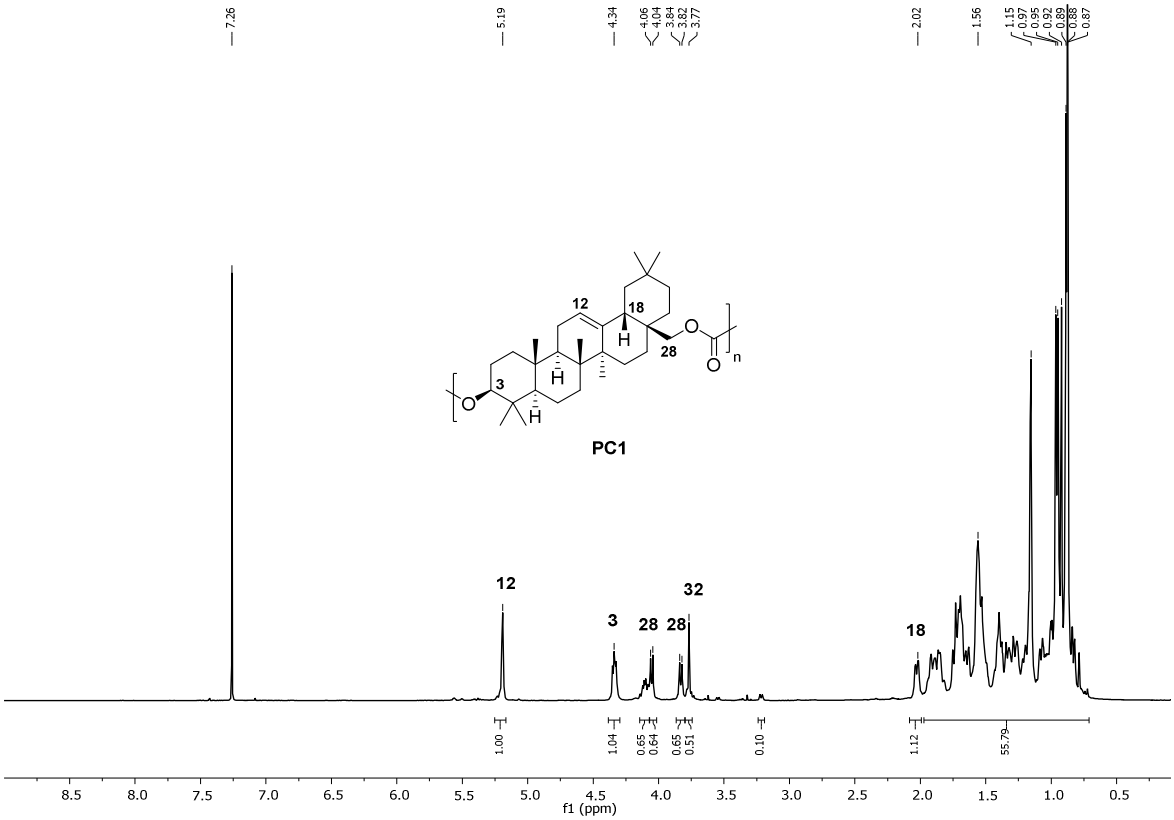

Figure 8.50. ^{1}H NMR spectrum of **PC1** in $CDCl_3$.

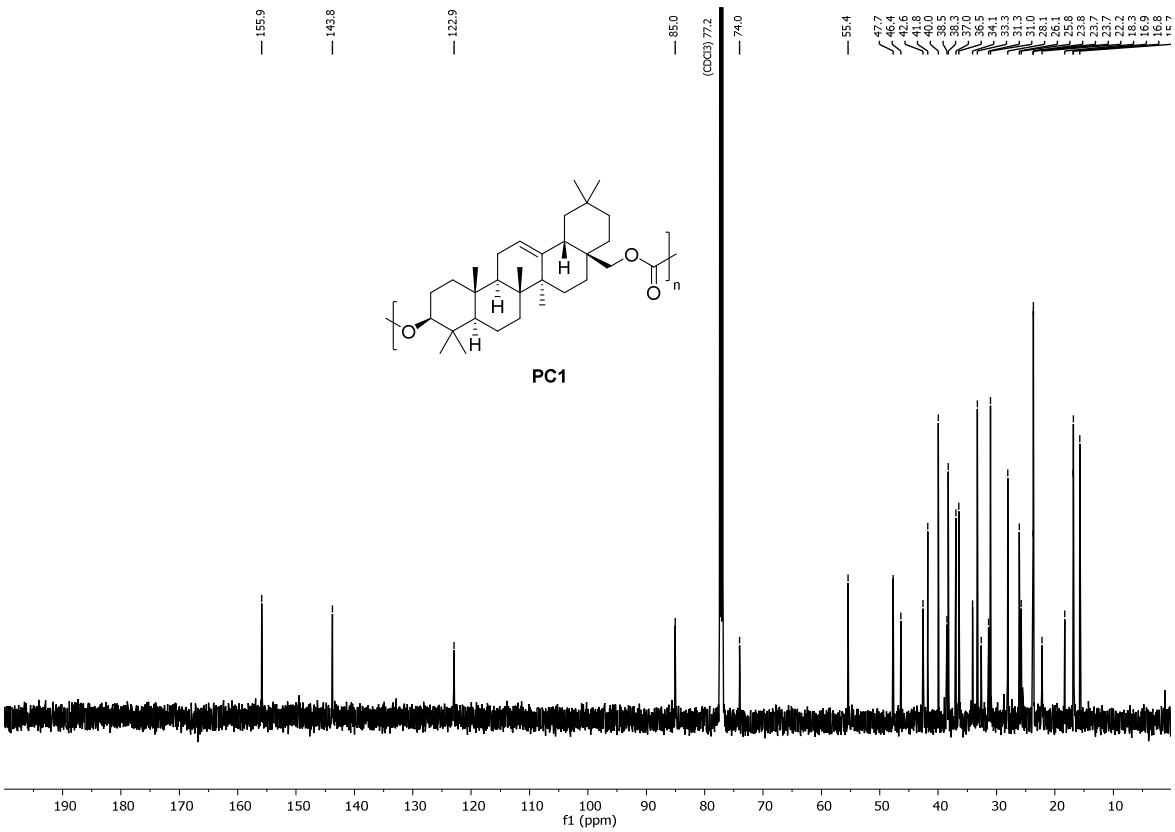

Figure 8.51. ^{13}C NMR spectrum of **PC1** in $CDCl_3$.

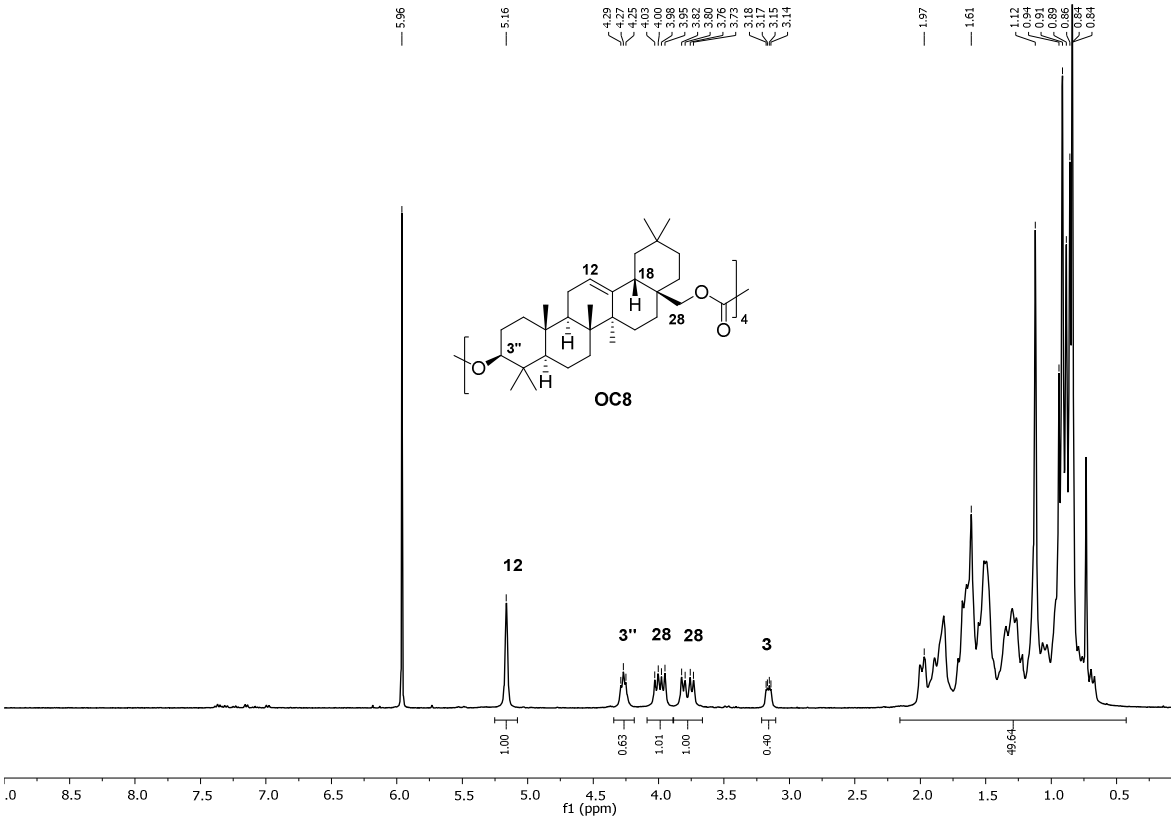

Figure 8.52. [1]H NMR spectrum of **OC8** in TeCA-d_2.

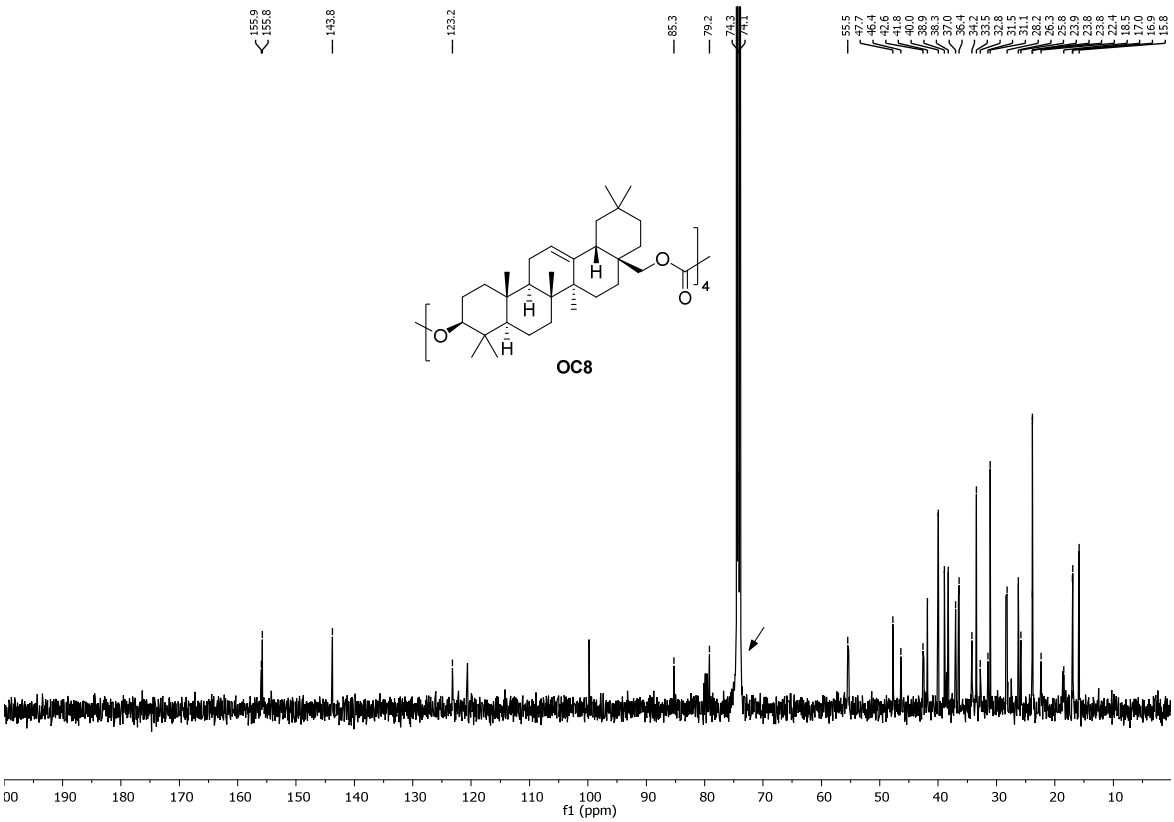

Figure 8.53. [13]C NMR spectrum of **OC8** in TeCA-d_2.

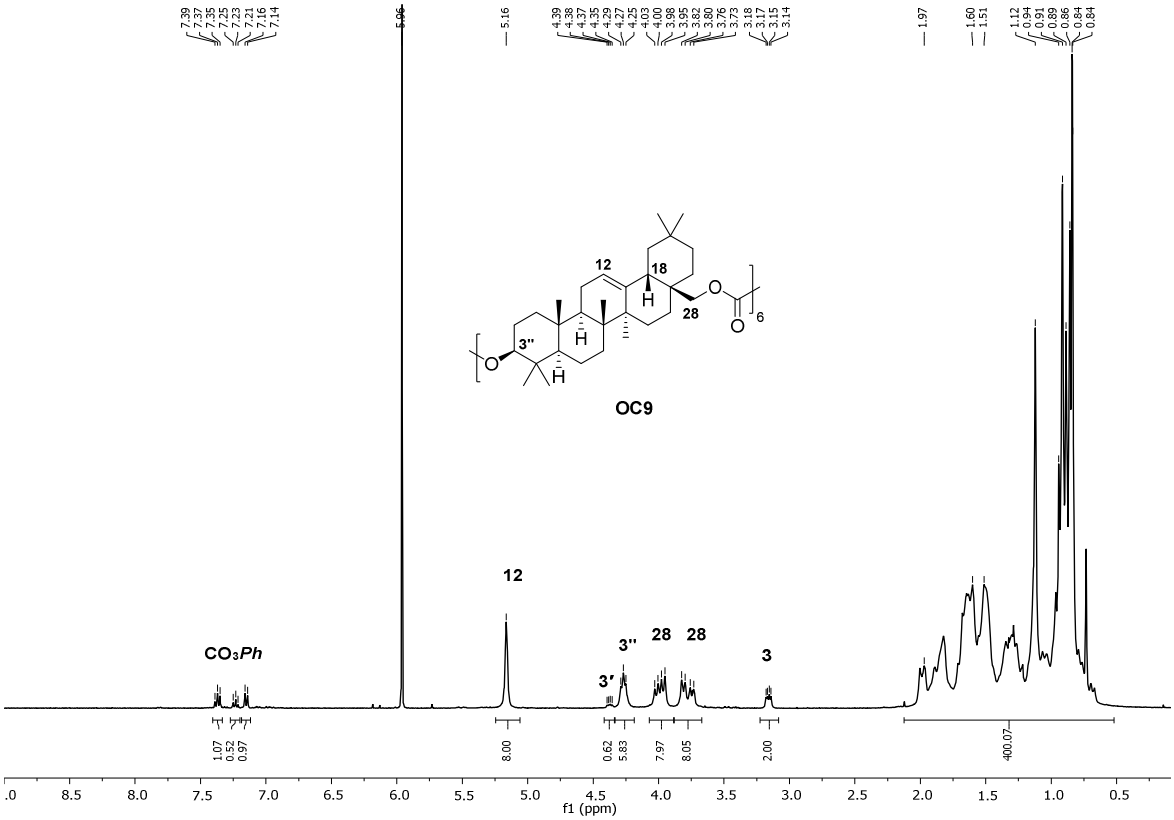

Figure 8.54. [1]H NMR spectrum of **OC9** in TeCA-d_2.

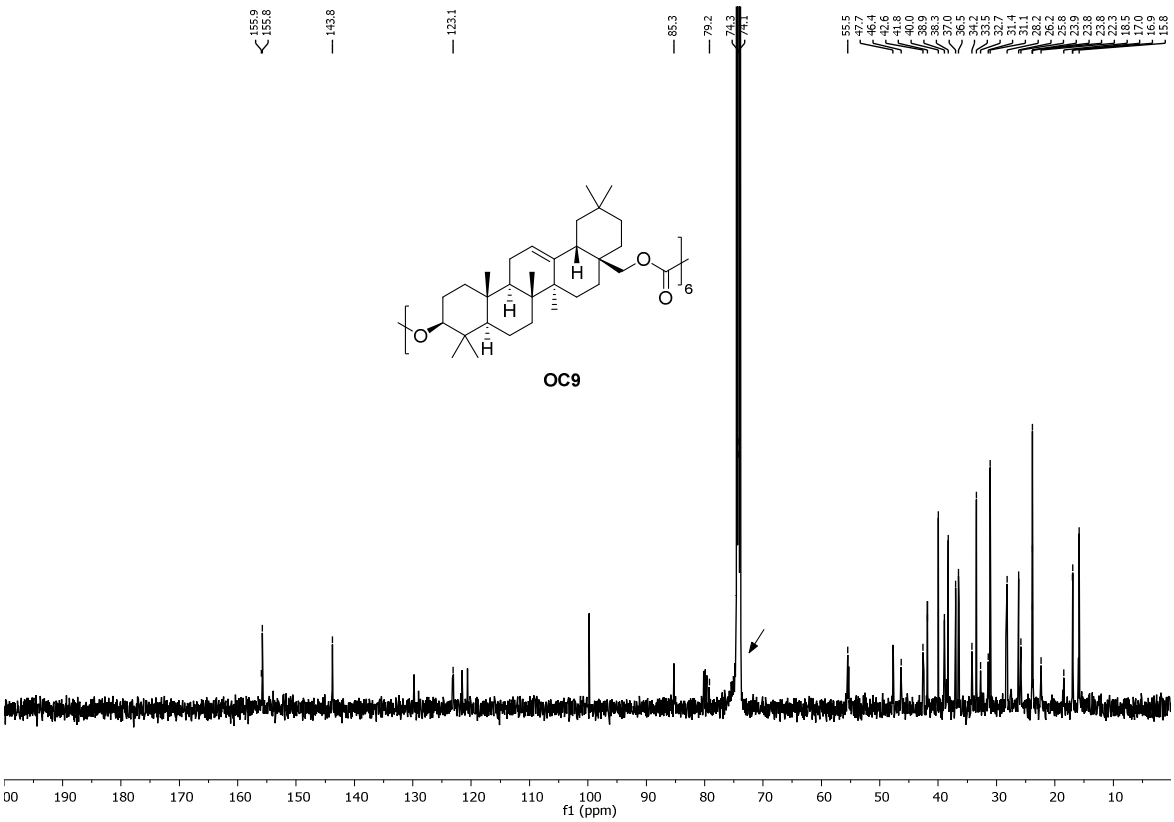

Figure 8.55. [13]C NMR spectrum of **OC9** in TeCA-d_2.

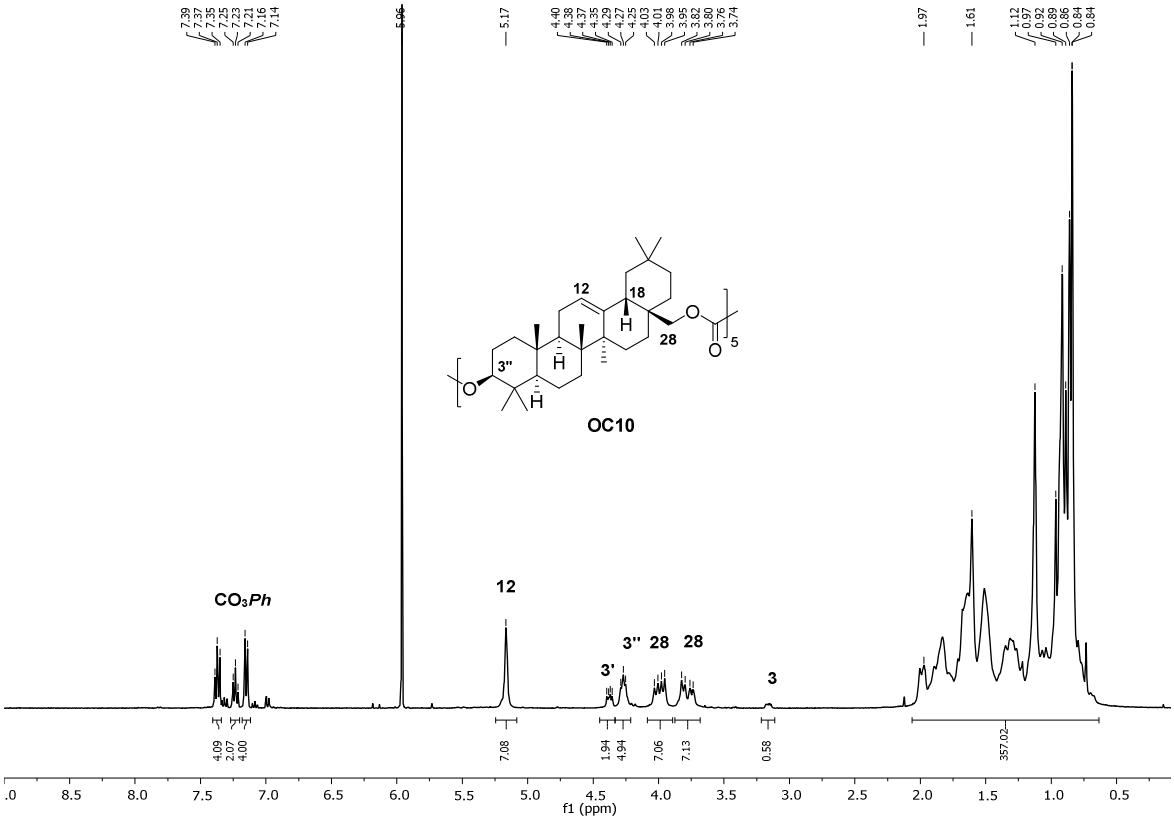

Figure 8.56. [1]H NMR spectrum of **OC10** in TeCA-d_2.

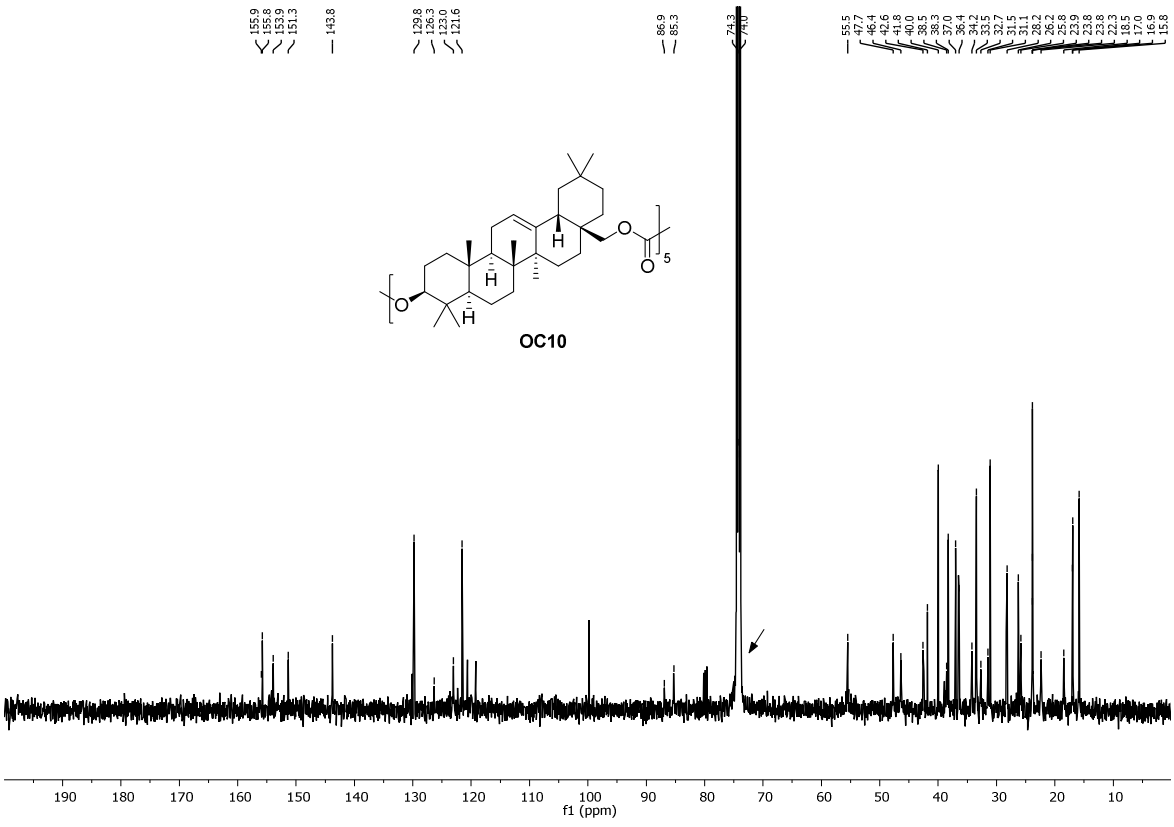

Figure 8.57. [13]C NMR spectrum of **OC10** in TeCA-d_2.

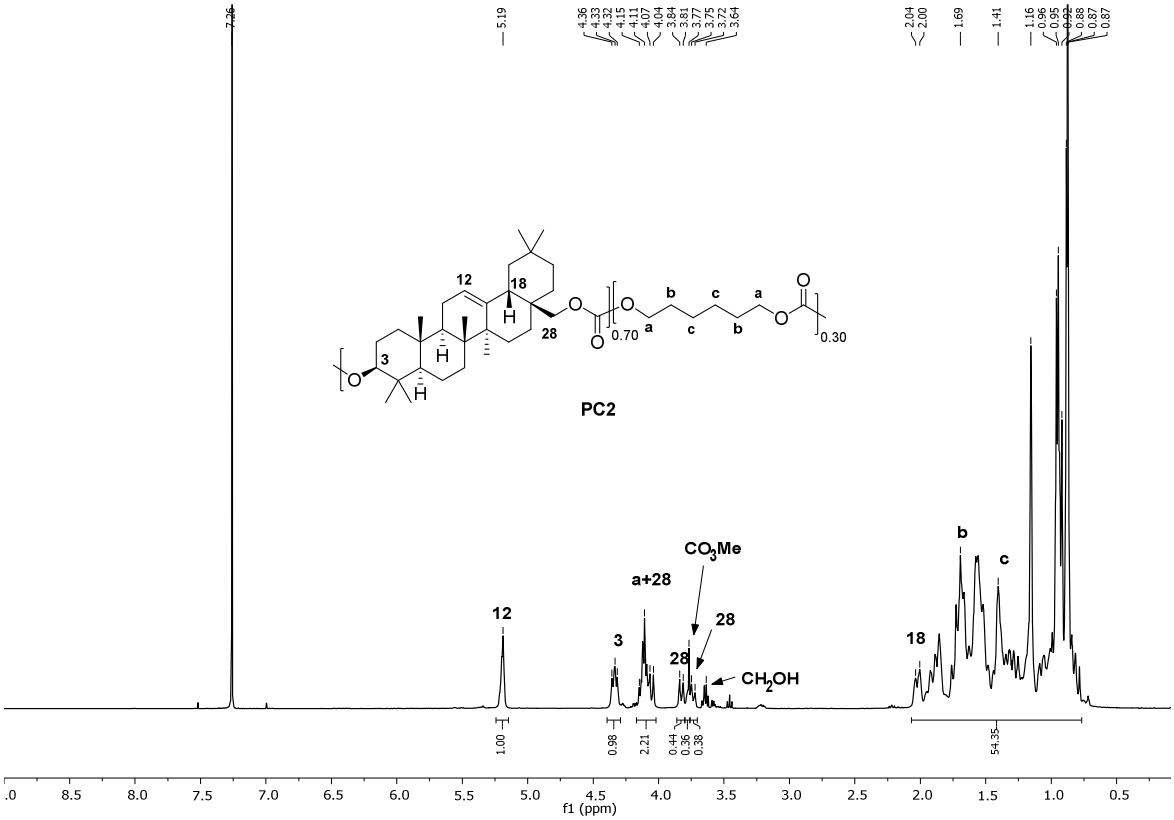

Figure 8.58. ^{1}H NMR spectrum of **PC2** in $CDCl_3$.

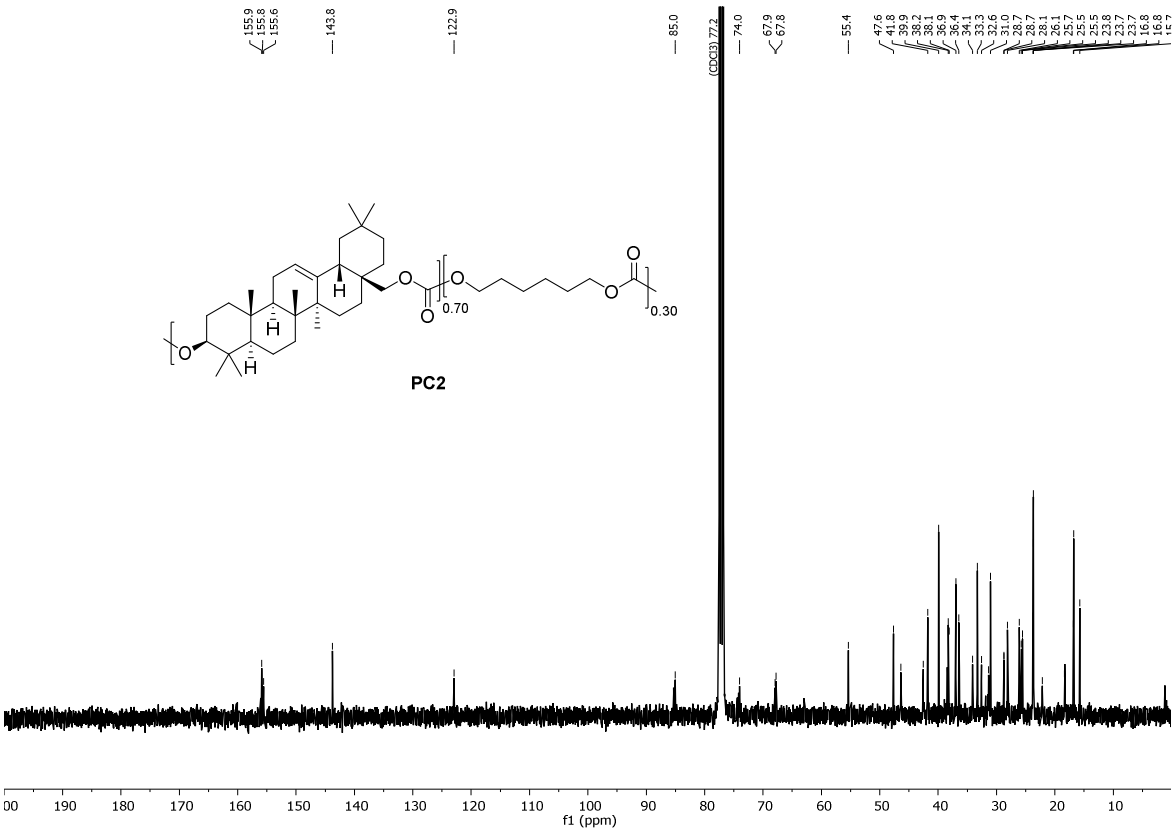

Figure 8.59. ^{13}C NMR spectrum of **PC2** in $CDCl_3$.

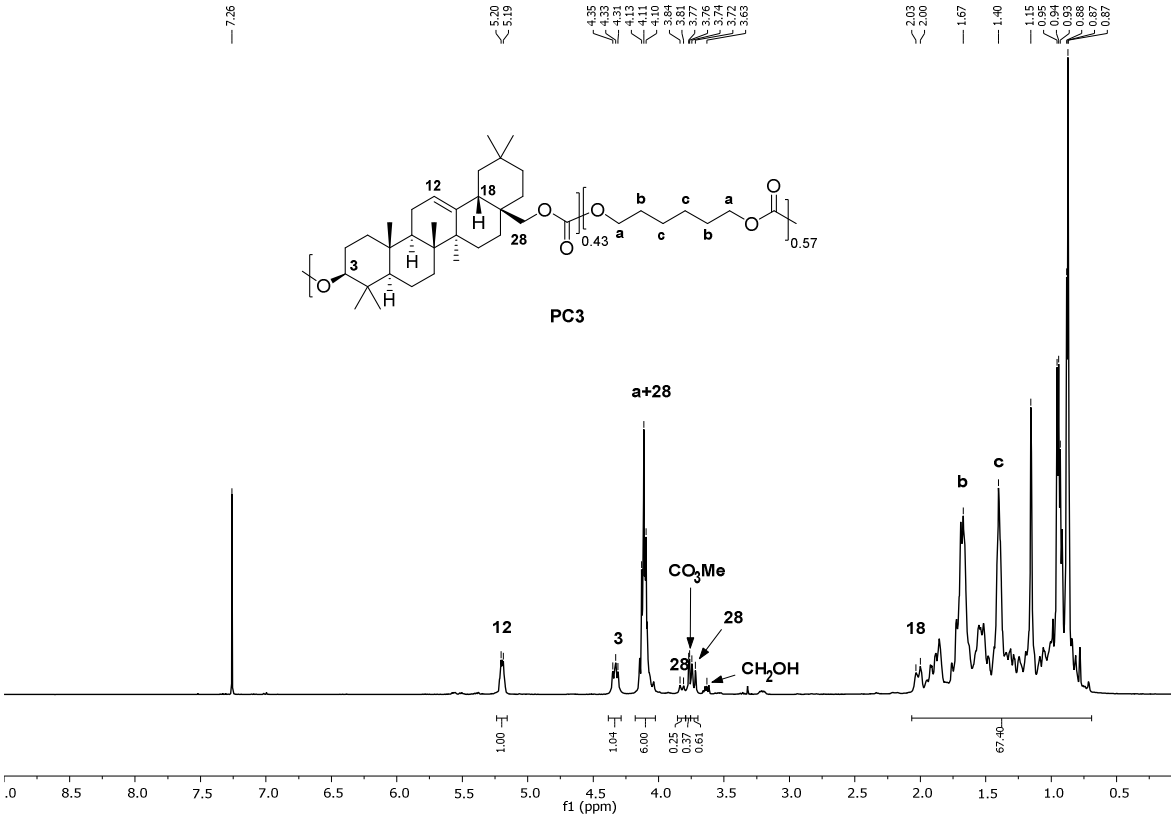

Figure 8.60. ^{1}H NMR spectrum of **PC3** in $CDCl_3$.

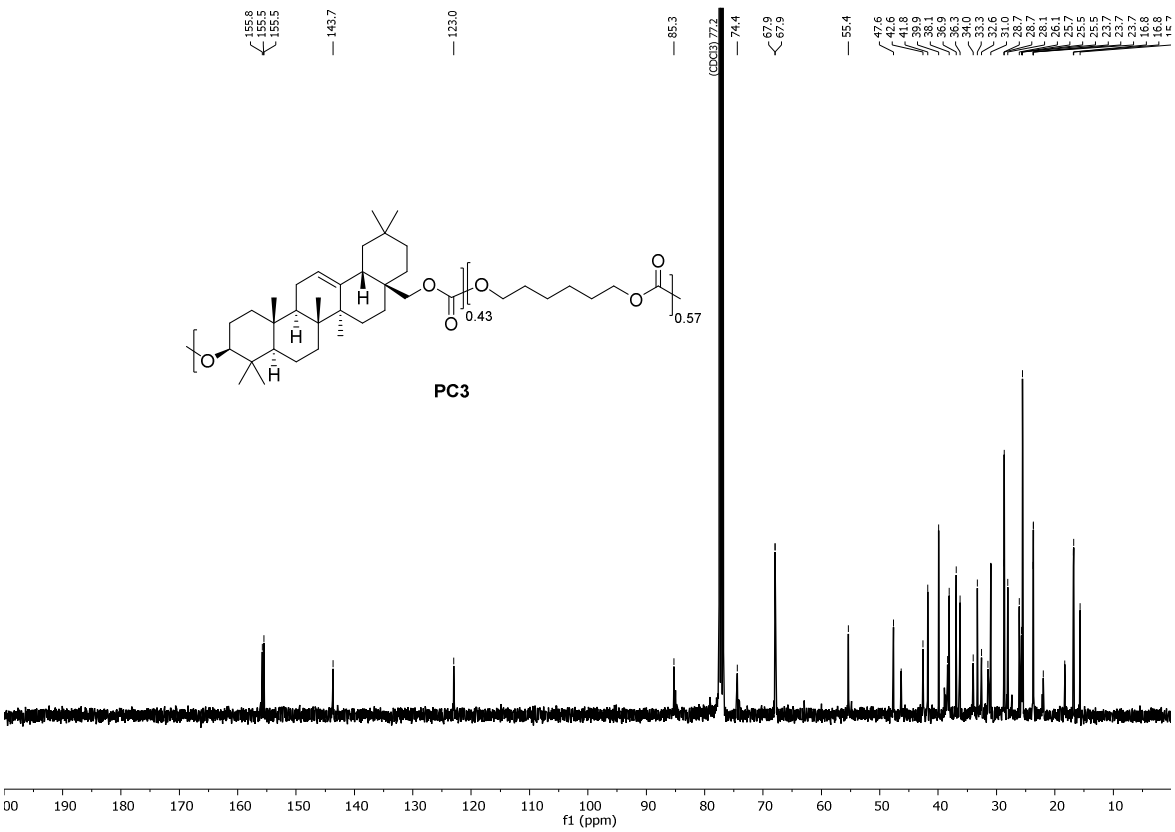

Figure 8.61. ^{13}C NMR spectrum of **PC3** in $CDCl_3$.

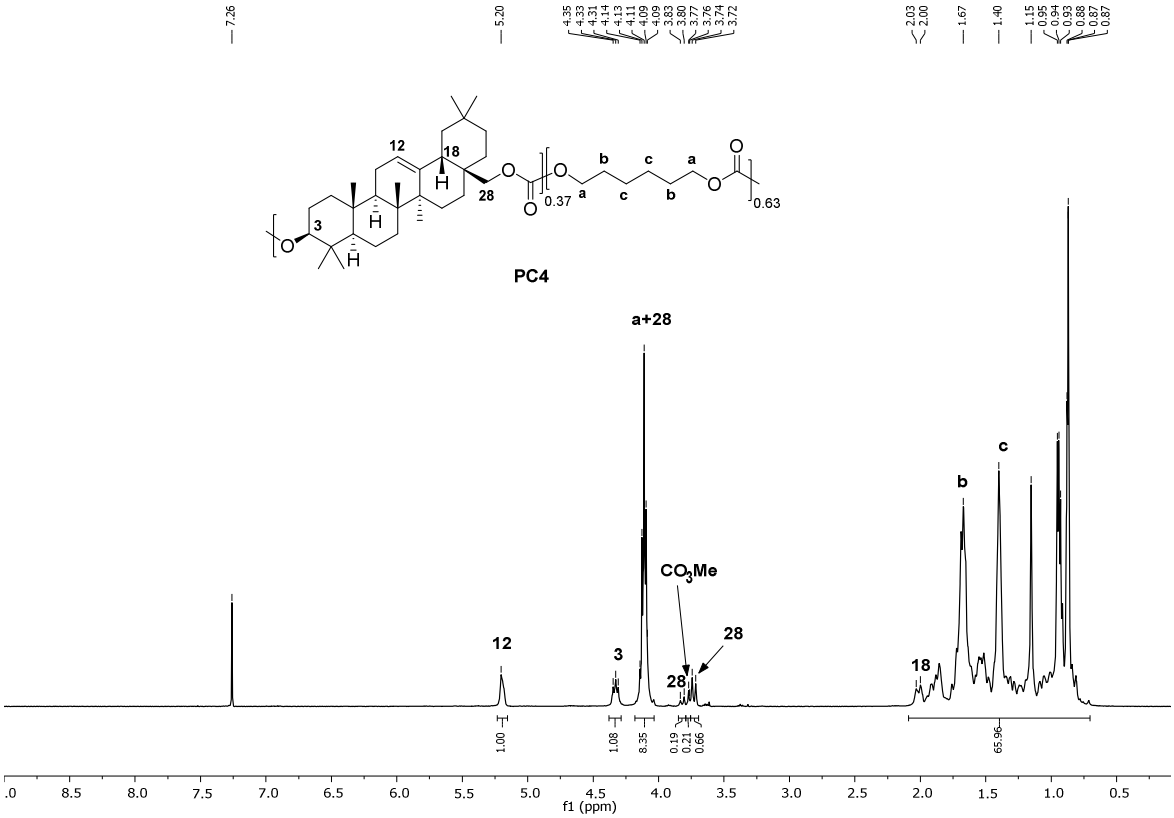

Figure 8.62. ^{1}H NMR spectrum of **PC4** in $CDCl_3$.

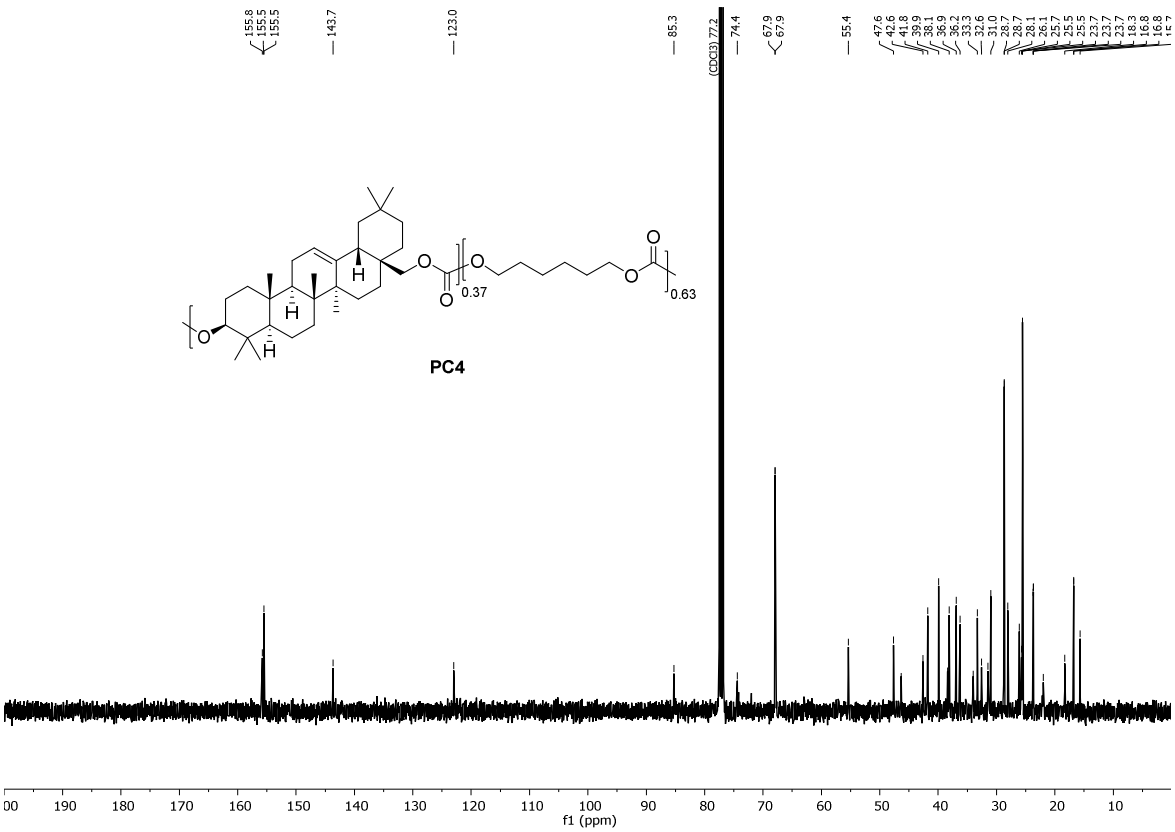

Figure 8.63. ^{13}C NMR spectrum of **PC4** in $CDCl_3$.

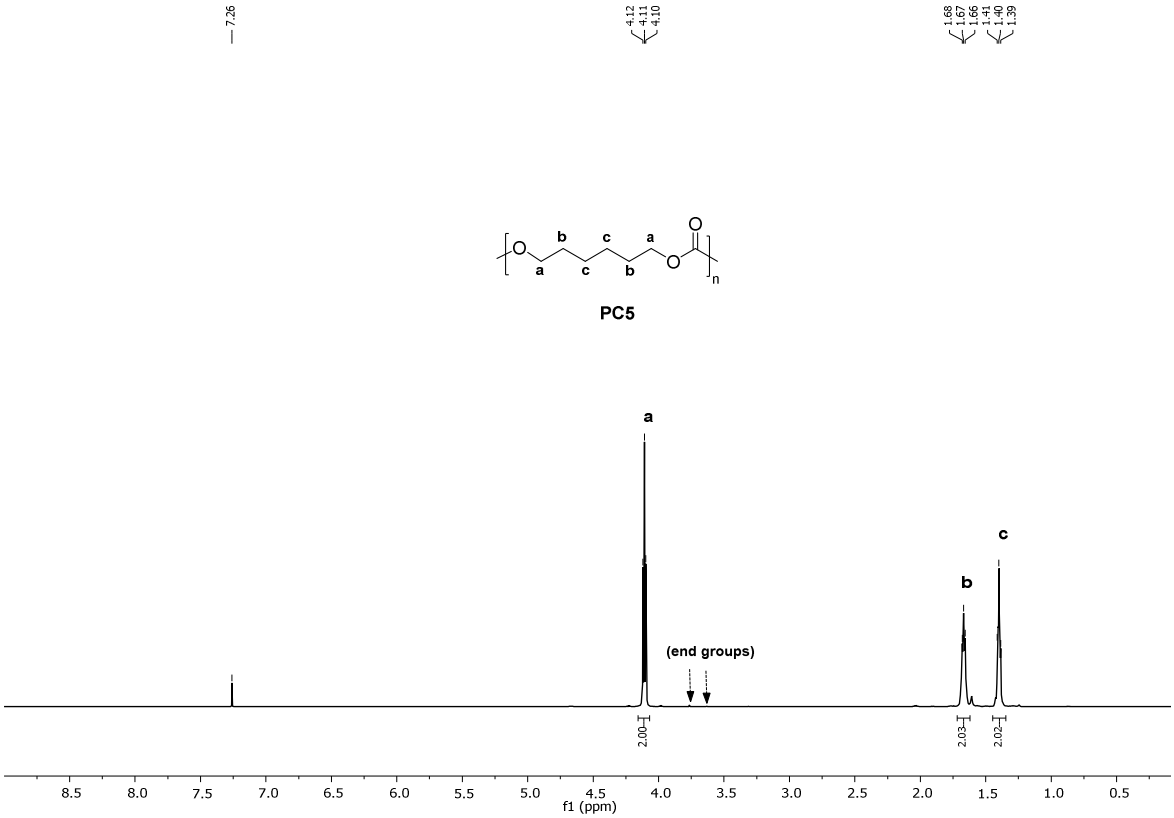

Figure 8.64. ^{1}H NMR spectrum of **PC5** in $CDCl_3$.

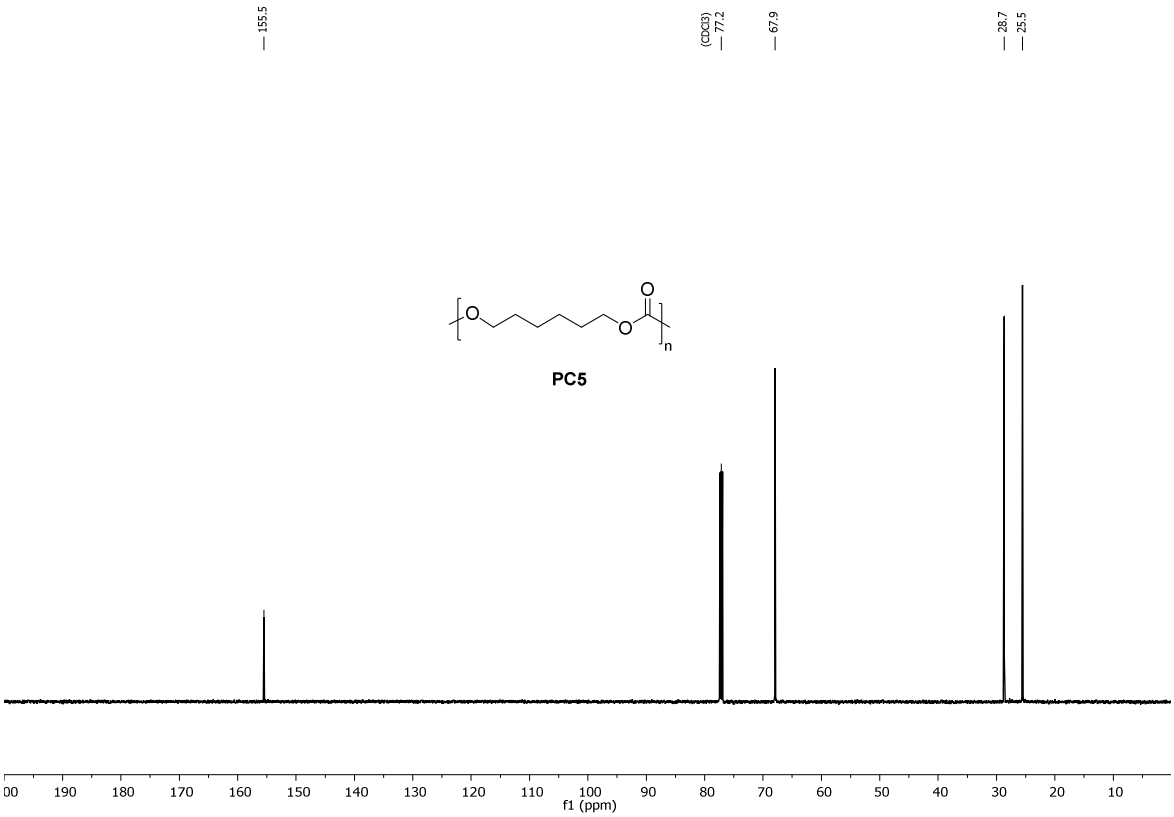

Figure 8.65. ^{13}C NMR spectrum of **PC5** in $CDCl_3$.

8.5. References

(1) Bhushan, S.; Kalia, K.; Sharma, M.; Singh, B.; Ahuja, P. S. Processing of Apple Pomace for Bioactive Molecules. *Crit. Rev. Biotechnol.* **2008**, *28* (4), 285–296.

(2) Kauser, S.; Murtaza, M. A.; Hussain, A.; Imran, M.; Kabir, K.; Najam, A.; An, Q. U.; Akram, S.; Fatima, H.; Batool, S. A.; Shehzad, A.; Yaqub, S. Apple Pomace, a Bioresource of Functional and Nutritional Components with Potential of Utilization in Different Food Formulations: A Review. *Food Chemistry Advances* **2024**, *4*, 100598.

(3) Jäger, S.; Trojan, H.; Kopp, T.; Laszczyk, M. N.; Scheffler, A. Pentacyclic Triterpene Distribution in Various Plants – Rich Sources for a New Group of Multi-Potent Plant Extracts. *Molecules* **2009**, *14* (6), 2016–2031.

(4) Cláudio, A. F. M.; Cognigni, A.; De Faria, E. L. P.; Silvestre, A. J. D.; Zirbs, R.; Freire, M. G.; Bica, K. Valorization of Olive Tree Leaves: Extraction of Oleanolic Acid Using Aqueous Solutions of Surface-Active Ionic Liquids. *Sep. Purif. Technol.* **2018**, *204*, 30–37.

(5) Kaur, R.; Singh, P.; Tanwar, S.; Varshney, G.; Yadav, S. Assessment of Bio-Based Polyurethanes: Perspective on Applications and Bio-Degradation. *Macromol* **2022**, *2* (3), 284–314.

(6) Cywar, R. M.; Rorrer, N. A.; Hoyt, C. B.; Beckham, G. T.; Chen, E. Y.-X. Bio-Based Polymers with Performance-Advantaged Properties. *Nat. Rev. Mater.* **2021**, *7* (2), 83–103.

(7) Liu, L.; Liang, W.; Zhang, Y.; Fu, Q. Nanoencapsulation in Polymeric Materials: Weaving Magical Coats for Microorganisms. *Nano Today* **2023**, *52*, 101973.

(8) Berezina, N.; Martelli, S. M. Bio-Based Polymers and Materials. In *Renewable Resources for Biorefineries*; Lin, C., Luque, R., Eds.; The Royal Society of Chemistry, 2014; pp 1–28.

(9) Chen, G.-Q.; Patel, M. K. Plastics Derived from Biological Sources: Present and Future: A Technical and Environmental Review. *Chem. Rev.* **2012**, *112* (4), 2082–2099.

(10) Isikgor, F. H.; Becer, C. R. Lignocellulosic Biomass: A Sustainable Platform for the Production of Bio-Based Chemicals and Polymers. *Polym. Chem.* **2015**, *6* (25), 4497–4559.

(11) Gregory, D. A.; Taylor, C. S.; Fricker, A. T. R.; Asare, E.; Tetali, S. S. V.; Haycock, J. W.; Roy, I. Polyhydroxyalkanoates and Their Advances for Biomedical Applications. *Trends Mol. Med.* **2022**, *28* (4), 331–342.

(12) Mehrpouya, M.; Vahabi, H.; Barletta, M.; Laheurte, P.; Langlois, V. Additive Manufacturing of Polyhydroxyalkanoates (PHAs) Biopolymers: Materials, Printing Techniques, and Applications. *Mater. Sci. Eng., C* **2021**, *127*, 112216.

(13) Lv, J.; Lv, X.; Ma, M.; Oh, D.-H.; Jiang, Z.; Fu, X. Chitin and Chitin-Based Biomaterials: A Review of Advances in Processing and Food Applications. *Carbohydr. Polym.* **2023**, *299*, 120142.

(14) El-Araby, A.; Janati, W.; Ullah, R.; Ercisli, S.; Errachidi, F. Chitosan, Chitosan Derivatives, and Chitosan-Based Nanocomposites: Eco-Friendly Materials for Advanced Applications (a Review). *Front. Chem.* **2024**, *11*, 1327426.
(15) Ewing, T. A.; Nouse, N.; Van Lint, M.; Van Haveren, J.; Hugenholtz, J.; Van Es, D. S. Fermentation for the Production of Biobased Chemicals in a Circular Economy: A Perspective for the Period 2022–2050. *Green Chem.* **2022**, *24* (17), 6373–6405.
(16) Gallezot, P. Conversion of Biomass to Selected Chemical Products. *Chem. Soc. Rev.* **2012**, *41* (4), 1538–1558.
(17) Xue, Z.; Ma, M.-G.; Li, Z.; Mu, T. Advances in the Conversion of Glucose and Cellulose to 5-Hydroxymethylfurfural over Heterogeneous Catalysts. *RSC Adv.* **2016**, *6* (101), 98874–98892.
(18) Rubin, E. M. Genomics of Cellulosic Biofuels. *Nature* **2008**, *454* (7206), 841–845.
(19) Mankar, A. R.; Pandey, A.; Modak, A.; Pant, K. K. Pretreatment of Lignocellulosic Biomass: A Review on Recent Advances. *Bioresource Technology* **2021**, *334*, 125235.
(20) Li, M.; Wilkins, M. Lignin Bioconversion into Valuable Products: Fractionation, Depolymerization, Aromatic Compound Conversion, and Bioproduct Formation. *Syst. Microbiol. Biomanuf.* **2021**, *1* (2), 166–185.
(21) Javanmard, A.; Wan Daud, W. M. A.; Patah, M. F. A.; Zuki, F. M.; Ai, S. P.; Azman, D. Q.; Chen, W.-H. Breaking Barriers for a Green Future: A Comprehensive Study on Pre-Treatment Techniques for Empty Fruit Bunches in the Bio-Based Economy. *Process Saf. Environ. Prot.* **2024**, *182*, 535–558.
(22) Sun, Z.; Fridrich, B.; De Santi, A.; Elangovan, S.; Barta, K. Bright Side of Lignin Depolymerization: Toward New Platform Chemicals. *Chem. Rev.* **2018**, *118* (2), 614–678.
(23) Salam, U.; Ullah, S.; Tang, Z.-H.; Elateeq, A. A.; Khan, Y.; Khan, J.; Khan, A.; Ali, S. Plant Metabolomics: An Overview of the Role of Primary and Secondary Metabolites against Different Environmental Stress Factors. *Life* **2023**, *13* (3), 706.
(24) Elshafie, H. S.; Camele, I.; Mohamed, A. A. A Comprehensive Review on the Biological, Agricultural and Pharmaceutical Properties of Secondary Metabolites Based-Plant Origin. *Int. J. Mol. Sci.* **2023**, *24* (4), 3266.
(25) Huang, X.-Q.; Dudareva, N. Plant Specialized Metabolism. *Curr. Biol.* **2023**, *33* (11), R473–R478.
(26) Ninkuu, V.; Zhang, L.; Yan, J.; Fu, Z.; Yang, T.; Zeng, H. Biochemistry of Terpenes and Recent Advances in Plant Protection. *Int. J. Mol. Sci.* **2021**, *22* (11), 5710.
(27) Yousaf, H. K.; Shan, T.; Chen, X.; Ma, K.; Shi, X.; Desneux, N.; Biondi, A.; Gao, X. Impact of the Secondary Plant Metabolite Cucurbitacin B on the Demographical Traits of the Melon Aphid, Aphis Gossypii. *Sci Rep* **2018**, *8* (1), 16473.
(28) Isah, T. Stress and Defense Responses in Plant Secondary Metabolites Production. *Biol. Res.* **2019**, *52* (1), 39.
(29) Razak, A. M.; Tan, J. K.; Mohd Said, M. M.; Makpol, S. Modulating Effects of Zingiberaceae Phenolic Compounds on Neurotrophic Factors and Their Potential as

Neuroprotectants in Brain Disorders and Age-Associated Neurodegenerative Disorders: A Review. *Nutrients* **2023**, *15* (11), 2564.

(30) Pichersky, E.; Raguso, R. A. Why Do Plants Produce so Many Terpenoid Compounds? *New Phytol.* **2018**, *220* (3), 692–702.

(31) Christianson, D. W. Structural and Chemical Biology of Terpenoid Cyclases. *Chem. Rev.* **2017**, *117* (17), 11570–11648.

(32) Pollier, J.; Goossens, A. Oleanolic Acid. *Phytochemistry* **2012**, *77*, 10–15.

(33) Feng, Y.; Morgan, R. M. L.; Fraser, P. D.; Hellgardt, K.; Nixon, P. J. Crystal Structure of Geranylgeranyl Pyrophosphate Synthase (CrtE) Involved in Cyanobacterial Terpenoid Biosynthesis. *Front. Plant Sci.* **2020**, *11*, 589.

(34) Liang, P.-H. Reaction Kinetics, Catalytic Mechanisms, Conformational Changes, and Inhibitor Design for Prenyltransferases. *Biochemistry* **2009**, *48* (28), 6562–6570.

(35) Micera, M.; Botto, A.; Geddo, F.; Antoniotti, S.; Bertea, C. M.; Levi, R.; Gallo, M. P.; Querio, G. Squalene: More than a Step toward Sterols. *Antioxidants* **2020**, *9* (8), 688.

(36) Lozano-Grande, M. A.; Gorinstein, S.; Espitia-Rangel, E.; Dávila-Ortiz, G.; Martínez-Ayala, A. L. Plant Sources, Extraction Methods, and Uses of Squalene. *Int. J. Agron.* **2018**, *2018*, 1–13.

(37) Xu, R.; Fazio, G. C.; Matsuda, S. P. T. On the Origins of Triterpenoid Skeletal Diversity. *Phytochemistry* **2004**, *65* (3), 261–291.

(38) Thimmappa, R.; Geisler, K.; Louveau, T.; O'Maille, P.; Osbourn, A. Triterpene Biosynthesis in Plants. *Annu. Rev. Plant Biol.* **2014**, *65* (1), 225–257.

(39) Brendolise, C.; Yauk, Y.; Eberhard, E. D.; Wang, M.; Chagne, D.; Andre, C.; Greenwood, D. R.; Beuning, L. L. An Unusual Plant Triterpene Synthase with Predominant A-amyrin-producing Activity Identified by Characterizing Oxidosqualene Cyclases from *Malus* × *Domestica*. *FEBS J.* **2011**, *278* (14), 2485–2499.

(40) Martelanc, M.; Vovk, I.; Simonovska, B. Determination of Three Major Triterpenoids in Epicuticular Wax of Cabbage (Brassica Oleracea L.) by High-Performance Liquid Chromatography with UV and Mass Spectrometric Detection. *J. Chromatogr. A* **2007**, *1164* (1–2), 145–152.

(41) Bauer, S.; Schulte, E.; Thier, H.-P. Composition of the Surface Wax from Tomatoes: II. Quantification of the Components at the Ripe Red Stage and during Ripening. *Eur. Food Res. Technol.* **2004**, *219* (5), 487–491.

(42) Li, D.; Pan, C.; Lu, J.; Zaman, W.; Zhao, H.; Zhang, J.; Lü, S. Lupeol Accumulation Correlates with Auxin in the Epidermis of Castor. *Molecules* **2021**, *26* (10), 2978.

(43) Fukushima, E. O.; Seki, H.; Ohyama, K.; Ono, E.; Umemoto, N.; Mizutani, M.; Saito, K.; Muranaka, T. CYP716A Subfamily Members Are Multifunctional Oxidases in Triterpenoid Biosynthesis. *Plant Cell Physiol.* **2011**, *52* (12), 2050–2061.

(44) Orihara, Y.; Ebizuka, Y. Production of Triterpene Acids by Cell-Suspension Cultures of Olea Europaea. In *Olives and Olive Oil in Health and Disease Prevention*; Elsevier, 2010; pp 341–347.

(45) Srisawat, P.; Fukushima, E. O.; Yasumoto, S.; Robertlee, J.; Suzuki, H.; Seki, H.; Muranaka, T. Identification of Oxidosqualene Cyclases from the Medicinal Legume Tree *Bauhinia Forficata* : A Step toward Discovering Preponderant A-amyrin-producing Activity. *New Phytol.* **2019**, *224* (1), 352–366.

(46) Sandeep; Misra, R. C.; Chanotiya, C. S.; Mukhopadhyay, P.; Ghosh, S. Oxidosqualene Cyclase and CYP716 Enzymes Contribute to Triterpene Structural Diversity in the Medicinal Tree Banaba. *New Phytol.* **2019**, *222* (1), 408–424.

(47) Kushiro, T.; Ebizuka, Y. Triterpenes. In *Comprehensive Natural Products II*; Elsevier, 2010; pp 673–708.

(48) Wu, S.; Zhang, F.; Xiong, W.; Molnár, I.; Liang, J.; Ji, A.; Li, Y.; Wang, C.; Wang, S.; Liu, Z.; Wu, R.; Duan, L. An Unexpected Oxidosqualene Cyclase Active Site Architecture in the *Iris Tectorum* Multifunctional α-Amyrin Synthase. *ACS Catal.* **2020**, *10* (16), 9515–9520.

(49) Fang, Y.; Xiao, H. The Transport of Triterpenoids. *Biotechnol. Notes* **2021**, *2*, 11–17.

(50) Samuels, L.; Kunst, L.; Jetter, R. Sealing Plant Surfaces: Cuticular Wax Formation by Epidermal Cells. *Annu. Rev. Plant Biol.* **2008**, *59* (1), 683–707.

(51) Morita, M.; Shibuya, M.; Kushiro, T.; Masuda, K.; Ebizuka, Y. Molecular Cloning and Functional Expression of Triterpene Synthases from Pea (*Pisum Sativum*): New A-amyrin-producing Enzyme Is a Multifunctional Triterpene Synthase. *Eur. J. Biochem.* **2000**, *267* (12), 3453–3460.

(52) Laszczyk, M.; Jäger, S.; Simon-Haarhaus, B.; Scheffler, A.; Schempp, C. Physical, Chemical and Pharmacological Characterization of a New Oleogel-Forming Triterpene Extract from the Outer Bark of Birch (Betulae Cortex). *Planta Med.* **2006**, *72* (15), 1389–1395.

(53) Jeong, G.-S.; Bae, J.-S. Anti-Inflammatory Effects of Triterpenoids; Naturally Occurring and Synthetic Agents. *Mini-Rev. Org. Chem.* **2014**, *11* (3), 316–329.

(54) Wolska, K.; Grudniak, A.; Fiecek, B.; Kraczkiewicz-Dowjat, A.; Kurek, A. Antibacterial Activity of Oleanolic and Ursolic Acids and Their Derivatives. *Cent. Eur. J. Biol.* **2010**, *5* (5), 543–553.

(55) Wu, H.; Morris-Natschke, S. L.; Xu, X.; Yang, M.; Cheng, Y.; Yu, S.; Lee, K. Recent Advances in Natural anti-HIV Triterpenoids and Analogs. *Med. Res. Rev.* **2020**, *40* (6), 2339–2385.

(56) Salvador, J. A. R.; Moreira, V. M.; Gonçalves, B. M. F.; Leal, A. S.; Jing, Y. Ursane-Type Pentacyclic Triterpenoids as Useful Platforms to Discover Anticancer Drugs. *Nat. Prod. Rep.* **2012**, *29* (12), 1463.

(57) Xu, X.; Ma, X.; Wang, X.; Zhu, J.; Wang, J.; Yan, N.; Chen, J. Catalyst-Free Synthesis of Betulin-Based Polyurethane Elastomers with Outstanding Mechanical Properties and Solvent Resistance. *ACS Appl. Polym. Mater.* **2023**, *5* (10), 8260–8269.

(58) Cargnin, S. T.; Gnoatto, S. B. Ursolic Acid from Apple Pomace and Traditional Plants: A Valuable Triterpenoid with Functional Properties. *Food Chem.* **2017**, *220*, 477–489.

(59) Wiebel, M.; Bensberg, K.; Wende, L.; Grandrath, R.; Plitzko, K.; Bohrmann-Linde, C.; Kirsch, S. F.; Schebb, N. H. Efficient and Simple Extraction Protocol for Triterpenic Acids from Apples. *J. Chem. Educ.* **2024**, *101* (5), 2087–2093.

(60) Fan, J.-P.; Liao, D.-D.; Zhang, X.-H. Ultrasonic Assisted Extraction of Ursolic Acid from Apple Pomace: A Novel and Facile Technique. *Sep. Sci.* **2016**, *51* (8), 1344–1350.

(61) Cláudio, A. F. M.; Cognigni, A.; De Faria, E. L. P.; Silvestre, A. J. D.; Zirbs, R.; Freire, M. G.; Bica, K. Valorization of Olive Tree Leaves: Extraction of Oleanolic Acid Using Aqueous Solutions of Surface-Active Ionic Liquids. *Sep. Purif. Technol.* **2018**, *204*, 30–37.

(62) Yang, Y.-H.; Dai, S.-Y.; Deng, F.-H.; Peng, L.-H.; Li, C.; Pei, Y.-H. Recent Advances in Medicinal Chemistry of Oleanolic Acid Derivatives. *Phytochemistry* **2022**, *203*, 113397.

(63) Verma, N.; Raghuvanshi, D. S.; Singh, R. V. Recent Advances in the Chemistry and Biology of Oleanolic Acid and Its Derivatives. *European Journal of Medicinal Chemistry* **2024**, 116619.

(64) Li, J.; Qiu, W.-W.; Li, H.; Zou, H.; Gao, L.-X.; Liu, T.; Yang, F.; Li, J.-Y.; Tang, J. Synthesis and Biological Evaluation of Oleanolic Acid Derivatives as Novel Inhibitors of Protein Tyrosine Phosphatase 1B. *Heterocycles* **2012**, *85* (5), 1117.

(65) Moad, G.; Rizzardo, E.; Thang, S. H. Toward Living Radical Polymerization. *Acc. Chem. Res.* **2008**, *41* (9), 1133–1142.

(66) *Handbook of Radical Polymerization*, 1st ed.; Matyjaszewski, K., Davis, T. P., Eds.; Wiley, 2002.

(67) Nesvadba, P. Radical Polymerization in Industry. In *Encyclopedia of Radicals in Chemistry, Biology and Materials*; Wiley, 2012.

(68) Matyjaszewski, K.; Tsarevsky, N. V. Macromolecular Engineering by Atom Transfer Radical Polymerization. *J. Am. Chem. Soc.* **2014**, *136* (18), 6513–6533.

(69) Pirman, T.; Ocepek, M.; Likozar, B. Radical Polymerization of Acrylates, Methacrylates, and Styrene: Biobased Approaches, Mechanism, Kinetics, Secondary Reactions, and Modeling. *Ind. Eng. Chem. Res.* **2021**, *60* (26), 9347–9367.

(70) Scheren, P. A. G. M.; Russell, G. T.; Sangster, D. F.; Gilbert, R. G.; German, A. L. Chain-Length-Dependent Termination Rate Processes in Free-Radical Polymerizations. 3. Styrene Polymerizations with and without Added Inert Diluent as an Experimental Test of Model. *Macromolecules* **1995**, *28* (10), 3637–3649.

(71) Nakamura, Y.; Yamago, S. Termination Mechanism in the Radical Polymerization of Methyl Methacrylate and Styrene Determined by the Reaction of Structurally Well-Defined Polymer End Radicals. *Macromolecules* **2015**, *48* (18), 6450–6456.

(72) Corrigan, N.; Jung, K.; Moad, G.; Hawker, C. J.; Matyjaszewski, K.; Boyer, C. Reversible-Deactivation Radical Polymerization (Controlled/Living Radical Polymerization): From Discovery to Materials Design and Applications. *Progress in Polymer Science* **2020**, *111*, 101311.

(73) Dworakowska, S.; Lorandi, F.; Gorczyński, A.; Matyjaszewski, K. Toward Green Atom Transfer Radical Polymerization: Current Status and Future Challenges. *Advanced Science* **2022**, *9* (19), 2106076.
(74) Moad, G. Living and Controlled Reversible-activation Polymerization (RAP) on the Way to Reversible-deactivation Radical Polymerization (RDRP). *Polymer International* **2023**, *72* (10), 861–868.
(75) Antonopoulou, M.-N.; Jones, G. R.; Kroeger, A. A.; Pei, Z.; Coote, M. L.; Truong, N. P.; Anastasaki, A. Acid-Triggered Radical Polymerization of Vinyl Monomers. *Nat. Synth* **2024**, *3* (3), 347–356.
(76) Matioszek, D.; Mazières, S.; Brusylovets, O.; Lin, C. Y.; Coote, M. L.; Destarac, M.; Harrisson, S. Experimental and Theoretical Comparison of Addition–Fragmentation Pathways of Diseleno- and Dithiocarbamate RAFT Agents. *Macromolecules* **2019**, *52* (9), 3376–3386.
(77) Perrier, S. *50th Anniversary Perspective*: RAFT Polymerization—A User Guide. *Macromolecules* **2017**, *50* (19), 7433–7447.
(78) Bingham, N. M.; Abousalman-Rezvani, Z.; Collins, K.; Roth, P. J. Thiocarbonyl Chemistry in Polymer Science. *Polym. Chem.* **2022**, *13* (20), 2880–2901.
(79) Izadi, F.; Arthur-Baidoo, E.; Strover, L. T.; Yu, L.; Coote, M. L.; Moad, G.; Denifl, S. Selective Bond Cleavage in RAFT Agents Promoted by Low-Energy Electron Attachment. *Angew Chem Int Ed* **2021**, *60* (35), 19128–19132.
(80) Moad, G.; Rizzardo, E.; Thang, S. H. Living Radical Polymerization by the RAFT Process. *Aust. J. Chem.* **2005**, *58* (6), 379.
(81) Quinn, J. F.; Moad, G.; Barner-Kowollik, C. RAFT Polymerization: Mechanistic Considerations. In *RAFT Polymerization*; Moad, G., Rizzardo, E., Eds.; Wiley, 2021; pp 95–137.
(82) Jenkins, A. D.; Jones, R. G.; Moad, G. Terminology for Reversible-Deactivation Radical Polymerization Previously Called "Controlled" Radical or "Living" Radical Polymerization (IUPAC Recommendations 2010). *Pure and Applied Chemistry* **2009**, *82* (2), 483–491.
(83) Mori, H. Living Radical Polymerization: Reversible Addition-Fragmentation Chain Transfer (RAFT) Polymerization. In *Encyclopedia of Polymeric Nanomaterials*; Kobayashi, S., Müllen, K., Eds.; Springer Berlin Heidelberg: Berlin, Heidelberg, 2015; pp 1148–1155.
(84) Moad, G.; Rizzardo, E.; Thang, S. H. Radical Addition–Fragmentation Chemistry in Polymer Synthesis. *Polymer* **2008**, *49* (5), 1079–1131.
(85) Truong, N. P.; Jones, G. R.; Bradford, K. G. E.; Konkolewicz, D.; Anastasaki, A. A Comparison of RAFT and ATRP Methods for Controlled Radical Polymerization. *Nat Rev Chem* **2021**, *5* (12), 859–869.
(86) Keddie, D. J.; Moad, G.; Rizzardo, E.; Thang, S. H. RAFT Agent Design and Synthesis. *Macromolecules* **2012**, *45* (13), 5321–5342.
(87) Fliedel, C.; Poli, R. Homolytically Weak Metal-Carbon Bonds Make Robust Controlled Radical Polymerizations Systems for "Less-Activated Monomers." *J. Organomet. Chem.* **2019**, *880*, 241–252.

(88) Moad, G. Dithioesters in RAFT Polymerization. In *RAFT Polymerization*; Moad, G., Rizzardo, E., Eds.; Wiley, 2021; pp 223–358.
(89) Nwoko, T.; Nguyen, K.; Saha, N. K.; Barner-Kowollik, C.; Konkolewicz, D. Rate Retardation Trends in RAFT – an Emerging Monomer Classification Tool? *Polym. Chem.* **2024**, *15* (11), 1052–1061.
(90) Moad, G. Mechanism and Kinetics of Dithiobenzoate-Mediated RAFT Polymerization – Status of the Dilemma. *Macro Chemistry & Physics* **2014**, *215* (1), 9–26.
(91) Barner-Kowollik, C.; Buback, M.; Charleux, B.; Coote, M. L.; Drache, M.; Fukuda, T.; Goto, A.; Klumperman, B.; Lowe, A. B.; Mcleary, J. B.; Moad, G.; Monteiro, M. J.; Sanderson, R. D.; Tonge, M. P.; Vana, P. Mechanism and Kinetics of Dithiobenzoate-mediated RAFT Polymerization. I. The Current Situation. *J. Polym. Sci. A Polym. Chem.* **2006**, *44* (20), 5809–5831.
(92) Bradford, K. G. E.; Petit, L. M.; Whitfield, R.; Anastasaki, A.; Barner-Kowollik, C.; Konkolewicz, D. Ubiquitous Nature of Rate Retardation in Reversible Addition–Fragmentation Chain Transfer Polymerization. *J. Am. Chem. Soc.* **2021**, *143* (42), 17769–17777.
(93) Rizzardo, E.; Chen, M.; Chong, B.; Moad, G.; Skidmore, M.; Thang, S. H. RAFT Polymerization: Adding to the Picture. *Macromol. Symp.* **2007**, *248* (1), 104–116.
(94) Gody, G.; Maschmeyer, T.; Zetterlund, P. B.; Perrier, S. Exploitation of the Degenerative Transfer Mechanism in RAFT Polymerization for Synthesis of Polymer of High Livingness at Full Monomer Conversion. *Macromolecules* **2014**, *47* (2), 639–649.
(95) Hartlieb, M. Photo-Iniferter RAFT Polymerization. *Macromol. Rapid Commun.* **2022**, *43* (1), 2100514.
(96) Hill, M. R.; Carmean, R. N.; Sumerlin, B. S. Expanding the Scope of RAFT Polymerization: Recent Advances and New Horizons. *Macromolecules* **2015**, *48* (16), 5459–5469.
(97) Gody, G.; Maschmeyer, T.; Zetterlund, P. B.; Perrier, S. Rapid and Quantitative One-Pot Synthesis of Sequence-Controlled Polymers by Radical Polymerization. *Nat Commun* **2013**, *4* (1), 2505.
(98) Clothier, G. K. K.; Guimarães, T. R.; Khan, M.; Moad, G.; Perrier, S.; Zetterlund, P. B. Exploitation of the Nanoreactor Concept for Efficient Synthesis of Multiblock Copolymers via MacroRAFT-Mediated Emulsion Polymerization. *ACS Macro Lett.* **2019**, *8* (8), 989–995.
(99) Khan, M.; Guimarães, T. R.; Zhou, D.; Moad, G.; Perrier, S.; Zetterlund, P. B. Exploitation of Compartmentalization in RAFT Miniemulsion Polymerization to Increase the Degree of Livingness. *J. Polym. Sci. Part A: Polym. Chem.* **2019**, *57* (18), 1938–1946.
(100) Nothling, M. D.; Fu, Q.; Reyhani, A.; Allison-Logan, S.; Jung, K.; Zhu, J.; Kamigaito, M.; Boyer, C.; Qiao, G. G. Progress and Perspectives Beyond Traditional RAFT Polymerization. *Adv. Sci.* **2020**, *7* (20), 2001656.

(101) Lehnen, A.-C.; Kurki, J. A. M.; Hartlieb, M. The Difference between Photo-Iniferter and Conventional RAFT Polymerization: High Livingness Enables the Straightforward Synthesis of Multiblock Copolymers. *Polym. Chem.* **2022**, *13* (11), 1537–1546.
(102) Somarathna, H. M. C. C.; Raman, S. N.; Mohotti, D.; Mutalib, A. A.; Badri, K. H. The Use of Polyurethane for Structural and Infrastructural Engineering Applications: A State-of-the-Art Review. *Constr. Build. Mater.* **2018**, *190*, 995–1014.
(103) Krol, P. Synthesis Methods, Chemical Structures and Phase Structures of Linear Polyurethanes. Properties and Applications of Linear Polyurethanes in Polyurethane Elastomers, Copolymers and Ionomers. *Prog. Mater. Sci.* **2007**, *52* (6), 915–1015.
(104) Ristić, I.; Cakić, S.; Vukić, N.; Teofilović, V.; Tanasić, J.; Pilić, B. The Influence of Soft Segment Structure on the Properties of Polyurethanes. *Polymers* **2023**, *15* (18), 3755.
(105) Delebecq, E.; Pascault, J.-P.; Boutevin, B.; Ganachaud, F. On the Versatility of Urethane/Urea Bonds: Reversibility, Blocked Isocyanate, and Non-Isocyanate Polyurethane. *Chem. Rev.* **2013**, *113* (1), 80–118.
(106) Akindoyo, J. O.; Beg, M. D. H.; Ghazali, S.; Islam, M. R.; Jeyaratnam, N.; Yuvaraj, A. R. Polyurethane Types, Synthesis and Applications – a Review. *RSC Adv.* **2016**, *6* (115), 114453–114482.
(107) Guo, Z.; Ding, X.; Wang, Y. How To Get Isocyanate? *ACS Omega* **2024**, *9* (10), 11168–11180.
(108) Hayes, G.; Laurel, M.; MacKinnon, D.; Zhao, T.; Houck, H. A.; Becer, C. R. Polymers without Petrochemicals: Sustainable Routes to Conventional Monomers. *Chem. Rev.* **2023**, *123* (5), 2609–2734.
(109) Kreye, O.; Mutlu, H.; Meier, M. A. R. Sustainable Routes to Polyurethane Precursors. *Green Chem.* **2013**, *15* (6), 1431.
(110) Golling, F. E.; Pires, R.; Hecking, A.; Weikard, J.; Richter, F.; Danielmeier, K.; Dijkstra, D. Polyurethanes for Coatings and Adhesives – Chemistry and Applications. *Polym. Int.* **2019**, *68* (5), 848–855.
(111) *Springer Handbook of Aerogels*; Aegerter, M. A., Leventis, N., Koebel, M., Steiner Iii, S. A., Eds.; Springer Handbooks; Springer International Publishing: Cham, 2023.
(112) Guo, Y.; Muuronen, M.; Lucas, F.; Sijbesma, R. P.; Tomović, Ž. Catalysts for Isocyanate Cyclotrimerization. *ChemCatChem* **2023**, *15* (10), e202201362.
(113) Gomez-Lopez, A.; Elizalde, F.; Calvo, I.; Sardon, H. Trends in Non-Isocyanate Polyurethane (NIPU) Development. *Chem. Commun.* **2021**, *57* (92), 12254–12265.
(114) Aomchad, V.; Cristòfol, À.; Della Monica, F.; Limburg, B.; D'Elia, V.; Kleij, A. W. Recent Progress in the Catalytic Transformation of Carbon Dioxide into Biosourced Organic Carbonates. *Green Chem.* **2021**, *23* (3), 1077–1113.
(115) Wang, Y.; Xia, Y.; Hua, Z.; Zhang, C.; Zhang, X. Chemoselective Ring-Opening Copolymerization of Five-Membered Cyclic Carbonates and Carbonyl Sulfide toward Poly(Thioether)s. *Polym. Chem.* **2022**, *13* (37), 5397–5403.

(116) Blain, M.; Cornille, A.; Boutevin, B.; Auvergne, R.; Benazet, D.; Andrioletti, B.; Caillol, S. Hydrogen Bonds Prevent Obtaining High Molar Mass PHU s. *J. Appl. Polym. Sci.* **2017**, *134* (45), 44958.

(117) Gomez-Lopez, A.; Panchireddy, S.; Grignard, B.; Calvo, I.; Jerome, C.; Detrembleur, C.; Sardon, H. Poly(Hydroxyurethane) Adhesives and Coatings: State-of-the-Art and Future Directions. *ACS Sustainable Chem. Eng.* **2021**, *9* (29), 9541–9562.

(118) Gomez-Lopez, A.; Ayensa, N.; Grignard, B.; Irusta, L.; Calvo, I.; Müller, A. J.; Detrembleur, C.; Sardon, H. Enhanced and Reusable Poly(Hydroxy Urethane)-Based Low Temperature Hot-Melt Adhesives. *ACS Polym. Au* **2022**, *2* (3), 194–207.

(119) Schmidt, S.; Gatti, F. J.; Luitz, M.; Ritter, B. S.; Bruchmann, B.; Mülhaupt, R. Erythritol Dicarbonate as Intermediate for Solvent- and Isocyanate-Free Tailoring of Bio-Based Polyhydroxyurethane Thermoplastics and Thermoplastic Elastomers. *Macromolecules* **2017**, *50* (6), 2296–2303.

(120) Yuen, A.; Bossion, A.; Gómez-Bengoa, E.; Ruipérez, F.; Isik, M.; Hedrick, J. L.; Mecerreyes, D.; Yang, Y. Y.; Sardon, H. Room Temperature Synthesis of Non-Isocyanate Polyurethanes (NIPUs) Using Highly Reactive N-Substituted 8-Membered Cyclic Carbonates. *Polym. Chem.* **2016**, *7* (11), 2105–2111.

(121) Hosokawa, S.; Nagao, A.; Hashimoto, Y.; Matsune, A.; Okazoe, T.; Suzuki, C.; Wada, H.; Kakiuchi, T.; Tsuda, A. Non-Isocyanate Polyurethane Synthesis by Polycondensation of Alkylene and Arylene Bis(Fluoroalkyl) Bis(Carbonate)s with Diamines. *Bull. Chem. Soc. Jpn.* **2023**, *96* (7), 663–670.

(122) Kébir, N.; Nouigues, S.; Moranne, P.; Burel, F. Nonisocyanate Thermoplastic Polyurethane Elastomers Based on Poly(Ethylene Glycol) Prepared through the Transurethanization Approach. *J. Appl. Polym. Sci.* **2017**, *134* (45), 44991.

(123) Fidalgo, D. M.; Kolender, A. A.; Varela, O. Stereoregular Poly- *O* -methyl [*m,n*]-polyurethanes Derived from D -mannitol. *J. Polym. Sci. A Polym. Chem.* **2013**, *51* (2), 463–470.

(124) Sardon, H.; Engler, A. C.; Chan, J. M. W.; Coady, D. J.; O'Brien, J. M.; Mecerreyes, D.; Yang, Y. Y.; Hedrick, J. L. Homogeneous Isocyanate- and Catalyst-Free Synthesis of Polyurethanes in Aqueous Media. *Green Chem.* **2013**, *15* (5), 1121.

(125) Wang, T.; Deng, H.; Zeng, H.; Shen, J.; Xie, F.; Zhang, C. Self-Blowing Non-Isocyanate Polyurethane Foams from Cyclic Carbonate Linseed Oil. *ACS Sustainable Resour. Manage.* **2024**, *1* (3), 462–470.

(126) Blattmann, H.; Lauth, M.; Mülhaupt, R. Flexible and Bio-Based Nonisocyanate Polyurethane (NIPU) Foams. *Macro Materials & Eng* **2016**, *301* (8), 944–952.

(127) Amezúa-Arranz, C.; Santiago-Calvo, M.; Rodríguez-Pérez, M.-Á. A New Synthesis Route to Produce Isocyanate-Free Polyurethane Foams. *Eur. Polym. J.* **2023**, *197*, 112366.

(128) Bourguignon, M.; Grignard, B.; Detrembleur, C. Water-Induced Self-Blown Non-Isocyanate Polyurethane Foams. *Angew. Chem. Int. Ed.* **2022**, *61* (51), e202213422.

(129) Lee, E.; Kim, M.; Moon, I.; Kim, J. Multi-Objective Optimization for Sustainable and Economical Polycarbonate Production with Reaction Kinetics Inference for Real-World Industrial Process. *Chem. Eng. J.* **2024**, *490*, 151484.
(130) Fukuoka, S.; Kawamura, M.; Komiya, K.; Tojo, M.; Hachiya, H.; Hasegawa, K.; Aminaka, M.; Okamoto, H.; Fukawa, I.; Konno, S. A Novel Non-Phosgene Polycarbonate Production Process Using by-Product CO_2 as Starting Material. *Green Chem.* **2003**, *5* (5), 497–507.
(131) Liu, B.; Wei, D.; Wang, C.; Wang, B.; Zhu, J. Refined Kinetic Model for the Simulation of Polycarbonate Synthesis via Continuous Melt Transesterification. *Chem. Eng. Sci.* **2024**, *300*, 120618.
(132) An, H.; Yang, Z.; Bi, K.; Xu, F.; Huo, F.; Li, C.; Fang, W.; Zhang, Z.; Lan, X.; Zhang, S. Highly Efficient and Selective Synthesis of Methyl Carbonate-Ended Polycarbonate Precursors from Dimethyl Carbonate and Bisphenol A. *Ind. Eng. Chem. Res.* **2020**, *59* (31), 13948–13955.
(133) Shi, D.; Heyte, S.; Capron, M.; Paul, S. Catalytic Processes for the Direct Synthesis of Dimethyl Carbonate from CO_2 and Methanol: A Review. *Green Chem.* **2022**, *24* (3), 1067–1089.
(134) Haba, O.; Itakura, I.; Ueda, M.; Kuze, S. Synthesis of Polycarbonate from Dimethyl Carbonate and Bisphenol-a through a Non-Phosgene Process. *J. Polym. Sci. A Polym. Chem.* **1999**, *37* (13), 2087–2093.
(135) Tsuda, A.; Ozawa, N.; Muranaka, R.; Kuwahara, T.; Matsune, A.; Liang, F. Photo-on-Demand *In Situ* Phosgenation Reactions That Cross Three Phases of a Heterogeneous Solution of Chloroform and Aqueous NaOH. *ACS Omega* **2023**, *8* (30), 27802–27810.
(136) Khalili Sadrabad, E.; Hashemi, S. A.; Nadjarzadeh, A.; Askari, E.; Akrami Mohajeri, F.; Ramroudi, F. Bisphenol A Release from Food and Beverage Containers – A Review. *Food Sci. Nutr.* **2023**, *11* (7), 3718–3728.
(137) Wei, P.; Bhat, G. A.; Darensbourg, D. J. Enabling New Approaches: Recent Advances in Processing Aliphatic Polycarbonate-Based Materials. *Angew. Chem. Int. Ed.* **2023**, *62* (48), e202307507.
(138) Park, J. H.; Jeon, J. Y.; Lee, J. J.; Jang, Y.; Varghese, J. K.; Lee, B. Y. Preparation of High-Molecular-Weight Aliphatic Polycarbonates by Condensation Polymerization of Diols and Dimethyl Carbonate. *Macromolecules* **2013**, *46* (9), 3301–3308.
(139) Tempelaar, S.; Mespouille, L.; Coulembier, O.; Dubois, P.; Dove, A. P. Synthesis and Post-Polymerisation Modifications of Aliphatic Poly(Carbonate)s Prepared by Ring-Opening Polymerisation. *Chem. Soc. Rev.* **2013**, *42* (3), 1312–1336.
(140) Zhu, W.; Huang, X.; Li, C.; Xiao, Y.; Zhang, D.; Guan, G. High-molecular-weight Aliphatic Polycarbonates by Melt Polycondensation of Dimethyl Carbonate and Aliphatic Diols: Synthesis and Characterization. *Polym. Int.* **2011**, *60* (7), 1060–1067.

(141) Saxon, D. J.; Luke, A. M.; Sajjad, H.; Tolman, W. B.; Reineke, T. M. Next-Generation Polymers: Isosorbide as a Renewable Alternative. *Prog. Polym. Sci.* **2020**, *101*, 101196.

(142) Yang, Z.; Liu, L.; An, H.; Li, C.; Zhang, Z.; Fang, W.; Xu, F.; Zhang, S. Cost-Effective Synthesis of High Molecular Weight Biobased Polycarbonate via Melt Polymerization of Isosorbide and Dimethyl Carbonate. *ACS Sustainable Chem. Eng.* **2020**, *8* (27), 9968–9979.

(143) Qian, W.; Ma, X.; Fu, M.; Chen, M.; Yang, Z.; Su, Q.; Cheng, W. Tailoring the Molecular Weight of Isosorbide-Derived Polycarbonates *via* Regulating the H-Bond Donor/Acceptor Ability of Task-Specific Ionic Liquid Catalysts. *Green Chem.* **2024**, *26* (6), 3406–3417.

(144) Yu, W.; Maynard, E.; Chiaradia, V.; Arno, M. C.; Dove, A. P. Aliphatic Polycarbonates from Cyclic Carbonate Monomers and Their Application as Biomaterials. *Chem. Rev.* **2021**, *121* (18), 10865–10907.

(145) Mikami, K.; Lonnecker, A. T.; Gustafson, T. P.; Zinnel, N. F.; Pai, P.-J.; Russell, D. H.; Wooley, K. L. Polycarbonates Derived from Glucose via an Organocatalytic Approach. *J. Am. Chem. Soc.* **2013**, *135* (18), 6826–6829.

(146) Gregory, G. L.; Jenisch, L. M.; Charles, B.; Kociok-Köhn, G.; Buchard, A. Polymers from Sugars and CO_2 : Synthesis and Polymerization of a D -Mannose-Based Cyclic Carbonate. *Macromolecules* **2016**, *49* (19), 7165–7169.

(147) Xu, J.; Feng, E.; Song, J. Renaissance of Aliphatic Polycarbonates: New Techniques and Biomedical Applications. *J. Appl. Polym. Sci.* **2014**, *131* (5), app.39822.

(148) Yang, G.-W.; Xie, R.; Zhang, Y.-Y.; Xu, C.-K.; Wu, G.-P. Evolution of Copolymers of Epoxides and CO_2 : Catalysts, Monomers, Architectures, and Applications. *Chem. Rev.* **2024**, *124* (21), 12305–12380.

(149) Hauenstein, O.; Reiter, M.; Agarwal, S.; Rieger, B.; Greiner, A. Bio-Based Polycarbonate from Limonene Oxide and CO_2 with High Molecular Weight, Excellent Thermal Resistance, Hardness and Transparency. *Green Chem.* **2016**, *18* (3), 760–770.

(150) Ma, Z.; Jia, Y.-G.; Zhu, X. X. Glycopolymers Bearing Galactose and Betulin: Synthesis, Encapsulation, and Lectin Recognition. *Biomacromolecules* **2017**, *18* (11), 3812–3818.

(151) Jeromenok, J.; Böhlmann, W.; Jäger, C.; Weber, J. Carbon Dioxide Adsorption in Betulin-Based Micro- and Macroporous Polyurethanes. *ChemistryOpen* **2013**, *2* (1), 17–20.

(152) Curia, S.; Dautle, S.; Satterfield, B.; Yorke, K.; Cranley, C. E.; Dobson, B. E.; La Scala, J. J.; Soh, L.; Gordon, M. B.; Stanzione, J. F. Betulin-Based Thermoplastics and Thermosets through Sustainable and Industrially Viable Approaches: New Insights for the Valorization of an Underutilized Resource. *ACS Sustainable Chem. Eng.* **2019**, *7* (19), 16371–16381.

(153) Okada, M.; Suzuki, K.; Mawatari, Y.; Tabata, M. Biopolyester Prepared Using Unsaturated Betulin (Betulinol) Extracted from Outer Birch Bark and Dicarboxylic

Acid Dichlorides and Its Thermal-Induced Crosslinking. *Eur. Polym. J.* **2019**, *113*, 12–17.

(154) Ma, Z.; Chen, Y.; Zuo, W.; Zhu, M. Synthesis and Fabrication of a Betulin-Containing Polyolefin Electrospun Fibrous Mat for Antibacterial Applications. *ACS Biomater. Sci. Eng.* **2022**, *8* (12), 5110–5118.

(155) Shanmugam, M. K.; Nguyen, A. H.; Kumar, A. P.; Tan, B. K. H.; Sethi, G. Targeted Inhibition of Tumor Proliferation, Survival, and Metastasis by Pentacyclic Triterpenoids: Potential Role in Prevention and Therapy of Cancer. *Cancer Lett.* **2012**, *320* (2), 158–170.

(156) Cargnin, S. T.; Gnoatto, S. B. Ursolic Acid from Apple Pomace and Traditional Plants: A Valuable Triterpenoid with Functional Properties. *Food Chem.* **2017**, *220*, 477–489.

(157) Teoh, E. S. Secondary Metabolites of Plants. In *Medicinal Orchids of Asia*; Springer International Publishing: Cham, 2016; pp 59–73.

(158) Kim, S.; Lee, H.; Lee, S.; Yoon, Y.; Choi, K.-H. Antimicrobial Action of Oleanolic Acid on Listeria Monocytogenes, Enterococcus Faecium, and Enterococcus Faecalis. *PLoS ONE* **2015**, *10* (3), e0118800.

(159) Wang, Y.-S.; Li, G.-L.; Zhu, S.-B.; Jing, F.-C.; Liu, R.-D.; Li, S.-S.; He, J.; Lei, J.-D. A Self-Assembled Nanoparticle Platform Based on Amphiphilic Oleanolic Acid Polyprodrug for Cancer Therapy. *Chin. J. Polym. Sci.* **2020**, *38* (8), 819–829.

(160) Butkevičiūtė, A.; Janulis, V.; Kviklys, D. Triterpene Content in Flesh and Peel of Apples Grown on Different Rootstocks. *Plants* **2022**, *11* (9), 1247.

(161) Kumbham, S.; Paul, M.; Bhatt, H.; Ghosh, B.; Biswas, S. Oleanolic Acid-Conjugated Poly (D, L-Lactide)-Based Micelles for Effective Delivery of Doxorubicin and Combination Chemotherapy in Oral Cancer. *J. Mol. Liq.* **2020**, *320*, 114389.

(162) Shanmugam, M. K.; Dai, X.; Kumar, A. P.; Tan, B. K. H.; Sethi, G.; Bishayee, A. Oleanolic Acid and Its Synthetic Derivatives for the Prevention and Therapy of Cancer: Preclinical and Clinical Evidence. *Cancer Lett.* **2014**, *346* (2), 206–216.

(163) Liby, K. T.; Yore, M. M.; Sporn, M. B. Triterpenoids and Rexinoids as Multifunctional Agents for the Prevention and Treatment of Cancer. *Nat. Rev. Cancer* **2007**, *7* (5), 357–369.

(164) Jeong, D. W.; Kim, Y. H.; Kim, H. H.; Ji, H. Y.; Yoo, S. D.; Choi, W. R.; Lee, S. M.; Han, C.-K.; Lee, H. S. Dose-Linear Pharmacokinetics of Oleanolic Acid after Intravenous and Oral Administration in Rats. *Biopharm. Drug Dispos.* **2007**, *28* (2), 51–57.

(165) Manker, L. P.; Dick, G. R.; Demongeot, A.; Hedou, M. A.; Rayroud, C.; Rambert, T.; Jones, M. J.; Sulaeva, I.; Vieli, M.; Leterrier, Y.; Potthast, A.; Maréchal, F.; Michaud, V.; Klok, H.-A.; Luterbacher, J. S. Sustainable Polyesters via Direct Functionalization of Lignocellulosic Sugars. *Nat. Chem.* **2022**, *14* (9), 976–984.

(166) Kong, X.; Qi, H.; Curtis, J. M. Synthesis and Characterization of High-Molecular Weight Aliphatic Polyesters from Monomers Derived from Renewable Resources. *J. Appl. Polym. Sci.* **2014**, *131* (15), 40579.

(167) Laanesoo, S.; Bonjour, O.; Parve, J.; Parve, O.; Matt, L.; Vares, L.; Jannasch, P. Poly(Alkanoyl Isosorbide Methacrylate)s: From Amorphous to Semicrystalline and Liquid Crystalline Biobased Materials. *Biomacromolecules* **2021**, *22* (2), 640–648.
(168) Matt, L.; Parve, J.; Parve, O.; Pehk, T.; Pham, T. H.; Liblikas, I.; Vares, L.; Jannasch, P. Enzymatic Synthesis and Polymerization of Isosorbide-Based Monomethacrylates for High- T_g Plastics. *ACS Sustainable Chem. Eng.* **2018**, *6* (12), 17382–17390.
(169) Nguyen, H. T. H.; Qi, P.; Rostagno, M.; Feteha, A.; Miller, S. A. The Quest for High Glass Transition Temperature Bioplastics. *J. Mater. Chem. A* **2018**, *6* (20), 9298–9331.
(170) Veith, C.; Diot-Néant, F.; Miller, S. A.; Allais, F. Synthesis and Polymerization of Bio-Based Acrylates: A Review. *Polym. Chem.* **2020**, *11* (47), 7452–7470.
(171) Fouilloux, H.; Thomas, C. M. Production and Polymerization of Biobased Acrylates and Analogs. *Macromol. Rapid Commun.* **2021**, *42* (3), 2000530.
(172) Lenges, R. *BASF broadens its Monomers Portfolio and launches bio-based 2-Octyl Acrylate*. News Release. https://www.basf.com/global/en/media/news-releases/2023/09/p-23-315.html (accessed 2024-06-21).
(173) Wittig, E. *Evonik obtains Certification for VISIOMER® Terra biobased methacrylates*. Press Release. https://methyl-methacrylate-monomers.evonik.com/en/evonik-obtains-certification-for-visiomer-terra-biobased-methacrylates-195948.html (accessed 2024-06-21).
(174) Plaisance, A. *Arkema increases its bio-based offer with a new range of mass balance acrylic materials*. Press Release. https://www.arkema.com/global/en/media/newslist/news/global/products/2022/20221121-new-range-mass-balance-acrylic-materials/ (accessed 2024-06-21).
(175) Karahan, O.; Aydin, K.; Edizer, S.; Odabasi, N.; Avci, D. Development of Reactive Methacrylates Based on Glycidyl Methacrylate: Development of Reactive Methacrylates. *J. Polym. Sci., Part A: Polym. Chem.* **2010**, *48* (17), 3787–3796.
(176) Lopez, J.; Pletscher, S.; Aemissegger, A.; Bucher, C.; Gallou, F. *N* -Butylpyrrolidinone as Alternative Solvent for Solid-Phase Peptide Synthesis. *Org. Process Res. Dev.* **2018**, *22* (4), 494–503.
(177) Sherwood, J.; Parker, H. L.; Moonen, K.; Farmer, T. J.; Hunt, A. J. N-Butylpyrrolidinone as a Dipolar Aprotic Solvent for Organic Synthesis. *Green Chem.* **2016**, *18* (14), 3990–3996.
(178) Tobiszewski, M.; Bystrzanowska, M. Monetary Values Estimates of Solvent Emissions. *Green Chem.* **2020**, *22* (22), 7983–7988.
(179) Li, H.; Zhang, X.; Zhang, X.; Yang, B.; Wei, Y. Stable Biocompatible Cross-Linked Fluorescent Polymeric Nanoparticles Based on AIE Dye and Itaconic Anhydride. *Colloids Surf., B* **2014**, *121*, 347–353.
(180) Javakhishvili, I.; Kasama, T.; Jankova, K.; Hvilsted, S. RAFT Copolymerization of Itaconic Anhydride and 2-Methoxyethyl Acrylate: A Multifunctional Scaffold for Preparation of "Clickable" Gold Nanoparticles. *Chem. Commun.* **2013**, *49* (42), 4803.

(181) Grassie, N. Recent Work on the Thermal Degradation of Acrylate and Methacrylate Homopolymers and Copolymers. *Pure and Applied Chemistry* **1972**, *30* (1–2), 119–134.

(182) Bertini, F.; Audisio, G.; Zuev, V. V. Investigation on the Thermal Degradation of Poly-*n*-Alkyl Acrylates and Poly-*n*-Alkyl Methacrylates (C1–C12). *Polymer Degradation and Stability* **2005**, *89* (2), 233–239.

(183) Schild, H. G. Thermal Degradation of Poly(Methacrylic Acid): Further Studies Applying TGA/FTIR. *J. Polym. Sci., Part A: Polym. Chem.* **1993**, *31* (9), 2403–2405.

(184) Porter, C. E.; Blum, F. D. Thermal Characterization of PMMA Thin Films Using Modulated Differential Scanning Calorimetry. *Macromolecules* **2000**, *33* (19), 7016–7020.

(185) Teng, H.; Koike, K.; Zhou, D.; Satoh, Z.; Koike, Y.; Okamoto, Y. High Glass Transition Temperatures of Poly(Methyl Methacrylate) Prepared by Free Radical Initiators. *J. Polym. Sci. A Polym. Chem.* **2009**, *47* (1), 315–317.

(186) Yu, J. M.; Dubois, P.; Jérôme, R. Synthesis and Properties of Poly[Isobornyl Methacrylate (IBMA)- *b* -Butadiene (BD)- *b* -IBMA] Copolymers: New Thermoplastic Elastomers of a Large Service Temperature Range. *Macromolecules* **1996**, *29* (23), 7316–7322.

(187) Gallagher, J. J.; Hillmyer, M. A.; Reineke, T. M. Isosorbide-Based Polymethacrylates. *ACS Sustainable Chem. Eng.* **2015**, *3* (4), 662–667.

(188) Droesbeke, M. A.; Simula, A.; Asua, J. M.; Du Prez, F. E. Biosourced Terpenoids for the Development of Sustainable Acrylic Pressure-Sensitive Adhesives *via* Emulsion Polymerisation. *Green Chem.* **2020**, *22* (14), 4561–4569.

(189) Matsuo, K.; Nelb, G. W.; Nelb, R. G.; Stockmayer, W. H. Kinetics of Free-Radical Polymerization of Vinylidene Chloride in Homogeneous N-Methylpyrrolidone Solution. *Macromolecules* **1977**, *10* (3), 654–658.

(190) Santanakrishnan, S.; Tang, L.; Hutchinson, R. A.; Stach, M.; Lacík, I.; Schrooten, J.; Hesse, P.; Buback, M. Kinetics and Modeling of Batch and Semibatch Aqueous-Phase NVP Free-Radical Polymerization. *Macromolecular Reaction Engineering* **2010**, *4* (8), 499–509.

(191) Chattopadhyay, D. K.; Raju, K. V. S. N. Structural Engineering of Polyurethane Coatings for High Performance Applications. *Prog. Polym. Sci.* **2007**, *32* (3), 352–418.

(192) Golling, F. E.; Pires, R.; Hecking, A.; Weikard, J.; Richter, F.; Danielmeier, K.; Dijkstra, D. Polyurethanes for Coatings and Adhesives – Chemistry and Applications. *Polym. Int.* **2019**, *68* (5), 848–855.

(193) Chattopadhyay, D. K.; Webster, D. C. Thermal Stability and Flame Retardancy of Polyurethanes. *Prog. Polym. Sci.* **2009**, *34* (10), 1068–1133.

(194) Decostanzi, M.; Auvergne, R.; Darroman, E.; Boutevin, B.; Caillol, S. Reactivity and Kinetics of HDI-Iminooxadiazinedione: Application to Polyurethane Synthesis. *Eur. Polym. J.* **2017**, *96*, 443–451.

(195) Charlon, M.; Heinrich, B.; Matter, Y.; Couzigné, E.; Donnio, B.; Avérous, L. Synthesis, Structure and Properties of Fully Biobased Thermoplastic Polyurethanes, Obtained from a Diisocyanate Based on Modified Dimer Fatty Acids, and Different Renewable Diols. *Eur. Polym. J.* **2014**, *61*, 197–205.
(196) Desai, Y.; Jariwala, S.; Gupta, R. K. Bio-Based Polyurethanes and Their Applications. In *ACS Symposium Series*; Gupta, R. K., Ed.; American Chemical Society: Washington, DC, 2023; Vol. 1453, pp 1–14.
(197) Zenner, M. D.; Xia, Y.; Chen, J. S.; Kessler, M. R. Polyurethanes from Isosorbide-Based Diisocyanates. *ChemSusChem* **2013**, *6* (7), 1182–1185.
(198) Neumann, C. N. D.; Bulach, W. D.; Rehahn, M.; Klein, R. Water-Free Synthesis of Polyurethane Foams Using Highly Reactive Diisocyanates Derived from 5-Hydroxymethylfurfural. *Macromol. Rapid Commun.* **2011**, *32* (17), 1373–1378.
(199) Akay, O.; Altinkok, C.; Acik, G.; Yuce, H.; Ege, G. K. A Bio-Based and Non-Toxic Polyurethane Film Derived from Luffa Cylindrica Cellulose and L-Lysine Diisocyanate Ethyl Ester. *Eur. Polym. J.* **2021**, *161*, 110856.
(200) Li, Y.; Luo, X.; Hu, S. Lignocellulosic Biomass-Based Polyols for Polyurethane Applications. In *Bio-based Polyols and Polyurethanes*; SpringerBriefs in Molecular Science; Springer International Publishing: Cham, 2015; pp 45–64.
(201) Furtwengler, P.; Avérous, L. Renewable Polyols for Advanced Polyurethane Foams from Diverse Biomass Resources. *Polym. Chem.* **2018**, *9* (32), 4258–4287.
(202) Lligadas, G.; Ronda, J. C.; Galià, M.; Cádiz, V. Oleic and Undecylenic Acids as Renewable Feedstocks in the Synthesis of Polyols and Polyurethanes. *Polymers* **2010**, *2* (4), 440–453.
(203) Lligadas, G.; Ronda, J. C.; Galià, M.; Cádiz, V. Plant Oils as Platform Chemicals for Polyurethane Synthesis: Current State-of-the-Art. *Biomacromolecules* **2010**, *11* (11), 2825–2835.
(204) Fontana, G.; Bruno, M.; Notarbartolo, M.; Labbozzetta, M.; Poma, P.; Spinella, A.; Rosselli, S. Cytotoxicity of Oleanolic and Ursolic Acid Derivatives toward Hepatocellular Carcinoma and Evaluation of NF-κB Involvement. *Bioorganic Chemistry* **2019**, *90*, 103054.
(205) Li, W.; Zeng, H.; Xu, M.; Huang, C.; Tao, L.; Li, J.; Zhang, T.; Chen, H.; Xia, J.; Li, C.; Li, X. Oleanolic Acid Improves Obesity-Related Inflammation and Insulin Resistance by Regulating Macrophages Activation. *Front. Pharmacol.* **2021**, *12*, 697483.
(206) Khwaza, V.; Oyedeji, O. O.; Aderibigbe, B. A. Antiviral Activities of Oleanolic Acid and Its Analogues. *Molecules* **2018**, *23* (9), 2300.
(207) Jessewitsch, T.; Saou, N.; Steinlein, L.; Bensberg, K.; Kirsch, S. F.; Delaittre, G. Oleanolic Acid-Derived High-Glass-Transition-Temperature Methacrylic Polymers. *ACS Sustainable Chem. Eng.* **2024**, *12* (52), 18499–18507.
(208) Jiang, L.; Ren, Z.; Zhao, W.; Liu, W.; Liu, H.; Zhu, C. Synthesis and Structure/Properties Characterizations of Four Polyurethane Model Hard Segments. *R. Soc. Open Sci.* **2018**, *5* (7), 180536.

(209) Peng, F.; Yang, X.; Zhu, Y.; Wang, G. Effect of the Symmetry of Polyether Glycols on Structure-Morphology-Property Behavior of Polyurethane Elastomers. *Polymer* **2022**, *239*, 124429.
(210) Ristić, I.; Cakić, S.; Vukić, N.; Teofilović, V.; Tanasić, J.; Pilić, B. The Influence of Soft Segment Structure on the Properties of Polyurethanes. *Polymers* **2023**, *15* (18), 3755.
(211) Wu, C.-H.; Chen, C.-W.; Chen, P.-H.; Chen, Y.-S.; Chuan, F.-S.; Rwei, S.-P. Characteristics of Polycarbonate Soft Segment-Based Thermoplastic Polyurethane. *Appl. Sci.* **2021**, *11* (12), 5359.
(212) Deneme, I.; Yıldız, T. A.; Kayaci, N.; Usta, H. The Hansen Solubility Approach towards Green Solvent Processing: N-Channel Organic Field-Effect Transistors under Ambient Conditions. *J. Mater. Chem. C* **2024**, *12* (11), 3854–3864.
(213) Belmokaddem, F.-Z.; Dagonneau, J.; Lhomme, J.; Blanc, R.; Garduno-Alva, A.; Maliverney, C.; Baceiredo, A.; Maerten, E.; Fleury, E.; Méchin, F. Novel Nucleophilic/Basic and Acidic Organocatalysts for Reaction between Poorly Reactive Diisocyanate and Diols. *Des. Monomers Polym.* **2016**, *19* (4), 347–360.
(214) Lim, J. Y. C.; Lin, Q.; Liu, C. K.; Guo, L.; Xue, K.; Loh, X. J. Zinc Diethyldithiocarbamate as a Catalyst for Synthesising Biomedically-Relevant Thermogelling Polyurethanes. *Mater. Adv.* **2020**, *1* (9), 3221–3232.
(215) Wu, L.; Liu, W.; Ye, J.; Cheng, R. Fast Cyclotrimerization of a Wide Range of Isocyanates to Isocyanurates over Acid/Base Conjugates under Bulk Conditions. *Catal. Commun.* **2020**, *145*, 106097.
(216) Gorbunova, M.; Anokhin, D. V.; Abukaev, A.; Ivanov, D. Impact of Soft Segment Composition on Phase Separation and Crystallization of Multi-Block Thermoplastic Polyurethanes Based on Poly(Butylene Adipate) Diol and Polycaprolactone Diol. *Crystals* **2023**, *13* (10), 1447.
(217) Zhang, C.; Ren, Z.; Yin, Z.; Qian, H.; Ma, D. Amide II and Amide III Bands in Polyurethane Model Soft and Hard Segments. *Polym. Bull.* **2008**, *60* (1), 97–101.
(218) Chiu, S.-J.; Liou, T.-H.; Tsai, C.-T.; Jian, X.-H. Characterization of Commercial Grades of Poly(Carbonate of Bisphenol A). *Int. J. Polym. Mater.* **2006**, *55* (11), 909–923.
(219) Eggenhuisen, T. M.; Hoeks, T. L. Degradation Mechanisms of Aromatic Polycarbonate. In *Reliability of Organic Compounds in Microelectronics and Optoelectronics*; Van Driel, W. D., Yazdan Mehr, M., Eds.; Springer International Publishing: Cham, 2022; pp 33–52.
(220) Rivaton, A. Recent Advances in Bisphenol-A Polycarbonate Photodegradation. *Polym. Degrad. Stab.* **1995**, *49* (1), 163–179.
(221) Trullemans, L.; Koelewijn, S.-F.; Scodeller, I.; Hendrickx, T.; Van Puyvelde, P.; Sels, B. F. A Guide towards Safe, Functional and Renewable BPA Alternatives by Rational Molecular Design: Structure–Property and Structure–Toxicity Relationships. *Polym. Chem.* **2021**, *12* (41), 5870–5901.
(222) Wang, H.; Xu, F.; Zhang, Z.; Feng, M.; Jiang, M.; Zhang, S. Bio-Based Polycarbonates: Progress and Prospects. *RSC Sustainability* **2023**, *1* (9), 2162–2179.

(223) Hauenstein, O.; Agarwal, S.; Greiner, A. Bio-Based Polycarbonate as Synthetic Toolbox. *Nat. Commun.* **2016**, *7* (1), 11862.
(224) Zhang, C.; Garrison, T. F.; Madbouly, S. A.; Kessler, M. R. Recent Advances in Vegetable Oil-Based Polymers and Their Composites. *Prog. Polym. Sci.* **2017**, *71*, 91–143.
(225) Hauenstein, O.; Reiter, M.; Agarwal, S.; Rieger, B.; Greiner, A. Bio-Based Polycarbonate from Limonene Oxide and CO_2 with High Molecular Weight, Excellent Thermal Resistance, Hardness and Transparency. *Green Chem.* **2016**, *18* (3), 760–770.
(226) Kindermann, N.; Cristòfol, À.; Kleij, A. W. Access to Biorenewable Polycarbonates with Unusual Glass-Transition Temperature (T_g) Modulation. *ACS Catal.* **2017**, *7* (6), 3860–3863.
(227) Mikami, K.; Lonnecker, A. T.; Gustafson, T. P.; Zinnel, N. F.; Pai, P.-J.; Russell, D. H.; Wooley, K. L. Polycarbonates Derived from Glucose via an Organocatalytic Approach. *J. Am. Chem. Soc.* **2013**, *135* (18), 6826–6829.
(228) Song, Y.; Ji, X.; Dong, M.; Li, R.; Lin, Y.-N.; Wang, H.; Wooley, K. L. Advancing the Development of Highly-Functionalizable Glucose-Based Polycarbonates by Tuning of the Glass Transition Temperature. *J. Am. Chem. Soc.* **2018**, *140* (47), 16053–16057.
(229) Gregory, G. L.; Jenisch, L. M.; Charles, B.; Kociok-Köhn, G.; Buchard, A. Polymers from Sugars and CO_2 : Synthesis and Polymerization of a D -Mannose-Based Cyclic Carbonate. *Macromolecules* **2016**, *49* (19), 7165–7169.
(230) Saxon, D. J.; Luke, A. M.; Sajjad, H.; Tolman, W. B.; Reineke, T. M. Next-Generation Polymers: Isosorbide as a Renewable Alternative. *Prog. Polym. Sci.* **2020**, *101*, 101196.
(231) Zhang, Z.; Xu, F.; He, H.; Ding, W.; Fang, W.; Sun, W.; Li, Z.; Zhang, S. Synthesis of High-Molecular Weight Isosorbide-Based Polycarbonates through Efficient Activation of Endo-Hydroxyl Groups by an Ionic Liquid. *Green Chem.* **2019**, *21* (14), 3891–3901.
(232) Sakakura, T.; Kohno, K. The Synthesis of Organic Carbonates from Carbon Dioxide. *Chem. Commun.* **2009**, No. 11, 1312.
(233) Wang, K.; Li, S.; Yu, M.; Liang, X. Enhancing DMC Production from CO2: Tuning Oxygen Vacancies and In Situ Water Removal. *Energies* **2024**, *17* (4), 839.
(234) Post, C.; Maniar, D.; Voet, V. S. D.; Folkersma, R.; Loos, K. Biobased 2,5-Bis(Hydroxymethyl)Furan as a Versatile Building Block for Sustainable Polymeric Materials. *ACS Omega* **2023**, *8* (10), 8991–9003.
(235) Choi, E. H.; Lee, J.; Son, S. U.; Song, C. Biomass-derived Furanic Polycarbonates: Mild Synthesis and Control of the Glass Transition Temperature. *J. Polym. Sci. Part A: Polym. Chem.* **2019**, *57* (17), 1796–1800.
(236) Panja, S. K.; Bag, B. G. Flower- and Grass-like Self-Assemblies of an Oleanane-Type Triterpenoid Erythrodiol: Application in the Removal of Toxic Dye from Water. *ACS Omega* **2020**, *5* (47), 30488–30494.

(237) Juan, M. E.; Wenzel, U.; Daniel, H.; Planas, J. M. Erythrodiol, a Natural Triterpenoid from Olives, Has Antiproliferative and Apoptotic Activity in HT-29 Human Adenocarcinoma Cells. *Mol. Nutr. Food Res.* **2008**, *52* (5), 595–599.

(238) Peñas-Fuentes, J. L.; Siles, E.; Rufino-Palomares, E. E.; Pérez-Jiménez, A.; Reyes-Zurita, F. J.; Lupiáñez, J. A.; Fuentes-Almagro, C.; Peragón-Sánchez, J. Effects of Erythrodiol on the Antioxidant Response and Proteome of HepG2 Cells. *Antioxidants* **2021**, *11* (1), 73.

(239) Martín, R.; Miana, M.; Jurado-López, R.; Martínez-Martínez, E.; Gómez-Hurtado, N.; Delgado, C.; Visitación Bartolomé, M.; San Román, J. A.; Cordova, C.; Lahera, V.; Nieto, M. L.; Cachofeiro, V. DIOL Triterpenes Block Profibrotic Effects of Angiotensin II and Protect from Cardiac Hypertrophy. *PLoS ONE* **2012**, *7* (7), e41545.

(240) Rodriguez-Rodriguez, R.; Perona, J. S.; Herrera, M. D.; Ruiz-Gutierrez, V. Triterpenic Compounds from "Orujo" Olive Oil Elicit Vasorelaxation in Aorta from Spontaneously Hypertensive Rats. *J. Agric. Food Chem.* **2006**, *54* (6), 2096–2102.

(241) Vanderhenst, R.; Miller, S. A. Polycarbonates from Biorenewable Diols via Carbonate Metathesis Polymerization. *Green Mater.* **2013**, *1* (2), 64–78.

(242) Ahmed, S.; Padilla-Gainza, V. M.; Gilkerson, R.; Narula, A.; Lozano, K. Processing-Structure–Property Relationships of Oleanolic Acid Loaded PLGA Fiber Membranes. *J. Mater. Sci.* **2023**, *58* (9), 4240–4255.

(243) Liu, W.; Zhu, W.; Li, C.; Guan, G.; Zhang, D.; Xiao, Y.; Zheng, L. Thermal Degradation Mechanism of Poly(Hexamethylene Carbonate). *Polym. Degrad. Stab.* **2015**, *112*, 70–77.

(244) Díaz-Celorio, E.; Franco, L.; Rodríguez-Galán, A.; Puiggalí, J. Synthesis of Glycolide/Trimethylene Carbonate Copolymers: Influence of Microstructure on Properties. *Eur. Polym. J.* **2012**, *48* (1), 60–73.

(245) Curia, S.; Dautle, S.; Satterfield, B.; Yorke, K.; Cranley, C. E.; Dobson, B. E.; La Scala, J. J.; Soh, L.; Gordon, M. B.; Stanzione, J. F. Betulin-Based Thermoplastics and Thermosets through Sustainable and Industrially Viable Approaches: New Insights for the Valorization of an Underutilized Resource. *ACS Sustainable Chem. Eng.* **2019**, *7* (19), 16371–16381.

(246) Jessewitsch, T.; Demeler, A. K.; Delaittre, G. Novel Bio-Based Thermoplastic Polyurethanes Derived From Oleanolic Acid. *submitted*.

(247) Siegu, W. M. K.; Djouonkep, L. D. W.; Selabi, N. B. S.; Bonku, E. M.; Cheng, Z.; Gauthier, M. Synergistic Effect and Structure–Property of Bio-Based 1,6-Hexanediol on Thermal, Mechanical and Degradation Properties of Biopolymers. *J. Polym. Environ.* **2023**, *31* (3), 1144–1159.

(248) Díez-Poza, C.; Sessini, V.; Jaraba Cabrera, D.; Mosquera, M. E. G.; Whiteoak, C. J. Non-Isocyanate Polyurethanes (NIPUs) Incorporating Isomers of Abundant Sugar-Derived 1,4:3,6-Dianhydrohexitols. *ACS Appl. Polym. Mater.* **2024**, *6* (23), 14695–14706.

(249) Mu, T.; Wei, B.; Zhu, D.; Yu, B. Site-Selective C-H Hydroxylation of Pentacyclic Triterpenoids Directed by Transient Chiral Pyridine-Imino Groups. *Nat. Commun.* **2020**, *11* (1), 4371.

(250) Wolfgang, J. D.; White, B. T.; Long, T. E. Non-isocyanate Polyurethanes from 1,1′-Carbonyldiimidazole: A Polycondensation Approach. *Macromol. Rapid Commun.* **2021**, *42* (13), 2100163.

(251) Choi, E. H.; Lee, J.; Son, S. U.; Song, C. Biomass-derived Furanic Polycarbonates: Mild Synthesis and Control of the Glass Transition Temperature. *J. Polym. Sci., Part A:Polym. Chem.* **2019**, *57* (17), 1796–1800.

(252) Olsson, J. V.; Hult, D.; García-Gallego, S.; Malkoch, M. Fluoride-Promoted Carbonylation Polymerization: A Facile Step-Growth Technique to Polycarbonates. *Chem. Sci.* **2017**, *8* (7), 4853–4857.

(253) Sehn, T.; Huber, B.; Fanelli, J.; Mutlu, H. Straightforward Synthesis of Aliphatic Polydithiocarbonates from Commercially Available Starting Materials. *Polym. Chem.* **2022**, *13* (42), 5965–5973.

(254) Tan, E. W. P.; Hedrick, J. L.; Arrechea, P. L.; Erdmann, T.; Kiyek, V.; Lottier, S.; Yang, Y. Y.; Park, N. H. Overcoming Barriers in Polycarbonate Synthesis: A Streamlined Approach for the Synthesis of Cyclic Carbonate Monomers. *Macromolecules* **2021**, *54* (4), 1767–1774.

(255) Häfliger, F.; Truong, N. P.; Wang, H. S.; Anastasaki, A. Fate of the RAFT End-Group in the Thermal Depolymerization of Polymethacrylates. *ACS Macro Lett.* **2023**, *12* (9), 1207–1212.

(256) Young, J. B.; Hughes, R. W.; Tamura, A. M.; Bailey, L. S.; Stewart, K. A.; Sumerlin, B. S. Bulk Depolymerization of Poly(Methyl Methacrylate) via Chain-End Initiation for Catalyst-Free Reversion to Monomer. *Chem* **2023**, *9* (9), 2669–2682.

(257) Wang, H. S.; Truong, N. P.; Pei, Z.; Coote, M. L.; Anastasaki, A. Reversing RAFT Polymerization: Near-Quantitative Monomer Generation Via a Catalyst-Free Depolymerization Approach. *J. Am. Chem. Soc.* **2022**, *144* (10), 4678–4684.

(258) Bensberg, K. *Studien Zu Oxidationsreaktionen Vermittelt Durch Hypervalente Iod(V)-Verbindungen Und Der Derivatisierung Pentacyclischer Triterpenoide.* Dissertation, Bergische Universität Wuppertal, Wuppertal, 2024.

(259) Wong, M. H. L.; Bryan, H. K.; Copple, I. M.; Jenkins, R. E.; Chiu, P. H.; Bibby, J.; Berry, N. G.; Kitteringham, N. R.; Goldring, C. E.; O'Neill, P. M.; Park, B. K. Design and Synthesis of Irreversible Analogues of Bardoxolone Methyl for the Identification of Pharmacologically Relevant Targets and Interaction Sites. *J. Med. Chem.* **2016**, *59* (6), 2396–2409.

8.6. Acknowledgements

My sincere thanks go to my supervisor *Prof. Dr. Guillaume Delaittre* for kindly welcoming me into his research group and for the opportunity to contribute to the university's sustainable apple collaboration project, which broadened my perspective. I am grateful for the valuable advice and encouragement during complex problem-solving. The professional discussions were consistently helpful and steered me in the right direction.

Furthermore, I would especially like to thank *Prof. Dr. Hatice Mutlu* for providing a second opinion on this dissertation, as well as for her time and thoughtful evaluation. I would like to express my gratitude to *Prof. Dr. Robert Göstl* and *Prof. Dr. Fabian Mohr* for being part of the examination committee.

I am grateful to *Sen. Prof. Dr. Ullrich Scherf*, who supervised me during my previous studies and provided valuable scientific support.

I owe special thanks to *Sylwia Adamczyk* for carrying out numerous SEC, TGA, and DSC measurements, and to *Anke Helfer* for her technical advice and support with the SEC system.

Thanks to *Felix Niebisch*, I have been able to pursue this goal from the very beginning of our studies. Further, I would like to sincerely thank all the AKGD group members for the incredibly inspiring time, especially *Gero Bramlage*, *Katerina Mathianaki*, *Dr. Gürbüz Dursun*, *Audrey Kieffer*, *Dr. Seçkin Merve Altuncu*, *Dr. Max Linhorst*, *Nathalie Bolten*, *Andreas Sternad*, and *Achim Vankann*. In this regard, I would also like to thank *Naima Saou*, *Lena Steinlein*, and *Aysha Demeler* for the excellent teamwork.

Lastly, I would like to express my heartfelt thanks to *Laura* and my family, who supported me emotionally, morally, and in all my decisions.